# Biogeomorphology from Space

## A comprehensive Analysis of the Corridor of the Naryn River in Kyrgyzstan based on Remote Sensing

by Florian Betz

A Dissertation Presented in Partial Fulfillment
of the Requirements for the Degree
Dr. rer. nat.

Faculty of Mathematics and Geography
Catholic University Eichstätt-Ingolstadt
Germany 2021

Submission Date: 11.01.2021

1st supervisor: Prof. Dr. Bernd Cyffka

2nd supervisor: apl. Prof. Dr. Gregory Egger

Date of oral examination: 07.05.2021

*To Magdalena*
*For all the support in the years full of ups and downs*

# Abstract

In the arid and semi-arid climate of Central Asia, the endorheic rivers and their ecosystems play a crucial role as regional hotspots of biodiversity and for the provision of ecosystem services for local people. The Naryn River in Kyrgyzstan as the object of interest of this thesis is one of these rivers. On a flow length of more than 600 km, it is still in a widely natural condition making it an interesting study object in a world where most large rivers are distorted by anthropogenic activities. Despite this relevance, no comprehensive scientific studies are available about the Naryn River except water resource related research. In particular, large scale information about the structure and functioning of the Naryn River system from an interdisciplinary perspective is missing. Against this background, this thesis aims to fill the research gap and deliver up-to-date information about the Naryn River corridor with a special focus on biogeomorphology, i.e. the dynamic interaction between hydromorphology and vegetation. First, this thesis delivers the necessary background information about the Naryn River corridor including a general overview, an assessment of ecosystem services, a field based overview of the structure of the riparian ecosystems and an in-depth analysis of hydrology. Basing upon this background, remote sensing methods adapted to the data-scarce environment of Central Asia are used to derive various parameters of the structure of the Naryn River on the scale from reaches to the entire river corridor. Then, the large scale biogeomorphological structures and dynamics are assessed based on dense time series of multispectral satellite imagery. From the results, it becomes obvious that the structure of the corridor of the Naryn River is heterogeneous and mainly controlled by geological contraints. Only in a laterally unconfined segment, dynamic braided river reaches can form. In these reaches, the majority of biogeomorphological interactions take place.
The outcome of this thesis is on the one hand the provision of large scale and up-to-date information about the structure and functioning of the Naryn River corridor as a basis for further research or decision making. On the other hand, this thesis presents innovative remote sensing methods for large scale characterization of river corridors. In particular, an approach for the characterization of dynamic processes of biogeomorphological interactions on a large scale is developed based on time series analysis of satellite imagery. This approach can complement biogeomorphological research on smaller spatial scales by delivering spatially and temporally continuous information for entire river corridors. This has the potential to obtain new insights of the processes and emergence of structure in river systems across multiple scales.

# Contents

# List of Figures

# List of Tables

# 1 Introduction

## 1.1 Setting the stage

In the arid and semi-arid climate of Central Asia, the endorheic rivers and their ecosystems play a crucial role as regional hotspots of biodiversity (Karthe et al., 2015). This is especially true for the upstream sections of the rivers where they are often still in a widely natural condition without damns or embankments. One of these rivers is the Naryn River in Kyrgyzstan (Fig. 1.1). Be-

Figure 1.1: An impression of the Naryn River in the central part of its catchment

sides its ecological relevance, the Naryn River provides manifold ecosystem services to people living in the villages along its banks. The floodplain forests along this river deliver wood and harvestable fruits for local people, serve as pastoral land and help mitigating erosion (Betz et al., 2015a,b). Furthermore, forestry has a high relevance in the Kyrgyz policy making, increasing the forest cover is a relevant administrative goal of the environmental management (Scheuber et al., 2000; Fisher et al., 2004). Floodplain forests are one major forest type and contribute 5.2% of the Kyrgyz forest cover (Zholdosheva, 2010). On the floodplains of the Naryn as the largest river a fundamental share of the Kyrgyz riparian forest grows. From a global perspective, the Naryn is of particular interest as this river is still in a widely natural state on a flow length of more than 600 km (Betz et al., 2016, 2018). In a world where more than half of the large river corridors are fragmented by dams and natural processes are disturbed by embankments or intensive land use in the riparian zone the Naryn becomes a rare refugium for widely undisturbed natural river dynamics (Tockner and Stanford, 2002; Nilsson et al., 2005; Grill et al., 2015). Despite the national and international importance of the Naryn River, there is no systematic assessment of the river and its accompanying floodplains prior to the work of the author of this thesis (Betz et al., 2015b). This is especially a relevant issue as there are plans for dam construction expected to have significant effects on the functioning of the river system. Main reason for the lack of governmental monitoring action are the economic and political challenges related to the ongoing transformation Kyrgyzstan undergoes after its independence following the breakdown of the Soviet Union in 1991 (Schmidt,

2013). The Soviet legacy is still highly present in Kyrgyzstan and contemporary environmental decision making like the dam construction at the upper Naryn River cannot be understood without having a look into history.
In the international river science community, it has become common sense that a comprehensive analysis of a river system needs to be highly interdisciplinary taking into account hydrology, geomorphology, ecology as well as the human dimension (Gilvear et al., 2016a, see Fig. 1.2). This

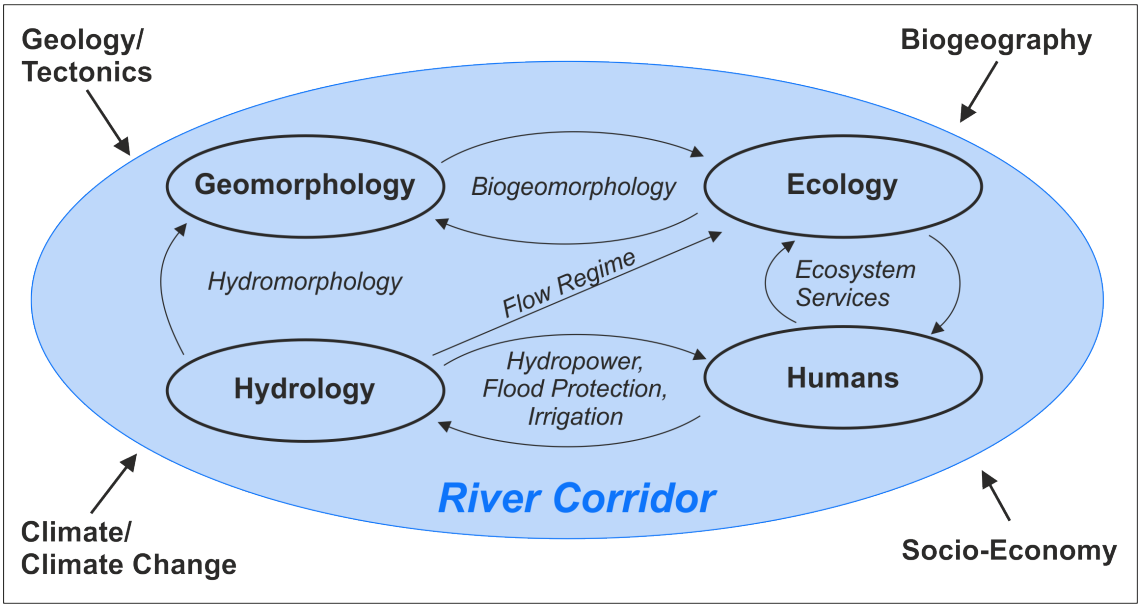


Figure 1.2: Scheme of the holistic perspective on the river corridor of the Naryn River as considered as background for this thesis; the arrows highlight connections of the river corridor components treated in this thesis

figure highlights the manifold relationships between the different disciplines. Hydrology as the key driver of river dynamics is influenced by climate as well as the ongoing climate change (Döll and Zhang, 2010; Milner et al., 2017). It has a direct influence on geomorphology which itself is constrained by the geological setting and tectonics. A further link exists to vegetation which is regarded to control landform development while geomorphological dynamics are vice versa expected to govern vegetation establishment and development. The abundance of certain species as well as the community composition is governed by the larger scale biogeography, i.e. the location within a certain floristic kingdom or - on a smaller scale - a certain ecoregion. Finally, living in the Anthropocene (Crutzen, 2002), the human dimension plays a critical role in many river systems worldwide. This human role is twofold. First, humans benefit from ecosystem services provided by the riverine ecosystems. The use of ecosystem services, however, can also affect these ecosystems. A second, even more relevant human impact is the building of dams for hydropower generation, flood protection or irrigation water storage. The altered hydrological regime arising from the dam construction can have manifold effects on the river corridor (Nilsson et al., 2005; Petts and Gurnell, 2005; Poff and Zimmerman, 2010). Despite this acknowledgment of the interdisciplinary, the international scientific community has so far considered the Naryn River only from a hydrological perspective as one of the major headwater streams in Central Asia.
This thesis arises from the transdisciplinary research project *Ecosystem Assessment and Capacity Building for sustainable Management of Floodplains along the Central Asian Rivers Tarim*

*and Naryn* (EcoCAR) running from 2014-2017 (Betz et al., 2015b). This project focused on the detailed analysis of structure and functioning of the riparian ecotones along these two rivers as well as the assessment of related ecosystem services. The results are then used to make suggestions for a more sustainable management of these rivers. In addition to the research, capacity building was a strong focus of EcoCAR to facilitate early career scientists on the Master and PhD level to carry out modern monitoring and interdisciplinary river research. Against this applied background, this thesis uses a state-of-the-art scientific understanding of river systems which is presented in the subsequent sections and presents comprehensive scientific information about the structure and functioning of the Naryn River system. For this assessment, I base upon the concepts of ***riverscapes*** as framework for the large scale analysis of river systems and ***biogeomorphology*** as theoretical grounding for investigating the interaction of hydrology, geomorphology and ecology. I merge these two concepts and propose ways for a river corridor wide assessment of biogeomorphological structure and dynamics of large river corridors.

## 1.2 Riverscapes - A framework for large scale river assessment

*Roots in fluvial geomorphology*

Scientific analysis of rivers date back at least until the end of the 19th century (Wohl, 2014). In this time, large scale perspectives such as Davies (1899) cycle of erosion governed the view on rivers. This theory belonging to the so-called *evolutionary approaches* considered the development of landscapes over geological time scales linking tectonic uplift and denudation by erosion (Davies, 1899). With the beginning of the 20th century, *functional approaches* emerged focusing on the contemporary processes measurable in the field. For instance, Gilbert (1914) presented his concept of sediment transport as function of discharge, channel gradient and grain-size. This concept was refined later by Lane (1955) who presented the relationship between discharge Q, channel gradient S, sediment availability $Q_S$ and median grain-size $D_{50}$.

$$Q \cdot S \propto Q_S \cdot D_{50} \tag{1.1}$$

This assumption lead to the formulation of the theory of the dynamic equilibrium by Hack (1960). In this theory, a river section will react on changes in the discharge or sediment availability until the available energy in terms of discharge and gradient is in balance with the availability of sediment in a specific grain-size (see equation 1.1). If changes occur in discharge or sediment availability for instance during flood events or after the introduction of sediment via e.g. a landslide, the river erosion or deposition of sediment will happen until the river section is in balance again (Hack, 1960; Fryirs and Brierley, 2013). Thus, as long as the boundary conditions in terms of sediment availability or discharge do not undergo significant changes, a river will adjust to these conditions and behave under a specific process-form relationship (Fryirs and Brierley, 2013). However, the ability for adjustment is constrained by the geological history of the river (Phillips, 2007, 2011). This was first analyzed in depth by the seminal work of Schumm (1977) who noted that rivers are systems following certain physical laws but have a geological history controlling their actual form. This implies that the cause-effect relationships are dependent on the time scale under investigation. On shorter time scales, characteristics like the elevation distribution of the catchment or the channel gradient may be considered as static variables. On larger time scales, however, they will of course follow the geological development of the region (Schumm and Lichty, 1965; Lane and Richards, 1997). Contemporary theoretical frameworks in fluvial geomorphology consider rivers

as complex systems operating across a range of different spatial and temporal scales (Piégay, 2016). This cross-scalar perspective on river systems has been found useful in riverine ecology and interdisciplinary studies as well (e.g. Thoms and Parsons, 2002; Thorp et al., 2006). Thus, this multi-scale perspective originating from fluvial geomorphology is today widely accepted as template for all kind of river science (Brierley, 2015).

*Contemporary approaches to river assessment and definition of scales*

In an application oriented context, multi-scale perspectives have been suggested to obtain in-depth knowledge of the structure and functioning of a river corridor (Brierley and Fryirs, 2005; Fryirs and Brierley, 2013; Gurnell et al., 2016b). This knowledge is then used to identify potential pressures on the system and discuss an adaption of management or restoration measures (Gurnell et al., 2016b). Applied river science in our days explicitly argues for a multi-scale perspective when carrying out the river characterization as basis for management. Or - as Fryirs and Brierley (2013, 322) point out in their application oriented textbook on river system analysis *'Know your catchment!'*. Numerous theoretical frameworks exist for describing this multi-scale character (Frissell et al., 1986; Petts and Amoros, 1996; Montgomery and Buffington, 1997, 1998; Habersack, 2000; Fausch et al., 2002; Benda et al., 2004; Brierley and Fryirs, 2005; Thorp et al., 2006; Dollar et al., 2007; Rinaldi et al., 2015). This list is far from being complete but gives an impression of the wide range of existing frameworks. All of these schemes have a different focus resulting in different theoretical perceptions of the spatial and temporal organization of river systems. In a recent study, Gurnell et al. (2016b) reviewed the common ground of the most relevant frameworks and synthesized them to a own framework. Within this study, they gave a comprehensive overview of the spatial and temporal scales which I adapt for this thesis (see Table 1.1). The majority of this table is directly taken from Gurnell et al. (2016b). I added the scale of the river corridor as additional scale between the entire landscape unit and the river segment (Table 1.1). The scale of landscape units still includes the hillslopes and the entire river network while the segment is just a part of an entire river network. Most concepts of spatial organizations of rivers focus on the longitudinal and lateral pattern of abiotic or biotic variables (Ward et al., 2002; Thorp et al., 2006; Gurnell et al., 2016a). This additional river corridor scale includes the entire area along a river from headwater to outlet connected to the hydrological and geomorphological processes in the river channel. This follows the process oriented perception of Hupp and Osterkamp (1996) and includes the active channel as well as the adjacent floodplain. When using the term *'large scale'* within this thesis, I refer to the scales from the segment to the entire catchment with a focus on the spatial organization of the river corridor.

*Changes in large scale perception of river corridors in geomorphology and ecology*

An early large scale view on rivers is the downstream hydraulic geometry in geomorphology (Leopold and Maddock, 1953). Due to the mass continuity equation of the discharge written as Q = wdv (Q is the discharge in $m^3s^{-1}$, w is the river channel width in m, d is the average water depth in m and v is the flow velocity in $ms^{-1}$), any change of the discharge should cause changes in the channel cross section and the flow velocity (Ferguson, 1986). As discharge is expected to increase with increasing drainage area, channel variables have been expected to change in predictable manner along the longitudinal profile of a river (Leopold and Maddock, 1953; Leopold et al., 1964; Ferguson, 1986; Knighton, 1999). In a purely functional perception of rivers, the channel form would be predictable along the longitudinal profile as it would arise solely from the

Table 1.1: Scales of fluvial system analysis (based on Gurnell et al., 2016b)

| Unit | Description | Spatial Dimension | Temporal Dimension |
|---|---|---|---|
| Region | Area containing a characteristic climate, geology and species composition | > $10^4$ km2 | > $10^4$ Years |
| Catchment | Area drained by a river and its tributaries | 5 x $10^4$ $km^2$ | $10^3$ Years |
| Landscape Unit | Part of the catchment with the similar topographic properties | 10 $km^2$ – 10 $km^3$ | $10^2$ – $10^3$ Years |
| River Corridor | Part of the catchment connected to the hydrological and geomorphological processes happening within the channel of a particular river | 10 $km^1$ – 10 $km^2$ | $10^1$ – $10^2$ Years |
| Segment | Section of a river corridor with similar valley morphology and energy conditions | 10 $km^1$ – 10 $km^2$ | $10^1$ – $10^2$ Years |
| Reach | Section of a river where the boundary conditions are sufficiently uniform to assume homogeneous process-form relationships | $10^{-1}$ – $10^1$ km | $10^1$ – $10^2$ Years |
| Geomorphic Unit | area created by erosion or sedimentation of sediment, often in association with vegetation | $10^0$ – $10^2$ m | $10^0$ – $10^1$ Years |
| Hydraulic Unit | Distinct patch with homogeneous flow conditions indicated by similar sediment characteristics | $10^{-1}$ – $10^1$ m | $10^{-1}$ – $10^1$ Years |
| River Element | Single element of the riverine landscape, for instance a piece of large woody debris | 10–2 – $10^1$ m | $10^{-2}$ – $10^0$ Years |

contemporary physical process regime. This view manifested in the idea of a sediment source, transfer and deposition zone in the fluvial system of Schumm (1977). Despite its early publication date, this concept is still used in fluvial geomorphology (e.g. Barker et al. 2009; Parker et al. 2015; Gleason 2015). The idea of a predictable downstream continuum of river variables has also been adapted in riverine ecology. Inspired by the work of Leopold and Maddock (1953), Vannote et al. (1980) presented their river continuum concept which is still considered to be among the most influential papers in riverine ecology in the 20th century (Thorp et al., 2006). Assuming that the abiotic controlling variables change in a continuous way along the longitudinal profile, Vannote et al. (1980) argue that the abundance and composition of species should follow a longitudinal gradient as well. Extending this longitudinal perception of riverine ecosystem pattern, Junk et al. (1989) introduced the flood pulse concept. They argue that regular floods create and modify the lateral connectivity between channel and floodplain. Ward (1989) combined these ideas to his

concept of four dimensions of a river corridor. In addition to the longitudinal focus of the river continuum concept and the lateral dimension of the flood pulse concept, he added a vertical dimension focusing on surface-groundwater interactions and its ecological consequences as well as a temporal dimension to understand the reaction of riverine ecosystems. A special emphasis on the temporal dynamics of riverine ecosystems has been given later by the natural flow regime paradigm introduced by Poff et al. (1997).
The idea of a gradual, predictable downstream continuum of abiotic and biotic variables has experienced fundamental criticism. Arguing from a geomorphological perspective, Montgomery (1999) argued that rivers are organized in process domains controlled by geological boundary conditions rather than in a gradual downstream pattern. Similarly, the spatial organization of riverine ecosystems has been considered as patchy and discontinuous since the early 2000s (Poole, 2002; Ward et al., 2002; Benda et al., 2004). A more recent framework emphasizing the discontinuous, patchy nature of rivers is the *riverine ecosystem synthesis* (Thorp et al., 2006, 2008; Gilvear et al., 2016a). Following the idea of Montgomery (1999), it considers a river network being spatially organized in diverse process domains. Geology, climate, vegetation and soils are assumed to form specific boundary conditions under which runoff and sediment transport happen forming a specific biophysical habitat (Thorp et al., 2006, 2008). More recently, advances in the collection and processing of large scale geographical data like satellite imagery or airborne LiDAR allowed an empirical analysis of the riverscape theories developed since the 1980s. These more recent advances underpinned the theoretical views on rivers as complex, patchy and hierarchical systems (Fonstad and Andrew Marcus, 2010; Alber and Piégay, 2011; Carbonneau et al., 2012; Bertrand et al., 2013; Notebaert and Piégay, 2013; Michez et al., 2017).

*Riverscapes*

The idea of riverscapes arises from the debate about the spatial organization of rivers with its interaction of abiotic and biotic processes. Leopold and Marchand (1968) was among the first to use the term for describing the large scale description of a river corridor (Carbonneau et al., 2012). The modern era of the concept started in the early 2000s. In this period, riverine ecologists started to discover the spatial structure of river corridors (Fausch et al., 2002; Poole, 2002; Ward et al., 2002; Wiens, 2002).

> *[. . . ] we perceive a need to conceptualize rivers not as sampling points, lines, or gradients, but as spatially continuous longitudinal and lateral mosaics. As such, heterogeneity in the river landscape, or riverscape, becomes the focus of study (Fausch et al., 2002, p. 3, in Carbonneau et al., 2012)*

The idea of riverscapes has first been introduced by Leopold and Marchand (1968) who used the term for describing the large scale biophysical structure of a river corridor (Carbonneau et al., 2012). In the early 2000s, the concept has been re-discovered when Fausch et al. (2002) envisioned a continuous monitoring of habitats along rivers instead of spatially loose sampling plots. Later, this vision used to become reality when remote sensing and GIS techniques became available (Alber and Piégay, 2011; Carbonneau et al., 2012). In our days, ready-to-use GIS toolboxes have become available allowing an operational application for practitioners (Roux et al., 2015). Nevertheless, obtaining continuous information for river corridors or entire networks is still challenging and river science just recently started to work on larger spatial scales using modern methods of GIS and remote sensing (Piégay et al., 2019; Tomsett and Leyland, 2019). Despite the technological progress, so far the idea of riverscapes focuses on a spatial perspective. Of course, observing

changes over time in river corridors has a certain tradition (Carbonneau and Piégay, 2012). However, a focus has been on the use of individual time steps represented by single aerial images, UAV surveys or satellite scenes (e.g. Bertoldi et al. 2011; Henshaw et al. 2013; Räpple et al. 2017; Bizzi et al. 2019). Imagery time series representing a continuum in time have only rarely been used for assessing river corridors. Among the few examples is the work of Marchetti et al. (2016) and Marchetti et al. (2020) who used MODIS time series with a temporal resolution of 16 days to assess hydromorphological and vegetation dynamics of the Paraná River in Southern America.

## 1.3 Biogeomorphology as interdisciplinary view on river corridors

One relatively new scientific discipline emerging from the integrative view on rivers as complex ecosystems is bio- or ecogeomorphology[1]. This new discipline focuses on the interaction between geomorphological and ecological processes (Hupp and Osterkamp, 2013). River corridors with their interaction of hydrological, geomorphological and ecological processes are predestined to be analyzed from a biogeomorphological perspective (Gurnell, 2014; Wohl, 2017). Balke et al. (2014) even referred to rivers as *biogeomorphological ecosystems*. Corenblit et al. (2015a) formalized this idea and posed three central questions to fluvial biogeomorphology:

- Which are the effects of hydromorphology on vegetation?
- Which are the effects of vegetation on the abiotic environment?
- What are the feedbacks between geomorphological landforms and vegetation?

There is a rich body of literature documenting the impact of hydromorphology on vegetation (Naiman and Décamps, 1997; Tabacchi et al., 1998; Edwards et al., 1999; Bendix and Hupp, 2000; Amoros and Bornette, 2002; Karrenberg et al., 2002, 2003; Naiman et al., 2005; Bornette et al., 2008; Tockner et al., 2010). For instance, *Populus* and *Salix* have been identified as dominant genera within the zone regularly disturbed by floods. Rapid growth after seed establishment, the ability for vegetative as well as generative succession and resistance to flooding have been found as key criteria for the success of these genera in the highly disturbed fluvial environment (Karrenberg et al., 2002, 2003; Bornette et al., 2008; Politti et al., 2018).
There are two basic mechanisms of vegetation acting on hydromorphological processes. First, vegetation traps fine sediment via a local reduction of flow velocity (Corenblit et al., 2009b). Second, plant roots increase the cohesive forces within a sediment body reducing the erodibility (Simon and Collison, 2002; Karrenberg et al., 2003; Pollen-Bankhead and Simon, 2010). The effects of these basic mechanisms on river channel development have already been emphasized in early studies (Hupp and Osterkamp, 1996; Robertson and Augspurger, 1999). A special focus of research has been on fluvial islands where the accumulation of fine sediment within patches of vegetation on gravel bars has been documented as key factor for landform development (Edwards et al., 1999; Kollmann et al., 1999; Gurnell et al., 2001; Gurnell and Petts, 2006; Francis et al., 2009; Wintenberger et al., 2015). Within the study of fluvial islands, the analysis of large woody debris (LWD) has gained a certain attendance (Collins et al., 2012). LWD has the ability to modify the flow velocity and hydraulic forces on gravel bars during flood events modulating the initial

[1] In this thesis, I regard these two terms to be synonym and use *biogeomorphology*. Nevertheless, some authors point to slight differences in the foci of eco- and biogeomorphology (see e.g. Wheaton et al., 2011).

deposition of fine sediment (Piégay and Gurnell, 1997; Gurnell et al., 2005; Gurnell and Petts, 2006; Wohl, 2013; Wohl and Scott, 2017). In addition, the species of the *Salicaceae* family can regenerate vegetatively from LWD (Karrenberg et al., 2002). These two factors lead to a certain role of large woody debris in initial landform development (Francis et al., 2009; Collins et al., 2012; Wintenberger et al., 2015).
Older studies tended to focus on disciplinary aspects, i.e. the influence of hydromorphology on vegetation or vice versa. More recently, the study of feedback mechanisms between landform and vegetation development gained increasing interest. One aspect considering evolutionary time scales is the construction of ecological niches via the co-evolution of landforms and plant species (Odling-Smee et al., 2003; Corenblit et al., 2015b). However, currently there is only very few empirical evidence for this hypothesis (Corenblit et al., 2015a). More empirical work has been done on the concept of *ecosystem engineers* in the sense of Jones et al. (1994). Ecosystem engineers are species which modify their habitat for instance via the accumulation of fine sediment and enhance the habitat suitability also for other species. Areas where this habitat modification by means of the interaction of *ecosystem engineers* with their abiotic environment is particularly strong are considered as *biogeomorphic feedback windows* (Eichel et al., 2016; Hortobágyi et al., 2017). Building upon these ideas, (Corenblit et al., 2007) and Corenblit et al. (2009a) suggested a conceptual model of biogeomorphological succession. In this model, four succession stages are discriminated:

1. A geomorphological stage, where the hydraulic forces are too high to allow the establishment and growth of vegetation

2. A pioneer stage, where vegetation begins to germinate after the deposition of seeds or due to vegetative rejuvenation from large woody debris. To facilitate an initial establishment of vegetation, the disturbance needs to be reduced for a certain period. This is the case for instance if there is one year with a lower flood magnitude (*Window of opportunity* sensu Balke et al., 2014).

3. A biogeomorphological stage, in which the growth of pioneer vegetation leads to an increasing influence on the hydromorphological processes; vegetation is already sufficiently resistant against hydraulic forces and causes deposition of fine sediment and protects against erosion. In this stage, the interaction between hydromorphological and ecological processes is considered to be strongest.

4. An ecological stage where the vegetation is only influenced by hydromorphological disturbance during exceptional flood events. In this stage ecological factors like the concurrence for light and nutrients control the development of the vegetation structure.

In a synthesis of different conceptual models of fluvial biogeomorphology, Gurnell et al. (2016a) added permanently inundated areas as fifth succession stage. Figure 1.3 gives a graphical overview of all five biogeomorphological succession stages. These succession stages can represent on the one hand a temporal development. Sediment can be deposited and form a new gravel bar where initial vegetation can establish and develop further. On the other hand, the different succession stages can occur at the same time and form a specific spatial pattern representing different biogeomorphological process regimes (Corenblit et al., 2009a; Wintenberger et al., 2015; Gurnell et al., 2016a). The temporal as well as the spatial perspective have in common that the influence of hydromorphology decreases from the permanent inundation stage to the ecological stage. On

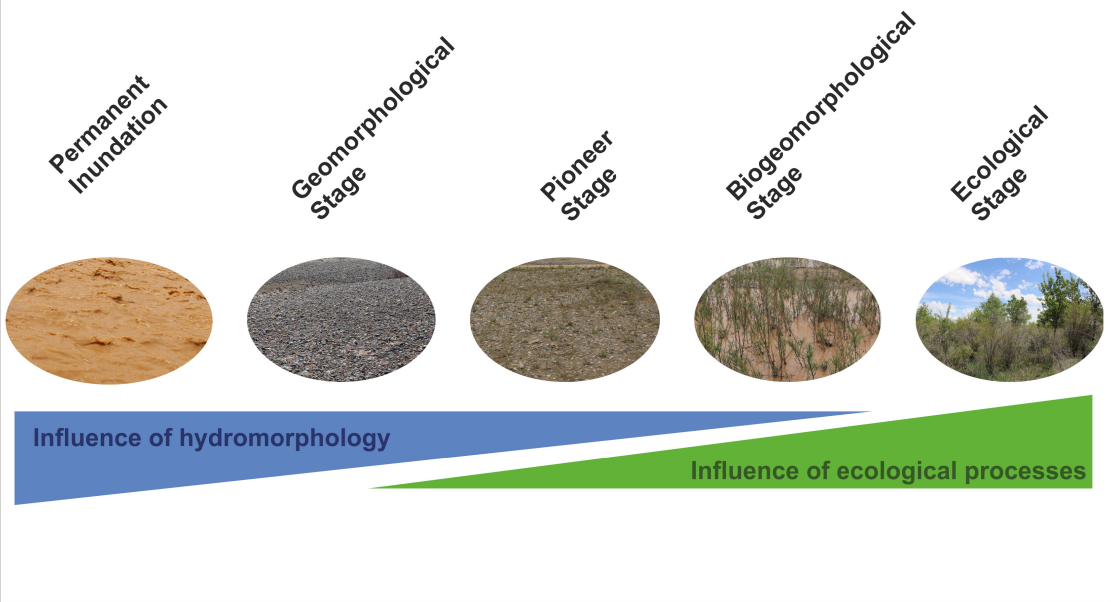


Figure 1.3: Conceptual model of biogeomorphological succession following Corenblit et al., 2007, 2009a and Gurnell et al., 2016a

the contrary, the influence of ecological processes increase after the initial establishment of pioneer vegetation from the pioneer to the ecological stage. From the spatial perspective, there is a lateral dimension where the ecological stage is considered to exist mainly at the river corridor margins while the permanent inundation stage and the geomorphological stage are expected to occur mainly close to the thalweg of the active channel. In addition, there is also a longitudinal dimension with differences of the relative contribution of each succession stage to the total area of the river corridor (Gurnell et al., 2016a).

A very recent development is the application of resilience theory to biogeomorphological systems (Stallins and Corenblit, 2018; Thoms et al., 2018). In a broad sense, resilience can be understood as the capacity of a (natural) system to absorb disturbance without undergoing a regime change (Gunderson et al., 2012). There are two crucial concepts linked to biogeomorphology within resilience theory, adaptive cycles and panarchies (Allen and Holling, 2010; Allen et al., 2014; Stallins and Corenblit, 2018). A single adaptive cycle consists of four stages (Fig. 1.4). In the first stage, available resources are exploited, for instance, seeds available in the seed bank of a gravel bar germinate. The conservation of resources is the second stage. An example is the establishment of individual plants after the seed germination. Third adaptive cycle stage is the release of resources. This release might be caused by the erosion of the gravel bar with the established saplings or the mortality of the plants due to a disturbance. In the fourth stage, the system is reorganized e.g. via the availability of fresh sediment after the erosion of a gravel bar (Allen and Holling, 2010; Allen et al., 2014; Stallins and Corenblit, 2018). The processes within the four stages of the adaptive cycle hold the system within a certain range of structures and functions (Stallins and Corenblit, 2018). At the point of reorganization, the adaptive cycle can repeat itself using the resources available from the release stage. Alternatively, it can adapt to new conditions (Stallins and Corenblit, 2018). Different adaptive cycles can co-exist over a range of temporal and spatial scales comprising a panarchy (Gunderson and Holling, 2002; Allen and Holling, 2010).

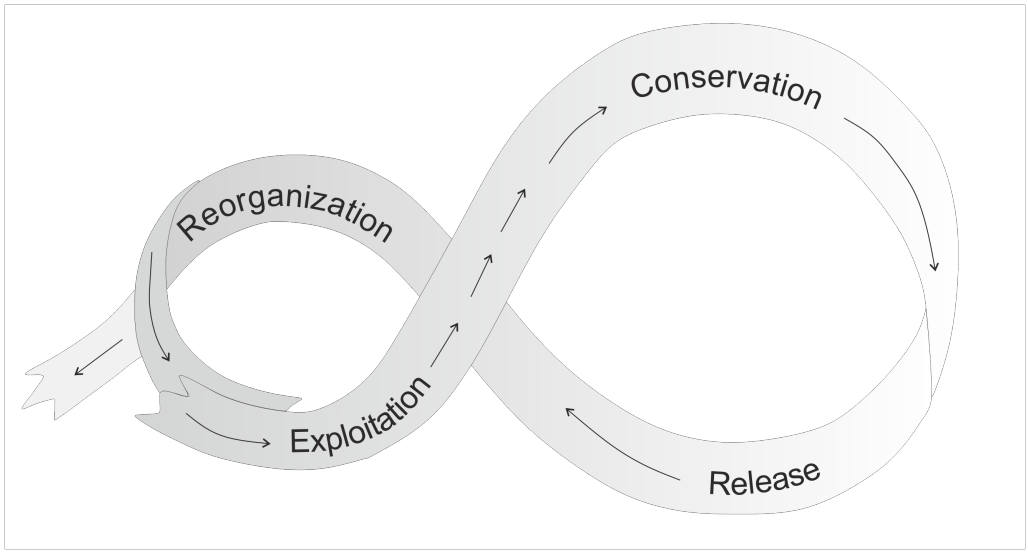


Figure 1.4: Concept of adaptive cycles (modified from Gunderson and Holling, 2002 and Stallins and Corenblit, 2018)

Different adaptive cycles can be linked in different ways. On the one hand, they can *revolt* and change to a new system state operating under a different adaptive cycle when the environmental conditions change. On the other hand, the system can also *remember* the former state and return to a regime comprising an adaptive cycle under which it was operating before (Gunderson et al., 2012; Allen et al., 2014).
Stallins and Corenblit (2018) adapted this theoretical approach to the biogeomorphological succession of coastal dunes. Figure 1.5 shows the conceptual model of panarchy they applied. It treats each succession stage as an individual adaptive cycle operating under a specific process regime. Within the geomorphological stage, the variability of the substrate and its reorganization during disturbance events are the characteristic cycle. In the pioneer stage, initial plant establishment and potential mortality due to disturbance governs the process regime. During the biogeomorphological stage, seasonal variations in disturbance form the adaptive cycle. Finally, in the ecological stage, longterm disturbance governs the adaptive cycle (Stallins and Corenblit, 2018). The different adaptive cycles respectively the different biogeomorphological succession stages are linked via *revolt* and *remember* mechanisms. This means that changing environmental conditions can force an adaptive cycle to switch to a new state (e.g. from the geomorphological to the pioneer stage if there are suitable conditions). On the contrary, an adaptive cycle can also return to a previous state (e.g. from the pioneer to the geomorphological stage if all seedlings are removed during a flood event). The adaptive cycle of the geomorphological stage is considered to operate on the smallest spatio-temporal scales while the cycle of the ecological stage is expected to represent the largest spatial and temporal scales.
This model is in fact an extension of the concept of biogeomorphological succession suggested by Corenblit et al. (2007, 2009a). Thus, the application of resilience theory treating biogeomorphological succession as a set of adaptive cycles linked in a panarchy is also promising for the fluvial environment. However, while Stallins and Corenblit (2018) suggested quantitative indicators for the analysis of coastal dunes, there is to my knowledge no empirical work done yet to apply resilience theory to the biogeomorphology of riverine ecosystems.

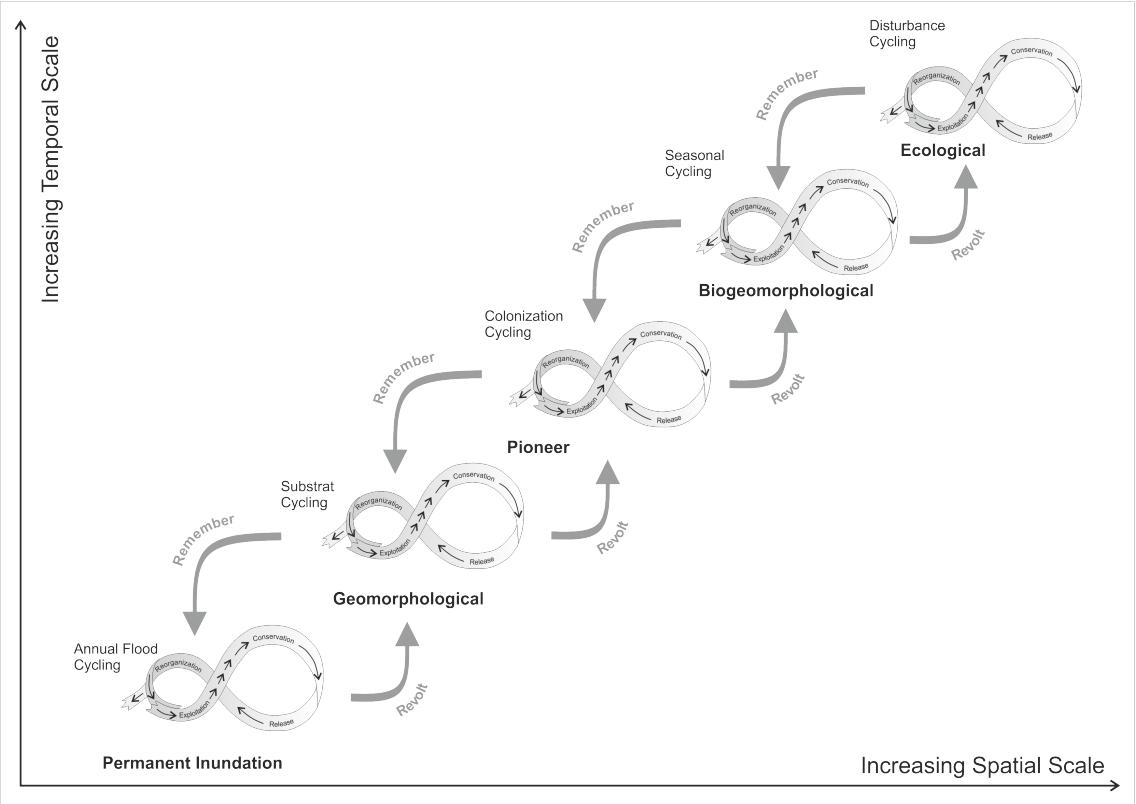


Figure 1.5: Adaptive cycles of a panarchy of a biogeomorphological system (modified from Stallins and Corenblit, 2018)

## 1.4 Remote sensing for the large scale assessment of river corridors

Most widely used frameworks for river corridor characterization such as the *Riverstyles* framework (Brierley and Fryirs, 2005), the *fluvial audit* (Sear et al., 2010) or the *Morphological Quality Index* (Rinaldi et al., 2013) rely on field based measurements and expert opinion. Nevertheless, all of these conceptual frameworks acknowledge the multi-scale nested structure of river systems and the need for large scale observations on the river corridor to the catchment scale. In addition, the conceptual frameworks see the temporal aspect of river systems and highlight the relevance of past trajectories to analyze the response of the system to disturbance. In their seminal paper, Fausch et al. (2002) argued for the need to move beyond spatially and temporally loose field sampling for a management relevant analysis of rivers and envisioned the development of *riverscapes* as spatially continuous representation of river characteristics. Here, remote sensing can play a key role as airborne and especially spaceborne imagery and DEMs provide spatially continuous data over large areas (Bizzi et al., 2016; Gilvear et al., 2016b). Thus, river scientists have a long time used remotely sensed data for their work. Before satellite imagery became more widely available in the 1970s, aerial photography along with stereo-photogrammetry has been the method of choice for studying rivers (Gilvear and Bryant, 2016). As airborne imagery is captured routinely in many countries at least in Europe and other western countries (Bizzi et al., 2016), such data is a valuable and cost-efficient data source and is still widely used in fluvial geomorphology (e.g. Lane et al.,

2010; Alber and Piégay, 2017; Bakker and Lane, 2017). A great advance for remote sensing of rivers has been the availability of LIDAR (Light Detection and Ranging) based on laser data. This method allows the derivation of highly precise digital elevation data as well as the delineation of vegetation structure from 3D point clouds (Bailly et al., 2012). DEMs derived from airborne LIDAR have become the standard for all terrain related purposes in river studies such as flood risk assessment (Carbonneau and Piégay, 2012). But LIDAR has also been used for analysis beyond DEM generation such as the habitat characterization of entire river networks (e.g. Demarchi et al., 2016; Michez et al., 2017).
Since the early 2000s, higher resolution satellite imagery such as Ikonos, Quickbird or WorldView became available having a sub-meter spatial resolution (Gilvear et al., 2016b). With this imagery it became possible to map narrow rivers as well as smaller instream features with a sufficient accuracy. Scholars used this new opportunities to develop remote sensing methods for habitat mapping from remotely sensed imagery (Marcus et al., 2003; Legleiter et al., 2004; Legleiter and Goodchild, 2005). New methods have been developed to assess different riverscape parameters from space, among them water depth (Legleiter et al., 2009; Legleiter and Roberts, 2009), the grain-size characteristics of the channel (Carbonneau et al., 2004; Black et al., 2014; Legleiter et al., 2016) or even flow velocity (Hugue et al., 2016). These technological advances allowed a spatially continuous view on rivers giving the opportunity to test theoretical frameworks such as the downstream hydraulic geometry in geomorphology or the river continuum concept in lotic ecology (Marcus and Fonstad, 2008; Fonstad and Andrew Marcus, 2010; Carbonneau et al., 2012). For this issue, discontinuities have to be detected within the riverscape. As soon as the river corridor is split into quasi-continuous units (e.g. segments of 100 m), statistical algorithms can be applied for their detection (Alber and Piégay, 2011). Different methods have been proposed for this issue like spatially constrained clustering (Brenden et al., 2008), breakpoint tests originally developed for time series analysis (Leviandier et al., 2012; Parker et al., 2012; Martínez-Fernández et al., 2016) or neural networks along with unsupervised clustering (Bizzi and Lerner, 2012; Schmitt et al., 2014). Meanwhile such large scale remote sensing studies have moved from a purely scientific to a more applied context. Within the European context, for instance, the riparian ecotones have been delineated for the entire European Union using a combination of existing datasets, a digital elevation model and multispectral satellite imagery (Clerici et al., 2011, 2013; Weissteiner et al., 2016).
Within a biogeomorphological context, remote sensing has been applied as well. Bertoldi et al. (2011) used annual ASTER imagery for detecting vegetation gain and loss along a 21 km long reach of the Tagliamento River in Northern Italy. The NDVI composites of this 15 m resolution sensor has been found useful to detect changes in vegetation cover in response to flood events. Later, Henshaw et al. (2013) transferred this approach to 30 m resolution LANDSAT TM imagery as this dataset has the longer archival record. They found LANDSAT a rich source of information for the assessment of the Tagliamento River even if the spatial resolution limited the potential application. More recently, Marchetti et al. (2016) used monthly time series of the MODIS sensor with 250 m spatial resolution to assess biogeomorphological dynamics of the Paraná River in Peru, the second-largest river system in Southern America after the Amazon. They explicitly used the phenological pattern of the NDVI to find clusters with specific spatio-temporal characteristics. However, these scholars did not link their findings explicitly to biogeomorphological or eco-hydrological theory. On a smaller spatial scale, photogrammetric analysis of aerial photographies or UAV imagery have been used to gain information about the reciprocal interaction of vegetation and landform development (Hortobagyi et al., 2016; Vautier et al., 2016; Räpple et al., 2017). On a larger scale, Thapa et al. (2016) used the classification of NDVI time series derived from LANDSAT imagery to analyze adaptive cycles of floodplain vegetation within resilience the-

ory.
All these methods have in common that they do not treat temporal dynamics at all or treat them on an annual basis using traditional change detection methods. In remote sensing science, a recent trend is the use of the full time series of the imagery archive e.g. of Landsat or more recently the European Sentinel mission to monitor the dynamics of terrestrial ecosytems and assess potential disturbances (Gómez et al., 2016). This development has been stimulated by the availability of open access satellite imagery, particularly by the opening of the Landsat archive in 2008 (Wulder et al., 2012) and the European Sentinel missions. In fact this led to a new era of 'Big Data' in the study of earth surface dynamics from space using dense time series and statistical analysis techniques and machine learning algorithms (Wulder and Coops, 2014; Gómez et al., 2016; Comber and Wulder, 2019). A key focus of this recent trend is the development of methods for the disturbance detection of (tropical) forest ecosystems (Verbesselt et al., 2010, 2012; DeVries et al., 2015; Verbesselt et al., 2016) or the detection of tipping points in large scale ecosystem development (Forkel et al., 2013). In addition, dense time series of satellite data have also been used for the detection and monitoring of flood events (Pulvirenti et al., 2011; Schlaffer et al., 2015) and the assessment of temporal dynamics of evapotranspiration (McCabe et al., 2017). However, to my knowledge studies using dense time series of satellite imagery have so far not been used for analyzing biogeomorphological dynamics in river corridors.

## 1.5 Research questions and outline of the thesis

Overall aim of this thesis is to provide information of the Naryn River corridor to guide further research on and conservation of this river system. I take an interdisciplinary perspective addressing all interactions of figure 1.2. As the Naryn River is still in a widely natural condition, it is possible to at least partially neglect contemporary human influence and use a biogeomorphological approach for investigating the relationship between hydrology, geomorphology and ecology. A focus is on the development of remote sensing based methods for analyzing biogeomorphological processes. This thesis focuses on a large scale and treats the scale from reach to the entire catchment with a focus on the river corridor and river segment (see table 1.1 for a definition of the scales). More specifically, I address the following research questions:

- How is the basic structure and functioning of the Naryn River system and how can open source remote sensing contribute to an assessment?
- How does the natural flow regime of the Naryn River look like and is it affected by global climate change?
- What is the extent and spatial distribution of the riparian zone and the riparian vegetation along the Naryn River?
- How can the biogeomorphological dynamics be assessed using remote sensing data?
- What is the relevance of the Naryn River and the riparian ecosystems for local people?
- What are the management implications of the findings of this thesis?

In chapter 2, I give a brief overview over the regional setting of the study area to give set the background for analysis. Besides climate, geology, tectonics and biogeography a special interest is on the post-socialist development of Kyrgyzstan as this is relevant to understand contemporary

environmental issues. In chapter 3, I go deeper into the aspect of ecosystem services of the Naryn floodplain forests. An analysis of the hydrology is presented in chapter 4. Beside general trend analysis for climate change assessment, I investigate the natural flow regime and assess the recurrence intervals of flood events. In chapter 5, the four field sites used for calibration and validation of the remote sensing analysis are introduced. This chapter gives a field based overview over the structure of the riparian areas of the Naryn River in order to facilitate the interpretation of the remote sensing results. In chapter 6, I derive the structure of the Naryn River corridor using a combination of terrain analysis, visual interpretation of high resolution of virtual globe imagery and multispectral remote sensing. This remote sensing derived structure gives a static view of the river corridor. In chapter 7, I use time series of Landsat and Sentinel-2 for assessing the dynamic interaction of hydrology, geomorphology and ecology from a remote sensing perspective. Each of these chapters except the regional overview is organized in an article-like form with a brief introduction to the chapter, methods, results and a brief, specific discussion. The various aspects from the different chapters are brought together to a synthesis in the discussion in chapter 8. A final conclusion is given in chapter 9.

# 2 Regional overview

## 2.1 Geographical setting

The subject of this thesis is the catchment of the upper Naryn River located in Central Asia (see Fig. 2.1). The Naryn River originates in Kyrgyzstan in the Tian Shan mountains and flows westwards. Soon after crossing the Kyrgyz-Uzbek border, it merges with the Kara Darya and forms the Syr Darya, where the Naryn contributes approximately 75 % of the discharge (Bernauer and Siegfried, 2012). Due to the arid climate, the Syr Darya is the main water supplier for the Ferghana Valley at the Kyrgyz-Kazakh border (where 50% of the Uzbek population lives) as well as for the downstream area in Kazakhstan (Bernauer and Siegfried, 2012; Sorg et al., 2014). In addition

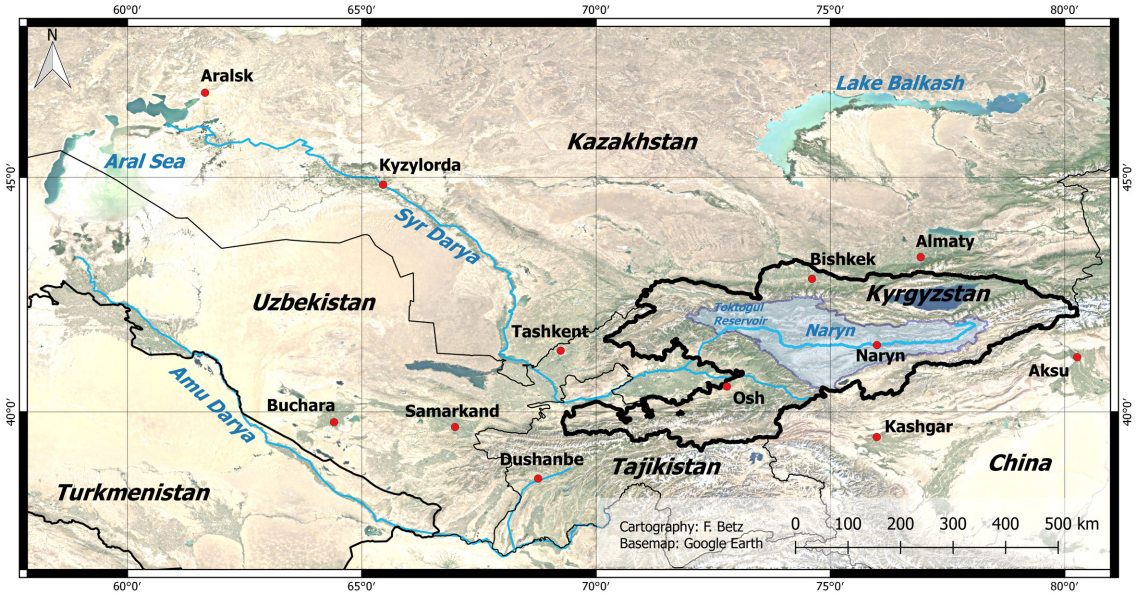


Figure 2.1: Regional overview of the study area; the light blue area indicates the catchment of the Naryn River under analysis in this thesis

to its relevance for irrigation water supply, the Syr Darya delivers a significant amount of water to the Aral Sea, an endhoreic lake well known for the environmental disaster happening after its dessication following intensive water withdrawal for agricultural irrigation (Micklin, 1988; Giese et al., 1998). Today, the Aral Sea split into two parts, a southern part forming the terminal lake of the Amu Darya ('Big Aral Sea') and a northern part forming the terminal lake of the Syr Darya ('Small Aral Sea'). The 'Big Aral Sea' still undergoes a dessication while the 'Small Aral Sea' is subject of restoration measures of the Kazakh government ending the declining trend of the water level (Micklin, 2016).

Approximately 90% of the discharge of the Syr Darya is regulated, the largest hydraulic construction is the Toktogul dam with its reservoir having a total volume of $19.5 \times 10^6$ km$^3$ (Antipova

et al., 2002; Bernauer and Siegfried, 2012). This reservoir has been established in the 1970s for collecting the water from the Naryn River for irrigation of the agricultural land in Uzbekistan and Kazakhstan. Upstream from the Kambar-Ata Dam at the inflow of the Toktogul reservoir, the catchment is still in a natural state without dams or embankments along the Naryn River (see Fig. 2.1 for an overview). This natural part of the Naryn (respectively the Syr Darya) catchment is the subject of this thesis, a detailed overview is given in figure 2.2. This catchment has an area of

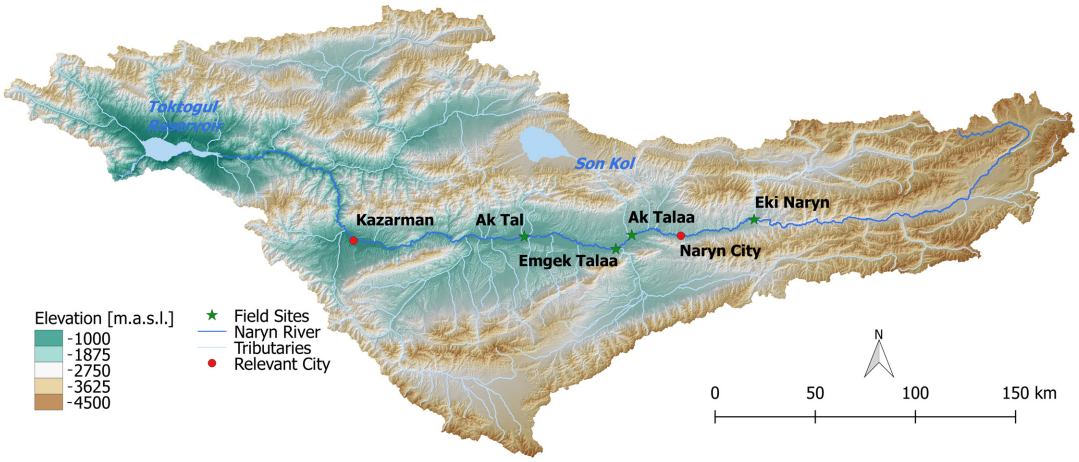


Figure 2.2: Overview of the Naryn catchment

52,130 km$^2$, the elevation ranges from 868 m at the Toktogul reservoir to 5133 m in the uppermost part in the Tian Shan mountains (values derived from the SRTM-1 DEM). The Naryn River itself originates in the Tian Shan mountains. On the first 277 km, the river is still named 'Big Naryn'. After the confluence with the 'Small Naryn' at Eki Naryn (Kyrgyz for 'Two Naryn'), it is officially termed 'Naryn' (see Fig. 2.2). From here, the river flows westwards across a wide, tectonically formed basin. Downstream from Kazarman, the Naryn River turns north and crosses a gorge before entering the Toktogul reservoir. The focus of this thesis is on the section of the Naryn River between Eki Naryn at an elevation of 2265 m and Kazarman at an elevation of 1260 m. In this section, the Naryn River is characterized by active braided river reaches where certain biogeomorphological dynamics can be expected for the remote sensing imagery analysis. In this river section, also the four field sites are located. In the following sections, I give a more detailed overview of the Naryn catchment with its physical geographical as well as anthropogenic characteristics.

## 2.2 Climate and hydrology

The climate in the Naryn catchment is highly continental with hot summers and cold winters. At the climate station Naryn City, average summer temperatures up to 25 °C occur, while winter averages are –25 °C. The precipitation is in general low with a clear rainy season in May and June. Annual average precipitation is 300 mm (see Fig. 2.3). One consequence of the low precipitation is the dominance of snow and glacier melt in the runoff generation. The actual glaciation of the Naryn catchment is approximately 2% contributing to about 10% of the total runoff of the Naryn River (Aizen et al., 1995; Kriegel et al., 2013). Due to this characteristics, the discharge regime

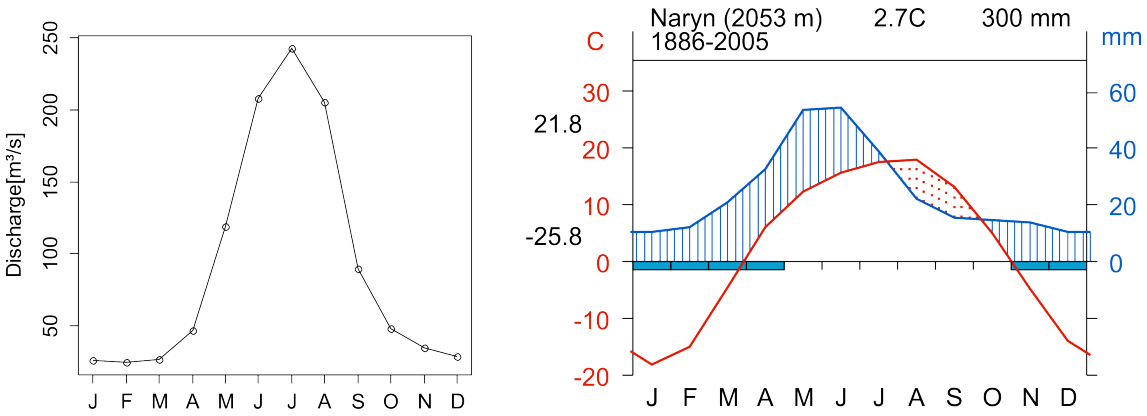


Figure 2.3: Hydrograph (l) and climate diagram (r) of Naryn City; data from http://neespi.sr.unh.edu, last access: 2020-12-28

has a clearly glacial behavior with one single peak in July (Fig. 2.3). Mean annual discharge at the station Naryn City is 92.12 $m^3/s$. At the inflow to the Toktogul reservoir at the station Uchterek, the average annual discharge is increasing to 323.33 $m^3/s$.

The hydrology undergoes substantial changes caused by the global climatic change. Increasing temperature leads to enhanced glacier melt causing an increase in the summer discharge (Hagg et al., 2013; Kriegel et al., 2013). In a short term perspective, this leads to an increase in summer discharge until a tipping point is reached where the water storage of the glaciers has become too small to sustain the runoff. From this point, the discharge will decrease until the glacier completely disappeared (Sorg et al., 2014). For the Naryn catchment, runoff from glacier melt is predicted to increase at least until 2040 (Gan et al., 2015). However, the complex effects of terrain as well as changes of temperature and precipitation lead to a more complex picture regarding the hydro-climatic changes within the Naryn catchment. A comprehensive, data-driven analysis of the hydrology and hydro-climatic changes is given in chapter 4.

## 2.3 Geology [1]

While data about the geomorphology of the Naryn River is still widely absent, publications exist about the larger scale geological structure of the region. From a tectonic point of view, the Tian Shan mountains belongs to the Central Asian Orogenic Belt and has been formed by the collision of the Eurasian Plate and the Indian Plate (De Grave et al., 2011). More specifically, the Kyrgyz Tian Shan is located on the margin of two microplates, the Kazakh Plate in the northwest and the Tarim microplate in the southeast (Shahgedanova, 2002; Thompson et al., 2002; Tibaldi et al., 2015). One consequence of this tectonic situation is a large number of faults crossing the Tian shan (see Fig. 2.5). In addition it causes an interplay of mountain ranges striking in an east-west direction and intramontane basins. The geology of the mountain ranges is in generally characterized by the Hercynides and Caledonides of the Tian Shan while the basins are characterized have a Cenozoic origin (De Grave et al. 2011, see Fig. 2.4). One of these basins is the Naryn Basin in the central part of the Naryn catchment (indicated with the yellow rectangle in Fig. 2.5). The course

[1] The geological overview presented here is based on a literature review conducted by Magdalena Lauermann within her master thesis. For more details, readers can refer to Lauermann (2016).

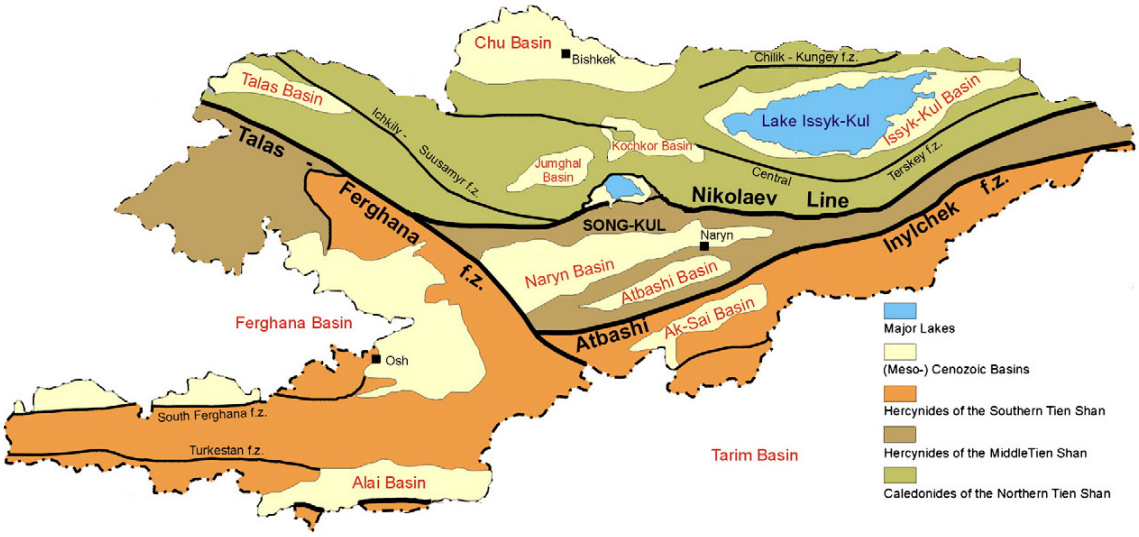


Figure 2.4: Overview of the large scale geological units of Kyrgyzstan (modified from De Grave et al., 2011)

of the Naryn River developed in association with two faults, the Kadjerty fault and the Central Naryn fault (Thompson et al., 2002, see Fig. 2.5).

Recent GPS based measurements have shown that the Tian Shan experiences an annual compression in north-south direction of approximately 13 ± 2 mm (Abdrakhmatov et al., 1996; Burtman, 2012) and an annual uplift of 1.0 ± 0.3 mm (Avouac et al., 1993). These active tectonics lead to several large landslides within the catchment. For the interpretation of the contemporary river corridor structure, the Beshkiol landslide is of the greatest relevance (Lauermann, 2016). It happened downstream from Ak Tal (Fig. 2.5) and has a total volume of approximately 10 $km^3$ filling the entire Naryn Valley on a length of 7 km. The river was not able to erode the landslide deposits and a 70 km long lake formed behind the Beshkiol dam existing for about 3000 years through the Holocene (Korup et al., 2006). The Naryn River finally turned north and cut a new valley instead of eroding the landslide deposits and using its original course. This cross valley is still visible today in form of a gorge between Ak Tal and Kazarman. Relicts of the lake morphology are also abundant. The terraces around Ak Tal are interpreted as former lake shores (Korup et al., 2006; Strom and Korup, 2006). Lauermann (2016) reconstructed the lake based on relief analysis and visual interpretation of a hillshade, the result is shown in figure 2.5.
At the transition from the Pleistocene to the Holocene, terraces have developed along many rivers in the Tian Shan (Thompson et al., 2002; Burgette et al., 2017). These terraces are important features of the Naryn catchment and exist along a relevant length within the river corridor analyzed in this thesis (Thompson et al., 2002; Burgette et al., 2017, see Fig. 2.6). A typical stratigraphy of these terraces has a several meter thick, slightly cemented layer of silty/clayey sediments followed by a layer of fluvial gravels. On top of the gravel layer, a silty/loamy layer is found, which is interpreted as loess deposits or paleo-floodplain deposits (Thompson et al., 2002). Where abundant, these terraces form the ultimate boundary of the recent river corridor and are relevant when interpreting the confinement of the Naryn River (Betz et al., 2018).

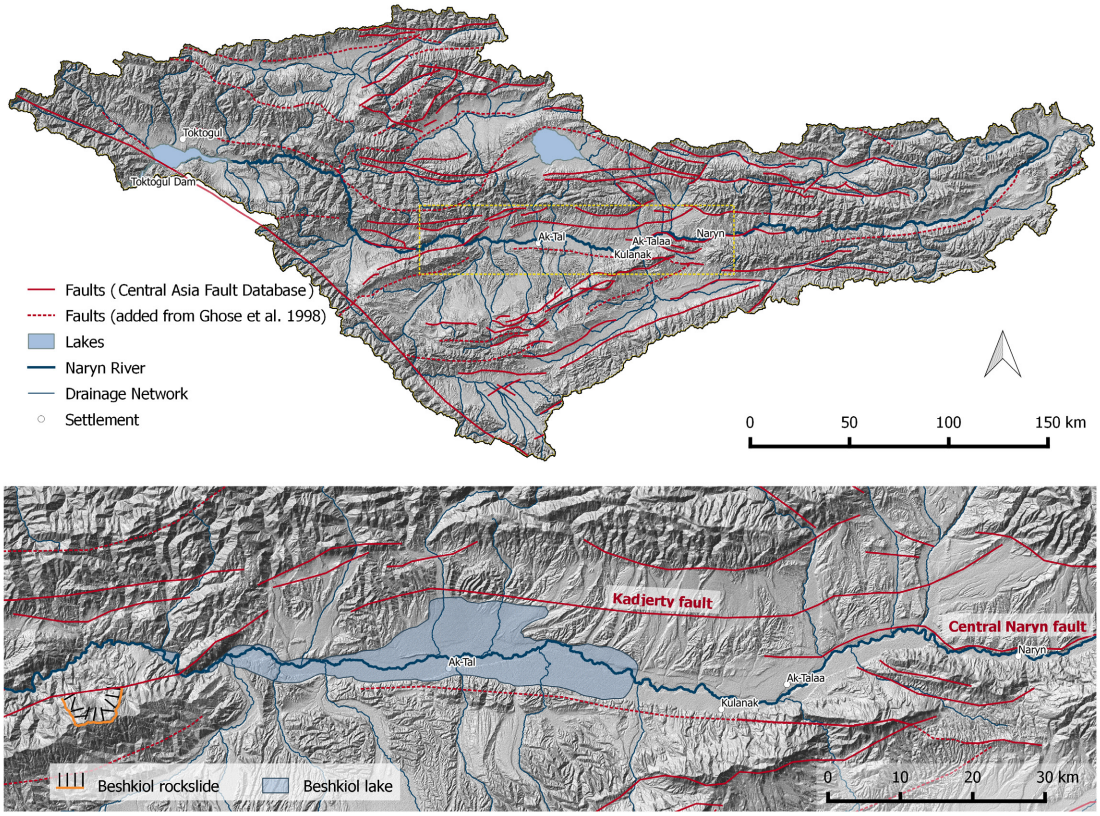


Figure 2.5: Faults in the Naryn catchment (source: Lauermann, 2016, 5; data from Mohadjer et al., 2016 and Ghose et al., 1998)

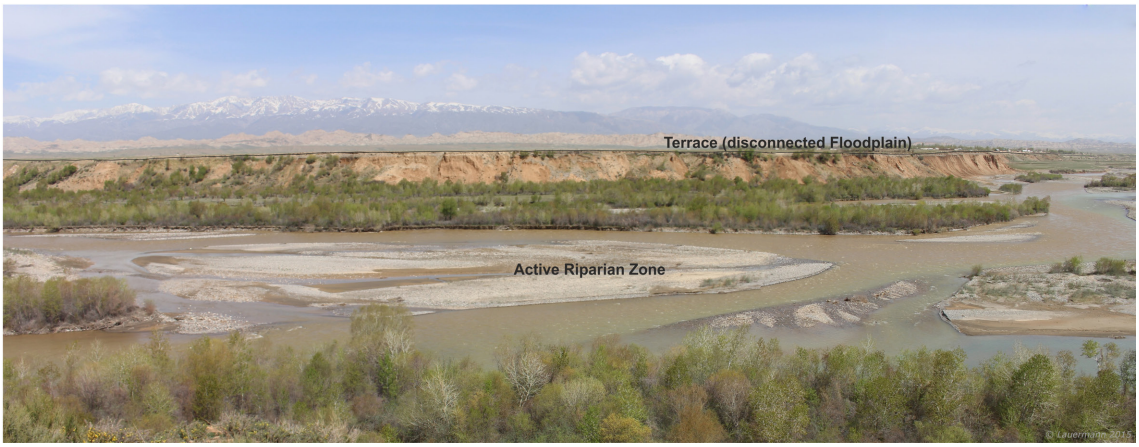


Figure 2.6: Terrace near the village of Emgek Talaa; the terrace is the boundary of the active riparian zone (*Photo: Magdalena Lauermann*)

## 2.4 Biogeography

Like Europe, Central Asia belongs to the Holarctic floristic kingdom covering almost the entire northern hemisphere (Schultz, 2005). According to Grubov (2010), the vegetation in the Naryn basin belongs to the Junggar-Turanian province, sub-province Tian Shan. However, the Tian Shan mountain range is at the interface of three floristic provinces, thus it is likely that species from different floristic provinces occur in the Tian Shan. Detailed international publications on the biogeography of Central Asia are scarce. The standard book regarding the botany of Central Asia is the *'Rastenija Central'noj Azii'* edited by Valerij Ivanovic Grubov (Hilbig and Jäger, 2010). However, as Central Asia is within the same floristic kingdom as Europe, taxa are similar what allows an evaluation at least of the genus based on European literature. More information on the spatial pattern of the ecosystems of Kyrgyzstan is available in Russian language based on research of the Kyrgyz Academy of Science (personal communication with Magdalena Lauermann). Here, an up-to-date review in the international literature would be highly valuable for the international research community. However, without sound knowledge of Russian, this information is not accessible for me, thus such review is beyond the scope of this section here.
Within the mountainous terrain of Kyrgyzstan, roughly three altitudinal belts can be discriminated (von Maydell, 1983; Scheuber et al., 2000). In an elevation below 1500 m, semi-deserts and steppes occur, between 1500 m and 4000 m, open forests and wildfruit forests dominate the landscape. Finally, above 4000 m, alpine meadows are the characteristic vegetation type. Forest cover is in general low in Kyrgyzstan and is in the range of 3.3-5.2% depending on the reference (von Maydell, 1983; Scheuber et al., 2000; Fisher et al., 2004). Following Fisher et al. (2004), four major forest types can be discriminated:

- Spruce forests with the dominating species *Picea schrenkiana* occur in elevations between 1700 m and 3000 m and are the dominating mountain forest type in the Tian Shan.
- Walnut-fruit forests occur at the northern and north-eastern slope of the Ferghana valley. This forest type has been cultivated already in ancient times and occurs in an elevation between 800 m and 2400 m. It is a Kyrgyz particularity and is regarded to have a high relevance due to its biodiversity and importance for local people (Schmidt, 2013).
- Juniper forests which occur in arid environments or in high mountain environments up to 3500 m.
- Floodplain forests occur along the rivers Chui, Talas and Naryn as well along their larger tributaries.

The latter forest type contributes to 5.2% of the total forest cover in Kyrgyzstan (Zholdosheva, 2010). While general publications mention floodplain forests as one of the forest types and attribute a high biodiversity to them, detailed studies about the structure of riparian ecosystems do not exist to my knowledge. A more detailed description of the floodplain ecosystems along the Naryn River is given in chapter 5.

## 2.5 An overview of the socio-economic structure along the Naryn River

The Naryn catchment is only sparsely populated with an average population density of 6 people/km$^2$ (CIESIN, 2005). Only one major city exists: Naryn City having a population of approximately

34,000 people (pers. communication, E. Baibagyshov, Fig. 2.7). Beside Naryn City a multitude of villages exist along the Naryn River and in the adjacent valleys. Despite the low population density, a consideration of the human dimension is relevant for a comprehensive understanding of the Naryn River corridor. History, socio-economy and politics influence the way an ecosystem is perceived, utilized and managed (Schmidt, 2017). In the Naryn region, the consideration of historical changes from the early modern era until the transformations of after the breakdown of the Soviet Union until the establishment of the new Silk Road in the 21st century is necessary to understand the current situation.

Figure 2.7: Naryn City, the only major city within the Naryn catchment

*A brief look into history*

Until the early modern era, the people in the Naryn region have been nomads and lived in subsistence from their livestock. The floodplains of the Naryn River have served as location for the winter camps and smaller permanent settlements (Anderson, 1999; Schmidt, 2013). Things began to change when the Russians began to enlarge their empire towards Central Asia in the 18th and 19th century. Until the 1870s, they conquered the area covering today's Kyrgyzstan, in 1868, they founded Naryn City as military base and built a bridge across the Naryn River (Schuyler, 1876 cited in Schmidt, 2013). During the Russian government, farmers from other parts of Russia settled down in the Kyrgyz territory and the rights of the nomads to access their pastures has been curtailed by new laws leading to a first period of sedentation in the region (Anderson, 1999). In 1917, the Russian revolution terminated the Czardom and the Soviet Union began to dominate the development of Central Asia. This was the beginning of a far-reaching development influencing the region until today. To support the development of socialism, new nations have been founded in Central Asia. The Kyrgyz Republic was first established in 1924 as Autonomous Kyrgyz Territory, then in 1926 it was included in the USSR as Kyrgyz Autonomous Socialist Soviet Republic and finally became full-fledged member of the USSR in 1936 (Schmidt, 2007). Until beginning of the 1940s, the sedentation of the nomads was 98% completed and agricultural production and livestock breeding have been collectivized (Anderson, 1999). During this time, a certain degree of industry was established mainly in northern Kyrgyzstan. However, agriculture and livestock production remained the focus of the Kyrgyz economy (Anderson, 1999; Steimann, 2011). During this time, also the potential for the construction of dams and reservoirs was discovered (see also section 2.6). With the perestroika in the 1980s, times began zu change and first initiatives for privatization and political liberalization started. As the Soviet Union was formally terminated in 1991, Kyrgyzstan became an independent state – for the first time in the history of this country (Anderson, 1999; Schmidt, 2007).

The independence had far-reaching consequences. The economy decreased dramatically leading to high unemployment rates and poverty (Anderson, 1999; Schmidt, 2013). An extensive emigration was the consequence. Between 1989 and 1999 approximately 688,000 people left Kyrgyzstan. Most of them were Russians who have come to Central Asia from the Russian part of the USSR (Schmidt and Sagynbekova, 2008). This emigration did not only modify the ethnic structure of the country but caused also a serious 'brain drain' as many well educated citizens left Kyrgyzstan (Schmidt and Sagynbekova, 2008). Another indicator for the enormous effects of the independence is the number of livestock. Figure 2.8 shows its development from 1990 until today. After

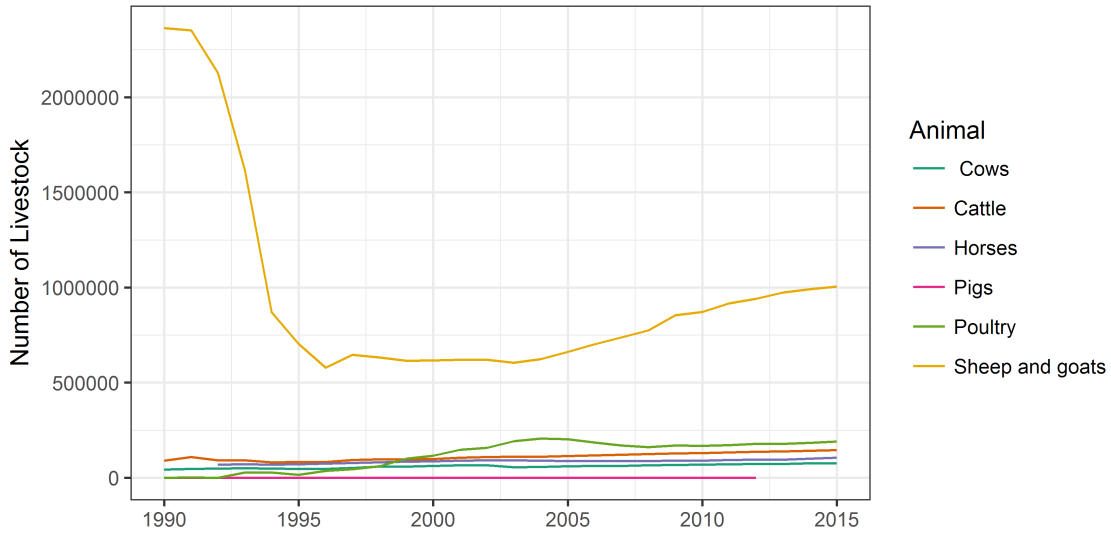


Figure 2.8: Livestock development in the Naryn oblast since 1990 (data from the National Statistical Committee of the Kyrgyz Republic, www.stat.kg, last access: 2020-12-28)

the breakdown of the collective production, a shortage in fodder but also in agrarian production in general led to mass slaughtering of the flocks (Farrington, 2005; Steimann, 2011). As reaction, the government started reforms and began with a privatization of the agricultural and pastoral land as well as with the livestocks. Despite some success of these measures visible in the slightly increasing trend in livestock, the level of the Soviet era was never reached again.
Also the political situation changed over time. After the official independence in August 1991, Kyrgyzstan became officially a representative democracy. Askar Akajew, who was already president of the SSR Kyrgyzstan since 1990 became the first president of the independent country (Anderson, 1999). As the leadership of Akajew became more and more dictatorial over the 1990s, societal tensions increased. These tensions culminated in the 'tulip revolution' in 2005 during which president Akajew has been ousted. New president became Kurmanbek Bakijew, who promised a more democratic leadership to the Kyrgyz people. But the high level of corruption around the president's family and the increasing living expenses lead again to social tensions (Cheterian, 2010). In April 2010, the tensions lead to violent demonstrations during which president Bakijew left the country towards Kazakhstan. A referendum in June 2010 lead to the formation of a interim government under the leadership of Rosa Otunbajewa (Cheterian, 2010). In the following elections in 2011, Almazbek Atambaev, the prime minister during the government Otunbaejewa, was elected as president (Deutsches Auswaertiges Amt, 2016). Parliament elections in October 2015

confirmed the governance of the social democratic party already being the strongest party in the 2011 elections. In the presidential elections in October 2017, Almazbek Atambaev followed the constitution and did not run for re-election (Deutsches Auswaertiges Amt, 2016). These successful elections might be interpreted as sign of beginning stability in Kyrgyz politics. However, the political future of Kyrgyzstan is still associated with manifold uncertainties.

*Societal challenges in contemporary Kyrgyzstan*

Today's society is still undergoing the fundamental transformations happening after the breakdown of the Soviet Union in 1991 (see Steimann 2011 or Schmidt 2013 for a detailed discussion). Despite manifold economic reformations having a certain success, the rural areas of Kyrgyzstan still suffer from the economic decline of the national economy happening after the independence (Schmidt, 2001; Schoch et al., 2010; Steimann, 2011). Before the Kyrgyz independence, the collective farms (kolkhozes) have been responsible for maintaining most rural infrastructure like the drinking water supply. After the liquidation of the kolkhozes following the Kyrgyz independence, the government was not able to conduct the maintenance and delegated it to the community level (Rost et al., 2015). However, the communities do not have the required know-how and financial resources to fulfill this duty (Steimann, 2011). Thus, it is not likely that the living standard of the rural population will increase significantly in a short term perspective. For instance, most households still get their drinking water from public standpipes. Furthermore, due to the lack of canalization, latrines in the backyard are still the standard sanitary in almost all households (Rost et al., 2015). Figure 2.9 shows typical scenes of contemporary living conditions in the villages along the Naryn River.

Like already during Soviet times, livestock breeding is still the major agricultural activity, just today smallholders and not collective farms are the main owners. In the villages along the Naryn River, people heard horses, cattle and sheep for subsistence but also as financial investment. If possible, the families buy livestock and sell it on local or regional markets in case there is a need for cash (Shamsiev, 2007; Schoch et al., 2010; Mestre, 2017). Thus, the slightly increasing livestock numbers in the Naryn oblast (Fig. 2.8) can be seen as an indicator of positive economic development. But of course, the increasing number of livestock causes also pressure on the pastures. Thus, pasture management and pasture degradation are ongoing issues in the Naryn Oblast (Hoppe et al., 2016). Another issue related to the breakdown of the Soviet Union is the direct dependence on nearby wood for heating and cooking as the centralized distribution of coal ended with the Soviet era and market price coal is too expensive for most families. Even though people collect dung and use it in a dried form as heating material, they still depend on the wood. The consequence is a high logging activity in the forests (Schmidt, 2013). Even if woodcutting recently became less severe due to a slightly increasing wealth of the people, logging is still a relevant issue also in the floodplain forests along the Naryn River.

Against this background, it is dubious if the people living in rural Kyrgyzstan can benefit directly from an ongoing economic development in the country (Dubashov et al., 2017). Up to date, no change of the living conditions is visible in the villages along the Naryn River. Citizens cannot move beyond the subsistence farming and livestock breeding. The only alternative is labor migration to Bishkek or abroad (Schmidt and Sagynbekova, 2008). In addition, interviews with local authorities support the point of view that the communities still lack in the financial resources even for basic infrastructure investments (like e.g. in the standpipes for drinking water supply). This lack in financial resources will have the consequence that peoples' dependence on nearby natural resources is likely to persist at least in near future (see chapter 3). Investments in alternative


Figure 2.9: Living conditions in rural Kyrgyzstan; a: Typical street scene in Ak Tal; b: Dried dung for heating in wintertime; c: Outhouse in the backyard is still the standard due to the lack of canalization; d: water supply from standpipe *(Photo d provided by Bernd Cyffka)*

technology like solar power plants, short rotation plantations or small hydropower only become possible solutions if there is funding from institutions on a national or - even more likely - international level.

## 2.6 Dams, hydropower and international water conflicts

Globally, there is a boom in hydropower construction leading to an ongoing fragmentation of natural river systems. Already in 2005, more than 45,000 hydropower dams with a height above 15 m existed and the number of dams is growing steadily (Nilsson et al., 2005; Zarfl et al., 2014). The hydropower potential of Kyrgyzstan has already been recognized by the Soviet decision makers and first dams and reservoirs have been constructed during this era. Also the current situation cannot be understood without having the Soviet history and the transformation processes after 1991 in mind. Thus, to get a comprehensive idea about the ongoing hydropower exploitation along the Naryn, it is important to enlarge the view to the entire region and have a look back in the history before 1991.
The Soviet planners recognized early the potential of Kyrgyzstan for reservoir construction. The glaciers in the Tian Shan deliver water resources and the mountainous topography is favorable for dam construction (Bernauer and Siegfried, 2012). Main focus for the intended management

of the Kyrgyz reservoirs was irrigation of the lowlands in Kazakhstan and Uzbekistan. As a consequence, the area of irrigated land in the Syr Darya Basin increased from 2 million ha in 1960 to a maximum of 3.5 million ha in 2000. Since 2000, a slight decline is observable (Fig. 2.10). From this figure, it becomes clear that the total area of irrigated land continued to increase also

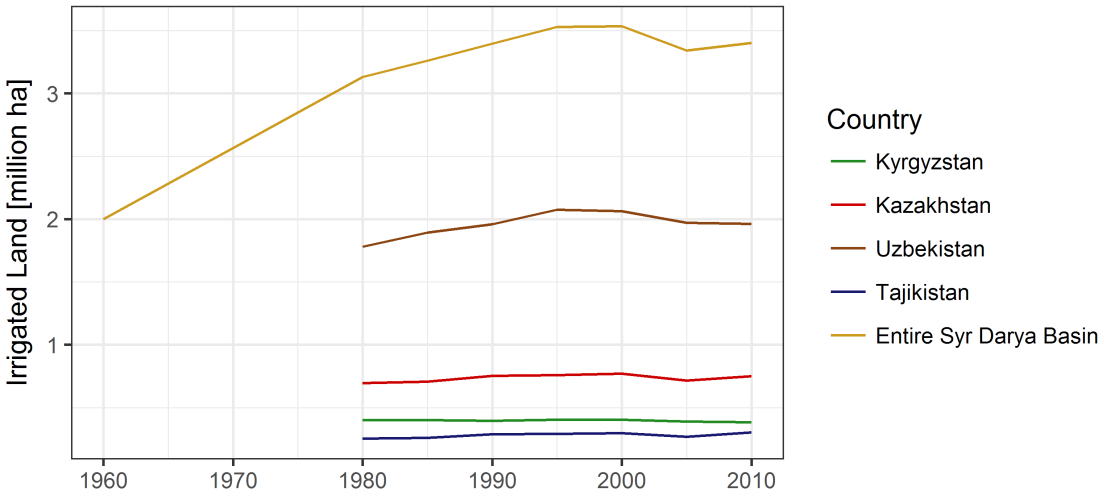


Figure 2.10: Development of irrigated land in the Syr Darya Basin (data from http://www.cawater-info.net and Bernauer and Siegfried, 2012; prior to 1980 only data for the entire basin was available)

after the breakdown of the Soviet Union in 1991 even if this development stopped around 2000. In addition to the overall development, the disparity between the upstream countries Kyrgyzstan and Tajikistan and the lowland countries Uzbekistan and Kazakhstan is obvious. While the upstream countries do not have extensive irrigated agriculture, they provide the majority of the water resources (Bernauer and Siegfried, 2012; Sorg et al., 2014). As a consequence, during Soviet times water was mainly withdrawn from the reservoirs in summer time for agriculture. Opposite, the downstream countries delivered coal, oil and gas to Kyrgyzstan and Tajikistan to supply them with fuel resources in winter time when the energy demand is the highest (Antipova et al., 2002; Bernauer and Siegfried, 2012). This compensation is necessary as the fossil fuel resources are quite unequally distributed across the countries (see table 2.1). Coal, oil and gas is mainly found

Table 2.1: Energy resources of the Central Asian Countries (from Trouchine and Giese, 2006)

| | Coal ($10^9$ tons) | Oil ($10^6$ tons) | Gas ($10^9$ $m^3$) | Uranium ($10^3$ tons) | Hydropower Potential ($10^9$ kwh/year) |
|---|---|---|---|---|---|
| Kyrgyzstan | 1.34 | 11.5 | 6.54 | 601 | 163 |
| Kazakhstan | 34.1 | 2,760 | 1841 | | 27 |
| Uzbekistan | 2 | 350 | 2,000 | 83.7 | 7 |
| Tajikistan | 0.67 | 5.4 | 9.2 | | 317 |
| Turkmenistan | | 75 | 2,860 | | 2 |

in the lowland countries Kazakhstan, Uzbekistan and Turkmenistan while Kyrgyzstan and Tajikistan only have the opportunity to use hydropower for energy production. The management of the existing reservoirs, however, optimized for summer irrigation did not allow sufficient energy production in winter time. For example, at the Toktogul reservoir - the largest reservoir of the Syr Darya Basin - 69% of the water has been released in summer time for irrigation before 1990. Only 31% has been available in winter time for the production of energy (Trouchine and Giese, 2006). With the breakdown of the Soviet Union in 1991, this compensation mechanism stopped working and the free delivery of fossil energy to the upstream countries was interrupted. As a consequence, the energy production of the thermal power plants in Kyrgyzstan sharply decreased from 4,108 GWh in 1988 to 1,631 in 1998 and 982 GWh in 1999 (Antipova et al., 2002; Bernauer and Siegfried, 2012). As a reaction, the Kyrgyz government decided to switch the management of the Toktogul reservoir from an 'irrigation mode' to a 'hydropower mode' where 66% of the water has been released in winter time for energy production (Trouchine and Giese, 2006). This allowed Kyrgyzstan to satisfy its energy demand in winter time but causes problems for the water supply of the agricultural areas in Kazakhstan and Uzbekistan. Furthermore, the release of water in the winter caused severe flood hazards in Uzbekistan (Bernauer and Siegfried, 2012). To solve this issue, international agreements guarantee a sufficient amount of water release from the Toktogul reservoir from April to October while Uzbekistan and Kazakhstan supply Kyrgyzstan with certain amounts of electricity, coal, oil and gas in winter time. Additionally, the two downstream countries agreed to buy the excess energy of 2,200 million KWh produced by the Toktogul hydropower plant during the summer releases (Bernauer and Siegfried, 2012; Sorg et al., 2014). However, the application of these agreements seems to have failed and the conflict between the wintertime energy demand of Kyrgyzstan and the summer time irrigation demand of Uzbekistan and Kazakhstan persists (Bernauer and Siegfried, 2012).

Against this background, there are ongoing plans to construct further dams and reservoirs upstream from the Toktogul reservoir. These dams could be managed with a focus on hydropower production for Kyrgyzstan while the Toktogul could be operated in an irrigation mode satisfying the need of the downstream countries (Abbink et al., 2010; Sorg et al., 2014). Figure 2.11 gives an overview of the existing and planned dams along the Naryn River under investigation. In addition, table 2.2 summarizes important facts about the dams including the length of the affected up- and downstream segment of the Naryn River. The Toktogul dam is the oldest dam and has been accomplished in 1974. With a maximum volume of 19.5 million $km^3$, the associated storage basin is the biggest reservoir in the Syr Darya catchment. Furthermore, the associated hydropower plant is able to produce 1,200 MW contributing to 91% of the total electricity of Kyrgyzstan (Antipova et al., 2002; Trouchine and Giese, 2006). Directly upstream from the Toktogul reservoir, the Kambar-Ata-2 dam is located. The construction of this dam originally started as early as 1986 together with a second dam. However, only one dam has been completed in 2010 as the political and economic situation didn't allow the further construction of the second Kambar-Ata dam. In addition to the dams close to the existing Toktogul reservoir, a cascade of four smaller reservoirs, the so-called Naryn Cascade is under construction (Urmambetova and Chymyrov, 2017). This project should be carried out by RusHydro and co-financed by Russia. However, RusHydro was not able to fulfill the contracts with the Kyrgyz government. Currently, Kyrgyzstan is looking for new investors for the hydropower projects along the upper Naryn River, a cooperation with a Czech investor seems to have failed (E. Baibagyshov, pers. communication). However, the plans are now withdrawn and as soon as a new investor is found, the construction is likely to be continued. More recently, there are plans for a smaller hydropower plant with 100 MW near the village of Emgek Talaa right downstream from Naryn City. Currently, this project is still in an early plan-

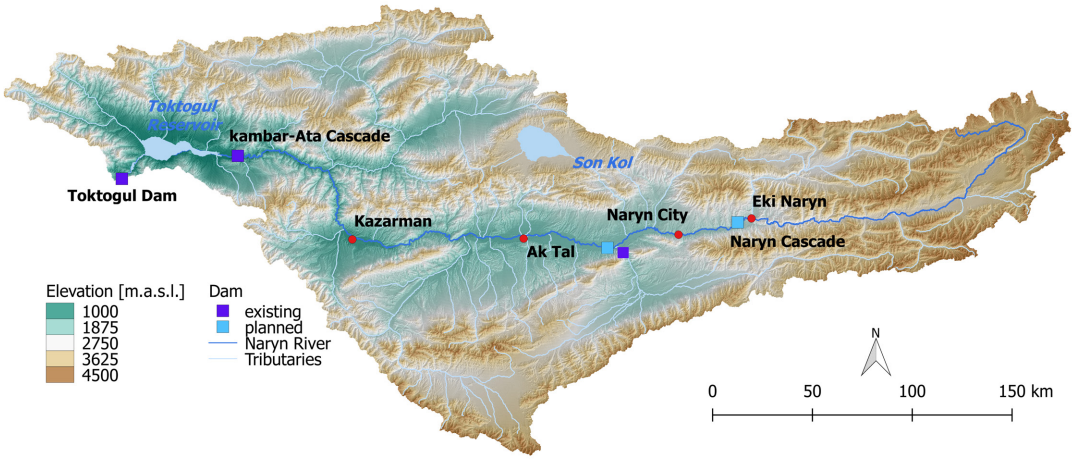


Figure 2.11: Hydropower dams along the Naryn River

Table 2.2: Important facts about the hydropower dams along the upper Naryn River

| Name | Status | Closing Year | Upstream Segment | Downstream Segment |
|---|---|---|---|---|
| Toktogul | built | 1974 | 753.57 km | 0 km |
| Kambar-Ata 1 | planned | —- | 88.59 km | 664.98 km |
| Kambar-Ata 2 | built | 2010 | 681.80 km | 71.77 km |
| Naryn Cascade | planned | —- | 404.00 km | 349.57 km |
| Emgek Talaa | planned | —- | 367.53 km | 386.47 km |

ning phase and initial geological and hydrological investigations are made. Intended starting date for construction is 2023. Contrary to the Naryn Cascade, the new plans are fostered by a private investor based in Kyrgyzstan, thus implementation problems like with RusHydro are unlikely to happen.

# 3 Ecosystem services of the Naryn floodplain forests

## 3.1 The relevance of ecosystem services for the Naryn River corridor assessment

The floodplain forests of the Naryn River provide manifold benefits for local people such as the provision of fuel wood or the protection against erosion. Since at least the Millenium Ecosystem Assessment Report (MA, 2005), the concept of ecosystem services has become dominant in describing this linkage between natural ecosystems and human well-being (Braat and de Groot, 2012; Costanza et al., 2017). Despite this concept is being more and more applied in research and practice, it has not been widely used in Kyrgyzstan. A recent review of 131 papers conducted by Shigaeva et al. (2013) showed that only 5 articles treated studied ecosystem services in Kyrgyzstan. Regarding the riparian ecosystem services at the Naryn River, there is even a total lack of research prior to the EcoCAR project.
A widely used scheme used for the assessment of human-nature interactions is the so-called ecosystem service cascade (Potschin and Haines-Young, 2011; Spangenberg et al., 2014; Potschin-Young et al., 2017). This framework starts with an analysis of the natural ecosystems including its structures and processes, then investigates how this contributes to human well-being as ecosystem services and, finally, tries to estimate people's benefits, partly in term of a monetary valuation (figure 3.1). A sound understanding of the biophysical structures and processes of the natural

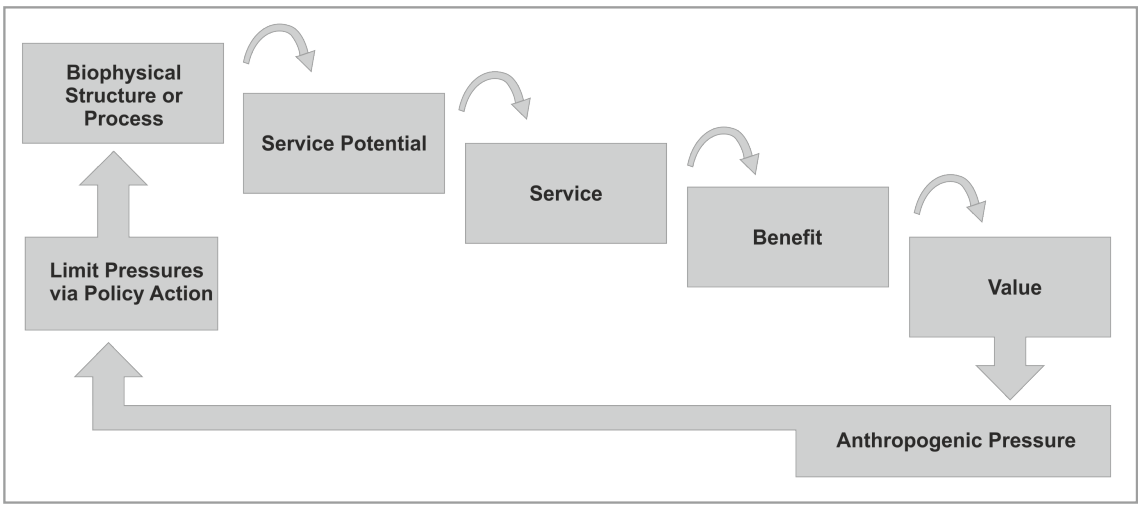


Figure 3.1: The ecosystem service cascade (based on Potschin and Haines-Young, 2011 and Spangenberg et al., 2014)

environment as well as the benefits and the values of the services are crucial for a science based

assessment and management of ecosystems services of the Naryn floodplain ecosystems. In this thesis, I focus on the first component of the cascade. Nevertheless, as no scientific literature is available yet, I want to give a brief overview of the socio-economic context in this chapter.

## 3.2 Methods

As no previous data has been available for making a statement about local peoples' demand for ecosystem services and associated values, an exploratory investigation has been conducted together with the colleagues from the Naryn State University. In a survey of 40 households in Ak Talaa and Ak Tal, people have been asked *'What does the floodplain forest mean for you?'*. The answers have than been grouped to categories during the analysis. Additionally, semi-structured interviews have been carried out with the local village administrations as well as with representatives of pasture and forest management. They have been asked for the role in their organization, the role of their institution for floodplain management, their perspective on ecological challenges and potential conflicts in ecosystem management. All household surveys and interviews have been conducted in Kyrgyz language with translation. Where market prices have been figured out, a monetary value was estimated for the respective service. Indirect valuation for non-market services using for instance the willingness-to-pay approach has not been carried out.

## 3.3 Results

### 3.3.1 Service potentials and services

There are a range of service potentials and actually used services provided by the Naryn floodplain forests. Figure 3.2 shows the actually used services. Clearly dominating service is the provision

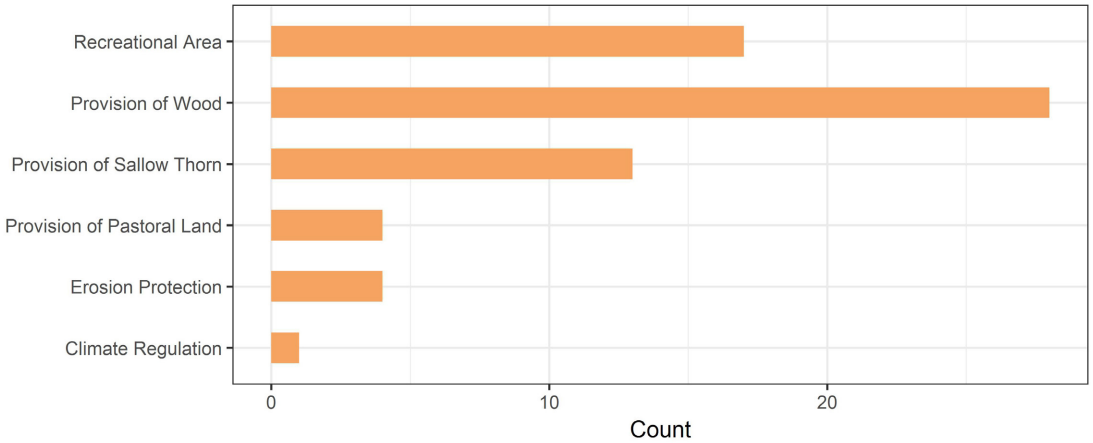


Figure 3.2: Ecosystem service demand of people living in the villages Ak Talaa, Emgek Talaa and Ak Tal

of wood followed by the provision of recreational area. Furthermore the provision of sallow thorn berries is regarded as a relevant service. The provision of pastoral land is mentioned as service only by 4 of the interrogated households. However, when conducting an interview with a representative of the pasture committee in Ak Tal, grazing in the floodplain forests was mentioned to have

a certain relevance. This contradiction might be explained by the responsibility of professional herders for selecting the pasture. Protection against erosion was mentioned 4 times in Ak Tal. In this village also the *ail okmotu* (mayor) is highly interested in the role of riparian vegetation in bank protection as high erosion rates are a risk for agricultural land belonging to the Ak Tal village. In addition to the erosion protection, climate regulation was mentioned once as regulating service. Flood protection as widely recognized riparian ecosystem service in Europe does not play any role at the Naryn River as there are no settlements or infrastructures in the zone prone to flooding. Despite this assessment gives a first overview over the actually used services, the societal demand might change over time (Spangenberg et al., 2015). Under the ongoing transformation in Kyrgyzstan and the slightly increasing economy (Dubashov et al., 2017), services beyond natural resources might become more important in the future. Thus, the services highlighted in this chapter give only a snapshot of the situation in 2015/16.

### 3.3.2 Benefits and values

The enjoyed ecosystem services offer various benefits for the people. Partly they have a market value and can be expressed in a monetary value, partly they are stated only qualitatively. The most obvious benefit is the supply with timber and non-timber forest resources. The value of wood collection for example can be expressed as the difference between the market price for coal (as subsidence for wood) and the price for the permission to collect wood. While 1 ton of coal costs 2500 KGS (approx. 35 EUR), the price for collecting 1 $m^3$ of wood is 250 KGS (approx. 4.50 EUR) being paid to the local forestry (Leschoz). Of course, the different caloric value makes a direct comparison difficult. Despite this issue, people state a saving when using wood instead of coal (see figure 3.3 as for illustration).

Figure 3.3: A flock of sheeps grazing in the floodplain forest (l); Timber collection in a village at the Naryn River (r)

The collected sallow thorn is processed to jam which is used in the families and sold on local markets. The market price for sallow thorn is 100 KGS (approx. 1.40 EUR) per kilogram. During the household survey it turned out that the income from selling sallow thorn is an important additional income for poorer families. When using the floodplain forests as pastoral land, people benefit from saving cost for additional fodder for their livestock during winter. However, this saving cannot be expressed in a monetary form with the collected data.
People stated also benefiting from 2 regulating services. First, they benefit from protection of their agricultural land via the mitigation/reduction of fluvial erosion. In case of an intact, resilient riparian vegetation cost intensive technical bank protection can be avoided or reduced. A second

benefit is the mitigation of climate change through the storage and sequestration of carbon in the biomass of the natural ecosystems. A further possible monetary value of carbon storage might be the participation in the REDD+ initiative, where developing countries get a financial compensation when they reduce their deforestation rate. In such case, a monetary value of carbon storage would be related to the global carbon market with fluctuating prices between 5 USD and 50 USD per ton of $CO_2$ (World Bank, 2016). Additionally, people benefit also from using the floodplains as recreational area nearby their homes as mobility usually is limited due to the transport costs. However, even this aspect is quite relevant for people, it cannot be assessed in terms of a market based value.

### 3.3.3 Anthropogenic pressures and current policy action

By using their services, people exert a certain pressure on the ecosystems. The main factors for the Naryn floodplain forests are woodcutting and livestock grazing. While the woodcutting affects the adult trees, grazing gives particular pressure on the young saplings leading to a decrease in forest rejuvenation. Especially in the mature floodplain forest the risk of degradation is high as the natural conditions and probably also grazing limit the seed germination and thus the rejuvenation (Rauschenberger, 2016).
Kyrgyzstan has manifold institutions for coping with environmental issues at different administrative levels (Scheuber et al., 2000; Schmidt, 2014). Most important stakeholder regarding the floodplain ecosystem services is the forestry administration (Leschoz) as this authority controls the access to the forest resources. Since 2010, the Leschoz introduced permission 'tickets' necessary to access forest resources. The amount of tickets sold to people is defined in a centralized way by the Department of Forest and Hunting in Bishkek taking into account the available amount of forest resources. In the interview with the Leschoz in Ak Tal, the responsible forester reported costs of 350 KGS (approximately 4.50 EUR) for the right to collect 1 $m^3$ of wood. In case of illegal collection the forest law provides a fine up to 10,000 KGS (approx. 125 EUR). Also the access right for livestock is sold. Here the price is 35 KGS (approximately 0.40 EUR) for 1 ha of forest pasture. The earnings generated by the access tickets as well as the fines go to the Forestry Department in Bishkek. Regarding grazing, there is a second relevant stakeholder: The pasture committees existing since 2009 are elected institutions in each municipality and take care for managing livestock affairs. Among others these committees organize (and potentially limit) the access to pastoral land. For instance, they organize the access permission to the forest pastures in a centralized way.

## 3.4 An Ecosystem service cascade for the Naryn floodplains

Placing the issues discussed above in the framework of the ecosystem service cascade, gives a conceptual model of ecosystem services for the Naryn floodplain forests (figure 3.4). While it gives a general overview, it does not claim to be the final result of ecosystem service research at the Naryn River. In fact it provides a framework to highlight ongoing research questions related to sustainable management of floodplain forests. The diverse parts of the cascade suggest that it is an interdisciplinary research issue.
People benefit from various ecosystem services provided by the floodplain forests of the Naryn River. In an overall evaluation, provisioning services such as the provision of timber, fruits and pastoral land are dominating. Additionally, the floodplain forests are an important recreational

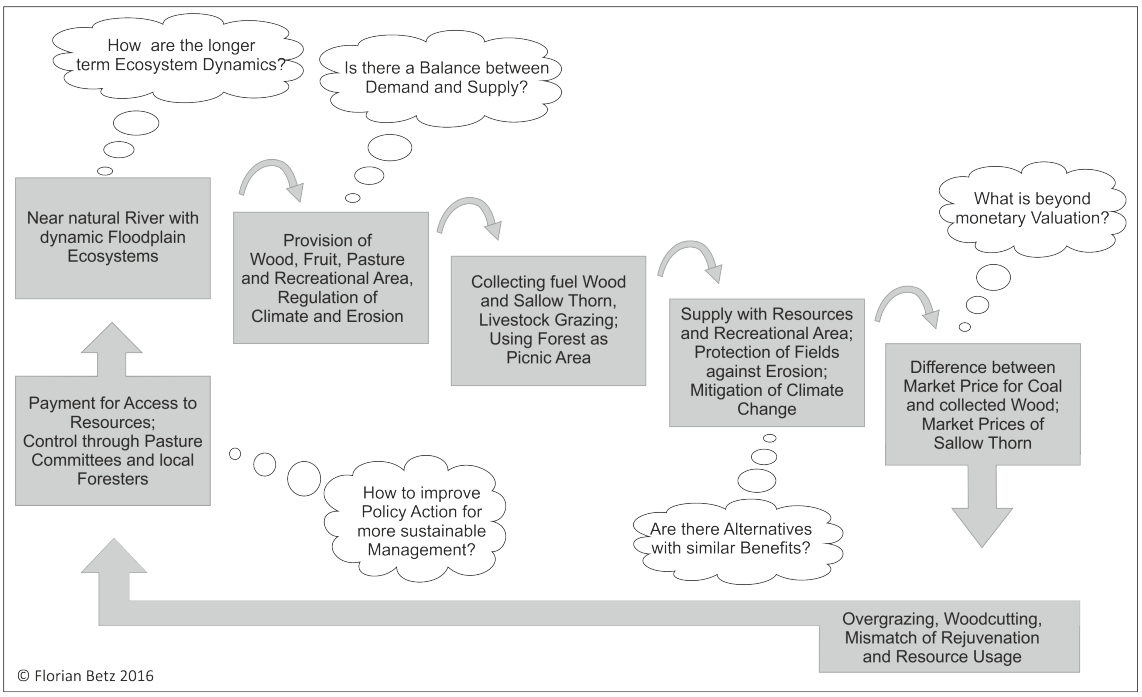


Figure 3.4: Ecosystem service cascade for the Naryn floodplain forests

area of the local villagers. A monetary valuation of these services is a critical issue, as ecosystem services are always societal constructions (Spangenberg and Settele, 2010; Spangenberg et al., 2015). The Kyrgyz Society is still in the transformation after the collapse of the Soviet Union in 1991. Thus the perception of ecosystem services from a societal but also from an institutional perspective is likely to undergo changes (Schmidt, 2013). Thus, even if an economic valuation can be done in a straightforward way like in case of the berries of the sallow thorn, the ecosystem service cascade goes beyond a simple pricing of natural resources. Rather, it is a template for analyzing the interaction of humans and their environment in a holistic, interdisciplinary way.

## 3.5 What is the contribution of this thesis to the ESS cascade?

Thinking about sustainable management of floodplain ecosystems – the aim of the EcoCAR project – there is the need for finding a balance between natural ecosystem development and peoples' dependence on resources for their well-being. The ecosystem service cascade is an appropriate framework to analyze the complex interaction between these two issues. However, it is beyond the scope of this thesis to analyze all parts of the ecosystem service cascade discussed above in a comprehensive way. As there is no data available for giving an overview over the socio-economic and political background of ecosystem services of the riparian ecosystems along the Naryn, I gave a brief outline about this based on own, exploratory research. Despite the results give a preliminary understanding about the human-environment interaction along the Naryn River, it is obvious that the limited data together with the changing societal background cannot result in a final statement on the socio-economic and political components of the cascade. Further research embedded in an ongoing dialog with the relevant stakeholders is necessary to make sound

suggestions for a more sustainable management. This thesis contributes with an analysis of the biophysical structure and dynamics of the Naryn River with its riparian ecosystems.

# 4 Hydrology and hydroclimatic changes in the Naryn catchment

## 4.1 Hydrological research in Central Asia

Water moving down the channel is the ultimate driver of geomorphological as well as for ecological dynamics within a river corridor (Junk et al., 1989; Poff et al., 1997; Lane and Richards, 1997; Church, 2002; Tockner et al., 2010). In the semi-arid to arid climate of Central Asia, discharge of the rivers is mainly generated from snow and glacier melt in the mountains (Immerzeel et al., 2010; Unger-Shayesteh et al., 2013). About 10% of the total runoff of the Naryn River is generated by the glaciers in the Tian Shan (Aizen et al., 1995; Kriegel et al., 2013). With rising temperatures the glaciers are expected to melt with the consequence of changing discharges in Central Asia (Aizen et al., 2007; Hagg et al., 2007; Sorg et al., 2012). Recent predictions forecast more unstable summer discharges due to the loss of glacier runoff (Hagg et al., 2007; Sorg et al., 2012; Gan et al., 2015). From a large scale perspective, this is a serious issue for the region as large parts of the agriculture along the inland rivers like the Syr Darya depend on irrigation (Sorg et al., 2014; Karthe et al., 2015). Furthermore, water conflicts between the upstream countries interested in hydropower production and the downstream countries with their need for irrigation water exist already today and might become more serious if the amount of available water resources decreases (Bernauer and Siegfried, 2012). Thus, research on hydrological change issues has mainly focused on the large scale issue of regional water availability or localized studies analyzing the relationship between climatic changes, glacier melt and runoff generation (see Sorg et al. 2012 and Unger-Shayesteh et al. 2013 for recent reviews).
For the geomorphological and especially the ecological dynamics not only the total amount of water is relevant but also the magnitude, frequency, duration and timing of the flood pulses. Together, these parameters form the natural flow regime of a river (Richter et al., 1996; Poff et al., 1997; Arthington et al., 2006; Hayes et al., 2018). This flow regime is among the most relevant determinants of riparian vegetation communities and changes might have significant consequences for the structure and the species composition of river corridors (Poff and Zimmerman, 2010; Hayes et al., 2018). Despite this relevance, there is a lack of research on the natural flow regime of the large headwater in Central Asia like the Naryn River - contrary to the widespread water resource studies. Thus, I go beyond the analysis of the amount of discharge in this thesis. I conduct trend analysis of discharge and climate time series on an annual as well as on a monthly basis in order to describe the effects of climate change on seasonal changes of temperature, precipitation and discharge. Furthermore, I analyze the frequency, timing and magnitude of flood pulses based on a daily discharge record for the gauge Naryn City. The hydrological analysis is completed by an assessment of the flood recurrence intervals for the Naryn River which are relevant for interpreting the results of the remote sensing analysis in chapters 6 and 7.

## 4.2 Data and methods

### 4.2.1 Data

Hydrological and climatological data have been downloaded from the data server of the Northern Eurasian earth science partnership initiative (http://neespi.sr.unh.edu [last access: 2020-12-28], Groisman and Bartalev 2007). On this platform, monthly discharge data of 18 gauging stations in the Naryn catchment are available. Data records start between 1931 and 1959 and end between 1987 and 2006. Table 4.1 gives a summary of the stations available for the Naryn Basin, their locations are given in figure 4.1. Additionally, I analyze trends of 3 climate stations in the Naryn basin. The stations Naryn City, Tian Shan and Susamyr have been selected as they provide time series for temperature and precipitation also beyond 2000 contrary to all other stations where the observation period is ending in the early 1990s. In addition to these monthly datasets, daily

Table 4.1: List of gauges and climate stations in the upper Naryn Basin used for the trend analysis (data downloaded from http://neespi.sr.unh.edu/maps/, last access: 2020-12-28)

| Name | NEESPI Code | Period | Catchment Area [km$^2$] | Longterm Average Discharge [m$^3$/s] |
|---|---|---|---|---|
| *Gauges* | | | | |
| Naryn City | 16055 | 1931-2017 | 10,347 | 92.117 |
| Kekirim | 16057 | 1933-1996 | 34,600 | 204.352 |
| Uchterek | 16059 | 1963-2006 | 47,077 | 323.333 |
| Big Nary | 16068 | 1937-2005 | 5,571 | 43.904 |
| Small Naryn | 16070 | 1939-2005 | 3,888 | 41.291 |
| Onara | 16072 | 1940-1988 | 1,320 | 10.019 |
| Dzhergetal | 16074 | 1932-1995 | 286 | 1.059 |
| Ak Tala | 16075 | 1934-1990 | 1,960 | 5.150 |
| At Bashe | 16076 | 1937-1995 | 1,500 | 17.711 |
| Koshtobe | 16080 | 1959-1993 | 3,710 | 30.542 |
| Tabylga | 16081 | 1950-1996 | 1,720 | 19.892 |
| Kekemeren | 16082 | 1944-1987 | 2,410 | 38.680 |
| Kekemeren | 16085 | 1933-1997 | 8,440 | 85.899 |
| Karakol | 16087 | 1950-1997 | 1,180 | 22.359 |
| Chaek | 16088 | 1954-1999 | 2,390 | 9.388 |
| Torkent | 16093 | 1950-1993 | 654 | 45.206 |
| Chichkan | 16096 | 1940-2006 | 917 | 17.389 |
| Ustasai | 16100 | 1930-2006 | 1,796 | 28.560 |
| *Climate Stations* | | | | |
| Naryn City | 36969 | 1886-2005 | | |
| Tian Shan | 36982 | 1930-2005 | | |
| Susamyr | 38358 | 1936-2005 | | |

discharge data is available for the gauge Naryn City for the period from 1988 to 2017, the period of the remote sensing analysis presented in chapter 7. This series has been provided by the hydro-

meteorological authority in Naryn, daily data prior to 1988 has not been available, respectively is archived in Bishkek and has not been accessible for this thesis. Most of the discharge series end around 1990 with the independence of Kyrgyzstan. This is a well-known issue in Central Asia,

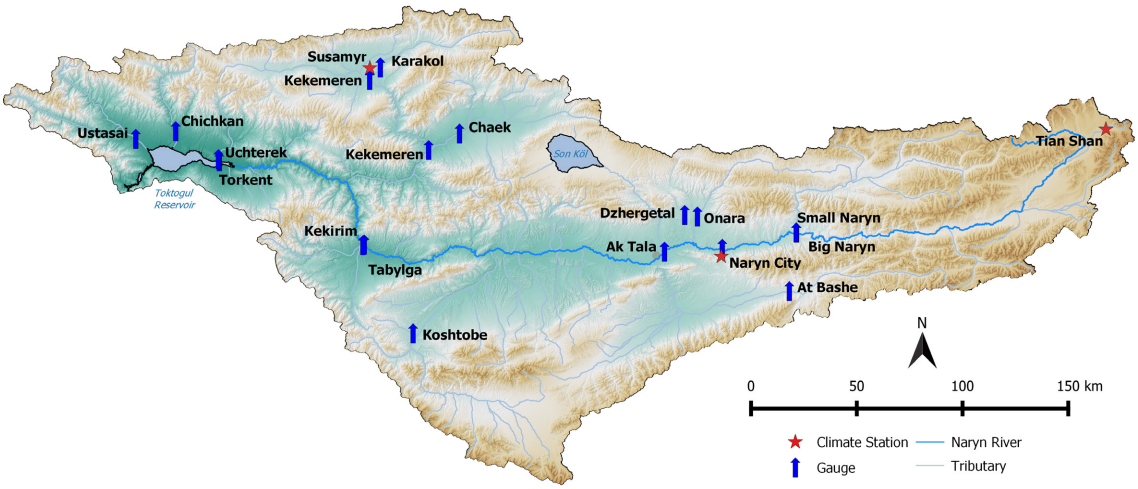


Figure 4.1: Locations of gauges and climate stations in the Naryn catchment

that hydro-meteorological observation stations have been shut down after the breakdown of the Soviet Union (Unger-Shayesteh et al., 2013). A further practical challenge is the fact that this daily series has been recorded in an analogue form and had to be digitized prior to analysis.

### 4.2.2 Trend analysis

I use the Mann-Kendall trend test for estimating the significance and the Sen Slope estimator for analyzing potential trends in the discharge and climate series. These approaches are robust, non-parametric methods and have been widely applied for hydrological time series analysis (Kundzewicz and Robson, 2004; Unger-Shayesteh et al., 2016). The Sen Slope is estimated as follows:

$$\beta = \frac{x_j - x_i}{j - i} \text{for all } i < j \tag{4.1}$$

where $x_i$ and $x_j$ are the hydrological or climatic variable in the year i or j. Based on $\beta$, the robust Theil-Sen trend line can be described:

$$x_l = \beta * t + \text{median}(x) - \text{median}(t) * \beta \tag{4.2}$$

After having estimated the trend magnitude, the significance has been estimated using the Mann-Kendall test (MK). For more details about the MK, readers can refer to Mann (1945) or Rougé et al. (2013).

$$S = \sum_{i}^{n-1} \sum_{j=i+1}^{n} \text{sgn}(x_j - x_i) \tag{4.3}$$

Where sgn is the sign of the difference between two distinct observations i and j and is defined as:

$$\mathrm{sgn}(x_j - x_i) = \begin{cases} +1 & x_j > x_i \\ 0 & x_j = x_i \\ -1 & x_j < x_i \end{cases} \tag{4.4}$$

Furthermore, n is the sample size. For $n \gg 8$, the test statistic is assumed to be approximately normal distributed with the mean E and the variance V following from equations 4.5 and 4.6.

$$E(S) = 0 \tag{4.5}$$

$$V(S) = \frac{1}{18}(n(n-1))(2n+5) - \sum_m t_m(m-1)(m+5) \tag{4.6}$$

Where t is the number of ties of extent m. Finally, the variable Z follows a standard normal distribution:

$$Z = \frac{S - \mathrm{sgn}(S)}{V(S)} \tag{4.7}$$

Thus, the null hypothesis *'no trend'* is rejected when $|Z| > Z_1 - \frac{a}{2}$, with $1-(\frac{a}{2})$ being the quantile of the standard normal distribution. As results we have *'no significant trend'* with $Z < 1.282$ (Rougé et al., 2013). The trend and significance estimation have been estimated for annually aggregated time series. As the length of the time series is not equal for all records, a comparison becomes difficult. To overcome this challenge, I performed the Sen slope estimation and the MK in an iterative way for all start and end points of the time series resulting in a period of longer than 30 years. The result of this approach can be visualized in so-called multiple trend plots as they have been recommended by Unger-Shayesteh et al. (2016). In addition to the trend assessment performed on the annual time series, seasonal trend tests on a monthly basis have been performed on the temperature and precipitation records of all climate stations as well as on the discharge time series with a record beyond the breakdown of the Soviet Union.

### 4.2.3 Flow regime analysis

To analyze the contemporary flow regime of the Naryn River, the daily dataset for Naryn City is used. Figure 4.2 shows the flow regime history plot of the daily series used for all analysis. As a first graphical description of the discharge, the flow duration curve has been generated as commonly accepted (Vogel and Fennessey, 1994, 1995). In addition to the flow duration curve as indicator of the magnitude of the flow regime, a wavelet power spectrum approach has been chosen to assess the periodicity of the discharge. Wavelet power spectra transfer a time series in the frequency domain what allows to analyze the seasonality of the discharge series without prior assumptions of the regime (White et al., 2005). Even if this approach has only rarely been used in flow regime analysis due to its complexity, it has been proved to be a useful indicator of flow regime (White et al., 2005; Lane, 2007; Agarwal et al., 2016). Following these graphical procedures, trend tests of the annual median and the annual maximum have been conducted using the Mann-Kendall trend test described above. To gain further insights in the ecologically relevant timing of the flood events, the day of the year with the maximum discharge has been extracted. Furthermore, the beginning and the end of the flooding season have been derived using a time series filtering approach originally developed for vegetation phenology analysis (Forkel et al.,

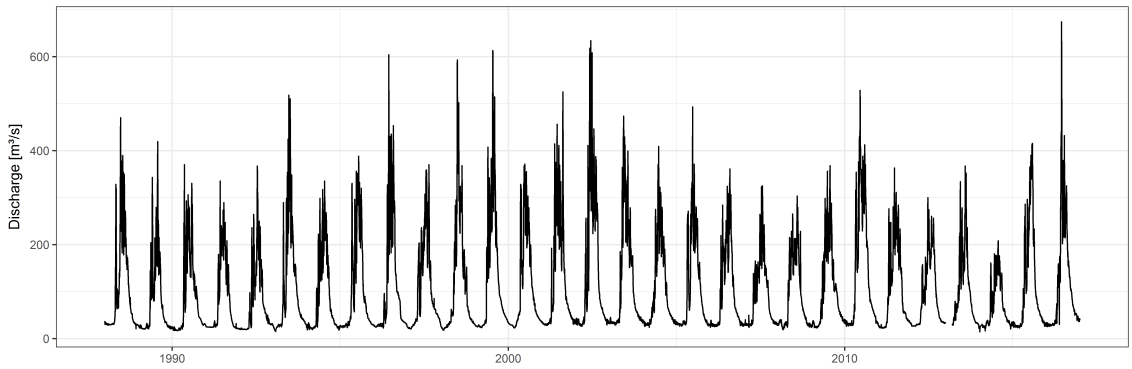


Figure 4.2: Daily discharge time series of the gauge Naryn City

2015). A spline function is fitted to the discharge data to perform the filtering. Then, the first derivative of the spline function is used to detect changes in the slope of the filtered discharge series. The beginning and the end of the flooding season can be estimated from significant changes in the slope (Forkel et al., 2015).

### 4.2.4 Flood recurrence interval estimation

Along with the flow regime analysis, an assessment of the flood probability is carried out applying methods of extreme value statistics. Due to the relatively short daily time series of 29 years only, the estimation of flood recurrence intervals is limited. Nevertheless, it gives an idea about the flood magnitudes during the study period from 1988 until 2017. Following Maniak (2016), the daily time series has been aggregated to annual maxima in order to avoid autocorrelation. The resulting time series has been tested on stationarity by means of evaluating the trend, the autocorrelation as well as the partial autocorrelation (Coles, 2001). In addition, the Kwiatkowski-Phillips-Schmidt-Shin (KPSS) test (Kwiatkowski et al., 1992) has been performed to underpin the assumption of stationarity. Figure 4.3 shows the time series of the annual maxima and the plots for the autocorrelation and partial autocorrelation. As the Mann-Kendall p-value of 0.50898 suggests that there is no significant trend of the annual maxima. In addition, there is no significant autocorrelation across all lags, stationarity can be assumed for the annual maxima from 1988 to 2017. This is also supported by the result of the KPSS test, which results in a p-value of 0.1 allowing to reject the hypothesis of non-stationarity.
After a positive result of the stationarity evaluation, a generalized extreme value (GEV) distribution has been fitted to the data using a maximum likelihood procedure implemented in the *evir* package in R (Pfaff and McNeil, 2012). After the fitting procedure, the goodness-of-fit has been tested using the Kolmogorov-Smirnov-test (Maniak, 2016). After successful evaluation, the fitted generalized extreme value distribution is used to estimate the recurrence intervals of the floods during the investigation period from 1988 to 2017.

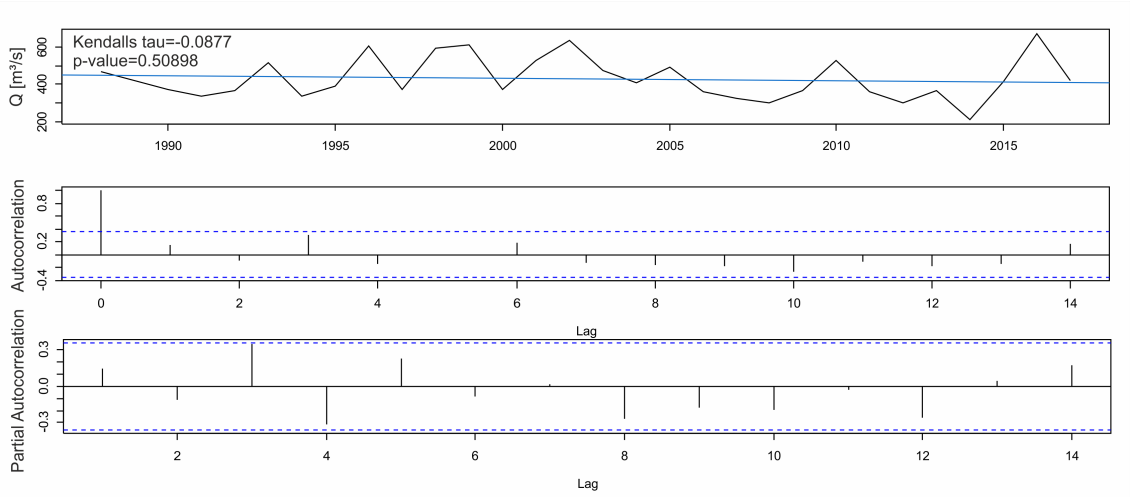


Figure 4.3: Time series of annual maxima of the gauge Naryn City and autocorrelation plots; the series does not show a significant trend or autocorrelation what satisfies the stationarity requirement for extreme value statistics

## 4.3 Results

### 4.3.1 Climate trends

Figure 4.4 and figure 4.5 show the temperature and precipitation changes for the selected stations. To enhance the comparability of the series, I used a period from 1937 to 2005 for analysis as this time span is fully covered from all three stations. The temperature increase is highly significant, for instance at the station Naryn City, the mean annual temperature rose from 1.5 °C to 3.9 °C. The precipitation is decreasing at all three stations, but the significance is varying. Susamyr in the western part of the catchment is showing a highly significant decrease, while the precipitation trend of the station Naryn City is not significant. A special case is the Tian Shan weather station which was relocated in 1997 (Giese et al., 2007). While showing no significant decrease of precipitation for period from 1936 to 2005, the decrease is significant under the 95% confidence interval when setting the endpoint of the time series to 1997. All annual trends have been summarized in table 4.2. The seasonal pattern shows increasing temperatures throughout the year with exception of the February for Susamyr and June for Naryn City, where temperatures show a slight, not significant decrease. This increase is highest in December while it is relatively small in summertime. For the precipitation there is a decrease in all seasons, only at the station Naryn City there is a slight increase in August and September. Even if not significant for all month, the strongest decrease of precipitation occurs for all climate stations in summer between June and September.

### 4.3.2 Discharge trends

The gauges Big Naryn, Small Naryn and Naryn City can be used to describe the hydrological trends of the upper Naryn River. The gauges Kekirim and Uchterek represent the entire Naryn Basin as they represent 65.77% respectively 89.48% of the entire Naryn catchment. However, Kekirim was shut down in 1996 while Uchterek was set up just in 1963. Thus, trends for these gauges have been calculated not for the entire series but for all 30 year periods within the existing

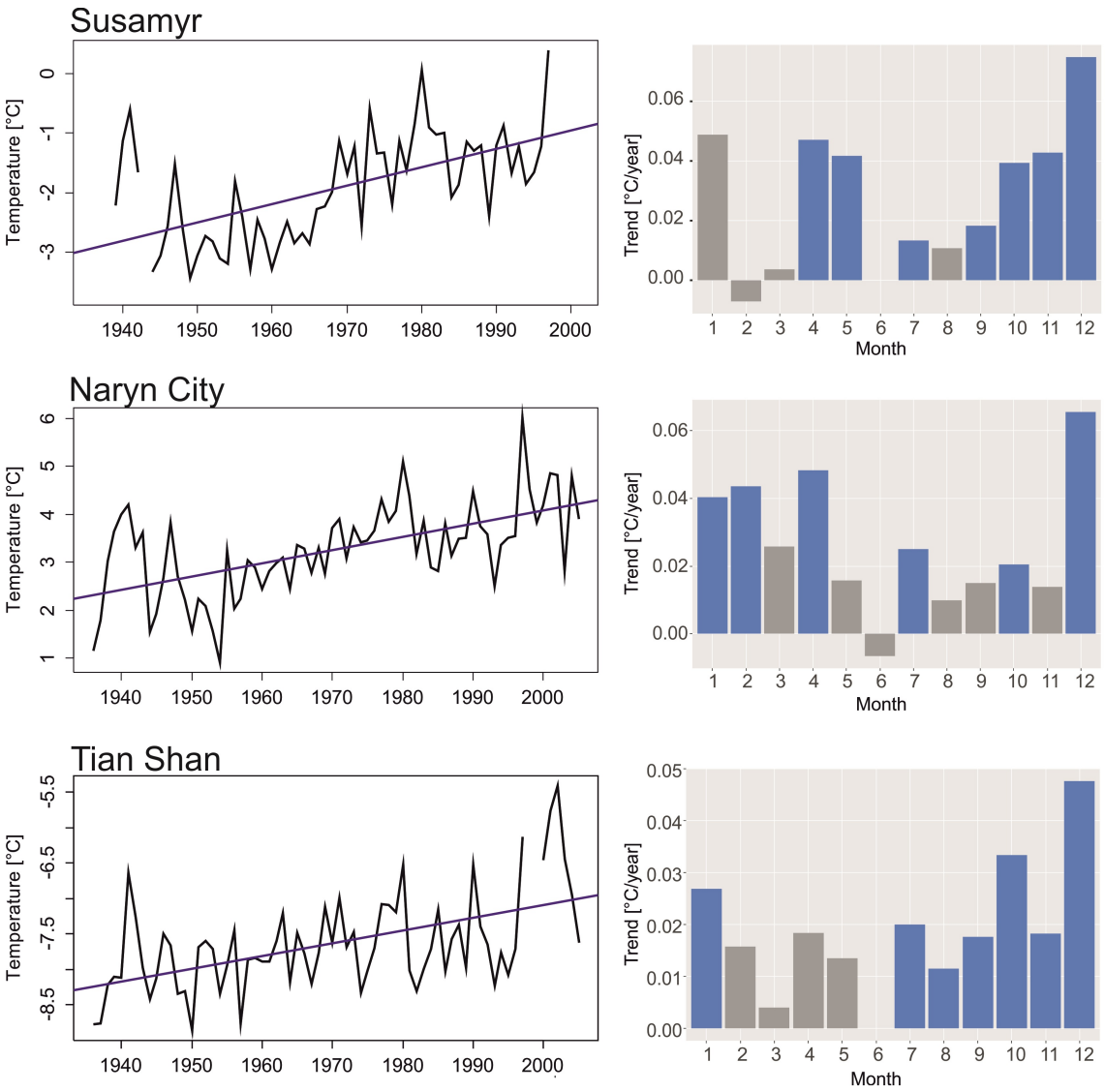


Figure 4.4: Results of the trends analysis of the temperature; The line graphs give the annual series, the bars the monthly temperature changes; blue bars indicate changes significant under the 95% confidence level

Table 4.2: Results of the annual trend analysis of the climate stations; T stands for the temperature, P for the precipitation

| Station | Trend (T) | P-Value (T) | Trend (P) | P-Value (P) |
|---|---|---|---|---|
| Susamyr | 0.035 | $4.01 \times 10^{-6}$ | -1.6 | 0.0037 |
| Naryn City | 0.029 | $4.78 \times 10^{-7}$ | -0.36 | 0.46 |
| Tian Shan (1937-2005) | 0.015 | $1.3 \times 10^{-6}$ | -0.044 | 0.94 |
| Tian Shan (1937-1997) | 0.0098 | 0.012 | -1.06 | 0.032 |

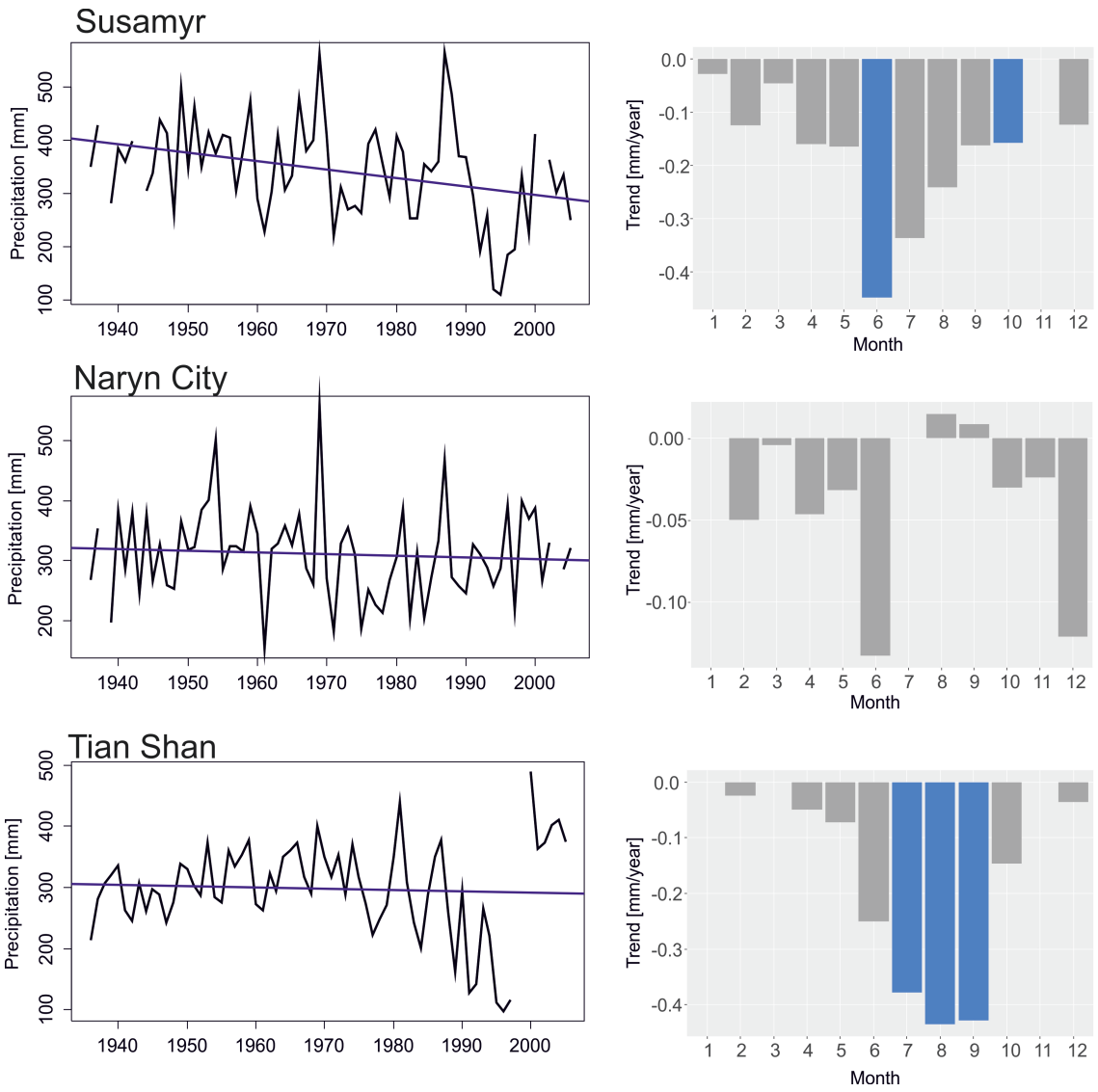


Figure 4.5: Results of the trends analysis of the precipitation; The line graphs give the annual series, the bars the monthly temperature changes; blue bars indicate changes significant under the 95% confidence level; for the behavior of the Tian Shan precipitation series, please refer to the explanation in the text

record. This allows to compare two time series even if they have only a short overlapping period. In addition to the gauges along the Naryn River, tributary trends of two sub-catchments have been analyzed using the gauges Chichkan and Ustasai. Table 4.3 summarizes the results from the discharge trend analysis and gives descriptive informations about the glaciation and the maximum elevation of the sub-catchments.
The Big Naryn shows a slightly increasing trend with a normalized Sen slope of 0.00149. However, the Mann-Kendall p-value of 0.278 suggests that this trend is not significant. On a monthly basis, increasing discharges can be observed throughout the entire year except in May and November, where slightly negative trend values occur (Fig. 4.6). The trend is strongest in June, nevertheless only from January to March trends significant under the 5% confidence levels exist. The gauge

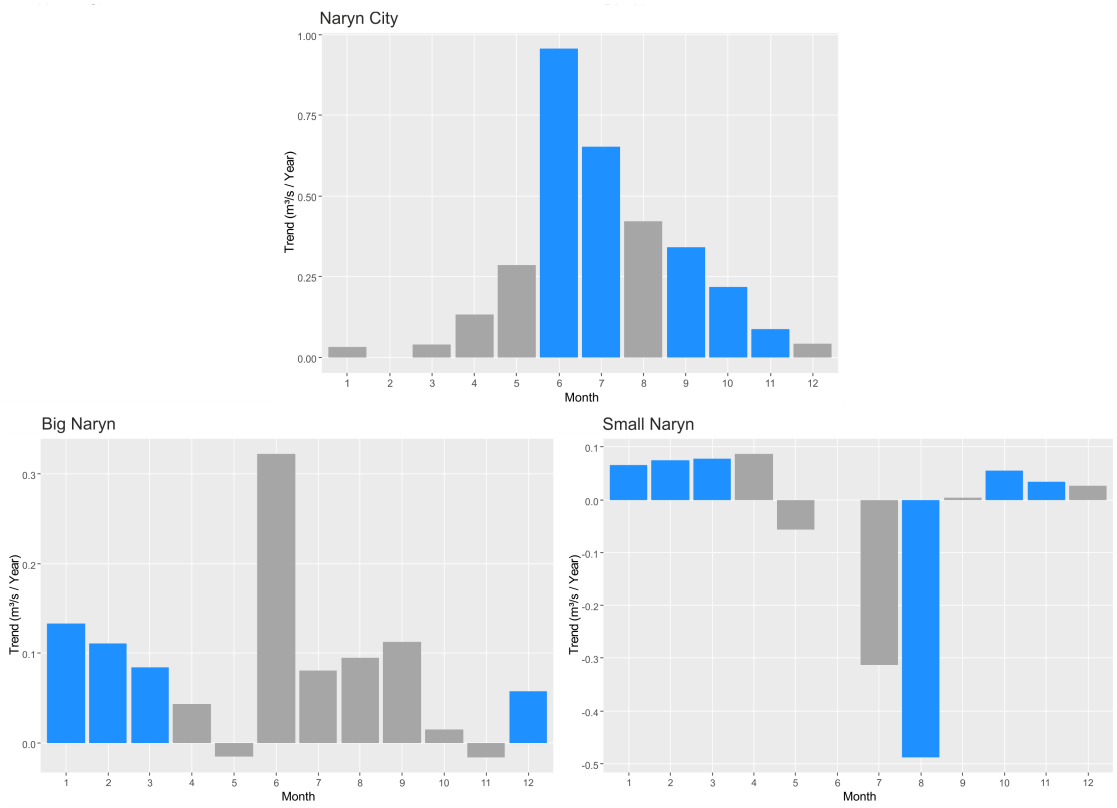


Figure 4.6: Seasonal trends of the gauges Naryn City as well as Big and Small Naryn; blue bars indicate trends significant under the 5% confidence level

in Naryn City shows also an increasing trend, with the latter being significant as the Mann-Kendall p-value of 0.0124 indicates. Similar to the Big Naryn, the trend is strongest in the summer months (Fig. 4.6). In June and July, the trends are significant. The Small Naryn, on the contrary, shows a different behavior. The trend is negative, even if not significant. Looking at the monthly trend analysis (Fig. 4.6), it becomes clear that the negative trend results from decreasing discharges between May and August. This negative summer trend is even significant under the 5% confidence level for August. In the winter season, slightly positive trends can be observed.

The two gauges representing the entire Naryn catchment are challenging to analyze as the one record ends in 1996 (Kekirim) and the other record starts in 1963 (Uchterek). Thus, I calculate the trends for all 30 year periods in the both series what allows to compare the trends in both time

Table 4.3: Trends and sub-catchment properties of the gauges analyzed in detail (glaciation from the World Glacier Inventory, relief parameters from the SRTM-1 DEM)

| Name | Trend | Normalized Trend* | P-Value | Glaciation | Maximal Elevation |
|---|---|---|---|---|---|
| Naryn City | 0.262 | 0.00284 | 0.0124 | 9.17% | 4962 m |
| Big Naryn | 0.0653 | 0.00149 | 0.278 | 10.67% | 4962 m |
| Small Naryn | -0.0516 | -0.00125 | 0.260 | 8.85% | 4894 m |
| Chichkan | 0.00939 | 0.000540 | 0.880 | 1.31% | 4078 m |
| Ustasai | 0.0118 | 0.000413 | 0.803 | 0.82% | 4186 m |

**normalized with the longterm average discharge*

series despite the different observation length (Unger-Shayesteh et al., 2016). The results of these analysis are shown in figure 4.7. From the 1930s to the 1970s, slightly positive trends can be observed for Kekirim and Naryn City even if they are not significant. Then, a period of negative trends follows until mid of the 1990s. These trends are more pronounced for Kekirim, where they are also significant (Fig. 4.7). At the end of this period of negative trends, the record of Uchterek begins while the one for Kekirim is ending. In the earliest observations of Uchterek, we still see the slightly negative trend even it is soon turning into positive. This switch from negative trend to positive trend also exists for Naryn City, even occuring slightly earlier. From the 1990s until the end of the record in 2005, Uchterek as well as Naryn City show clearly positive trends significant at least under the 10% confidence level.
Having a look at the two tributaries where the gauges have not been shut down in the 1990s, gives further insights in the hydrological changes of lower, less glaciated sub-catchments. Chichkan as well as Ustasai have negligible positive normalized trends of 0.000540 and 0.000413 respectively. The Mann-Kendall p-values greater than 0.8 (Table 4.3) clearly indicate non-significant trends, i.e. on an annual basis the discharge of these two gauges can be assumed to be constant. On a monthly basis, the discharge shows a heterogeneous image for Chichkan with increasing trends in the first half of the year and decreasing trends in the second half. However, there are no significant changes all year round (Fig. 4.8). Ustasai shows negative trends in July and August, while the rest of the year is characterized by positive trends which are strongest in April (significant under the 5% confidence level) and May.

### 4.3.3 Flow regime analysis

Figure 4.9 shows the flow duration curve of the gauge in Naryn City. The median of the daily discharge for the period from 1988 until 2017 is 53.1 $m^3s–1$, the 20% and 70% exceedance probabilities representing high and low flows (Vogel and Fennessey, 1994) are at 181 $m^3s–1$ and 29.5 $m^3s–1$ respectively. An additional parameter is the mean daily discharge for the period having a value of 102.26 $m^3s–1$. While the flow duration curve gives an indicator of the magnitude of discharge, the wavelet power spectrum represents the seasonality. Figure 4.10 shows the power spectrum of the daily discharge series. The time from 1988 to 2016 is drawn on the x-axis, the periodicity on the y-axis. The different color codes indicates the power spectrum with high values in yellow and low values in blue. The temporal scales with high power spectrum values can be interpreted to represent a relevant period of the flow regime, the scales with low values are less relevant. The highest power spectrum values appear at the scale around 1 year indicating the dominating summer floods. This signal is also constant over the entire observation period from 1988

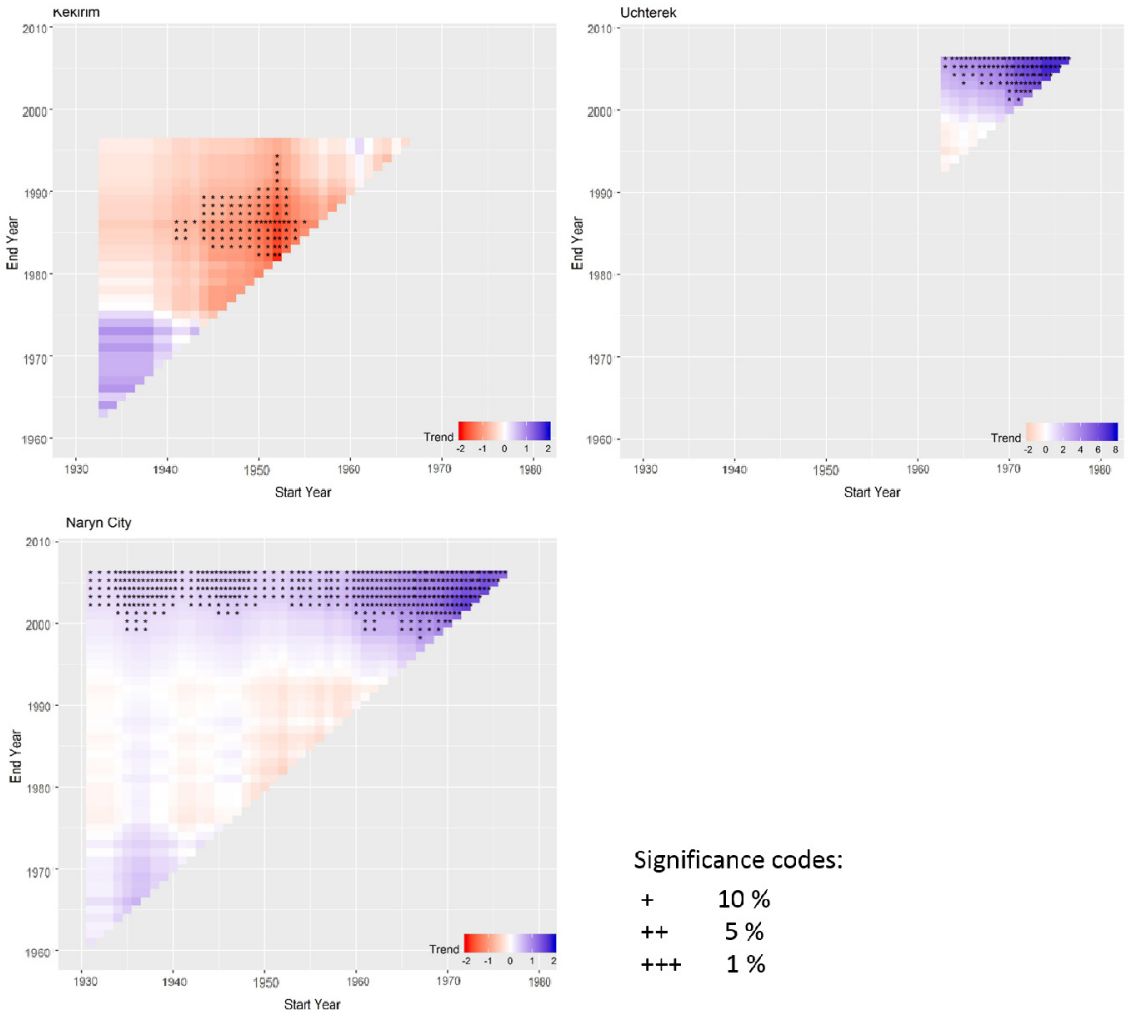


Figure 4.7: Multiple trend plots of the gauges Kekirim, Uchterek and - for comparison - Naryn City; each lattice in the plot indicates one 30-year period in the series, the color indicates the trend represented by the Sen Slope

to 2016. Beyond the annual periodicity, there are also weaker signals on longer time scales from 2 to 8 years which are unclear but might reflect longer term climatic cycles (White et al., 2005). Furthermore, there are inconstant signals on the scales from quarter years to a daily time scale. These signals reflect a certain 'flashiness' of the discharge and might be interpreted as reaction on precipitation events or snow melt following a warm weather period.
More information about the timing of the seasonal fluctuation of the discharge is given by the day of the year of the starting and end as well as the peak of the summer flood season. The temporal trajectory of these three indicators is given in Fig. 4.11. The flooding season starts between DOY (day of the year) 124 and 155 (May 4 and June 4 respectively), in median on DOY 140 (May 20). The end of the flooding season varies between DOY 233 (August 21) and DOY 261 (September 18). The median is DOY 247 (September 4). The annual peak has a higher variability with the earliest time at DOY 135 (May 15), soon after the start of the flooding season. The latest time is on DOY 235 respectively on August 23. All indicators of the flood timing undergo a slight,

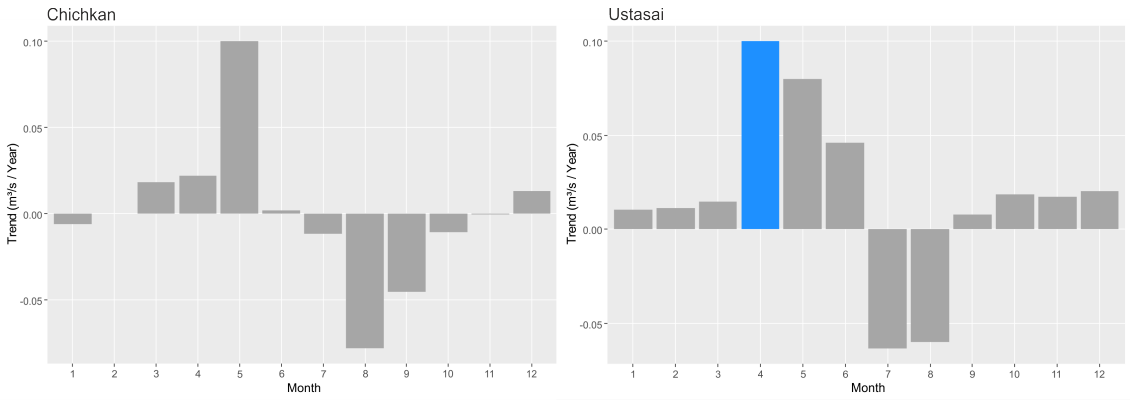


Figure 4.8: Seasonal trends of the gauges Chichkan and Ustasai; blue bars indicate trends significant under the 5% confidence level

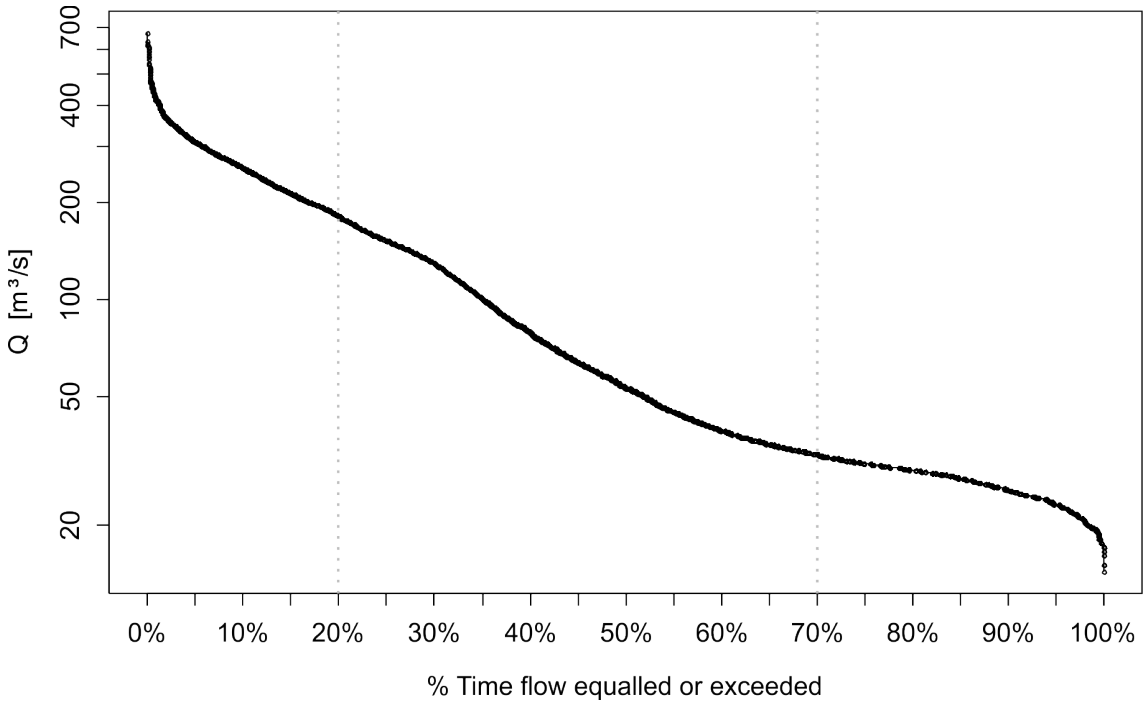


Figure 4.9: Flow duration curve for the gauge Naryn City for the period from 1988 to 2017

non-significant trend. Table 4.4 summarizes the trend estimation. From the trend estimation we

Table 4.4: Trend characteristics of the timing indicators of the annual floods

| Indicator | Min (DOY) | Max (DOY) | Median (DOY) | Sen slope | Trend | P-Value |
|---|---|---|---|---|---|---|
| Season Start | 124 | 155 | 140 | -0.342 | -9.9 | 0.374 |
| Flood Peak | 135 | 235 | 181 | 0.623 | 18.1 | 0.295 |
| Season End | 233 | 261 | 247 | 0.294 | 8.5 | 0.213 |

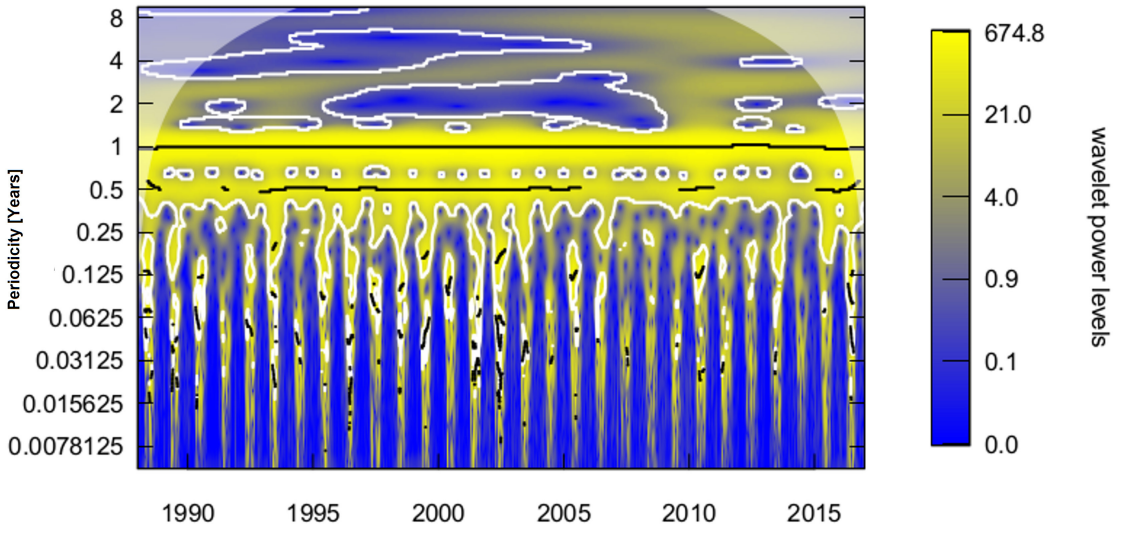


Figure 4.10: Wavelet power spectrum of the discharge series of the gauge Naryn City

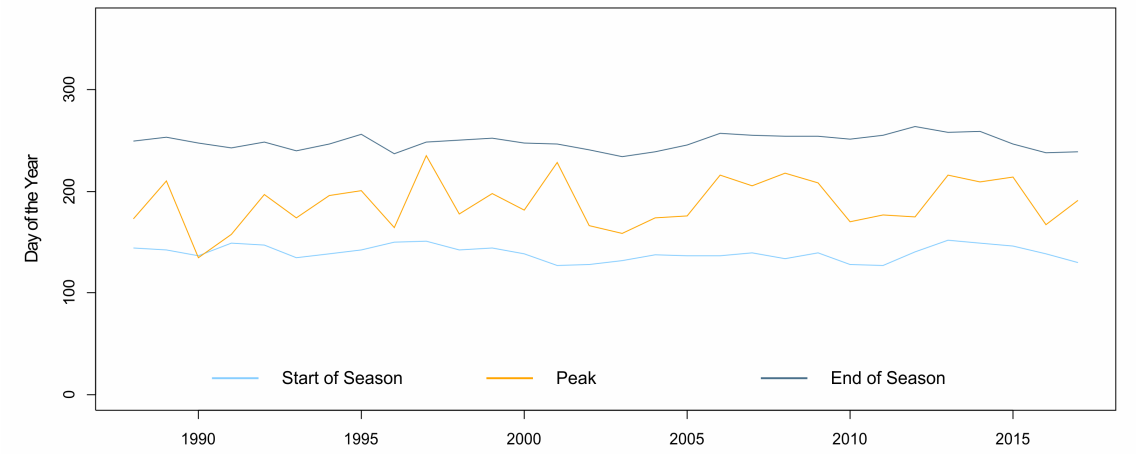


Figure 4.11: Temporal trajectory of the day of the year for the start, peak and end of the flooding season

see, that the start of the flooding season tends to begin almost 10 days earlier at 2016 compared to 1988. Similar, the end of the season tends to be later by 8 days. Thus, the flooding season tends to become longer over time even if there is no statistically significant evidence (yet) for this fact. The annual flood peak also tends to be later over the time observation period. However, it is highly variable with the earliest date in May and the latest date in August.

### 4.3.4 Flood recurrence interval estimation

The generalized extreme value distribution is a good representation of the empirical distribution of the annual discharge maxima of the Naryn River. Figure 4.12 shows a comparison of the empirical cumulative distribution of the annual maxima in the time series with the values derived from the fitted GEV distribution. In addition to the graphical assessment of the goodness-of-

fit, a Kolmogorov-Smirnov p-value of 0.5519 supports the successful fitting. The parameters of

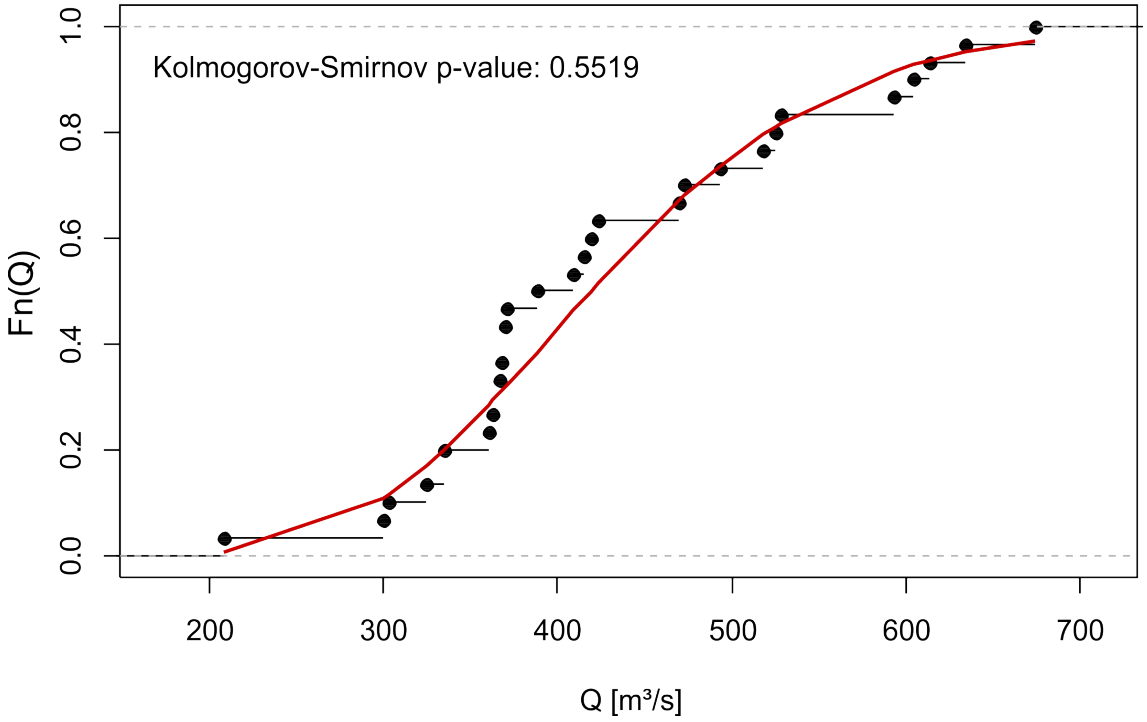


Figure 4.12: Comparison of the empirical cumulative distribution (black dots) of the annual discharge maxima for the gauge Naryn City with the values derived from the fitted generalized extreme value distribution (red line)

the fitted distribution are 0.1227714 for $\xi$, 97.6377614 for $\sigma$ and 384.3179243 for $\mu$ (see Pfaff and McNeil 2012 for the formulation of the parameters). After the successful fit, the recurrence intervals of all annual maxima can be calculated and drawn in a frequency-magnitude plot (Fig. 4.13). During the period from 1988 to 2017 no extreme event occurred, the event with the highest magnitude (674 $m^3s^{-1}$) occurred in 2016 and has a recurrence interval of 40.5 years. This absence of extreme events becomes also evident from the time series of annual maxima (Fig. 4.3), where events of similar magnitude could be observed already between 1996 and 2002. In addition to the recurrence intervals of the observed flood events, also the magnitudes of relevant return periods can be estimated. For instance, the median flood event (i.e. the 2-year flood) is widely recognized as the ecologically and geomorphologically relevant bankfull discharge (Wharton, 1995; Barker et al., 2009). The magnitude of the median flood event is at 419.31 $m^3s^{-1}$. Thus, the time where this discharge is exceeded can be considered as period where overbank flows are likely to occur. Also the magnitude of floods with a higher recurrence interval can be extrapolated from the fitted GEV. For instance, the 50-year flood is expected to have 687.02 $m^3s^{-1}$, a 100-year flood 727.49 $m^3s^{-1}$. However, due to the limited length of the time series available for the distribution fitting, an estimation of events with high recurrence intervals is critical and should be handled with caution (Maniak, 2016).

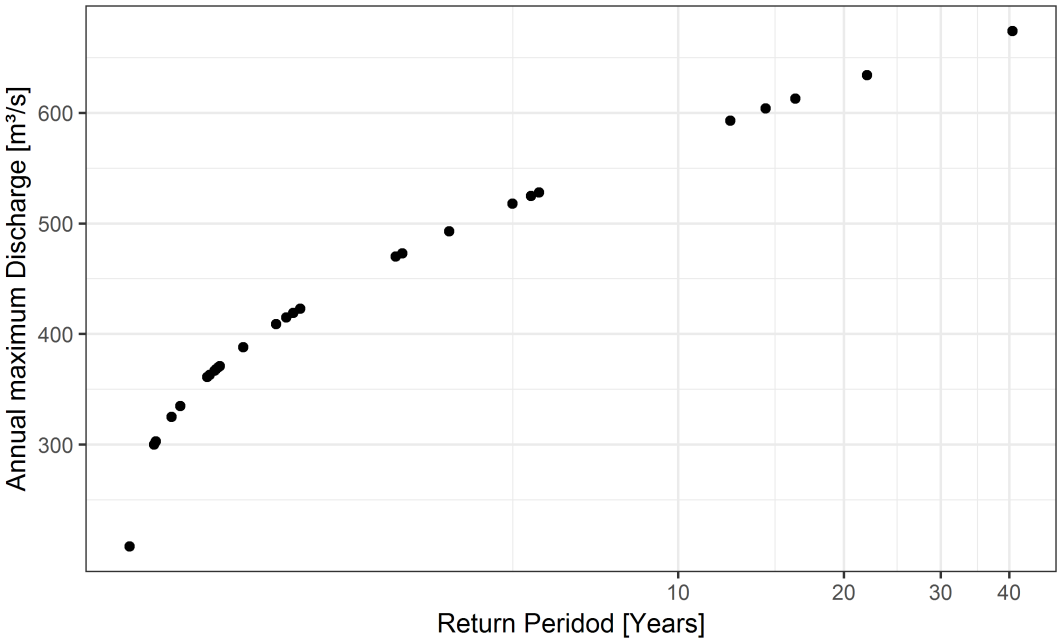


Figure 4.13: Frequency-magnitude plot of the annual maximum discharge of the gauge Naryn City

## 4.4 Evaluating the hydro-climatic setting of the Naryn River

Interpreting the results from the wavelet analysis with the clear annual periodicity (Fig. 4.10) and the flooding season between June and August (Table 4.4) allows to attribute a nivo-glacial to glacial discharge regime to the Naryn River. This in accordance with Kriegel et al. (2013) who analyzed the glacier runoff changes for the entire Naryn catchment. Furthermore, the wavelet power spectrum shows a certain 'flashiness' with sudden discharge variations on a daily time scale. The reason might be the low vegetation coverage and resulting high overland flow during precipitation events. The high suspended sediment loads which could be observed during the field campaigns after rainfall events (Fig. 4.14) support also the hypothesis of high soil erosion rates caused by a low infiltration and a high overland flow. However, up to date this is an assumption rather than a quantitatively supported result.

The dominance of the glacier melt in the runoff generation makes the hydrology of the Naryn catchment sensitive to global climate change. The globally rising temperatures can be observed also at the three climate stations in the Naryn catchment. This will lead to increased melting rates of the glaciers and thus to increased runoff. As soon as the water storage in the glaciers becomes too small, the runoff from the glaciers will decrease and the discharge in the glacier-fed river system is expected to become more unstable depending on the precipitation (Hagg et al. 2007; Sorg et al. 2014; Gan et al. 2015, see also Fig. 4.15). Having the entire Naryn River near the outlet at the Toktogul reservoir in view, the discharge is still increasing and has not reached the tipping point yet. Having a look at the multiple trend analysis (Fig. 4.7) suggests that the increase in discharge has even accelerated towards the end of the observation period. However, in the sub-catchment of the Small Naryn, the discharge already is decreasing even the trend is not statistically significant. Here, the tipping point seems to be crossed and the water storage in the glaciers cannot support the discharge in the Small Naryn anymore. This hypothesis is supported by the monthly trend analysis,

Figure 4.14: High suspended sediment load after precipitation event in Ak Tal - evidence for high overland flow rates?

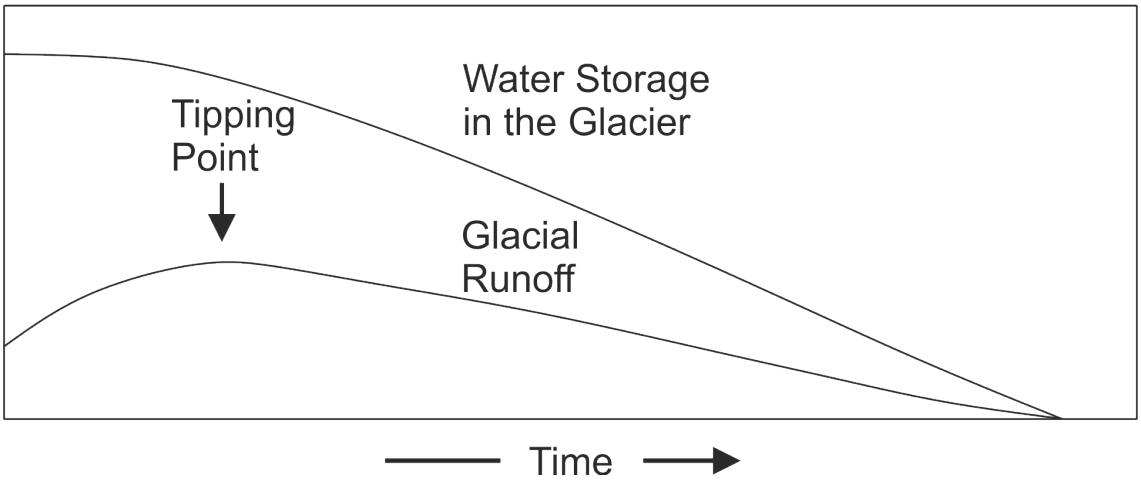


Figure 4.15: Tipping point between increase and decrease in glacier runoff following increased glacier melt (modified from Sorg et al. 2014)

where negative trends exist only during the summer months when the contribution of glacier melt is highest. On the contrary, the summer discharges of the Big Naryn River in the neighboring sub-catchment still show an increasing trend in the summer period (Fig. 4.6). This difference can be explained by a lower glacier share and slightly lower elevation of the Small Naryn catchment (Kriegel et al., 2013). This situation will even be intensified by decreasing summer precipitation. A completely different behavior can be observed at the gauges Chichkan and Ustasai representing sub-catchments with a very low glaciation of 1.31% and 0.83% respectively. On an annual basis, their discharge does not show any significant trend. On a monthly basis, the trends are strongest in spring from March to June rather than in summer. Thus, the observed changes are more likely to arise from changes in snow melt than from changes in glacier water storage. This fits together with the observation of increasing spring temperatures at the nearby climate station Susamyr.

From a flow regime point of view, the gauge in Naryn City is most relevant for the extensive riparian areas in the Central Naryn catchment as Uchterek is influenced by the operation of the Kambar-Ata dam and Kekirim has been shut down in 1996. Despite the longterm annual and seasonal changes observed for this gauge, there are no significant trends of the average as well as the maximum discharge over the study period of this thesis from 1988 to 2016 as proofed for the extreme value statistics in section 4.3.4. However, even the magnitude and frequency of the annual flood pulse have been stable over this period, there was a change in the timing. The flood season tends to begin earlier and end later, even if these trends are not statistically significant (Fig. 4.11, Table 4.4). However, once the critical tipping point is reached where the water storage in the glaciers cannot support the discharge for the flood pulse in summer anymore, the flow regime might change from glacial to nivo-glacial or even nivo-pluvial. This situation is likely to be intensified by the decreasing summer precipitation. While for the Naryn River itself, there is no evidence yet that this tipping point is approached, the Small Naryn River seems to have crossed it already.

In an overall evaluation, I conclude that the flow regime of the Naryn River is still in a natural condition and shows the natural dynamics governed by snow and glacier melt. This system is sensitive to climate change as the increasing temperatures reduce the amount of water storage in the glaciers what is likely to change the hydrological behavior of the Naryn River in a longterm perspective, first evidence already exists. Nevertheless, over the investigation period from 1988 to 2016, there was no significant change in the flow regime. Especially the timing and magnitude of the flood pulse did not change following the generally increasing discharge while instead the flood period becomes longer. Currently, there is no empirical evidence yet how the natural flow regime will adapt to the changing hydro-climatic conditions in the Naryn catchment. Rather than climate change, the plans of the hydropower dams upstream from Naryn City are a relevant threat for the flow regime. Thus, a careful monitoring of the discharge records is needed to improve the general understanding and see potential effects of climate change as well of anthropogenic impacts.

# 5 Field based overview of the Naryn River corridor structure

## 5.1 Introduction

The major interest of this thesis is the scale of river segments to the entire river corridor of the Naryn River (see chapter 1.2 for a definition of scales). Thus, detailed plot scale investigations of vegetation or local geomorphological properties are not the focus. Nevertheless, a field based understanding is required for the interpretation of the remote sensing results. In this chapter, I present the structure of the river corridor of the Naryn River based on four selected reaches distributed within the tectonically formed Naryn Basin between Eki Naryn and Ak Tal (Fig. 2.2). In each of the selected reaches, one representative transect is used for illustrating the basic morphological characteristics as well as the vegetation composition. For the latter, I use the concept of biogeomorphological succession (Corenblit et al., 2007) for structuring the assessment. It is beyond the aim of this thesis to present an in-depth analysis of structure of the river corridor and the floodplain ecosystems based on results from field investigations. Thus, rather than being a detailed quantitative analysis the results in this chapter are seen as descriptive background for the interpretation of the remote sensing analysis.

## 5.2 Data and methods

### 5.2.1 Ecosystem mapping

Two complementary approaches have been applied to assess the structure of the floodplain ecosystems in general and landform representations of the different biogeomorphological succession stages in particular. For the latter one, a total number of 111 field plots have been established each having a size of 30×30 m referring to the size of a single Landsat pixel. The data collection has been conducted in a stratified sampling design using the biogeomorphological succession stages of Corenblit et al. (2007) as strata. Criteria for plot selection has been homogeneity of vegetation and sediment characteristics what did not allow strict stratified random sampling. The criteria for identifying the succession stages in the field are listed in table 5.1. The vegetation composition of the biogeomorphological succession stages has then been assessed based on the number of plots where a certain number of species is occurring. In addition, within each plot, the woody vegetation cover has been estimated following the cover-abundance scheme of Braun-Blanquet (Dierschke, 1994; Wildi, 2017). The Braun-Blanquet cover-abundance values have then been transformed to cover values in percent using transformation values suggested by Tremp (2005). These cover values have been used for a cluster analysis conducted separately for the different succession stages. For clustering, I first computed the Canberra dissimilarity index. In a second step, I used hierarchical clustering with an average agglomeration method to find groups within the data (Legendre and Legendre, 2012; Wildi, 2017). The centroid of each plot has been recorded using a standard GPS device with a horizontal accuracy of approximately 2 m and was later used for calibrating the

Table 5.1: Field mapping indicators for the different biogeomorphological succession stages

| Succession Stage | Indicators |
|---|---|
| Permanently indundated zone | Covered by water during low flow season in early spring |
| Geomorphological Stage | Bare sediment surface; not flooded during the low flow season in early spring |
| Pioneer Stage | Juvenile individuals of woody species on bare sediment surface |
| Biogeomorphological Stage | Woody vegetation beyond the juvenile state; clear dominance of disturbance tolerant species; geomorphic evidence of disturbance like fresh fine sediment accumulation or flood marks; absence of herbal vegetation layer |
| Ecological Stage | Abundance of herbal vegetation layer and species intolerant to disturbance; consolidated sediment body with loamy texture |

remote sensing models. Instream units have not been assessed as they have not been accessible due to the high flow velocity and water depth of the Naryn River.
In addition to these plots, representative transects across four reaches have been mapped to assess the heterogeneity of the river corridor. The choice of the reaches has been made based on the river type but also on the accessibility of the reach. As a consequence of this accessibility requirement, all reaches are within the central Naryn Basin between Eki Naryn and Kazarman. The location of the field study reaches is shown in figure 2.2. Within every reach, a representative transect was chosen spanning the entire width of the river corridor. The elevation along the transects was recorded using a Trimble R8 differential GPS with a vertical accuracy of approximately 10 cm and a horizontal accuracy of below 0.5 m. The length of the transects varies between 290 m in Eki Naryn and 4,474 m in Ak Tal. The biogeomorphological succession stages of Corenblit et al. (2007) have been used for a stratification of the transects. Within each strata, the vegetation community has been categorized based on the dominant woody species and the Braun-Blanquet cover-abundance codes assessed for a representative 30×30 m plot within each stratum. In addition, the sediment characteristics have been assessed using the German soil mapping guideline (*'Bodenkundliche Kartieranleitung'*, AG Boden 2005) as framework. The thickness of the fine sediment layer has been determined as well.

### 5.2.2 Channel classification

The geomorphological channel classification is based on the interpretation of the planform characteristics analyzed based on high resolution *Google Earth* imagery and the channel gradient derived from the SRTM-1 DEM obtained in 2000 (see also chapter 6.2.4). For the planform characterization, I follow the approach suggested by Rinaldi et al. (2016) and Fryirs and Brierley (2013). In a first step, the confinement is determined based on the terminology of the *Riverstyles* framework (Fryirs et al., 2016). In a second step, the channel was separated into single- and multi-thread channels according to Rinaldi et al. (2016). The active channel width has been calculated as the average of ten measurements on the *Google Earth* imagery acquired in 2019. Then, the braiding index and the anabranching index are obtained from the imagery to have a quantitative measure of braiding intensity. The braiding index is calculated as the average number of channels separated by bars along 10 cross-sections in the reach spaced by the distance of active channel width (Egozi

and Ashmore, 2008; Rinaldi et al., 2016). The anabranching index is calculated in the same way just counting channels separated by vegetated islands (Rinaldi et al., 2016). Finally, a channel type is assigned to each study reach following the terminology of the *Riverstyles* framework.

## 5.3 Results

### 5.3.1 Channel classification and vegetation characterization along transects

The results from the geomorphological characterization of the field sites is summarized in table 5.2. The site in Eki Naryn is a special case as it is the only single-thread channel within the studied reaches. This site is confined by the hillslopes of the valley margin (see also Fig. 5.1 and 5.2) and has a small active channel width of 57.3 m only. A steep gradient and a braiding and anabranching index of 0, i.e. the absence of instream bars, as well as the proximity of hillslopes and channel characterize this reach as steep headwater. Under these conditions, it is hard for riparian vegetation

Table 5.2: Geomorphological characterization of the field sites; $W_{AC}$ is the active channel width, $B_I$ is the braiding index, $A_I$ the anabranching index

| Site | Confinement | Channel | Gradient | $W_{AC}$ | $B_I$ | $A_I$ |
|---|---|---|---|---|---|---|
| Eki Naryn | confined | single-thread | 0.00602 $mm^{-1}$ | 57.3 m | 0 | 0 |
| Ak Talaa | confined | multi-thread | 0.00494 $mm^{-1}$ | 134.2 m | 2 | 0 |
| Emgek Talaa | partly confined | multi-thread | 0.00391 $mm^{-1}$ | 257.4 m | 3.053 | 1.8 |
| Ak Tal | unconfined | multi-thread | 0.00255 $mm^{-1}$ | 823.1 m | 7.643 | 2.091 |

to establish. As a consequence, there is a lack of the pioneer and biogeomorphological succession stage at the Eki Naryn site (Fig. 5.1 and 5.2). The geomorphological stage at the channel margin is characterized by boulders without fine sediment. The zone between channel margin and hillslope is covered by *Juniperus spp.* (2), *Picea schrenkiana* (+), *Rosa spp.* (+), *Salix spp.* (1) and *Hippophae rhamnoides* (+). The understory is formed by diverse grass species resulting in a total coverage of 40-60%. The hillslope vegetation varies between the river banks. On the north-


Figure 5.1: Oblique photograph of the Eki Naryn field site showing the distribution of the biogeomorphological succession stages and the adjacent hillslope

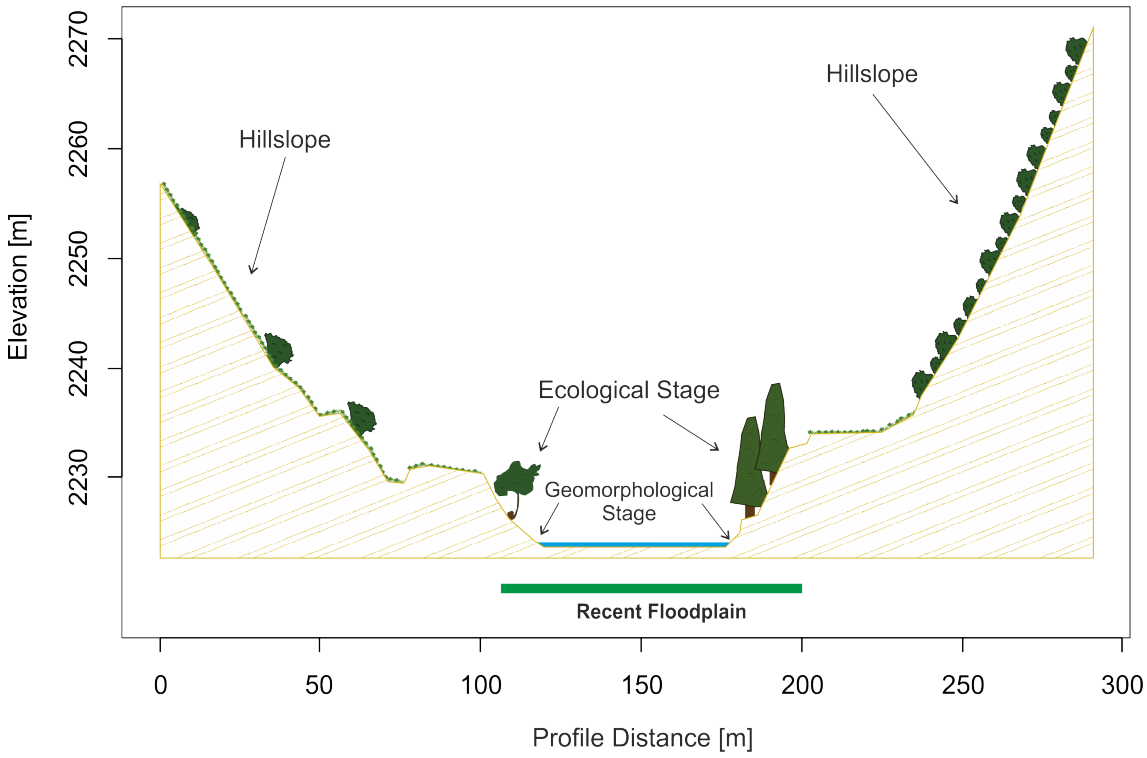


Figure 5.2: Transect across the Eki Naryn field site

exposed slope a dense coverage of *Juniperus spp.* (3) and *Rosa spp.* forms the vegetation (right margin in Fig. 5.1 and 5.2). On the contrary, the south-exposed slope has a smaller coverage with woody vegetation. The only shrub species which occurs is *Juniperus spp.* (+).

The field site in Ak Talaa shows also a confined valley setting. Contrary to Eki Naryn, this site is not confined by hillslopes but terraces. Furthermore, a floodplain pocket characterizes the site (5.3 and 5.4). In addition, also instream bars exist (braiding index=2) making Ak Talaa a multi-thread channel reach. The reason might be the smaller gradient of 0.00494 $mm^{-1}$ compared to Eki Naryn. With 134.2 m, the active channel width is considerably wider. In this setting, all biogeomorphological succession stages occur. The geomorphological stage occurs in form of gravel bars directly at the margin of the Naryn River as well as along the characteristic flood channel. On these gravel bars, pioneer vegetation sites exist with juvenile individuals of *Salix spp.* and *Populus spp*. Vegetation in the biogeomorphological succession stage exists predominantly on a point bar attached to the floodplain pocket (foreground in Fig. 5.3). Dominating species within the vegetation patch on the bar are *Populus nigra* (II), *Salix spp.* (2) , *Hippophae rhamnoides* (r) as well as *Tamarix spp.* (r). While the sedimentary body of the geomorphological and pioneer stage is made up of gravel with a matrix of sand, the biogeomorphological stage shows a stratigraphy of the gravel basis overlain by a 26 cm thick layer of loamy sand and a 4 cm thick top layer of sand. Within the ecological succession stage, different vegetation types occur on the southern (background in Fig. 5.3 resp. right side in Fig. 5.4) and northern river bank. On the southern bank, groups of *Populus nigra* (1) occur along with *Tamarix spp.* (+) and ground vegetation consisting of *Artemisia spp.* (2). The sediment stratigraphy in this setting is composed by the gravel basis overlain by a 25 cm thick layer of loamy sand. In the ecological stage of the northern river bank,

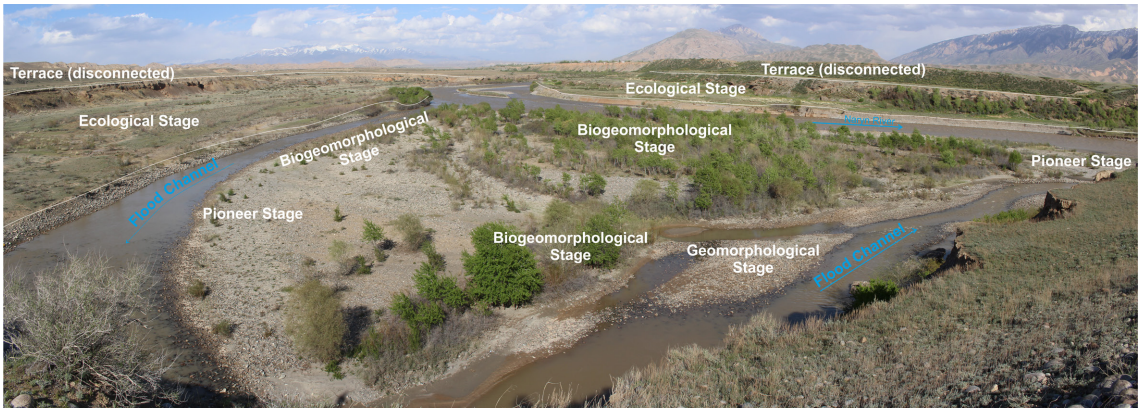


Figure 5.3: Oblique photograph of the Ak Talaa field site showing the distribution of the biogeomorphological succession stages

woody vegetation is scarce. Directly adjacent to the flood channel, there is a patch of *Tamarix spp.* (1) with a understory of *Artemisia spp.*. In further distance to the flood channel, *Artemisia spp.* becomes the dominant species (2). The only existing shrub is *Caragana spinosa* (+). The underground is similar to the southern river bank and is made up of a layer of loamy sand with a thickness up to 70 cm.

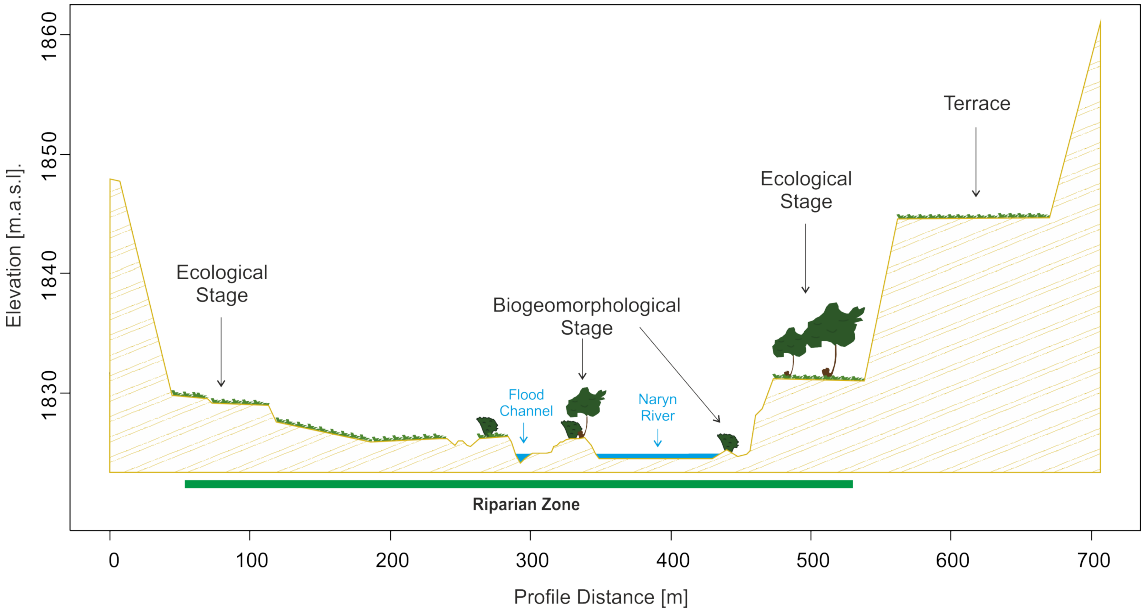


Figure 5.4: Transect across the Ak Talaa field site

The reach where the Emgek Talaa field site is located is partly confined by terraces (see Fig. 5.5 and 5.6). The average active channel width is 257.4 m, the gradient is 0.00391 $mm^{-1}$. With a braiding index of 3.053, the reach has clearly a multi-thread channel. In addition, an elongated island covered with vegetation leads to an anabranching index of 1.8 (see Fig. 5.5). Similar to Ak Talaa, the biogeomorphological succession stages are arranged in a sequence from the channel to the floodplain. The geomorphological stage is formed by instream and bank attached gravel

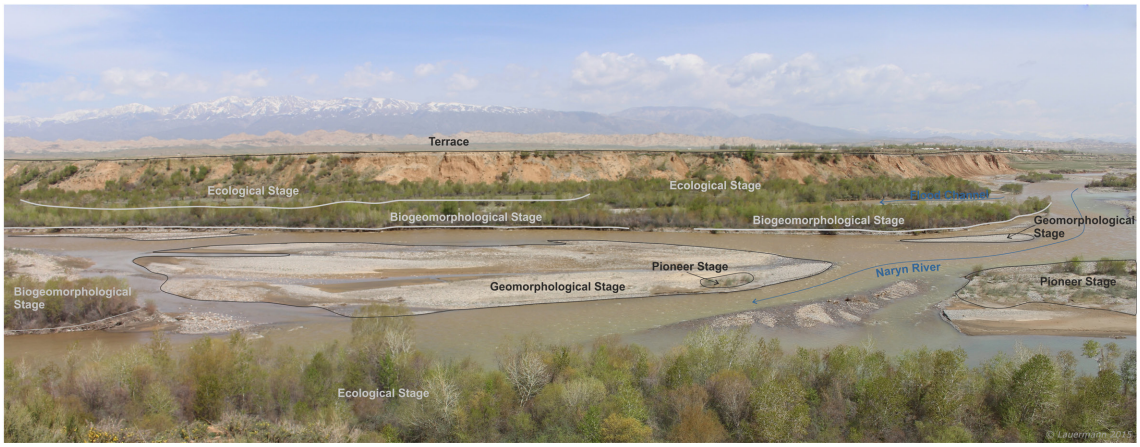


Figure 5.5: Oblique photograph of the Emgek Talaa field site showing the distribution of the biogeomorphological succession stages

bars (Fig. 5.5). On the gravel bars, patches with juvenile individuals of *Populus spp.*, *Salix spp.*, *Hippophae rhamnoides spp.* and *Tamarix spp.* form the pioneer stage of the biogeomorphological succession. The biogeomorphological stage is formed by dense patches of *Salix spp.* (1), *Salix babylonica* (1), *Populus nigra* (+) and *Hippophae rhamnoides* (1). The sedimentary body developing within this succession stage is composed by a sand layer with a thickness up to 2 cm above the gravel basis. However, due to the high flow velocity, the instream bars have not been accessible for investigation. Thus, the information about the geomorphological, pioneer and biogeomorphological succession stages arise from bank attached bars and details about the instream units are missing in the transect (Fig. 5.6). The ecological stage is characterized by an interplay of forested patches and open spaces (see Fig. 5.5). Dominating tree species is *Populus nigra* (1) along with further poplar species interpreted as hybrids of *Populus nigra* (r). In addition, different shrub species exist among them *Tamarix spp.*, *Rosa spp.*, *Berberis vulgaris* and *Caragana spinosa* (+). The understory within the ecological succession stage is dominated by *Artemisia spp.* (3-4) along with further herbaceous species. The sediment body of the ecological stage is formed by a layer up to 1 m thickness composed by loamy sand and loamy silt above the gravel basis. In addition, first stages of soil formation like humus accumulation in the top layer is observable.
The fourth field site is located in Ak Tal in a laterally unconfined valley setting leading to a much wider active channel (823.1 m). The channel gradient is the smallest of all investigated sites with a value of 0.00255 $mm^{-1}$. The gradient along with the unconfined valley setting might be the reason for the high braiding and anabranching indices of 7.643 and 2.091 respectively. This wide riverine landscape makes it difficult to see the different succession stages on the oblique photograph in Figure 5.7. Nevertheless, it becomes clear that there is a mosaic of patches in different succession stages within the active channel including bar gravel bars, densely vegetated sites as well as islands (Fig. 5.7). Similar to the other field sites, the geomorphological succession stage is characterized by gravel bars, partly covered with sand. The pioneer stage is formed by patches of juvenile *Populus spp.*, *Salix spp.*, *Hippophae spp.* and *Tamarix spp.*. In the biogeomorphological stage, *Hippophae rhamnoides* (3) is the dominating woody species along with *Salix spp.* (1), *Salix babylonica* (1), *Tamarix spp.* (+) and *Populus nigra* along with different hybrid poplar species (+). The sediment stratigraphy of this succession stage is dominated by a massive layer of loamy sand and sand with a thickness of up to 120 cm over the gravel basis. In the ecological stage, there are

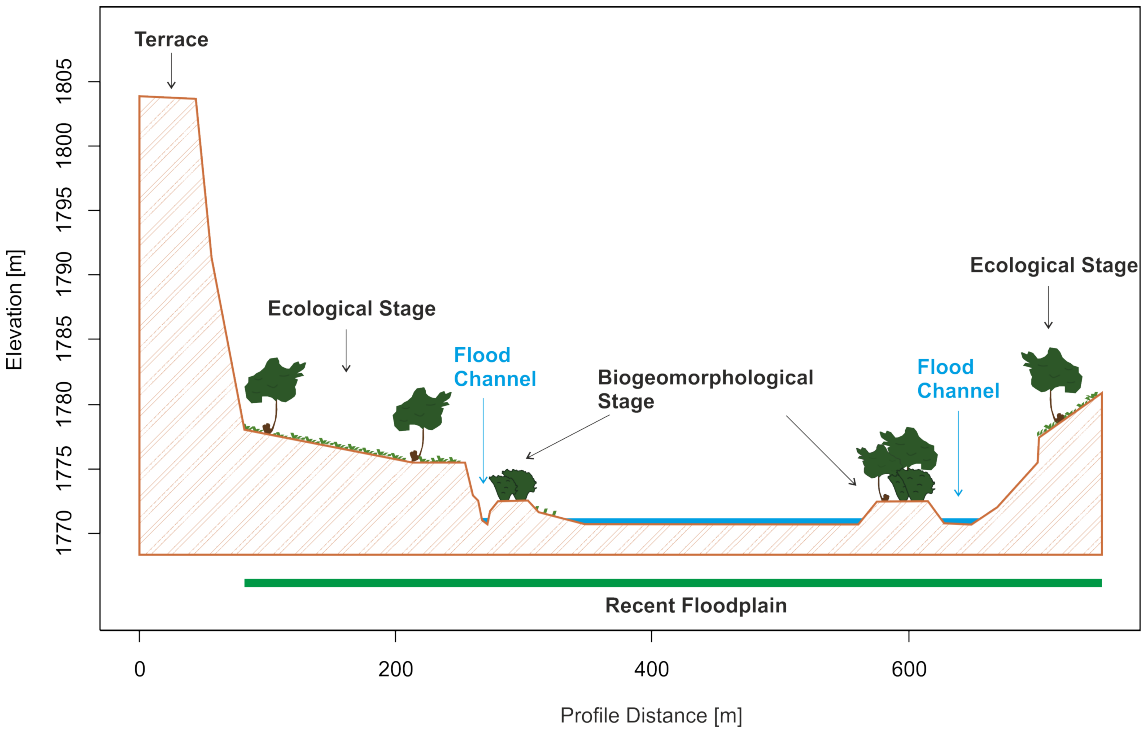


Figure 5.6: Transect across the Emgek Talaa field site

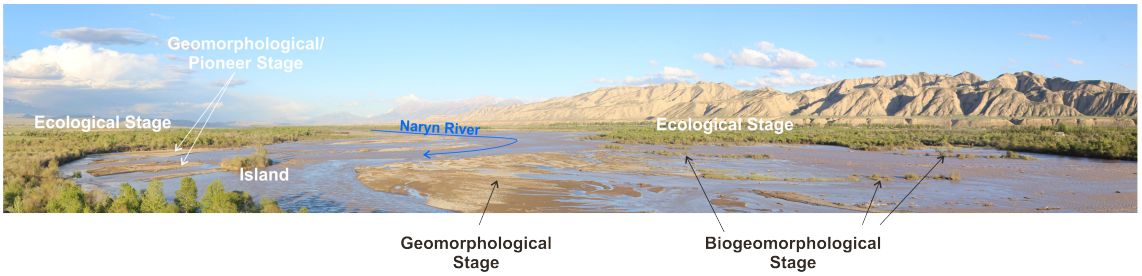


Figure 5.7: Oblique photograph of the field site in Ak Tal showing the different biogeomorphological successions stages

different types of forest and shrub cover over an understory of *Artemisia spp.* and other herbaceous species. The first type is composed of *Populus nigra* (2), *Tamarix spp.* (+), *Eleagnus angustifolia* (+), *Salix babylonica* (1), *Caragana spinosa* (+) as well as *Lonicera spp.* (r). A second type is composed of *Populus nigra* and other hybridized poplar species (2), *Salix babylonica* (1), *Salix alba* (r), *Berberis vulgaris* (+), *Rosa spp.* (+) and *Lonicera spp.* (r). A third type consists of *Hippophae rhamnoides* (3) along with *Populus nigra* (1) and *Salix spp.* (1). The sediment is less heterogeneous and is characterized by a more than 100 cm thick layer of loamy sand and silt over the gravel basis.

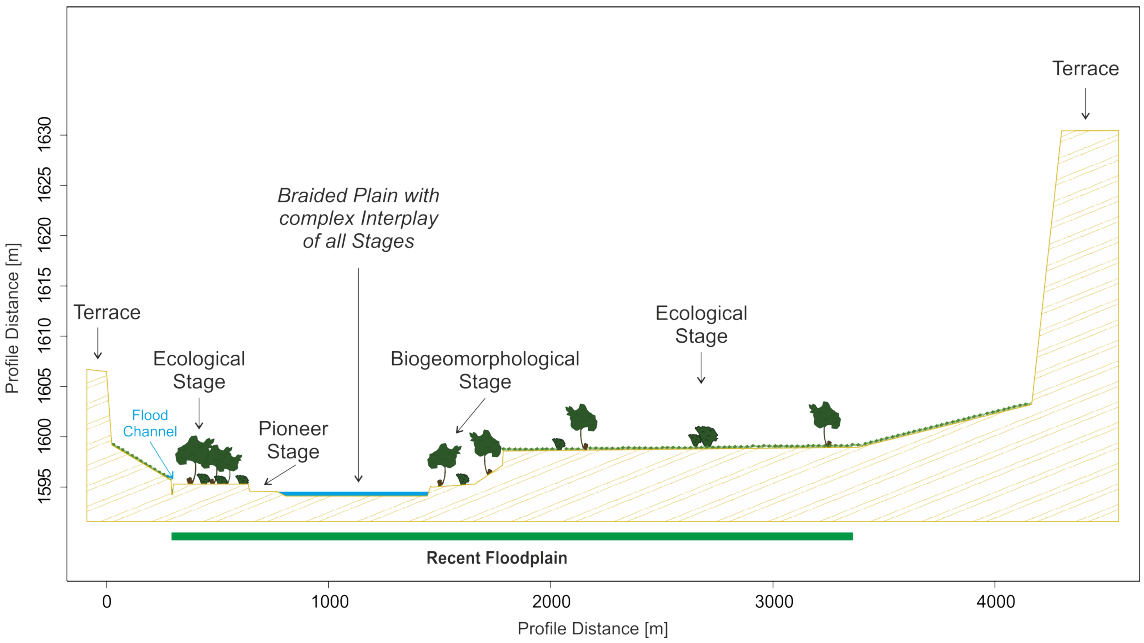


Figure 5.8: Transect across the field site in Ak Tal; Details about the instream units are missing as this part of the transect was not accessible due to the flow velocity of the Naryn River

### 5.3.2 Vegetation composition of the biogeomorphological succession stages

The vegetation composition differs among the different biogeomorphological succession stages. In this section, I focus on the biogeomorphologically relevant phanerophytes along with *Carex spp.* and *Phragmites australis* as further biogeomorphologically relevant plants. Figure 5.9 shows the counts of plots within different succession stages where specific genera are occurring. Within the

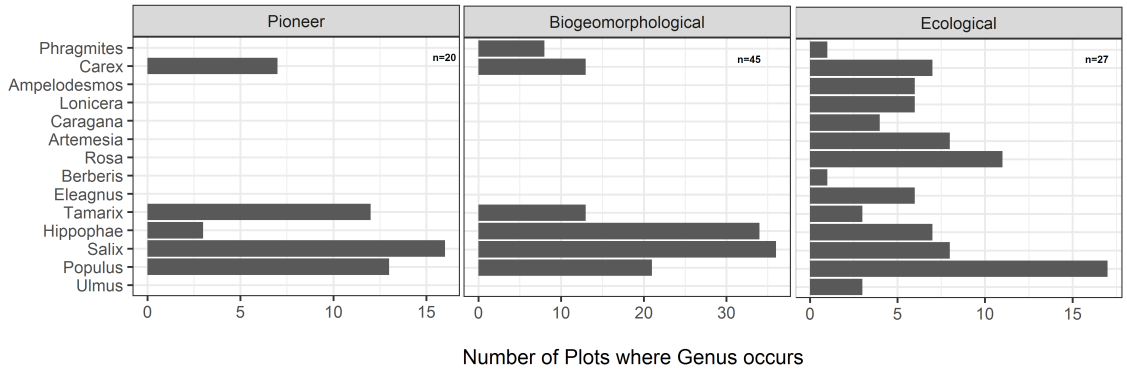


Figure 5.9: Counts of occurences of relevant genera within field plots in different succession stages

pioneer stage, the most frequently occurring genera are *Salix*, *Populus* and *Tamarix* along with *Hippophae*. In addition, *Carex* appears within plots in this succession stage. Further herbaceous genera are widely absent. In the biogeomorphological stage, still *Salix* is among the most frequent genera closely followed by *Hippophae*. Furthermore, *Populus* and *Tamarix* occur in a high number of plots. A relevant number of plots is also covered by *Carex* and/or *Phragmites*. Within the

ecological stage, the situation gets more complex. Still *Populus* is the most relevant genus. However, contrary to the pioneer and biogeomorphological stage also less flood disturbance tolerant genera. Among them, *Rosa* and *Artemisia* are the most frequent genera. Additionally, there are a range of further genera of phanerophytes relevant for the floodplain ecosystems along the Naryn River. The results of the cluster analysis reveal further insights in the structure of the riparian ecosystems (Fig. 5.10). Both - the vegetation in the pioneer stage and the biogeomorphological stage show two major groups divided into several subgroups. A closer look into the vegetation composition within these major groups shows that they stand for a wood series and a reed series in the biogeomorphological succession. While the wood series is split into a wide range of different vegetation types, the structure of the reed series is less complex. However, for a closer view into the structure of the subgroups more detailed field data is required and will be a task for future research in the Naryn floodplain research. The succession stages are associated with specific sedi-


Figure 5.10: Cluster analysis of the cover-abundance assessment of genera for the different biogeomorphological succession stages

ment types. Plots in the pioneer stage are mainly characterized by gravel surfaces, especially in the wood series. In the reed series, the plots tend to be associated with thick deposits of sandy-loamy sediments. In the biogeomorphological stage, sand deposits are likely to occur in the wood series while the reed series are still associated with thick sandy-loamy sediments. The ecological stage is characterized by typical floodplain sediments of a loamy layer of 0.5-2 m over a gravel surface.

## 5.4 Generalizing the information across the different field sites

Despite the different geomorphological settings of the four field sites, they share several common properties regarding the biogeomorphological succession stages. The geomorphological stages at all sites is composed by gravel bars, an indicator of the relatively high energy in the fluvial system, even the gradients show a decreasing trend from Eki Naryn to Ak Tal. For the pioneer

stage, small scale variations in grain-size, soil moisture and disturbance susceptibility are more relevant for the occurrence of juvenile phanerophytes than the location along the longitudinal profile as demonstrated by the master thesis of Rauschenberger (2016). An exception is the site in Eki Naryn, where no pioneer and biogeomorphological successions stage could be observed. *Salicaceae* are the relevant species family for the biogeomorphological succession stage. In addition, *Tamarix spp.* and especially *Hippophae rhamnoides* are relevant for biogeomorphic feedbacks of the fluvial system of the Naryn River. In the ecological stage, different vegetation communities occur with notable differences between the four field sites. On the Eki Naryn site, mountain species like *Picea schrenkiana* and *Juniperus turkestanica* are abundant in the ecological stage of the biogeomorphological succession. On the contrary, in Ak Tal, *Eleagnus angustifolia* exists as indicator of a less harsh climate. On all sites except the headwater site in Eki Naryn, most species are - similar to the biogeomorphological stage - of the family of *Salicaceae* (poplars and willows). However, additional shrub species like *Rosa spp.*, *Lonicera spp.* or *Berberis vulgaris* occur along with an understory of different herbaceous species indicating an ecological succession not influenced by the regular flood disturbance anymore. However, the vegetation in the ecological stage shows evidence of anthropogenic disturbance from woodcutting (Fig. 5.11) and grazing. Imanberdieva (2015) interpreted the occurrence of a vegetation type composed of *Artemisia spp.* and *Caragana spp.* as indicator of degradation. This type is also abundant in the ecological succession stage on the field sites in Ak Talaa, Emgek Talaa and Ak Tal. Thus, the geomorphological,

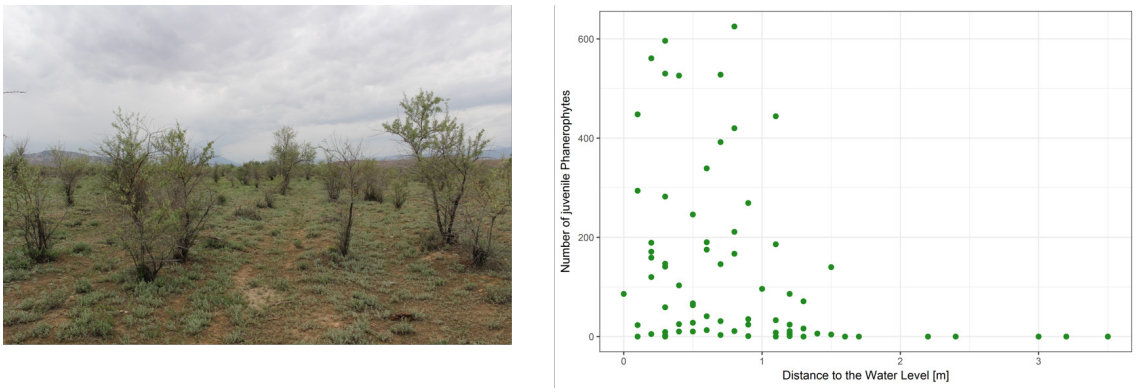


Figure 5.11: Evidence of woodcutting and following regrowth of the trees on the Emgek Talaa field site (l); number of juvenile phanerophytes and their relation to the distance above the active channel (r), data from Rauschenberger, 2016

pioneer and biogeomorphological succession stages can be assumed being in a natural state due to the high, unaffected hydro-morphological dynamics. In the ecological succession stage, however, anthropogenic disturbances have altered the natural structure of the riparian vegetation. Here, the succession governed by ecological processes like the concurrence for light or nutrients have been superimposed by the anthropogenic disturbances in form of woodcutting and livestock grazing. This has consequences for the interpretation of the remote sensing time series analysis. While it is possible to interpret the geomorphological, pioneer and biogeomorphological stage predominantly from a purely biogeomorphological perspective, the human factor is relevant for the development of the ecological succession stage.

# 6 Approaching the riverscape of the Naryn River from space [1]

## 6.1 Large scale characterization of the Naryn River

In this chapter, I present a basic characterization of the Naryn River corridor based on a combination of terrain analysis and multispectral remote sensing. I derive rather simple parameters like the catchment boundaries or the channel network but also more complex ones such as the riparian zone extent or the discrimination between the active channel and the floodplain. To assess the quality of the results, an evaluation of the results is carried out during several steps of the workflow proposed in this chapter. This is a core part of this thesis as to my knowledge so far no comprehensive assessment of the Naryn River corridor is available, neither in the international nor in the Russian scientific literature (where the information on the Russian literature comes from personal communication with my Kyrgyz colleagues Ermek Baibagyshov and Nadira Degembaeva). Beyond filling this research gap for the Naryn River, the approach presented in this chapter might be feasible for large scale characterization of other large rivers as well as it relies on commonly available open access data only.

## 6.2 Methods

### 6.2.1 Datasets used for the river corridor assessment in this chapter

For the river corridor characterization in this chapter, various datasets have been used (see table 6.1 for an overview). For the terrain analysis part, the SRTM-1 DEM has been used. This dataset has a resolution of 1 arcsecond resulting in a pixel size of 24.05 m when projected to UTM. The reported vertical accuracy is 16 m (Farr et al., 2007). However, in narrow river sections the accuracy might be even worse (Schwanghart and Scherler, 2017). SRTM-1 data is available under the public domain from the USGS earthexplorer (`https://earthexplorer.usgs.gov`, last access 2020-12-28). An alternative that has become recently available for the scientific community is the ALOS Global Digital Surface Model, which is also available in a resolution of 1 arcsecond. First tests show that this DEM is likely to outperform the SRTM-1 model regarding its accuracy (Schwanghart and Scherler, 2017). Unfortunately, this dataset was not available yet for Kyrgyzstan when the analysis for this thesis was carried out. For the multispectral analysis, Landsat OLI data has been used. This data is available as surface reflectance values from the espa interface of the USGS (`http://espa.cr.usgs.gov`, last access 2020-12-28).

A limitation is the resolution of the data. To assess the suitability of the intended datasets for the assessment of the Naryn River, the ratio of the active channel or river corridor width and the pixel size is used as a quantitative measure. This ratio should be $\gg 1$, i.e. the features of interest

[1] A shorter version of the remote sensing based characterization of the Naryn River has been published as Betz et al., 2020.

Table 6.1: Spaceborne datasets used for the river corridor characterization in this chapter and their main characteristics

| Dataset | Data Type | Spatial Resolution | Year of Acquisition |
|---|---|---|---|
| SRTM-1 | Elevation Data | 24.05 m | 2000 |
| Landsat | Multispectral Data | 30 m | 2015 |
| Google Earth | RGB images | 0.5-15 m | various |
| Bing Maps | RGB images | 0.5-15 m | various |
| Yandex Maps | RGB images | 0.5-15 m | various |

should have a width considerably larger than one pixel (Legleiter and Fonstad, 2012). Figure 6.1 shows the ratio of the active channel and the river corridor width and the pixel size of 30 m used for the large scale assessments in this thesis. The minimum for the active channel ratio is 2.25 and 4.88 for the river corridor width respectively. These values as well as the median ratios of 17.10 for the active channel and 36.75 for the river corridor indicate that a pixel size of 30 m is suitable for analyzing the corridor of the Naryn River. However, in the most narrow sections (which are located in the headwaters) only two pixels cover the active channel and limits the explanatory power of the 30 m resolution datasets for the headwater section of the Naryn River.

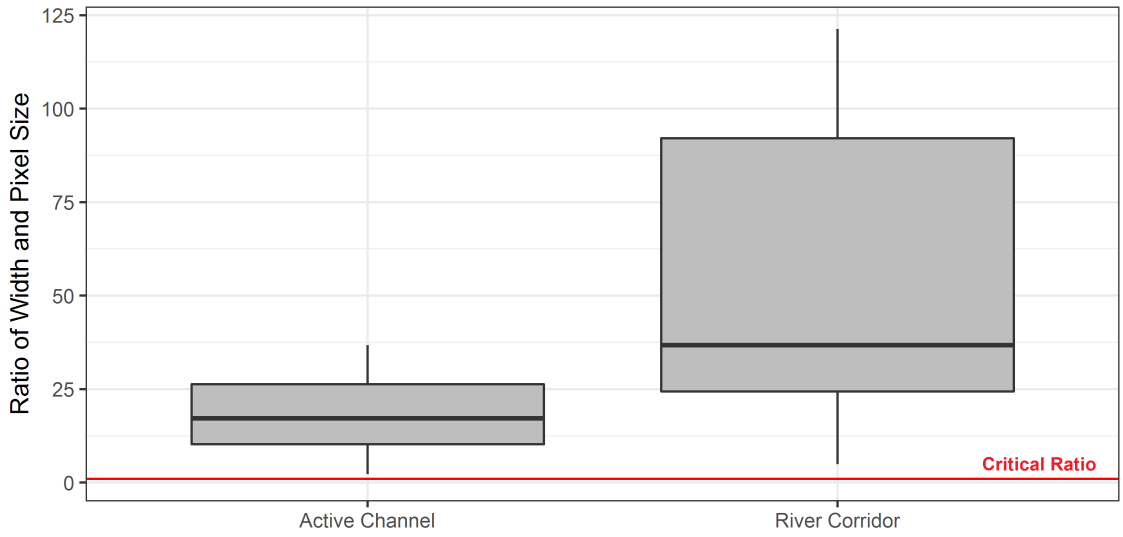


Figure 6.1: Ratios of river corridor features and Landsat's pixel size of 30 m measured for 50 random points along the Naryn River; the condition of a ratio $\gg 1$ is fulfilled for the entire river corridor width as well as for the active channel width at all points

### 6.2.2 Methodological overview of the remote sensing based assessment

Figure 6.2 shows an overview of the workflow used for the remote sensing based assessment of the river corridor along the Naryn. There are four sources of input data: the digital elevation model, the multispectral satellite imagery, discharge data of 18 gauges throughout the Naryn catchment

(see chapter 4) and imagery from different virtual globes. The DEM is used for delineating the

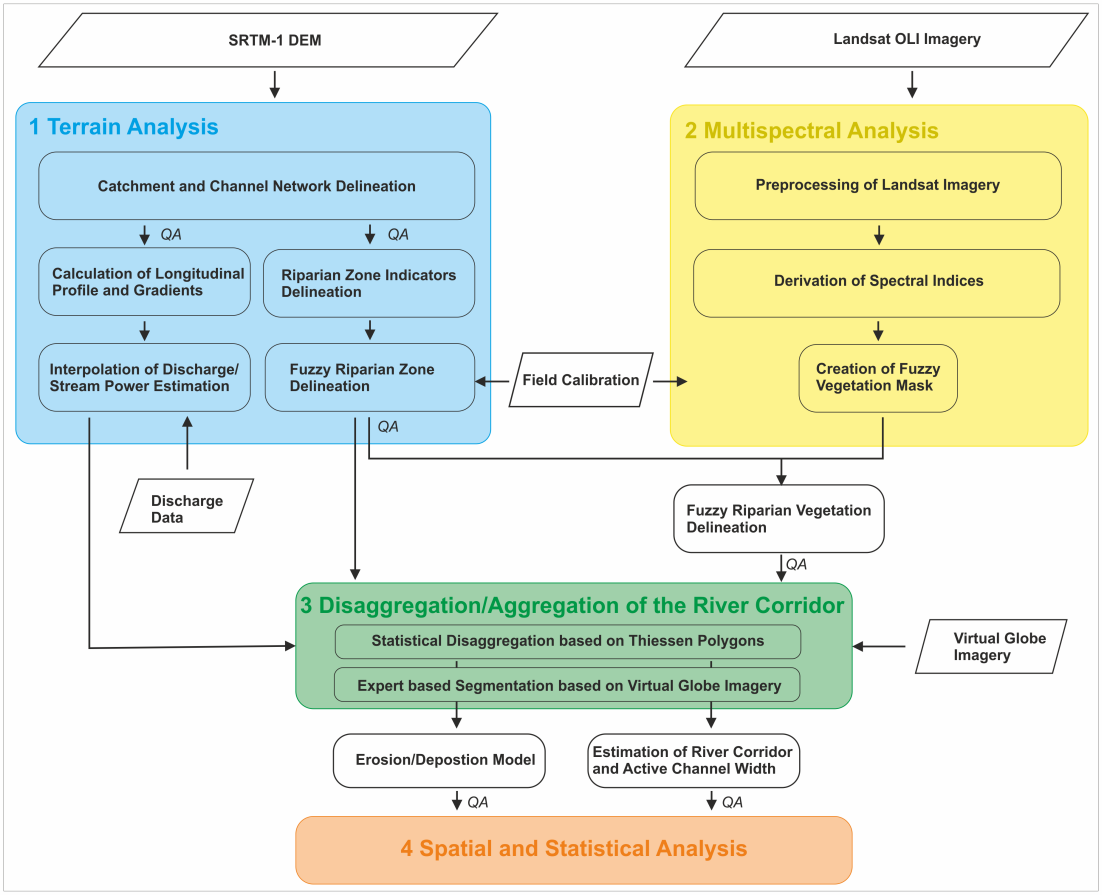


Figure 6.2: Simplified workflow for the remote sensing assessment of the river corridor along the Naryn River; QA stands for quality assessment and gives the location in the workflow where an evaluation of the results is conducted

catchment and the channel network (section 6.2.3). The channel line of the Naryn River extracted from this channel network is the basis for extracting the longitudinal profile including the channel gradients. In combination with the statistics from the discharge data, it is possible to interpolate the discharge for the entire channel network and estimate the stream power as measure of available energy in the system (section 6.2.5). The channel line is also input for diverse indicators used for the delineation of the riparian zone along the Naryn River based on a fuzzy logic model (along with calibration data from the field). As this is among the most crucial analysis steps in this thesis, extensive tests and validation is performed. The multispectral imagery process chain (section 6.2.7) starts with a preprocessing of the imagery. In a next step, the tasseled cap angle as relevant spectral index has been calculated. Based on this and field calibration, a vegetation mask is computed based on a fuzzy membership function. Combining the multispectral masks with the riparian zone mask in a fuzzy logic approach allows the estimation of the extent within the riparian zone covered with vegetation, water or bare earth.
In a next step, the entire river corridor is organized into segments based on a disaggregation/ag-

gregation framework. First, the entire corridor is split into segments of 100 m length representing a longitudinal continuum. In a second step, the segments are aggregated again to homogeneous reaches with similar planform characteristics based on a visual interpretation of virtual globe imagery (section 6.2.12). The disaggregated 100 m segments are then also the basis for an estimation of the river corridor as well as active channel width along with a confinement index. The homogeneous reaches are used for creating a simple, stream power based erosion/deposition model. All results are used for further spatial and statistical analysis of the river corridor of the Naryn.

### 6.2.3 Catchment and channel network delineation

Catchment area and channel network are among the most intuitive features of the fluvial system (Alber and Piégay, 2011; Roux et al., 2015). From a GIS and remote sensing perspective, it is crucial to obtain a realistic representation of these features and get an idea about the related uncertainty (Schwanghart and Heckmann, 2012). The derivation of catchments and channel networks from digital elevation models has meanwhile become a standard task in geomorphometry. Nevertheless, the underlying DEMs contain various sources of error such as spikes or depressions (Metz et al., 2011; Schwanghart and Heckmann, 2012; Schwanghart and Scherler, 2017). These DEM errors cause problems in the flow routing when computing the drainage direction or the flow accumulation. A common way to overcome this issue is to fill sinks in the DEM and to route through the 'hydrologically corrected' DEM (Planchon and Darboux, 2002; Wang and Liu, 2006). An alternative way to handle depressions and spikes in digital elevation data is to use a least cost path algorithm and conduct the flow routing through the unmodified DEM (Metz et al., 2011). Previous research described significant accuracy issues of the sink filling method when delineating river channels (Hengl et al., 2009; Metz et al., 2011; Lauermann et al., 2016; Betz et al., 2018). However, sink filling is still widely used and the accepted standard methods in many workflows. Thus, sink filling was tested against the least cost path channel delineation for the Naryn river. This testing arises from a work carried out together with Magdalena Lauermann and is described in full detail in Lauermann et al. (2016) and Betz et al. (2018). First, the flow accumulation has been computed for the SRTM-1 DEM hydrologically corrected by the algorithm of Wang and Liu (2006). Afterwards, the channel network has been extracted from the flow accumulation grid using values derived from channel heads which have been digitized from Soviet military maps to estimate the initiation threshold (see Lauermann et al. 2016 for full details). The sink filling and the channel network derivation have been conducted in SAGA GIS (Conrad et al., 2015). In the next step, a flow accumulation grid has been computed with a least cost path algorithm implemented in the *r.watershed* module in GRASS GIS (Metz et al., 2011). The extraction of the channel network has been conducted with the *r.stream* modules (Jasiewicz and Metz, 2011). From both channel networks, the Naryn River has been extracted. For the quality evaluation, these channel lines have been compared with a channel line digitized from Google Earth. Besides a visual evaluation, the distances of of the delineated river lines to the digitized reference line have been computed. The differences of these distances have been tested for significance using the nonparametric Mann-Whitney test.
For the catchment delineation, I used the GRASS GIS tool *r.watershed* along with *r.stream.basins* to compute the catchment boundaries. These tools work on unmodified elevation data as well. However, for the catchment delineation no quantitative assessment of the effect of sink filling has been conducted. I selected the Toktogul dam as outlet for the catchment computation. After the delineation, the summary statistics of the catchment such as area and elevation distribution have been derived.

### 6.2.4 Longitudinal profile and channel gradients

The longitudinal profile represents the relevant upstream-downstream component in a river system. Many attributes like the channel gradient are measured along the profile. The longitudinal profile is derived from the DEM and the river line by extracting all subsequent elevation values along the channel line and computing the cumulative distance along this line. A direct derivative of the longitudinal profile is the channel gradient $G_n$ respectively the channel slope $S_n$ of a channel segment n (where the gradient is the tangent of the slope). Thus, an intuitive way to compute a channel gradient would be to compute a slope grid in a GIS software (e.g. using the *r.slope.aspect* module in GRASS), extract the values for the channel segment of interest and take the mean of it. Then, the tangent of this mean is the channel gradient in m/m (Eq. 6.1).

$$G_n = \tan(S_n) = \tan(\frac{1}{n}\sum_{i=1}^{n} s_i) \tag{6.1}$$

However, this approach is very sensitive to errors in the underlying elevation data and is only reported here for comparison with the work of Lauermann (2016). An alternative option is the computation of the channel gradient from the longitudinal profile. In this case, the difference of the elevation at the first ($z_1$) and the last point ($z_i$) of a channel segment is taken and divided by the channel length of this segment. The channel segment can be calculated as the difference of the downstream distance of the last ($d_i$) and the first ($d_1$) point in the segment (Reinfelds et al., 2004; Barker et al., 2009):

$$G_n = \frac{\Delta z}{\Delta d} = \frac{z_1 - z_i}{d_i - d_1} \tag{6.2}$$

However, longitudinal profiles derived from the freely available digital elevation models commonly suffer from artifacts such as spikes or depressions (Reinfelds et al., 2004; Jain et al., 2006; Schwanghart and Scherler, 2017). Furthermore, if any 'hydrological correction' has been performed on the DEM before extracting the channel line, a step like profile might be observed (Schwanghart and Scherler, 2017). Thus, to obtain a realistic representation of the longitudinal profile, it is necessary to apply filter mechanisms to remove artifacts and noise from the DEM derived profile and keep at the same time all details like knick points or other discontinuities (Aiken and Brierley, 2013). Various methods have been proposed for smoothing longitudinal profiles like running average, smoothing splines or locally weighted regression. Furthermore, constrained quantile regression has recently been suggested as alternative method (Schwanghart and Scherler, 2017). Table 6.2 summarized different methods for longitudinal profile smoothing.

As the gradient is a crucial parameter and is likely to be influenced by the smoothing of the longitudinal profile, I test different methods against each other to obtain an estimate of the uncertainty. To test for the degree of smoothing, I use the residuals between the original longitudinal profile and the smoothed profile to compute the mean absolute residuals (MAR):

$$\mathrm{MAR} = \frac{1}{n}\sum_{i=1}^{n} |(z_{\mathrm{smooth}} - z_{\mathrm{orig}})_i| \tag{6.3}$$

where $(z_{\mathrm{smooth}} - z_{\mathrm{orig}})_i$ gives the residual at position i and n is the total number of computed residuals. Furthermore, the gradients calculated from the different longitudinal profiles are compared by means of boxplots and the nonparametric Kruskal-Wallis test. However, as no reference data is available e.g. from high resolution LiDAR data, no quantitative statement about the 'best' method

Table 6.2: Methods for longitudinal profile smoothing tested in this thesis

| Algorithm | Short description | Reference |
|---|---|---|
| Running Average | Elevation values are extracted from the DEM and averaged over a certain river length | Hayakawa and Oguchi, 2006 |
| Locally Weighted Regression | Locally weighted regression smoothing is applied to the elevation values along the longitudinal profile | Aiken and Brierley, 2013 |
| Outlier Removal and Interpolation | Downstream elevation values higher than upstream ones are identified as outliers, removed from the profile and then interpolated | Jain et al., 2006 |
| Constrained Quantile Regression | Values are smoothed by constrained quantile regression, where monotonically decreasing values are set as constraint | Schwanghart and Scherler, 2017 |

is possible and the final evaluation depends on experts opinion and a plausibility check.

### 6.2.5 Discharge interpolation and stream power estimation

To obtain the discharge for the entire longitudinal profile, the relationship between the flow accumulation and the discharge has been used. Knighton (1999) suggested a power law of the form $Q = a \times FA^b$ for describing this statistical relationship (where Q is the discharge, FA the flow accumulation and a and b empirical coefficients). For the calculation of the stream power, the 2-year return period flood is used for fitting this relationship as this discharge is assumed to represent the bankfull flow (Wharton, 1995; Barker et al., 2009; Bizzi and Lerner, 2015; Parker et al., 2015). For the Naryn catchment, all in all 18 gauges are available for the interpolation (Table 4.1). All time series have been clipped to the common observation period prior to analysis. Enhanced extreme value statistics for the derivation of the commonly used 2-year flood (Barker et al., 2009; Parker et al., 2015) is not meaningful for monthly discharge series. Thus, I use the median of the annual maximum discharge as approximation. The flow accumulation was calculated along with the channel extraction in GRASS GIS and extracted for the locations of the gauges. Then, a least-square fitting procedure was used to find the parameters a and b for the power law relating flow accumulation and discharge.
To have an idea of the bias introduced by using monthly values for the flood estimation, the gauge Naryn City can be used where daily data is available. For the daily discharge series, the extreme value statistics result in a 2-year flood of 419.2 $m^3s^{-1}$ (see chapter 4). The median of the annual maxima based on monthly averages is 265.97 $m^3s^{-1}$. Thus, using monthly values for calculating the stream power results in lower values. However, as the focus is on the spatial heterogeneity, the absolute values are less relevant than a sound interpolation. Nevertheless, it is necessary to be aware of this bias when comparing the stream power in this thesis with values reported in other studies.
The total stream power $\Omega$ ($Wm^{-1}$) is calculated from the channel gradient s, the unit weight of the

water $\gamma$ (9800Nm$^{-3}$) and the discharge Q (Knighton, 1999; Bizzi and Lerner, 2015). The discharge can be substituted by the flow accumulation FA and the estimated regression coefficients a and b.

$$\Omega = Q\gamma s = aFA^{b}\gamma s \tag{6.4}$$

While the total stream power is a measure of the energy inherent in a fluvial system, the specific stream power is widely recognized as indicator of the force locally available for sediment entrainment and transport (Knighton, 1999; Barker et al., 2009; Bizzi and Lerner, 2015; Parker et al., 2015). Thus, I use it in this thesis as indicator of the erosive forces of the Naryn River. The specific stream power $\omega$ (Wm$^{-2}$) is defined as the total stream power $\Omega$ divided by the active channel width $w_{AC}$:

$$\omega = \frac{\Omega}{w_{AC}} = \frac{aFA^{b}\gamma s}{w_{AC}} \tag{6.5}$$

The total stream power was calculated straightforward from the longitudinal profile derived gradient and the interpolated discharge. For the calculation of the specific stream power, the active channel widths are required which cannot be obtained from medium resolution elevation data directly (Schmitt et al., 2014; Bizzi and Lerner, 2015). I estimate the active channel width based on multispectral remote sensing for the disaggregated river corridor (see section 6.2.12). Based on these estimates, $\omega$ is computed for the 100 m segments of the disaggregated river corridor.

### 6.2.6 Delineation of the riparian zone [2]

*Geomorphological indicator delineation*

All in all six indicators have been tested for their suitability to represent the riparian zone (see table 6.3). In general, two groups of indicators can be distinguished. First, there are indicators for the proximity to the river channel, second their are indicators describing the local morphology of the valley floor. To the first category belongs the horizontal distance to the channel network which

Table 6.3: Indicators used for the delineation of the riparian zone (from Betz et al., 2018)

| Indicator (Abbreviation) | Reference |
|---|---|
| *Proximity Indicators* | |
| Horizontal Distance (HDist) | e.g. Ivits et al., 2009 |
| Vertical Distance above Channel Network (VDist) | Williams et al., 2000 |
| Path Distance Horizontal Distance and Slope (PathDist (Slope)) | Clerici et al., 2013 |
| Path Distance Horizontal Distance and Vertical Distance (PathDist (Vertical)) | this study |
| *Morphological Indicators* | |
| Multi Resolution Valley Bottom Flatness Index (MRVBF) | Gallant and Dowling, 2003 |
| Modified Topographic Index (MTI) | Manfreda et al., 2008 |

can be interpreted as simple buffer, a classical method for riparian zone delineation (e.g. Ivits

[2] The fuzzy logic approach for riparian zone delineation has been published as Betz et al. 2018; the methods and results for this topic presented in this thesis are taken in a slightly modified way from this publication

et al. 2009). A second, widely used indicator is the vertical distance above river channel (Williams et al., 2000). More sophisticated is the path distance calculated based on the horizontal distance to channel network and an additional cost factor (Clerici et al., 2013):

$$PD = HDist \times f_c \tag{6.6}$$

where HDist is the horizontal distance to the river channel and $f_c$ is the cost factor. Clerici et al. (2013) suggest to use the local slope as cost factor assuming that water is more likely to move across lower slope areas. Betz et al. (2018) suggest a modification of this indicator using the vertical distance above the river channel (VDist) as cost factor:

$$PD = HDist \times VDist \tag{6.7}$$

This is based on the assumption, that the connectivity to the river channel is higher if areas are close to the channel and relatively low.
The second group of indicators describe the local morphology of a pixel relative to its surrounding. A wide range of indicators for a quantitative description of the landscape have been developed over the past decades. Following Betz et al. (2018), I use two indicators. First is the multiresolution valley bottom flatness index suggested by Gallant and Dowling (2003). This index assumes that a pixel is more likely to be part of the riparian zone if it is relatively flat and relatively low compared to its surrounding. The algorithm for computing the MRVBF is implemented in the *r.valley.bottom* module in GRASS GIS. A second morphological indicator is the modified topographic index (Manfreda et al., 2008) which is defined as

$$MTI = \ln(a^n \tan\beta) \tag{6.8}$$

with a being the drainage area per unit contour line length, $\beta$ being the local slope and n a constant $< 1$ depending on the resolution of the DEM. The modified topographic index is implemented in the *r.hazard.flood* module in GRASS GIS. This module provides along with the MTI a straightforward binary classification of potentially flooded areas. However, a visual evaluation of this flood map for the field sites at the Naryn River has shown that it does not have the capability to serve as riparian zone indicator for the environmental setting and the available data.

*Fuzzy riparian zone delineation*

As discussed above, fuzzy logic offers a way to overcome the problem of crisp GIS data structures. For the case of the riparian zone, we could assume a pixel with a membership value of 1 as fully connected to the processes in the river channel while a pixel with a membership value of 0 is not connected at all and thus not part of the riparian zone. The main task is to create membership functions for the different riparian zone indicators. I follow the suggestion of Clerici et al. (2013) and use linear as well as inverse linear membership functions with calibration values derived from field mapping (equations 6.9 and 6.10).

$$\mu(x) \begin{cases} 0 & \text{for } x < x_{cal}(min) \\ \frac{x - x_{cal}(min)}{x_{cal}(max) - x_{cal}(min)} & \text{for } x_{cal}(min) \leq x \leq x_{cal}(max) \\ 1 & \text{for } x > x_{cal}(max) \end{cases} \tag{6.9}$$

$$\mu(x) \begin{cases} 1 - (\frac{x}{x_{cal}(max)}) & \text{for } x \leq x_{cal}(max) \\ 0 & \text{for } x > x_{cal}(max) \end{cases} \tag{6.10}$$

where $x_{cal}(min)$ and $x_{cal}(max)$ are the minimum respectively the maximum values the indicators take on the field calibration sites.

*Field calibration*

To obtain the required calibration values $x_{cal}(min)$ and $x_{cal}(max)$, data from field mapping is necessary. Three field sites have been chosen representing typical situations in the central part of the Naryn catchment (see Fig. 2.2). On the Ak Talaa site, the Naryn is deeply incised and the valley is confined by terraces. Consequently, the riparian zone is narrow and characterized by a relatively small floodplain pocket. Emgek Talaa has a partly confined valley setting, the riparian zone is wider compared to Ak Talaa. Furthermore, the braided plain contains bars and islands. However, the terraces characteristic for the central Naryn catchment are still abundant. The Ak Tal site is located in a laterally unconfined valley setting. Consequently, a wide braided plain and adjacent floodplain could develop. The cross sections of all three sites are given in Fig. 6.3.

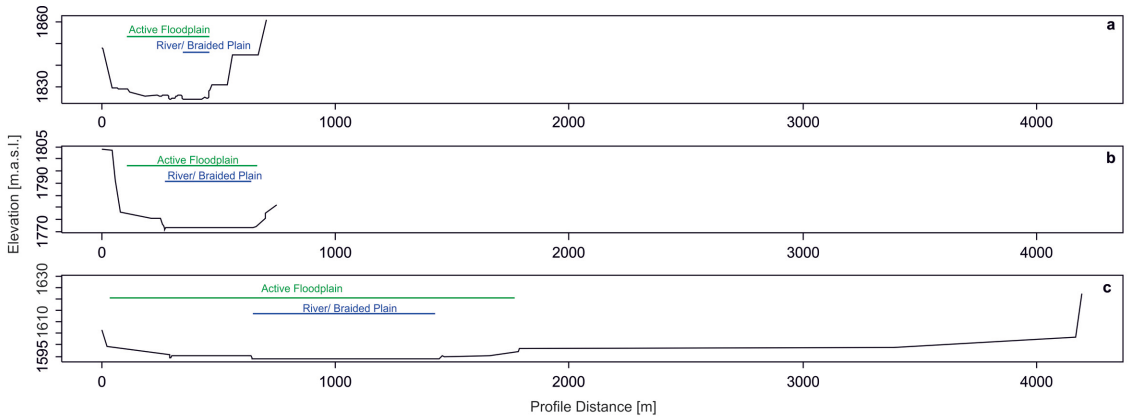


Figure 6.3: Transects across the calibration sites; a: Ak Talaa with a confined valley setting; b: Emgek Talaa with a partly confined valley setting and c: Ak Tal with laterally unconfined valley setting

Within the sites a total number of 111 ground control points have been collected across all biogeomorphological succession zones have. These zones include bare gravel bars within the channel, pioneer vegetation sites, developed vegetation within the active channel as well as points on the adjacent floodplain. After computing the indicators, their values have been extracted at the ground control point locations. Then, the summary statistics have been calculated to obtain the necessary values for $x_{cal}(min)$ and $x_{cal}(max)$.

*Validation*

The validation has been performed in a similar way as suggested by Clerici et al. (2013) using visual validation points. A total number of 250 points have been generated randomly within a 1500 m buffer around the river line of the Naryn River. Every point has been evaluated whether it is part of the riparian zone or not based on the visual interpretation of high resolution Google Earth imagery. For the validation itself, the membership value for the riparian zone membership rasters

have been extracted for the location of the validation points. If the membership value is >0 and the validation point indicates 'riparian zone', then the prediction was correct at this point. Also a prediction with a membership value of 0 and validation point indication of 'not riparian zone' is considered as correct. On the contrary the model is considered as incorrect if the membership value is 0 and the validation point is evaluated as 'riparian zone' or the membership value is >0 and 'not riparian zone' is stated for the point location. In this thesis, also very low membership values are interpreted as 'riparian zone'. These values might be used to tune the model and reduce an overestimation of the riparian zone extent via setting a minimum membership threshold.
For a quantitative assessment, the user's and producer's accuracy are computed. An overall accuracy measure is not meaningful for rare landcover classes like the riparian zone (Boschetti et al., 2004; Clerici et al., 2013). The producer's accuracy is calculated as the percentage of correctly classified validation points. The user's accuracy is calculated as the proportion of the points correctly classified as 'riparian zone' relative to the entire number of validation points predicted as 'riparian zone' (Olofsson et al., 2014). Additionally, the 95% confidence interval for the accuracy metrics has been calculated following the method suggested by Olofsson et al. (2014).

### 6.2.7 Preprocessing of Landsat imagery

To obtain meaningful ecological information from satellite imagery, preprocessing is required. This means, that the raw data stored as Digital Number (DN) in the image needs to be transformed to physically meaningful units (Easmus et al., 2016; Young et al., 2017). Figure 6.4 shows the preprocessing chain of the Landsat imagery used for this thesis.
The preprocessing starts with the geolocation and co-registration of the images. Then, the raw

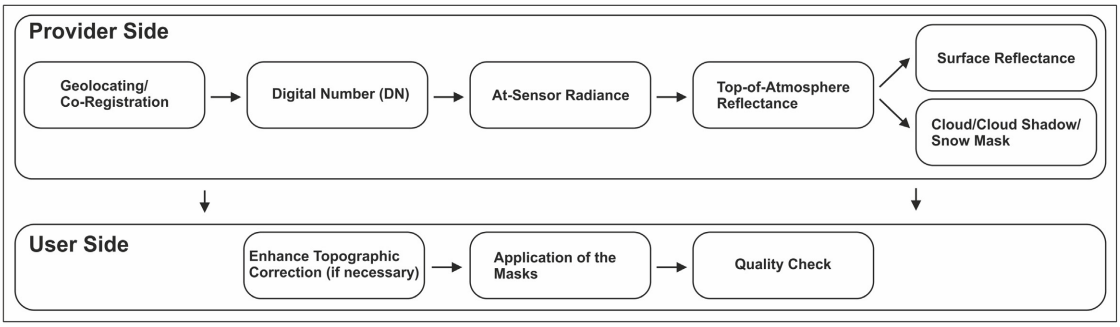


Figure 6.4: Preprocessing chain of the Landsat imagery; crucial steps are already conducted on the provider side

DNs are converted to at-sensor radiance values, i.e. the amount of energy emittance from the earth measured by the sensor (Easmus et al., 2016). For the OLI sensor on board of Landsat 8, this radiometric calibration is described in detail in Markham et al. (2014). In the next step, this measure of energy is converted to the top-of-atmosphere reflectance, where reflectance is the ratio of incoming and outgoing energy in a specific spectrum of the light. Taking into account the earth-sun distance and the solar elevation angle, it is possible to estimate the incoming energy on the earth surface, the radiance measured by the satellite sensor is the outgoing energy. Thus, it becomes possible to estimate the reflectance (Young et al., 2017). However, the earth's atmosphere leads to a bias as it absorbs, reflects and scatters some part of the incoming and outgoing radiation. Thus, to obtain unbiased information of the earth surface, it is necessary to correct for the atmospheric

effects. Vermote et al. (2016) presents all details about atmospheric correction for the Landsat OLI sensor in detail. In addition to this bias, clouds in the atmosphere may prohibit a look on the earth surface and cloud shadows might cause an additional bias of the sensor measurement. Thus, it is necessary to mask clouds and cloud shadows. For the Landsat sensors, Zhu and Woodcock (2012) and Zhu et al. (2015) present advanced methods for creating cloud and cloud shadow masks.
However, all of these preprocessing steps are on the provider side for Landsat imagery as the USGS offers a web-based processing platform for these steps (`http://espa.cr.usgs.gov/`, last access 2020-12-28). Thus, only the application of the cloud/cloud shadow mask as well as a quality check and - if necessary - an enhancement of the topographic correction is on the user side (Young et al., 2017). As the algorithms applied for the preprocessing at the USGS are highly sophisticated and can be expected to deliver reliable results (Young et al., 2017), only the application of the masks and a visual quality check have been carried out. The masks have been applied by setting all values in the spectral bands to NoData where clouds or cloud shadows have been detected. After this step, the imagery has been loaded to QGIS for a visual quality check e.g. for undetected clouds.

### 6.2.8 Derivation of spectral indices

For obtaining information about the vegetation, I decided to use the relatively recent tasseled cap angle (TCA) as spectral index (Powell et al., 2010). It is defined as:

$$\mathrm{TCA} = \arctan\left(\frac{\mathrm{TCG}}{\mathrm{TCB}}\right) \tag{6.11}$$

where TCG and TCB are the tasseled cap greenness and brightness respectively. The tasseled cap transformation of the Landsat imagery is basically a sort of principal component analysis, where the information content of the different spectral bands of Landsat is analyzed for the information content regarding vegetation (greenness), bare soil (brightness) or surface moisture (wetness) (Kauth and Thomas, 1976; Crist and Cicone, 1984; Baig et al., 2014). These indices are calculated weighted sum of all spectral bands of the Landsat sensor:

$$\mathrm{TCx} = f_1 \cdot B_1 + f_2 \cdot B_2 + ...f_n \cdot B_n \tag{6.12}$$

with f being the weight and B the spectral Band. The weights for the OLI sensor on Landsat 8 can be found in Baig et al. (2014). The tasseled cap transformation is available in the *RStoolbox* package in R (Leutner and Horning, 2016).

### 6.2.9 Creation of a fuzzy vegetation mask

Similar to the riparian zone indicators, fuzzy membership functions are created for the spectral indices, i.e. they are transformed into values between 0 and 1. In the interpretation, a TCA value of 0 would e.g. mean that this pixel is not vegetated, while a pixel value of 1 means dense green vegetation. A linear membership function has been chosen as appropriate for the fuzzification:

$$\mu(x) \begin{cases} 0 & \text{for } x < x_{cal}(\min) \\ \frac{x - x_{cal}(\min)}{x_{cal}(\max) - x_{cal}(\min)} & \text{for } x_{cal}(\min) \leq x \leq x_{cal}(\max) \\ 1 & \text{for } x > x_{cal}(\max) \end{cases} \tag{6.13}$$

where $x_{cal}(min)$ is the minimum TCA value representing dense vegetation (derived from field calibration) and $x_{cal}(max)$ is the maximum TCA occurring within the field calibration data.

### 6.2.10 Field calibration

The same 111 points like for the calibration of the riparian zone delineation are used (see chapter 5 for further details). The biogeomorphological succession phases of Corenblit et al. (2007, 2009a) have been used for a stratification of the sampling. Then again, the spectral index values for the location of the sampling point locations have been extracted and the summary statistics have been computed. To get a conservative estimation of the vegetation area, the TCA value corresponding to the 25% quantile of all calibration points classified as biogeomorphological phase has been chosen as $x_{cal}(min)$ for the vegetation membership function. This means that only pixels with a higher vegetation density will be considered as riparian vegetation. The maximum of all values for all points in the biogeomorphological and ecological succession stage has been taken as $x_{cal}(max)$.

### 6.2.11 Fuzzy Delineation of riparian vegetation

After having delineated the riparian zone and the fuzzy masks for vegetation and water, it is possible to delineate the fuzzy representations of the riparian vegetation and the surface water in the Naryn River corridor. Literally speaking, I assume that a pixel representing riparian vegetation is connected to the processes in the river channel and has a high vegetation cover. This means that a pixel should indicate membership values of >0 for the vegetation as well as for the riparian zone membership raster. From a technical perspective, I compute the fuzzy t-norm $\mu(x, y) = \min(x, y)$ (with $\mu$ being the membership value of two raster layers x and y). If a pixel resulting from this operation has a membership value $\mu(x, y) > 0$, it is classified as riparian vegetation.

### 6.2.12 Disaggregation and aggregation of the river corridor

For a meaningful interpretation of the remote sensing results, it is necessary to build spatial segments of the river corridors. The most simple segmentation is to build segments of a fixed length, e.g. 100 m or 1 km. However, in river science theory, the reach is the spatial unit for large scale analysis of river corridors (Fryirs and Brierley, 2013; Gurnell et al., 2016b). A reach is defined as follows:

> *A reach is defined as a length of river that operates under relatively consistent and characteristic boundary conditions such that a relatively uniform morphology results (Fryirs and Brierley, 2013, pp. 176)*

Several methods have been proposed for the automated delineation of reaches from continuous GIS data. There are several methods for delineating reaches from spatially continuous data (Brenden et al., 2008; Alber and Piégay, 2011; Leviandier et al., 2012; Parker et al., 2012; Martínez-Fernández et al., 2016, 2019). In this thesis, I base upon two complementary approaches. First, I disaggregate the river corridor in spatial units of 100 m length along the valley bottom following the method of Alber and Piégay (2011). These 100 m units are called disaggregated river corridor hereafter. These units are the spatial entity I use for the analysis of the longitudinal pattern of the Naryn River corridor. Also the derivation of the channel gradient, river corridor and active channel width as well as the confinement ratio are calculated on the basis of the DGOs. This allows to give a spatially continuous description of the river corridor attributes and the statistical analysis of

potential patterns. The geostatistical framework for the river corridor disaggregation is described in detail below.
However, the disaggregation does not result in homogeneous reaches. While Alber and Piégay (2011) and Roux et al. (2015) use statistical breakpoint tests for reach discrimination, I base upon an expert based separation of reaches using a channel classification framework adapted from the *Riverstyles Framework* (Brierley and Fryirs, 2005; Fryirs and Brierley, 2013). In this context, I define a reach boundary as a change in the river type assuming that a change in the planform type is associated with a change in the fundamental process-form-relationship. This method has the advantage that it allows a straightforward interpretation of the results and is less sensitive to uncertainties in the digital elevation data underlying the derivation of river corridor attributes like the stream power or the river corridor width.

*Disaggregation of the river corridor*

For the disaggregation, I base upon the approach of Alber and Piégay (2011) and use Thiessen polygonization (see Fig 6.5 for the workflow). In a first step, a buffer with a width much wider than the river corridor is created around the channel line. Then, the buffer polygon is converted to lines, and manually split into two lines accompanying the river. Afterwards, equally spaced points are created along these lines in the desired segmentation length (100 m for the case of the Naryn). In a third step, Thiessen polygons are created from these points. The resulting polygons

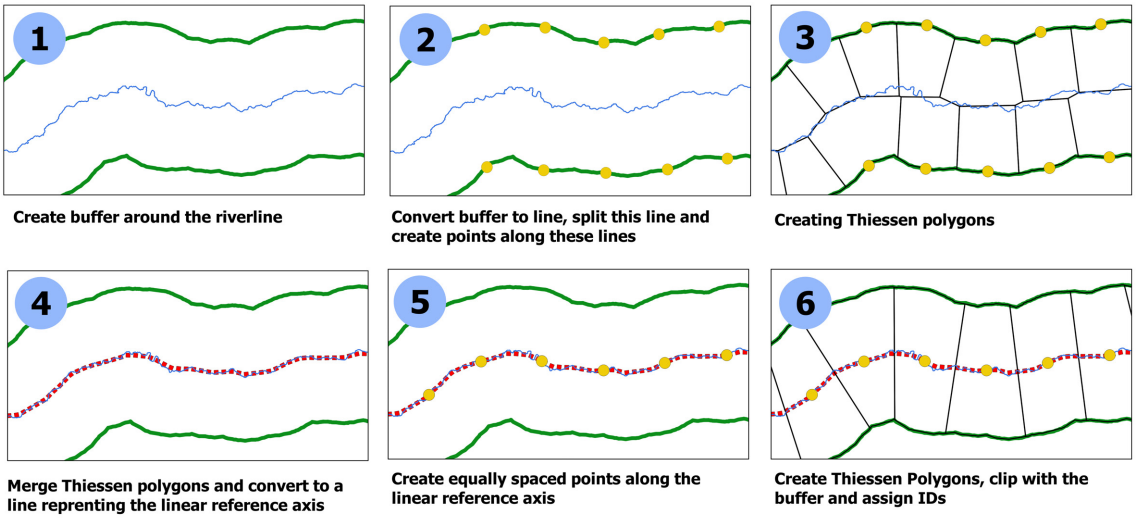


Figure 6.5: Disaggregation of the river corridor using Thiessen polygons (based on Alber and Piégay 2011)

are merged and converted to a line which refers to the linear reference axis of the buffer around the river line. Then again equally spaced points in the desired segmentation length are created along the linear reference axis. From these points Thiessen polygons are created. For convenience, these polygons can be clipped with the initially created buffer. Then, a unique ID is assigned to each polygon representing one river corridor segment as well as to the corresponding section of the channel line. The polygons can now be used to extract various river corridor attributes from the different raster datasets like the riparian vegetation extent for each polygon and link it to the longitudinal profile via the unique ID. This allows to link river corridor parameters derived from

the DEM and the Landsat imagery with parameters derived from the longitudinal profile. The disaggregation procedure has been implemented using the GIS capabilities of R (Lovelace et al., 2018).

*Expert based aggregation into homogeneous reaches*

Aggregation into homogeneous reaches has been performed based on the mapping of channel planform from high resolution virtual globe imagery where a reach boundary is defined as a change in planform. This explicitly assumes that there is a strict relationship between the observable planform and the underlying functional processes (Brierley and Fryirs, 2005; Fryirs and Brierley, 2013; Wheaton et al., 2015). For the mapping itself, manifold schemes for river channel classification have been proposed (Kondolf et al., 2016; Rinaldi et al., 2016). I base upon the *Riverstyles Framework* (Brierley and Fryirs, 2005) as well as a more recent classification scheme developed for the European Union (Rinaldi et al., 2016) for choosing variables for channel classification calling the result a *River Type*. To perform the mapping, the DEM derived Naryn River has been loaded to *QGIS* which allows the integration of various virtual globe imagery via the *QuickMapServices* plugin (QGIS Development Team, 2009). The channel line has been disaggregated into 100 m segments during the disaggregation procedure. Then, attribute fields for the desired attributes Valley Setting and River Type have been added. Then, the attributes have been manually assigned to the 100 m segments via the visual interpretation of the virtual globe imagery. Table 6.4 summarizes the distinguishing attributes for the 6 river types elaborated for the Naryn River. This approach allows a direct integration of the information obtained from the visual image interpretation with the automated DEM and remote sensing analysis.

Table 6.4: River types of the Naryn River and their distinguishing attributes

| Specification | Distinguishing Attributes |
|---|---|
| Gorge | Bedrock confined valley setting |
| Straight | Low sinuosity with no Extensive instream features and absent or discontinuous floodplains |
| Braided | Low sinuosity with extended gravel bars or islands, clearly identifiable main channel |
| Braided-anastomising | Low sinuosity with multiple channels; single channels show characteristics of braided rivers with extended bars and islands |
| Steep headwater | Low sinuosity with confined valley setting; instream geomorphic features like bars or islands as well as floodplains are widely absent |
| reservoir | Wide channel with Anthropogenic margins |

### 6.2.13 Width estimation and confinement

Based on the disaggregation of the river corridor into 100 m-segments, active channel width and confinement have been derived. Assuming that over a length of 100 m the area of the floodplain and the active channel are approximately rectangular, the simple formula for the area calculation of a rectangle $A_R$ = length $\times$ width can be used to obtain estimates of the width of the riparian corridor by dividing the derived river corridor area within the 100 m segment by the length of the

channel line within the 100-m segment (see Fig. 6.6). Furthermore, it is possible to discriminate

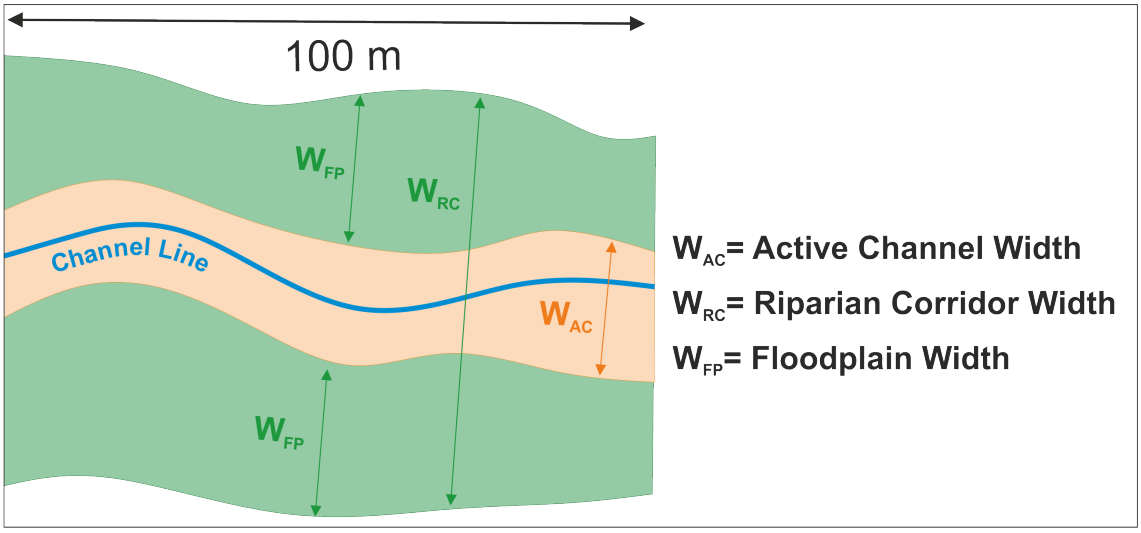


Figure 6.6: Scheme for the estimation of the different width parameters

the floodplain from the active channel. Following Schmitt et al. (2014), I use the vegetation cover as distinguishing attribute. Unvegetated areas are likely to belong to the active channel while the floodplain tends to be covered with vegetation. Thus, I can use the remote sensing derived vegetation cover and derive an estimate of the active channel width:

$$W_{AC} = \frac{A_{RC} - A_{veg}}{L_C} \tag{6.14}$$

where $W_{AC}$ is the active channel width, $A_{RC}$ and $A_{veg}$ the area of the river corridor respectively the vegetated area within the 100 m-segment and $L_C$ is the length of the channel line. Building the difference of river corridor width and active channel width results in the width of the floodplain. However, as the areas are not completely rectangular, the direct calculation fails when comparing to widths measured from high resolution imagery. Thus, rather than using the estimates from the geometric calculation directly, I use them as explanatory variables for a regression analysis with measured widths of the active channel and the river corridor. The measurements have been conducted on high resolution virtual globe imagery at 150 stratified random points using the Strahler order as strata (Lauermann, 2016). The number of points per stratum has been weighted by the length of the channel line per Strahler order:

$$n_{Si} = \frac{l_{Si}}{\sum_{S1}^{Sn} l_{Si}} n \tag{6.15}$$

where $n_S$ is the length of the number of random points for the $i^{th}$ Strahler order S and $l_{Si}$ is the length of the $i^{th}$ Strahler order and n is the total number of sampling points. The points as well as the measurements of the active channel widths have been provided by Magdalena Lauermann (see Lauermann 2016, 30-31 for details). The measured active channel and riparian corridor widths have been randomly split in a group of 105 points for fitting a linear model to the relationship between geometric estimate and measured widths. A group of 45 points has been used for validating

the regression model. The validation has been performed by a visual interpretation of a scatterplot with the measured and modeled values. Furthermore the Pearson correlation coefficient has been calculated for the test group as quantitative accuracy value.
The active channel width and the riparian corridor width can be used to compute the confinement ratio defined as the ratio of active channel width and river corridor width (Nicoll and Hickin, 2010; Schmitt et al., 2014). Equation 6.16 gives the computation of the ratio, with C being the confinement ratio, $W_{AC}$ being the active channel width and $W_{RC}$ the river corridor width respectively:

$$C = \frac{W_{AC}}{W_{RC}} \tag{6.16}$$

This ratio can be used as a continuous indicator of confinement as relevant controlling factor of planform development. To interpret the C values, I compare them with confinement mapped from high resolution virtual globe imagery. For the mapping, the categories *confined*, *partly confined* and *laterally unconfined* are used as defined in the *Riverstyles Framework* (Fryirs and Brierley, 2013; Fryirs et al., 2016, see also table 6.5).

Table 6.5: Attributes used for characterizing the Naryn River

| Specification | Distinguishing Attributes |
|---|---|
| confined | majority of the channel hits the valley margin or the terrace |
| partly confined | a minor share of the channel hits the valley margin or the terrace, often on just one side |
| laterally unconfined | only a minor share of the channel hits the valley margin or the terrace |

### 6.2.14 Erosion and deposition model [3]

To gain an overview of the channel processes, a simple model for evaluating the tendency towards erosion or deposition of sediment was created. The model is based on the principle, that a reach where the transport capacity exceeds the sediment load will have the tendency to erode while a reach where more sediment is available than the river is able to transport deposition will be dominating. If sediment load and transport capacity are in balance, the reach is regarded to be in dynamic equilibrium (Bizzi and Lerner, 2015; Parker et al., 2015). Parker et al. (2015) used this principle to construct a simple model for assessing the dominance of erosion or deposition in a river reach. He uses the ratio of the specific stream power in the reach under investigation with the upstream reach to calculate the stream power balance $\omega_{balance}$ (see Fig. 6.7).
If the ratio is << 1, the upstream stream power is greater than the one of the actual reach, thus it is likely that the sediment availability is high and the reach is deposition dominated. On the contrary, if the $\omega_{balance}$ is >> 1, the stream power is considerably higher than the one of the upstream reach and the reach under consideration is likely to have a sediment deficit causing a dominance of erosion (Fig. 6.7, Parker et al. 2015). If $\omega_{balance}$ is close to 1, the reach can be considered to be in

[3] A previous version of this model has been presented by Lauermann (2016) within her master thesis. The model approach presented here uses the same modeling workflow but improves the parameterization of channel gradients, discharge interpolation and channel width estimation. In addition, the segmentation of the river corridor has been conducted in a different, more detailed way.

dynamic equilibrium. Of course, these are simplified assumptions that cannot fully capture spatial and temporal dynamics of hydromorphological dynamics (Soar et al., 2017). Nevertheless, the model proofed to produce meaningful results also under the data-scarce conditions of Kyrgyzstan (Lauermann, 2016).

Due to the simple structure of the model, only the specific stream power along the longitudinal

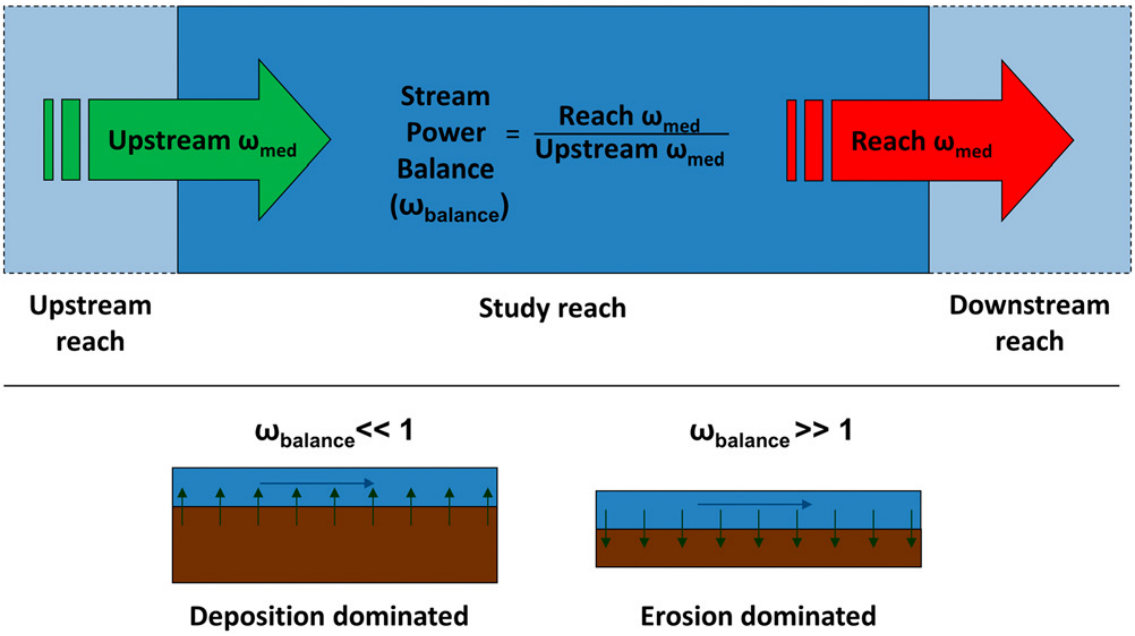


Figure 6.7: Principle of the calculation of stream power balances underlying the erosion and deposition model (from Parker et al. 2015, p. 408)

profile as well as a segmentation of the river into meaningful reaches is necessary for the parameterization (see sections 6.2.4,6.2.5 and 6.2.12 for their computation). The stream power balance values of each reach have been interpreted regarding the channel state following Lauermann (2016, p. 34):

- 0.0-0.7 Deposition
- 0.7-0.9 Deposition close to equilibrium
- 0.9-1.1 Dynamic equilibrium
- 1.1-1.3 Erosion close to equilibrium
- >1.3 Erosion

A quantitative validation of the model is not possible as no topographic measurements of channel changes are available for the Naryn River. Thus, I base upon Lauermann (2016) who used observations of the channel state based on indicators suggested by Sear et al. (2010, p. 130). At 21 points along the Naryn, the indicators have been observed and interpreted regarding the channel state. Then, observed and modeled channel state are checked for agreement.

## 6.3 Results

### 6.3.1 Catchment and channel network

*Catchment*

The catchment of the Naryn River has a size of 52,130 km$^2$, a figure of its delineation was already shown in figure 2.2 whereas the hypsometric curve of the catchment given in figure 6.8 is a new result. The maximum elevation is 5133 m in the Tian Shan in the eastern part of the catchment, the minimum elevation is 868 m at the outlet of the Toktogul reservoir. More than 50 % of the catchment are in an elevation above 2000 m a.s.l., approx. 20 % even in an altitude above 3000 m. This underpins the mountainous characteristic of the Naryn catchment. A further measure for

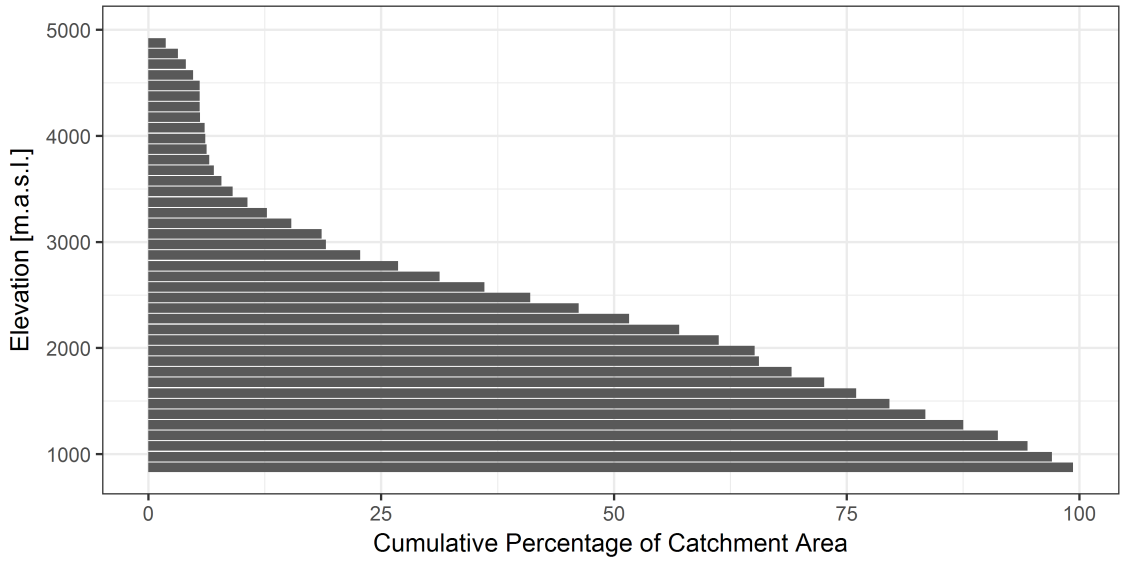


Figure 6.8: Hypsometric curve of the Naryn catchment; the maximum elevation of 5133 m does not show up in this diagram as it is only reached in one single pixel disappearing in the computation of the cumulative percentages

describing the elevation distribution in a catchment is the so-called hypsometric integral calculated as follows:

$$HI = \frac{z_{mean} - z_{min}}{z_{max} - z_{min}} \tag{6.17}$$

where $z_{min}$ is the elevation of the catchment outlet, $z_{max}$ the maximal and $z_{mean}$ the mean elevation in the catchment (Strahler, 1952; King, 1966). Despite the early development, this method is still being applied in modern geomorphological research (e.g. Cohen et al., 2008). The Naryn catchment has a hypsometric integral of 0.464, what could be interpreted as a landscape whose development is dominated by channel processes rather than diffuse hillslope erosion (Willgoose and Hancock, 1998). However, some caution is needed for the interpretation, as different parts of the catchment may be dominated by different process domains. For instance, the catchment of the Big Naryn River, i.e. the uppermost headwaters of the Naryn has a larger value of 0.531 what could be interpreted as a catchment with higher influence of hillslope processes (Willgoose and Hancock, 1998; Bishop et al., 2002).

*Quality assessment of the derived channel network*

Figure 6.9 shows the comparison of the channel line derived with the least cost path approach implemented in GRASS GIS with a channel line derived from a 'hydrologically corrected' DEM and the digitized Naryn River as reference. From the map view in this figure in becomes clear, that the channel line derived from the filled DEM results in an unrealistic representation of the Naryn River. This channel line cuts off entire meanders and represents the river as straight lines. In contrast, the channel line derived with the least cost path approach shows some bumps but represents the course of the Naryn in an appropriate way. In an overall evaluation for the entire

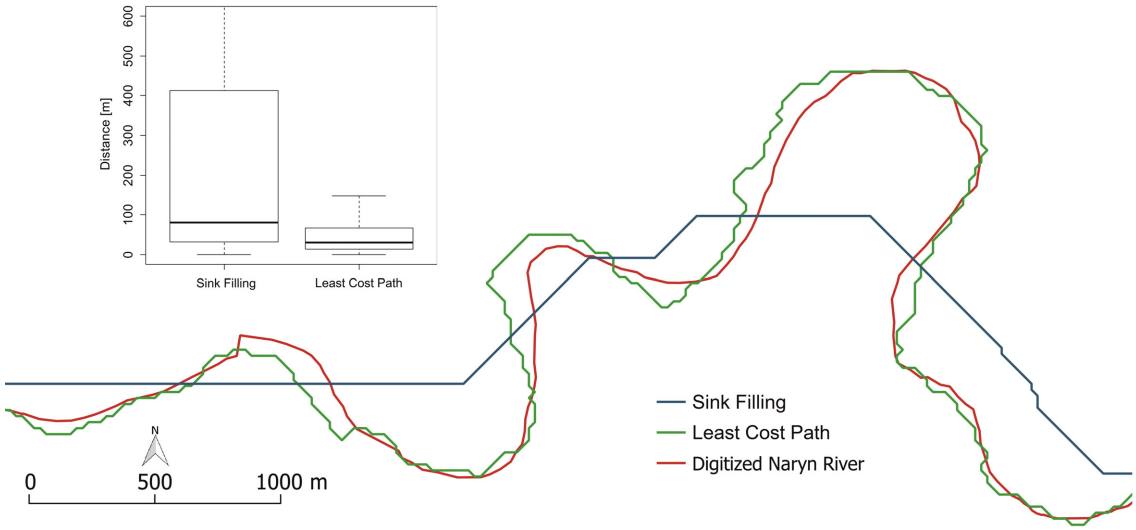


Figure 6.9: Comparison of different channel network delineation methods with a digitized river line; the difference of the two approaches shown in the boxplots is significant even under the 99% confidence interval (modified from Lauermann et al., 2016)

Naryn River, the median distance of the channel line delineated from the DEM treated with sink filling results to the digitized reference line is 79.94 m. Contrary, the channel line derived by means of the least cost path approach shows a median distance to the reference channel line of only 30.80 m. The p-value of $> 2.2 \times 10^{-16}$ suggests that the differences between the different channel delineation methods are significant even under the 99% confidence interval.

### 6.3.2 Longitudinal Profile and channel gradients

Figure 6.10 shows the longitudinal profile of the Naryn River as obtained from the SRTM-1 DEM without any filtering as well as the results of the different smoothing algorithms. From the original profile, it becomes clear, that there are several clearly identifiable realistic knick points especially in the upper part of the Naryn River. Nevertheless, the profile suffers from errors like the spikes at approximately 250 km and especially at approximately 500 km. Furthermore, heavy noise distorts the profile at around 600 km. Thus, even if already some details are observable the unfiltered longitudinal profile is evaluated as no realistic representation of the reality and further filtering is required for removing the obvious errors from the profile. The different smoothing algorithms handle these errors in different ways. The running average as well the outlier removal and interpolation method fail to remove the spikes at 500 km while the noise and the smaller spikes at 250

km are successfully removed by the latter one. The obvious knick points in the upper part of the river seem to be preserved well while new, 'staircase' like artifacts have been introduced especially be the running average. The locally weighted regression and the constrained quantile regression

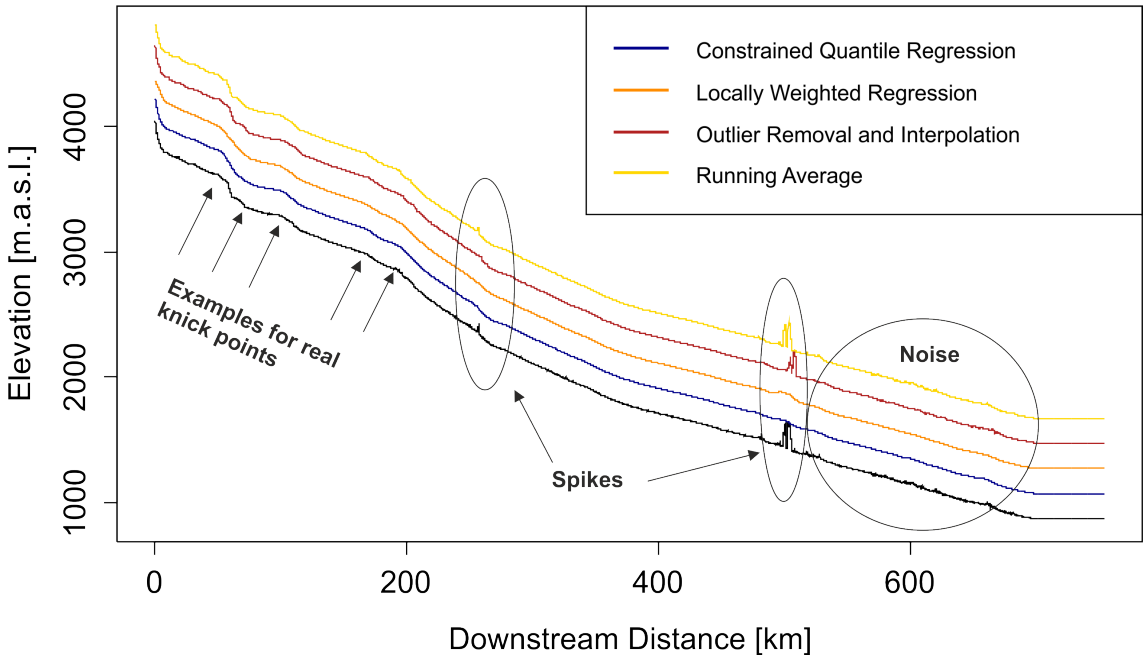


Figure 6.10: Differences between the unfiltered and filtered longitudinal profile; to enhance the readability, an offset of 200 m was introduced between the different profiles

are able to remove the spikes at 250 km and the noise around 600 km. The quantile regression removes also the significant spikes at 500 km, while the locally weighted regression smoothing results in an artificial knick point in this river section. Furthermore, this algorithm blurs knick points along the entire profile. Constrained quantile regression seems to keep knick points better. Furthermore, it ensures monotonically decreasing elevation values along the profile.
Having a look at the residual plots (Fig. 6.11) and the MAR values allows further insights in the modification of the original longitudinal profile by the smoothing algorithms. All algorithms have in common that the highest modification takes place in the section of the significant spikes at approx. 500 km. The regression methods reduce the original profile by up to 200 m in this section, the outlier removal and interpolation approach removes and fills elevation values there. The running average results in a much smaller modification in the spike section. Furthermore, all algorithms treat the noisy section at around 600 km and the smaller spike at 250 km. The MAR values help to assess the degree of modification of the algorithms. The running average results in the smallest MAR of 1.571, the largest values arises from the outlier removal and interpolation (9.831). This large value of the latter algorithm can be explained by the modifications between 0 and 250 km, which do not occur in the other smoothed profiles. Locally weighted regression and constrained quantile regression show similar MAR values of 4.1 and 3.312 respectively. The modification of the original profile only takes place in the area of the spikes and noise. In addition, the locally weighted regression shows an unrealistic modification at the beginning of the channel not occurring in the profile smoothed with the constrained quantile regression.
The main derivative of the longitudinal profile is the channel gradient. Figure 6.12 shows a com-

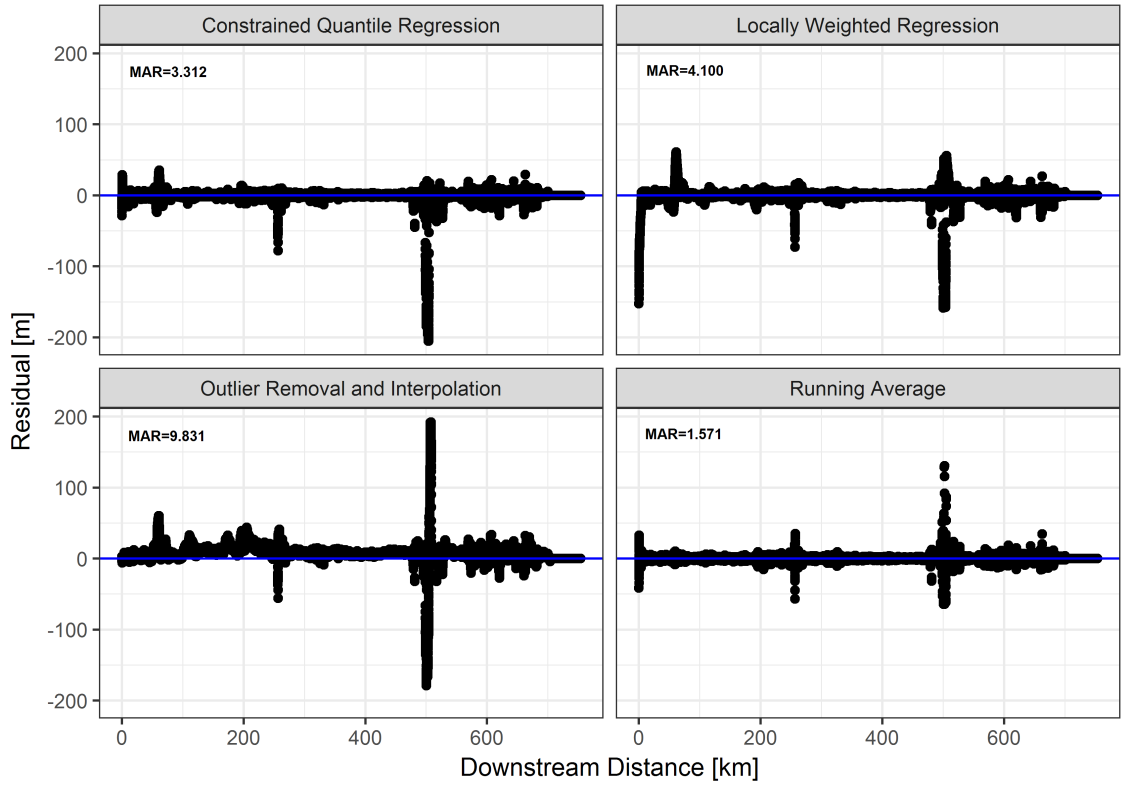


Figure 6.11: Residual plots of the longitudinal profile smoothing

parison of the different gradients arising from the different profile smoothing algorithms. The gradients derived from the GIS slopes result in obviously higher values than the other algorithms with a median value of 0.04017 while the median values of the other algorithms are 0 for the running average and the outlier removal and interpolation technique. Locally weighted regression and constrained quantile regression have slightly higher values of 0.003310 and 0.003382 respectively. Obvious are also the negative values of outlier removal and interpolation and running average indicating that the smoothed profile still does not show monotonically decreasing values. This is also true for the locally weighted regression, which results in negative gradients along 28.28 km of the river profile (the segment with the significant spikes in the original profile). From the smoothing algorithms, only the constrained quantile regression results in positive values only - non surprisingly as monotonically decreasing values have been the constraint for fitting the regression. All values show a significant number of outliers, especially the running average as well as the outlier removal and interpolation have large deviations from the median to the positive as well as to the negative direction (Fig. 6.12). This is an indicator of an insufficient smoothing of the profile. The gradients calculated based on the profile smoothed by locally weighted or constrained quantile regression show similar properties where the first has slightly fewer outliers and thus is slightly smoother as already expressed by the MAR values (see above). While the difference between the gradients derived from the GIS Slope and the smoothed longitudinal profiles is obvious, the difference within the latter group is less clear. Thus, a Kruskal-Wallis test was performed to test whether the differences between these four algorithms is significant. A p-value of $< 2.2 \times 10^{-16}$ with a chi-squared of 29077 indicate that the differences are indeed statistically significant. Also

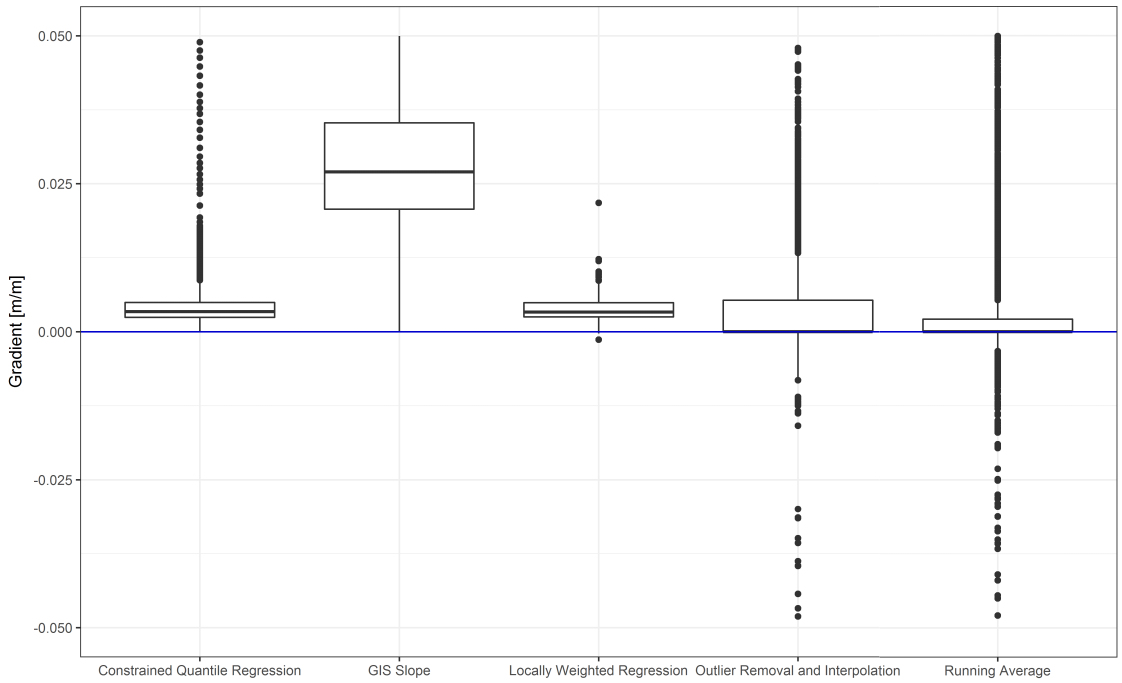


Figure 6.12: Comparison of channel gradients derived from the longitudinal profile smoothed with different algorithms

when testing the both regression algorithms for statistical significant differences by means of the Mann-Whitney U-test results is positive, i.e the differences are significant (p-value of $4.95 \times 10^{-8}$). In an overall evaluation, a smoothing of the longitudinal profile is necessary to remove unrealistic artifacts like spikes or noise which can cause for instance negative gradients which cannot occur from our physical understanding of longitudinal profiles. Only the constrained quantile regression fully satisfies this requirement, with a minor exception also the locally weighted regression. This disqualifies the running average and outlier removal and interpolation approach for the application at the Naryn River. Furthermore, the GIS Slope method results in unrealistic high gradient values which are not feasible. Summarizing all these facts leads to the result that the longitudinal profile smoothed with the constrained quantile regression is likely to be the best representation of the Naryn River and will be used for all subsequent analysis throughout this thesis.

### 6.3.3 Discharge interpolation and stream power estimation

The median average discharge for the 18 gauges in the Naryn catchment is in the range of 3.3 $m^3s^{-1}$ and 702.5 $m^3s^{-1}$, the flow accumulation varies between $2.23 \times 10^5$ cells and $8.23 \times 10^7$ cells. Figure 6.13 shows the result of the regression between these two variables. The fitted power law results in the equation:

$$Q = 0.0009757461 \times FA^{0.7375160073} \tag{6.18}$$

For nonlinear regression, the mean absolute error (MAE) gives a quantitative estimate of the goodness-of-fit as an r-squared is not meaningful (Ritz and Streibig, 2008; Spiess and Neumeyer,

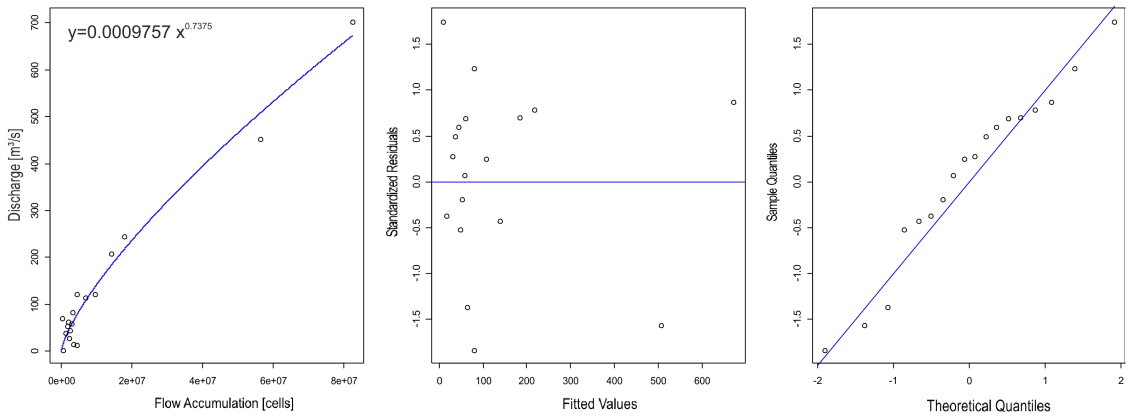


Figure 6.13: Modeled relationship between median annual maximum discharge and flow accumulation for 18 gauges in the Naryn catchment

2010). A MAE value of 27.3 $m^3s^{-1}$ gives a satisfying result. Furthermore, the interpretation of the residuals gives further insights in the quality of the nonlinear model. The z-transformed residuals scatter in a non-systematic way around 0. This implies that there is no systematic bias in the model supporting a successful model fit. The assumption of randomness is further supported by a normal distribution of the transformed residuals (Ritz and Streibig, 2008). The scatterplot of sampled and theoretical quantiles of the transformed residuals in figure 6.13 as well as the p-value of 0.5226 resulting from a Wilcoxon test on normality support the assumption of normal distributed residuals. Thus, the quality of the fitted regression model for interpolating the discharge can be accepted and equation 6.18 can be used for obtaining spatially continuous discharge estimates.
Figure 6.14 summarizes the main results from sections 6.3.2 and 6.3.3 and shows the longitudinal pattern of channel gradient, discharge and total stream power. The gradient ranges from a value of

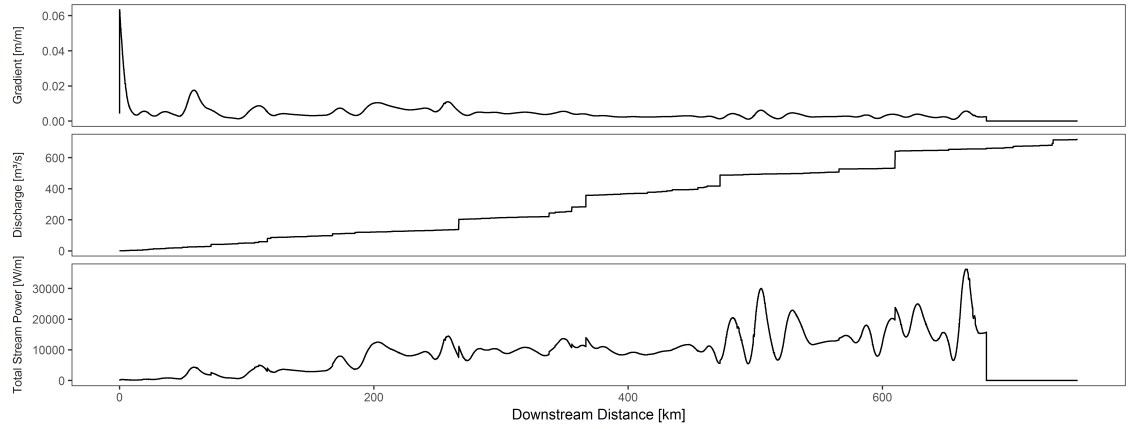


Figure 6.14: Longitudinal profile, channel gradient, interpolated discharge and total stream power along the Naryn River

0 to 0.0633 $mm^{-1}$ with a median of 0.0034 $mm^{-1}$ and has its maximum in the uppermost part of the Naryn River. The discharge increases in several steps indicating major tributaries of the Naryn River up to 716.29 $m^3s^{-1}$. Median discharge is 360.15 $m^3s^{-1}$. The total stream power shows a

more heterogeneous picture and has several peaks especially between 500 km and 650 km. The minimum is 0 $Wm^{-1}$ at the Toktogul reservoir, the maximum of 36,293 $Wm^{-1}$ directly before the drop to 0 at the Toktogul and a median value of 9084 $Wm^{-1}$. In general, the stream power shows an increasing trend with increasing downstream distance before the Toktogul reservoir (p-value of a linear trend model < 0.01). However, the downstream distance explains only 0.15 % of the total stream power variance.

### 6.3.4 Riparian zone delineation

*Parameterization of the membership functions*

The calibration of the membership functions is a crucial task for the subsequent modeling of the riparian zone. Fig. 6.15 shows the statistical distribution of the indicator variables. The proximity indicators are all right-skewed, an effect which is strongest for the path distances.

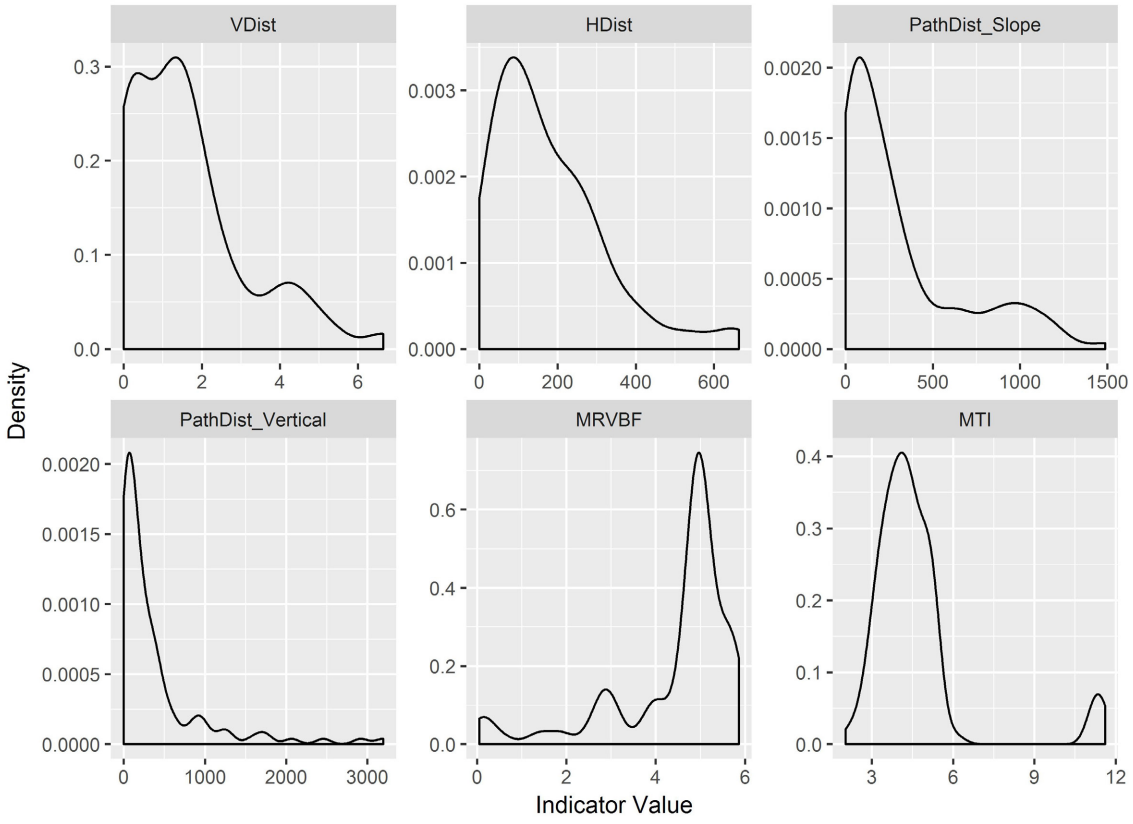


Figure 6.15: Statistical distribution of the indicator variables for the 111 calibration points

The vertical distance above the channel and the horizontal distance are less strongly skewed. On the contrary, the multiresolution valley bottom flatness index shows a strong skewness to the left while the modified topographic index is only moderately left-skewed. Consequently, the proximity indicators were fuzzified using the inverse linear function, while for the morphological indicators the linear fuzzification was applied. The calibration parameters $x_{cal}$(min) and $x_{cal}$(max) are summarized in Table 6.6.

Table 6.6: Calibration parameters for the fuzzy membership functions; for the parameterization of the inverse linear membership functions of the proximity indicators $x_{cal}$(min) is not required (for the abbreviations please refer to table 6.3)

| Indicator | $x_{cal}$(min) | $x_{cal}$(max) |
|---|---|---|
| HDist | - | 663.36 |
| VDist | - | 6.65 |
| PathDist(Slope) | - | 1487.98 |
| PathDist(Vertical) | - | 3196.38 |
| MRVBF | 0.05408 | 5.86052 |
| MTI | 2.034 | 11.612 |

*Single indicators*

Figure 6.16 shows the maps of the modeled membership functions for the six riparian zone indicators. It is obvious that the morphological indicators deliver membership values larger than 0 for

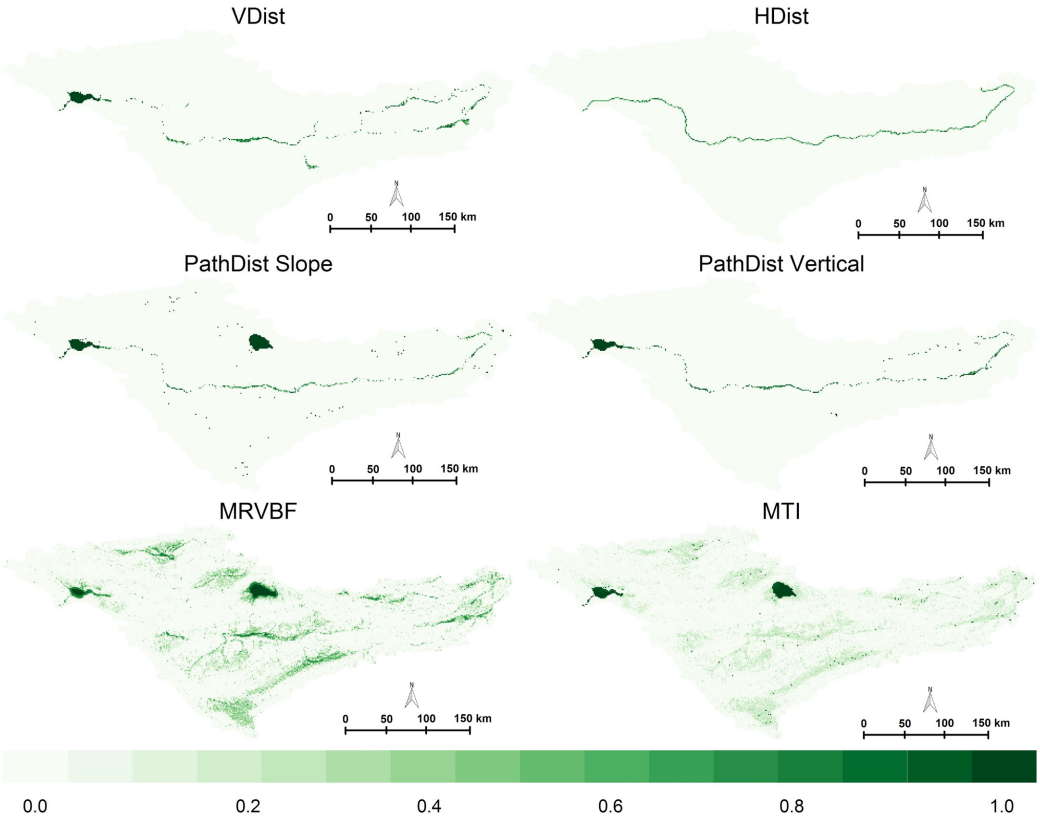


Figure 6.16: Membership function maps of the different riparian zone indicators

the entire catchment as long as the conditions fall within the calibration range of the membership model. The Toktogul Reservoir and lake Son Köl are clearly visible in most maps as they are rela-

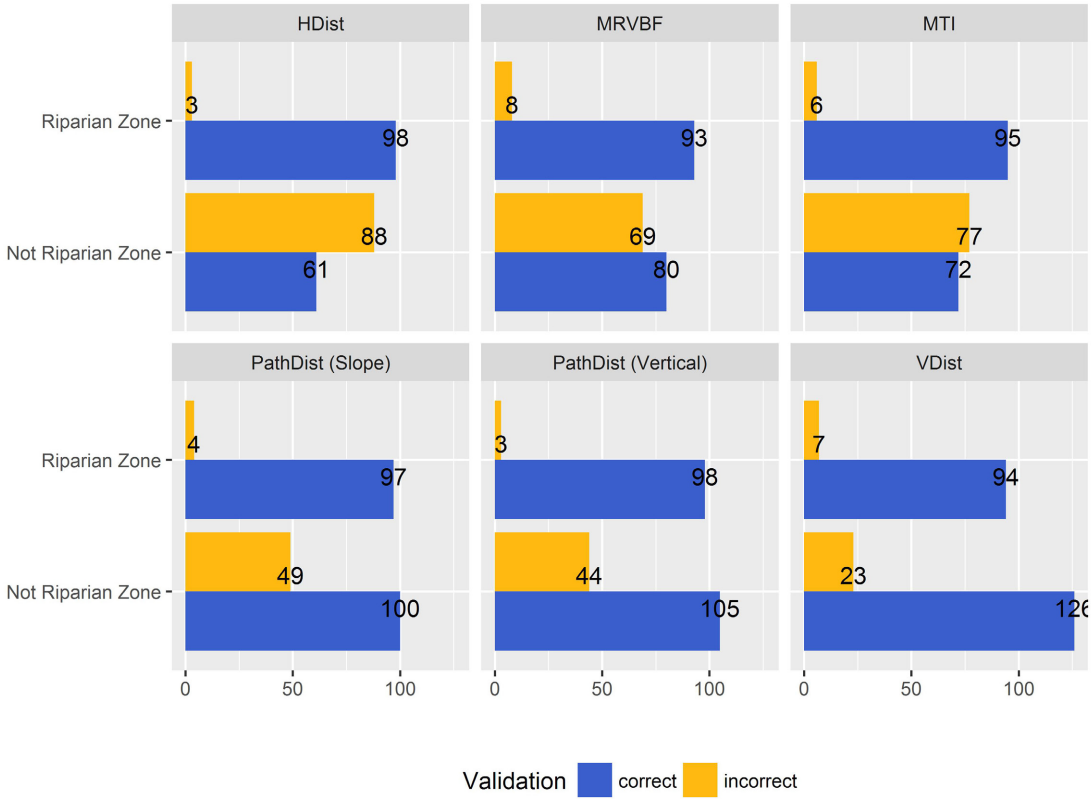


Figure 6.17: Performance of the single indicators regarding the 250 visual validation points. For the abbreviations refer to Table 6.3.

tively low and flat compared to the landscape around them (MRVBF) and have a large catchment area (MTI). The appearance of the proximity indicators is more heterogeneous. The horizontal distance (HDist) for instance does not represent the Toktogul Reservoir, while the path distance (PathDist Slope) shows membership degrees bigger than 0 for flat areas in a certain distance to the Naryn River like e.g. the Son Köl. The vertical distance above channel network (VDist) and the path distance with the VDist as the cost factor (PathDist Vertical) are quite similar on a larger scale, as they represent well the Toktogul Reservoir and do not include areas distant from the Naryn River.

The evaluation of all single indicators is shown in Fig. 6.17, and the quantitative accuracy is given in Table 6.7. The single indicators result in user's accuracies between 52.69±9.79% for the horizontal distance and 80.34±7.79% for the vertical distance above channel network. In general, the accuracy for the non-riparian validation points tends to be lower than that for the points of the riparian class. Thus, all indicators tend to overestimate the extent of the riparian zone. The indicator with the best performance is the vertical distance above channel network (VDist) with an user's accuracy of 80.34±7.79% followed by the path distance with VDist as the cost factor. The morphological indicators are worse than the proximity indicators with a user's accuracy of 55.23±9.75% for MTI and 57.41±9.69% for MRVBF. This result comes mainly from the non-riparian validation points, where only the horizontal distance has a worse performance compared to the morphological indicators (Fig. 6.17).

Table 6.7: Quantitative accuracies for the riparian zone class including the 95% confidence interval

| Indicator | Producer's Accuracy | User's Accuracy |
|---|---|---|
| *Single Indicators* | | |
| HDist | 97.03±3.33 % | 52.69±9.79 % |
| VDist | 93.07±4.98 % | 80.34±7.79 % |
| PathDist (Slope) | 96.04±3.82 % | 66.44±9.26 % |
| PathDist (Vertical) | 97.03±3.33 % | 69.01±9.06 % |
| MRVBF | 92.08±5.29 % | 57.41±9.69 % |
| MTI | 94.06±4.63 % | 55.23±9.75 % |
| *Inference Indicators* | | |
| HDist AND VDist | 92.08±5.29 % | 80.87±7.71 % |
| HDist OR VDist | 98.02±2.73 % | 52.66±9.79 % |
| VDist AND PathDist (Slope) | 92.08±5.29 % | 80.17±7.81% |
| VDIst OR PathDist (Slope) | 97.03±3.33 % | 66.67±9.24 % |
| VDist AND MRVBF | 88.12±6.34 % | 81.65±7.59 % |
| VDist AND MTI | 90.10±5.85 % | 81.98±7.53% |
| PathDist (Vertical) AND MRVBF | 89.11±6.11 % | 77.59±8.17 % |
| PathDist (Vertical) AND MTI | 91.09±5.58 % | 76.67±8.29 % |
| VDist AND (MRVBF OR MTI) | 91.09±5.58 % | 82.14±7.51 % |

*Inference indicators*

After evaluating the performance of the single indicators, I selected several combinations and built their fuzzy inferences. Figure 6.18 shows the maps of these inference values. I focused on combinations with the vertical distance above channel network and the path distance (vertical) as they showed the best performance in the validation of the single indicators. In the AND inference of HDist and VDist, I still see the "loss" of the Toktogul reservoir, the characteristics of the horizontal distance as single indicators. Similarly, for the OR inference of VDist and PathDist (Slope), still the Son Köl is included in the map due to its flat surface resulting in low path distance values. All other inference maps have a similar appearance at the first glance. The results of the validation of the riparian zone delineation with the inference indicators is shown in Table 6.7 and Fig. 6.19. The producer's accuracies decreased slightly and are now in the range from 88.12±6.34% to 97.03±3.33%. The user's accuracies, however, increased to a maximum of 82.14±7.51%. This increase mainly results from the reduced number of non-riparian validation points wrongly classified as riparian zone (Fig. 6.19). Thus, building the inference of different indicators helps solving the issue of overestimating the riparian zone extent. The highest accuracies still arise from the inferences with the vertical distance above channel network which was already the most successful single indicator. Interestingly, in terms of computed accuracy a simple combination of VDist and HDist shows already a high performance. However, in the visual interpretation we see the misrepresentation of the Toktogul reservoir which should appear as part of the riparian zone (Fig. 6.18). In contrast, inferences of the VDist and the morphological indicators MRVBF and MTI perform well according to the validation points and the visual evaluation. VDist and MRVBF have overall user's accuracy of 81.65±7.59%; VDist and MTI have 81.98±7.53%. To combine the advantages of the two morphological indicators, I decided to make an inference of VDist, MRVBF and MTI

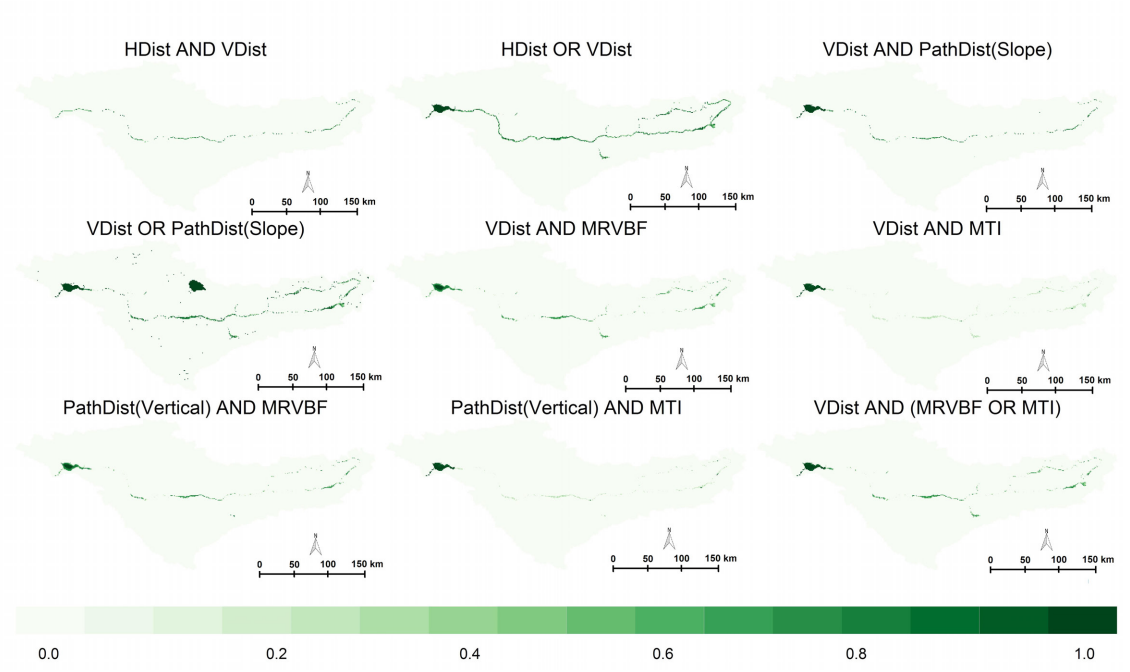


Figure 6.18: Maps of the inference values of selected indicators

(Table 6.7). This resulted in the best user's accuracy of 82.14±7.51%.

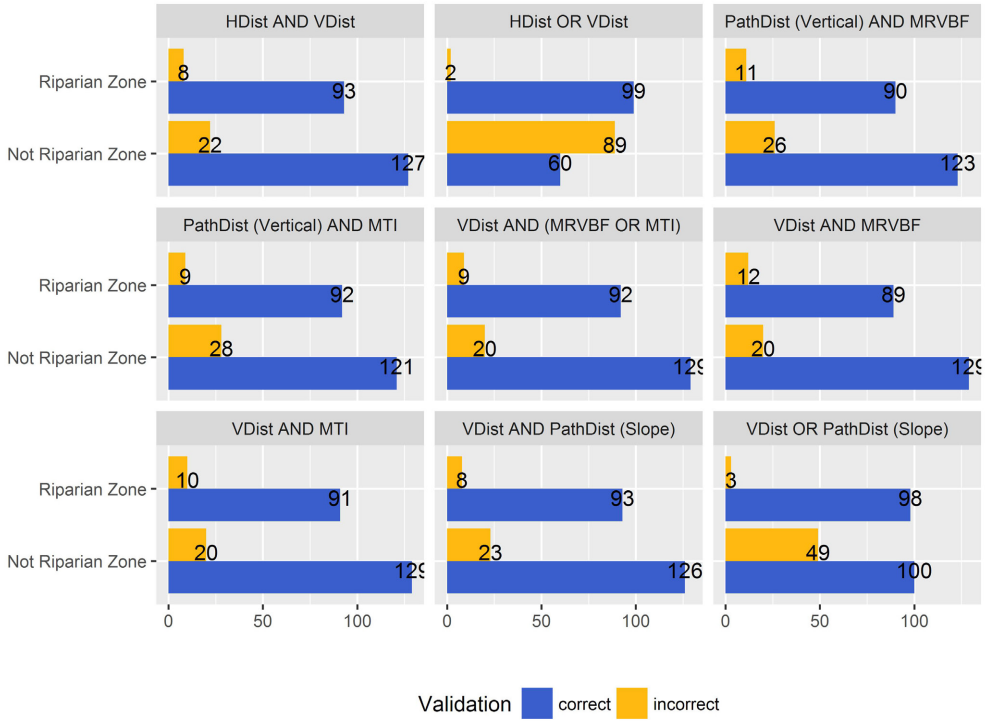


Figure 6.19: Validation of the riparian zone delineation with the inference of different indicators

*Application of the riparian zone model to the Naryn River corridor*

After having found the best model, I apply it to the entire river corridor of the Naryn. During the visual evaluation it turned out that manual cleaning of the modelled riparian zone was necessary at confluences with other rivers, an issue already described by Notebaert and Piégay (2013). Figure 6.20 shows the final map of the riparian zone distribution along the Naryn River.

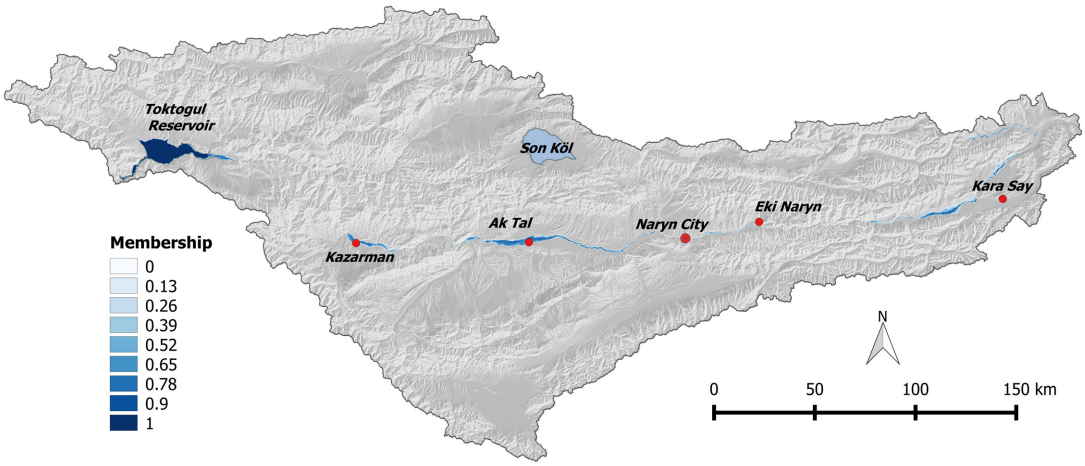


Figure 6.20: Distribution of the riparian zone along the Naryn River

The total area of the modeled riparian zone is 662.58 km$^2$. Excluding the 229 km$^2$ of the Toktogul reservoir, there are 443.58 km$^2$ of riparian zone with natural dynamics including the channel itself, instream bars and islands as well as the adjacent floodplain. The distribution of the riparian zone is not heterogeneous. There is a larger patch near the village Kara Say in the uppermost part of the river corridor followed by a narrow riparian zone. Downstream from Naryn City, the river corridor is getting wider again. The most extensive riparian zone is then found around Ak Tal. After crossing a gorge, the Naryn River is reaching another area with a wider riparian zone around Kazarman. Further downstream, the river enters a long, narrow gorge before entering the Toktogul reservoir.
For a more detailed investigation of the fuzzy riparian zone model in different valley settings, I refer to the field calibration sites. Figure 6.21 shows the modeled riparian zone on an rgb-composite of a Sentinel-2 image from June 2016. For the field calibration sites, the DEM derived channel line fits well to the channel visible on the satellite image even if the bumps are an evidence for the noise in the elevation data. The riparian zone model is also well in accordance with the valley morphology visible on the image. Nevertheless, the limits of accuracy become obvious at the fringe of the riparian zone. From the visual impression, the model seems to fit better for the partly confined and confined valley setting of Ak Talaa and Emgek Talaa. The fringe of the laterally unconfined Ak Tal site is noisy indicating the uncertainty in this valley morphology. Furthermore, there is a zonation within the riparian zone model. The channel and the braided plain show high membership values. Two clusters with lower membership values indicate different floodplain levels. This zonation is obvious for Ak Talaa and Emgek Talaa while it is less visible for Ak Tal.

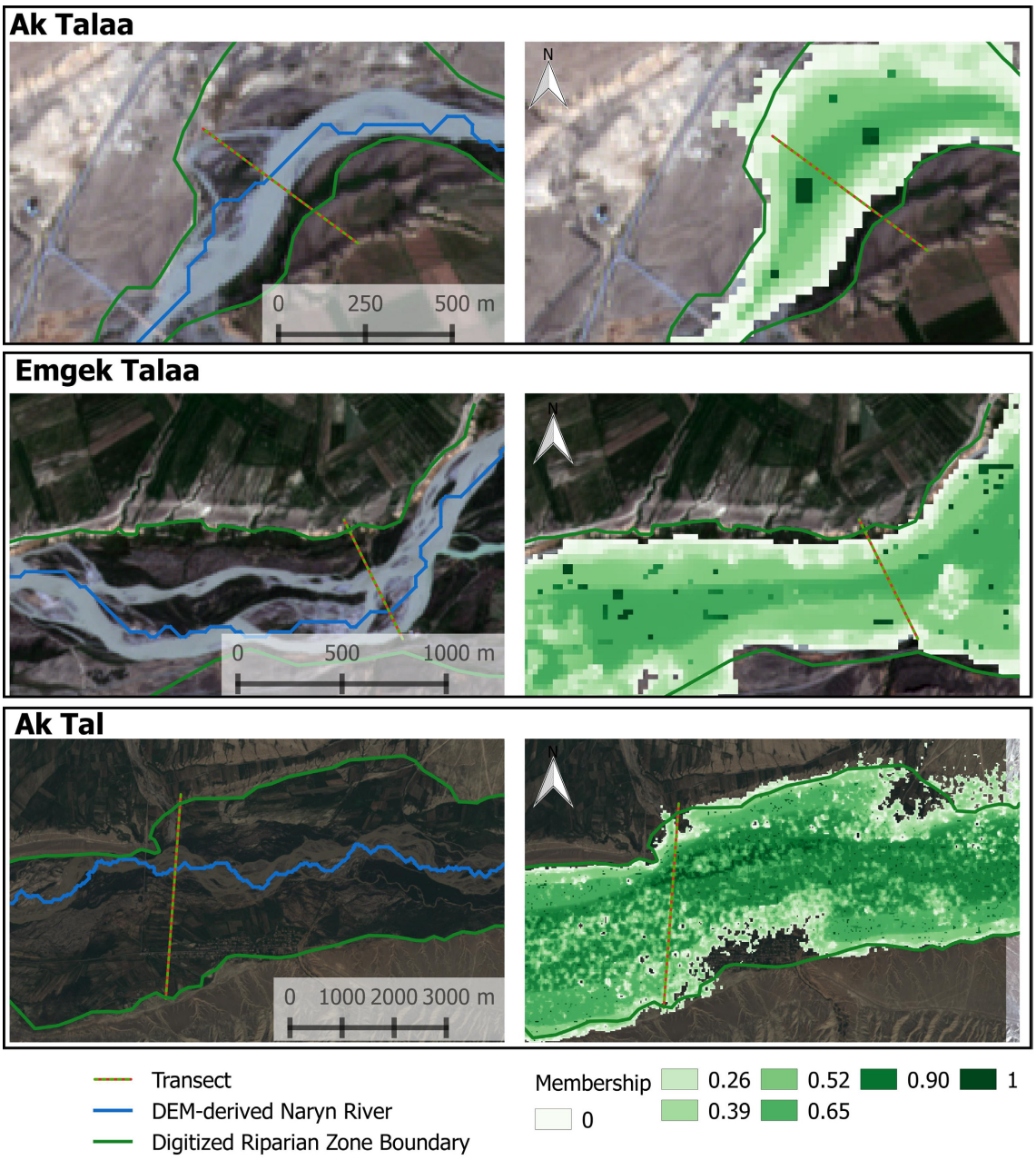


Figure 6.21: Modeled riparian zones for the calibration sites; Ak Talaa represents a confined, Emgek Talaa a partly confined and Ak Tal a laterally unconfined valley setting. For details about the valley morphology refer to Figure 6.3

### 6.3.5 Fuzzy delineation of riparian vegetation

The entire area of riparian vegetation for July 2015 is 231.99 km$^2$. The pattern of the riparian vegetation follows in general the pattern of the riparian zone. Figure 6.22 shows the spatial distribution of the riparian vegetation along the Naryn River. In the uppermost part of the river corridor, around the village of Kara Say, there is an area of more extensive riparian vegetation. Further

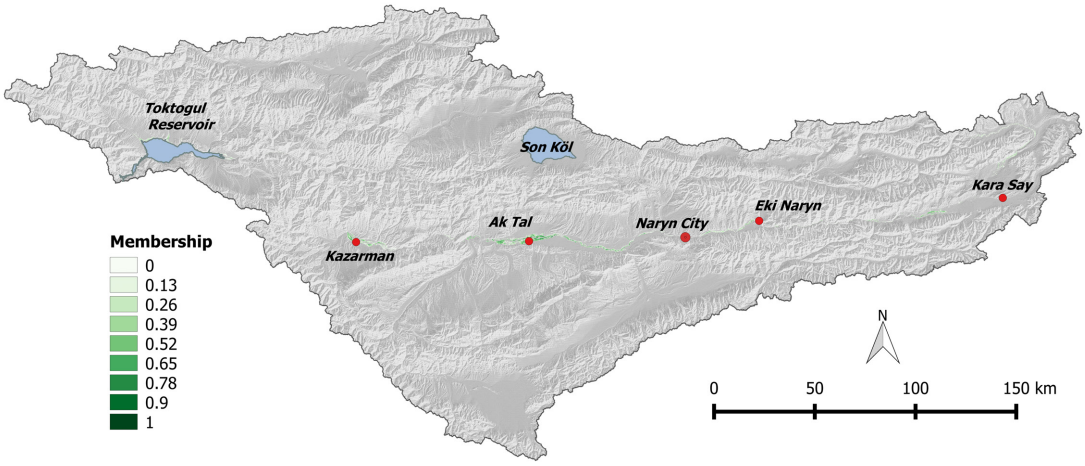


Figure 6.22: Distribution of riparian vegetation along the Naryn River

downstream, there is again riparian vegetation between Eki Naryn and Naryn City. The most

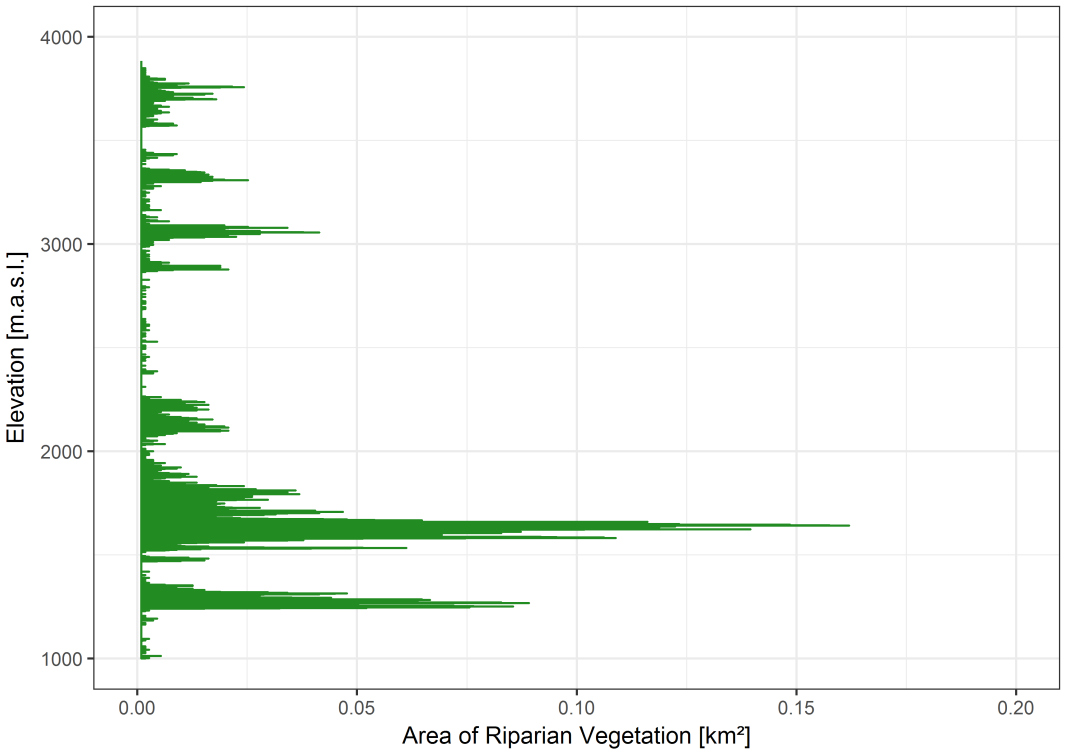


Figure 6.23: Distribution of the riparian vegetation across different elevation zones

extensive areas of riparian vegetation can be found around Ak Tal and Kazarman. Downstream from Kazarman, in the gorge leading to the Toktogul only occasional vegetated floodplain pockets exist. Finally, also at the fringe of the Toktogul reservoir vegetation exists even this cannot be considered as natural riparian vegetation. A direct derivative from the raster data set of riparian

vegetation is its elevation distribution (Fig. 6.23). There are several smaller peaks between 3000 and 4000 m.a.s.l. referring to the area around Kara Say. A next peak between 2000 and 2500 m.a.s.l. represents the riparian vegetation between Eki Naryn and Naryn City. The majority of riparian vegetation, however, is located between 1500 and 2000 m.a.s.l., including the area around Ak Tal at approximately 1600 m.a.s.l. The peak between 1000 and 1500 m.a.s.l. is representing the riparian area around Kazarman. The vegetation along the fringe of the Toktogul is not included as it does not represent a natural riparian ecosystem.

### 6.3.6 Disaggregation and aggregation of the river corridor

The segmentation of the Naryn River corridor into 100 m-segments using the Thiessen polygon method results in a total number of 5526 segments. These segments are the basis for the visual analysis of the longitudinal pattern of riparian zone as well as the riparian vegetation. Figure 6.24 shows the longitudinal pattern of riparian zone area as well as the area of riparian vegetation. While the general spatial distribution already became clear from the map, the longitudinal plot

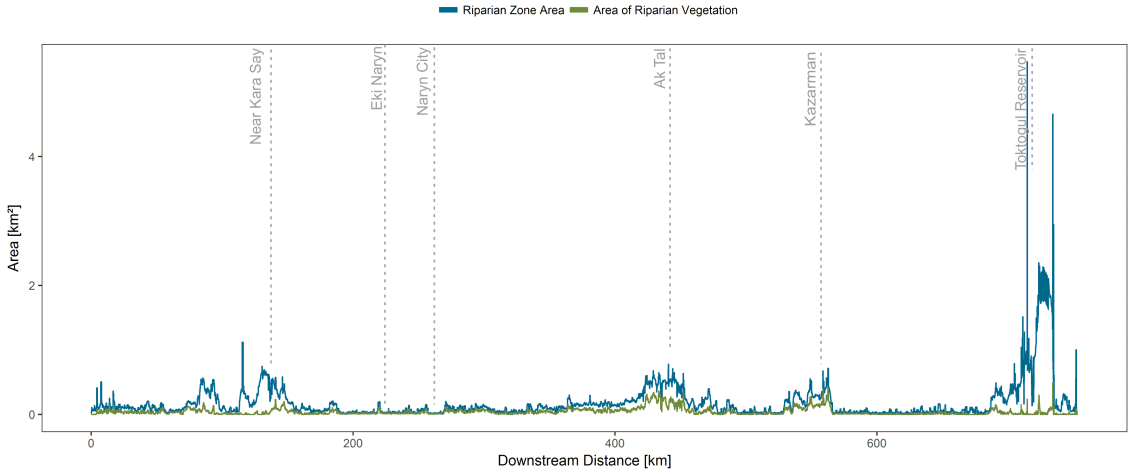


Figure 6.24: Longitudinal pattern of the area of riparian zone (blue) as well as riparian vegetation (green)

highlights better the structure of the river corridor. A large riparian zone occurs mainly in the upstream part near Kara Say and then again around Ak Tal and Kazarman. Also the Toktogul reservoir forms a large area connected to the Naryn River and thus a large area of riparian zone. But of course, we cannot expect natural riparian processes within this area. The pattern of riparian vegetation follows the general structure of the riparian zone width. Only at the Toktogul reservoir, the area of vegetation is much smaller than the riparian zone area due to the large water surface of the reservoir.

The expert based segmentation based on the discrimination of river types resulted in the delineation of 121 reaches. An overview of the distribution of the different river types within the river corridor is given in Figure 6.25. In the uppermost part upstream from Eki Naryn, steep headwaters are the dominating river type, even if shorter sections characterized as braided rivers occur. Between Eki Naryn and Naryn City, an interplay of straight and short braided reaches dominate the river corridor. Downstream from Naryn City, the braided reaches become longer, around Ak Tal also braided-wandering reaches occur. The braided and braided-wandering reaches around Ak Tal and

Kazarman are then interrupted by a gorge. Further downstream, a long gorge is leading towards the Toktogul reservoir. From an overall perspective, braided reaches are the dominant river type

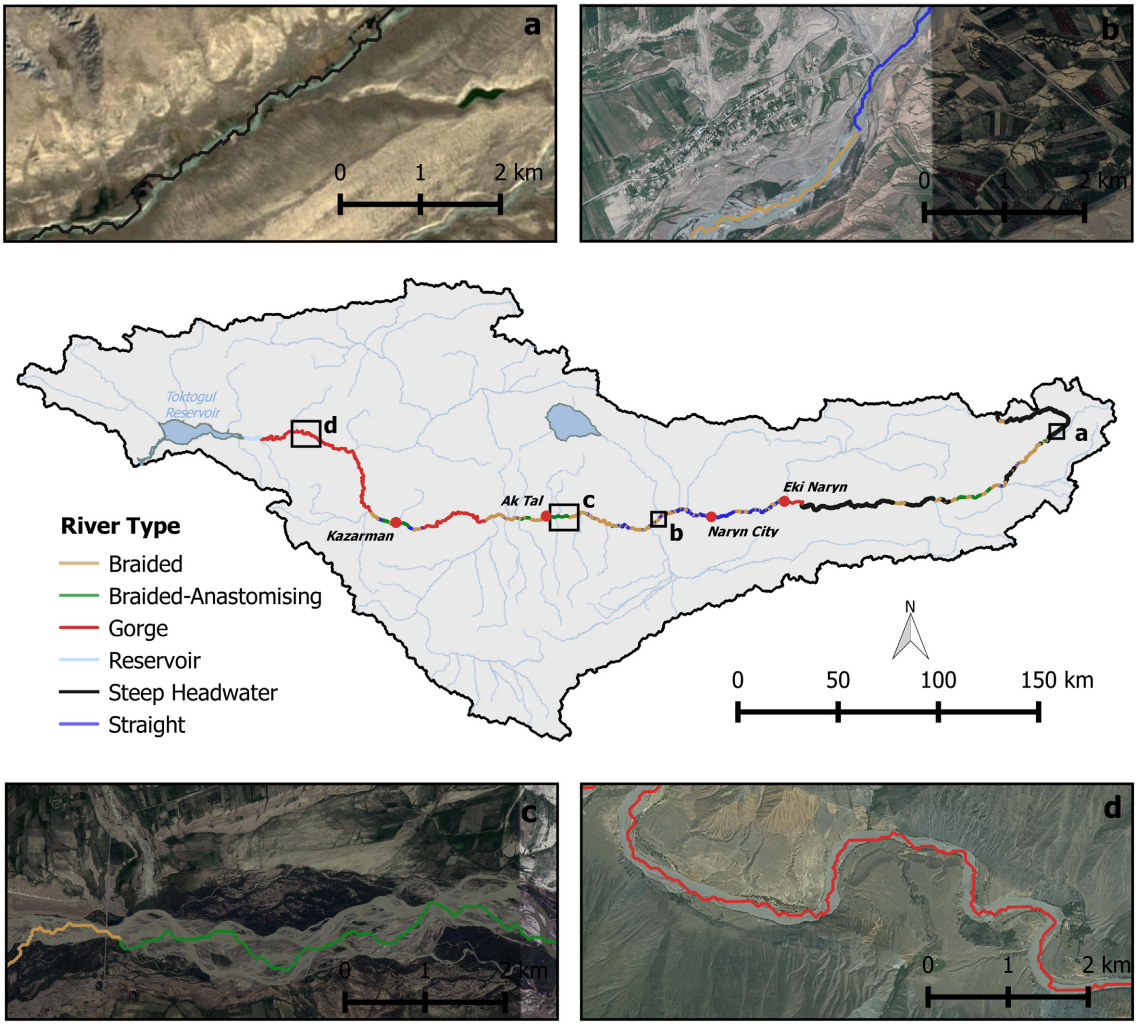


Figure 6.25: Distribution of river types along the Naryn River; The insets a-d give a more detailed impression of the respective river types

representing 211.30 km or 28.12% of the entire Naryn with its length of 753.66 km. Nearly the same dominance have gorges with 174.57 km (23.16%) and the steep headwaters with 167.40 km (22.21%). The high dominance of gorges arises from the 115.70 km long gorge upstream from the Toktogul reservoir. The other three river types contribute considerably less than the already mentioned ones. Straight reaches have an entire length of 77.21 km (10.24%), the Toktogul reservoir contributes to another 9.53% (71.83 km). A special case of braided rivers is the river type *'braided-anastomising'* which differs from braided reaches by the presence of secondary channels separated from a main channel with braided characteristics by vegetated islands (see Fig. 6.25c). This particular type has an entire length of 49.12 km contributing to 6.52% of the entire Naryn River. While braided river reaches are found along almost the entire river from the uppermost headwaters till Kazarman, braided-anastomising reaches occur only around Ak Tal and Kazarman.

### 6.3.7 Width estimation and confinement ratio as derivations from the disaggregated river corridor

*Width estimations*

The width estimations are crucial steps for assessing the geomorphic structure of the Naryn River corridor. Thus, the quality assessment is an important step during the analysis. Figure 6.26 shows the scatter plot of modeled and measured river corridor and active channel widths. For the river corridor, the model delivers accurate results, all values are close to the line indicating equal modeled and measured values. An correlation coefficient of 0.952 as quantitative accuracy metric supports this visual impression. The results for the active channel width are less accurate, there is a systematic bias with an overestimation of small and an underestimation of large active channel widths. The correlation coefficient of 0.84 also reflects this bias. Nevertheless, the width estimations from remote sensing go beyond simple scaling of widths over the Strahler orders or the downstream distance as applied in previous studies (e.g. Schmitt et al. 2014) what makes them useful despite the inherent uncertainty.

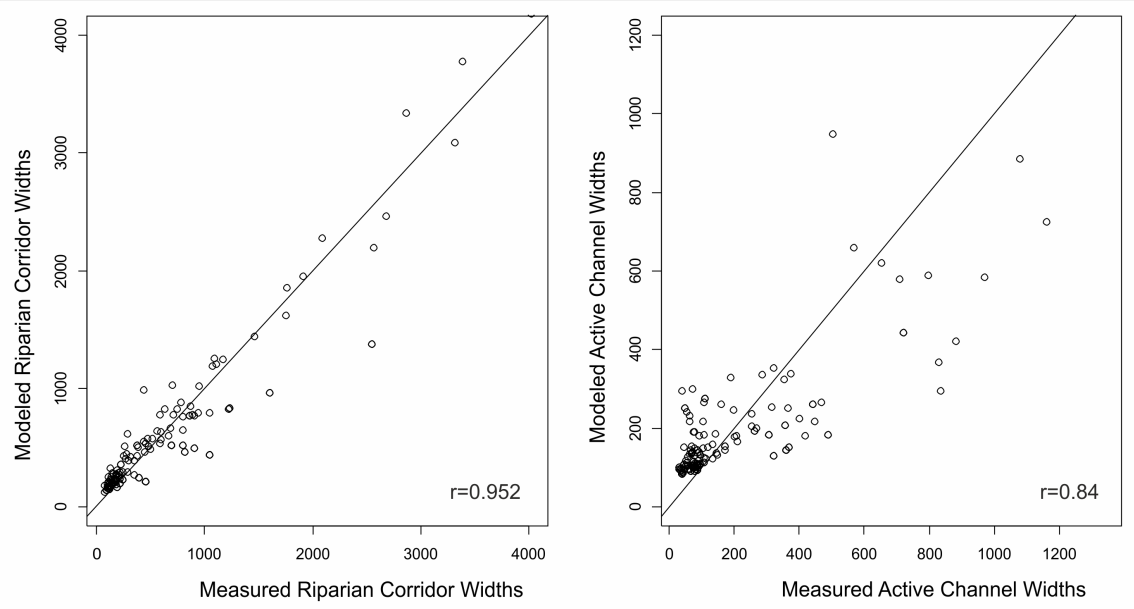


Figure 6.26: Validation of the river corridor and active channel width

The modeled river corridor width varies between 116.2 m and 26,511.5 m with a median of 346.1 m. The active channel width is in the range of 76.7 m and 9128 m having a median of 139.2 m. Figure 6.27 shows the associated longitudinal pattern of the values. The general pattern is the same with the largest widths above 10,000 m occurring at the Toktogul reservoir. Upstream from the Toktogul, a section of the Naryn with a very narrow river corridor and small active channel widths below 150 m dominates the riverine landscape. A wider river corridor (up to 5000 m) and higher active channel widths up to 1200 m occur around Kazarman and Ak Tal. Similar river corridor and active channel widths are again abundant around Kara Say.

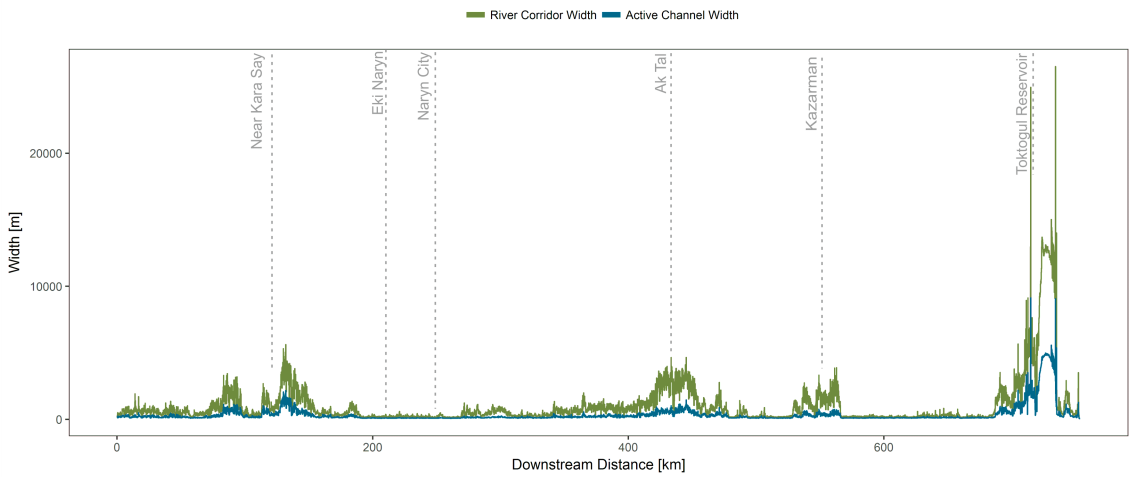


Figure 6.27: Longitudinal pattern of the river corridor (green) and active channel width (blue)

*Confinement ratio*

When having a look at the confinement, it is possible to compare the remote sensing derived confinement ratio (cr) with confinement mapped from high resolution virtual globe imagery according to the *Riverstyles Framework* (Brierley and Fryirs, 2005; Fryirs et al., 2016). Figure 6.28 shows the boxplots of the ratio for the different confinement types. The confined river sections

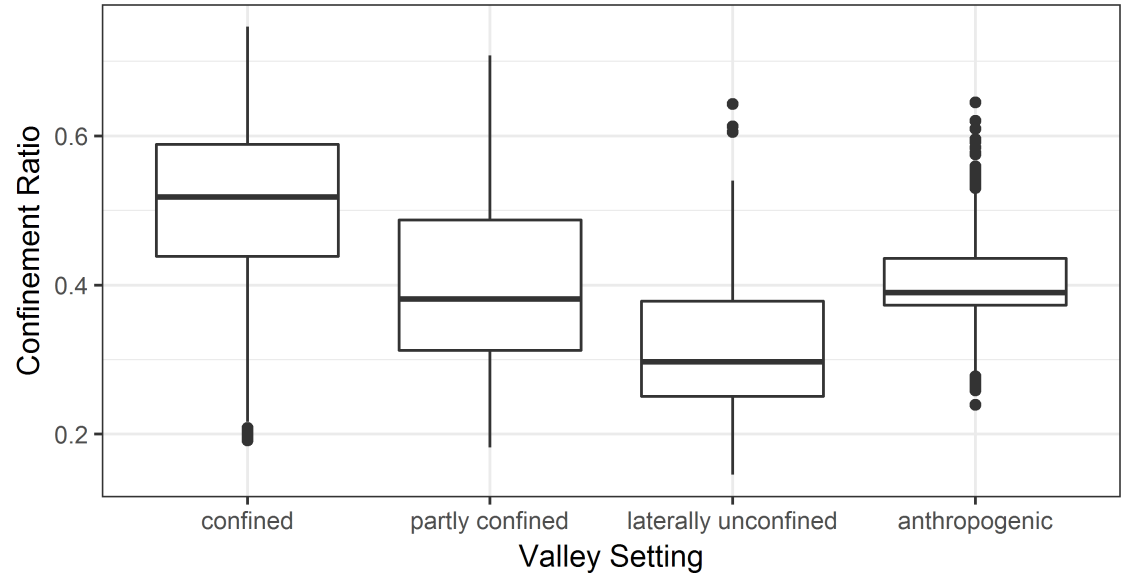


Figure 6.28: Confinement ratio values for different confinement types according to the *Riverstyles Framework*

have a median cr of 0.5176, the partly confined sections have a median cr of 0.3810, laterally unconfined sections show the smallest median cr with a value of 0.2967. The Toktogul reservoir classified as 'anthropogenic' has a median cr of 0.3898. A Kruskal-Wallis test supports the hy-

pothesis that the confinement ratio values differ significantly between the mapped confinement classes (Chi-squared=105030, p-value $< 2.2 \times 10^{-16}$). Thus, the confinement ratio can be considered as meaningful indicator of the geomorphologically relevant parameter confinement.
Having a look at the longitudinal pattern of the confinement ratio shows that the valley setting is

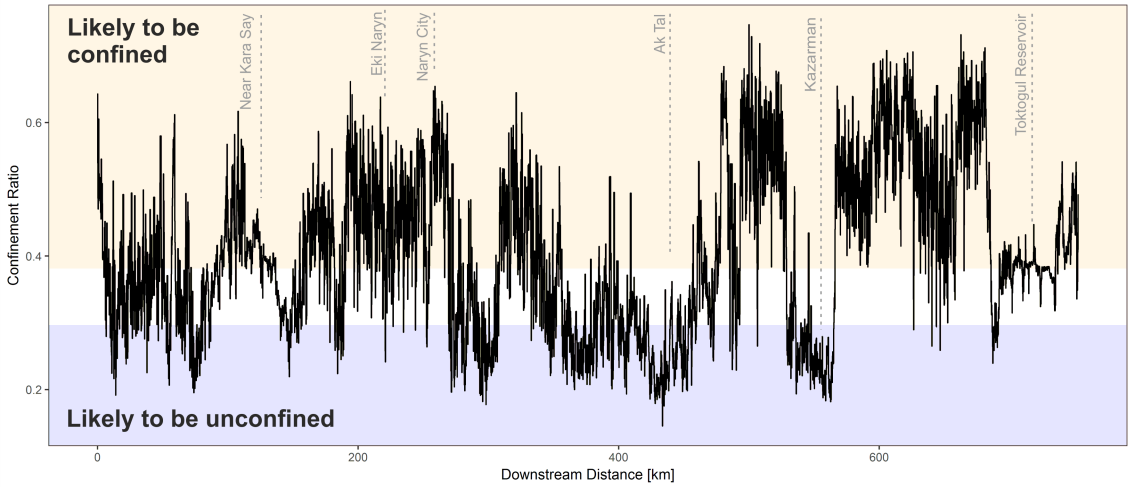


Figure 6.29: Longitudinal pattern of the confinement ratio as indicator of confinement; the colors indicate the boundaries between the valley settings based on the median values of the confinement ratio (Fig. 6.28)

heterogeneous along the Naryn River. The blue color indicates potentially unconfined sections, the yellow color potentially confined sections. The white band in between stands for partly confined sections. While this is only a first rough assessment, it becomes already clear that a major part of the Naryn River corridor tends to be confined or partly confined. 62.52% have a confinement ratio >0.3810 suggesting that these sections are likely to be confined or partly confined. Another 37.48% are likely to be laterally unconfined with a confinement ratio <0.2967. These unconfined river corridor sections occur mainly around Kazarman, between Naryn City and Ak Tal but also in the uppermost part of the river corridor near Kara Say. Clearly confined sections, on the contrary, exist between Ak Tal and Kazarman, between Kazarman and the Toktogul reservoir and around Eki Naryn. Despite this general patter, there is a high degree of heterogeneity reflecting the smaller scale variability of the river corridor along the Naryn.

*Erosion and deposition model*

Figure 6.30 shows the longitudinal pattern of the stream power balances along with the interpretation of the dominating channel state. Clearly erosion dominated reaches occur predominantly on the first 300 kilometers of the Naryn River. On the following 300 km, there is an interplay of shorter reaches alternating dominated by erosion and deposition respectively equilibrium or close to equilibrium. Then, a 150 km long clearly erosion dominated reach leads to the Toktogul reservoir being - of course - clearly deposition dominated. All in all, erosion is the major channel state for the reaches upstream from Naryn City. Along 340.30 km, this state could be identified making up 45.15% of the total river length. A deposition dominated channel state is also relevant and is predicted along 184.35 km (24.46%). 105.75 km (14.03%) of the Naryn River are in a dynamic equilibrium state where sediment input from upstream and transport capacity are regarded to be

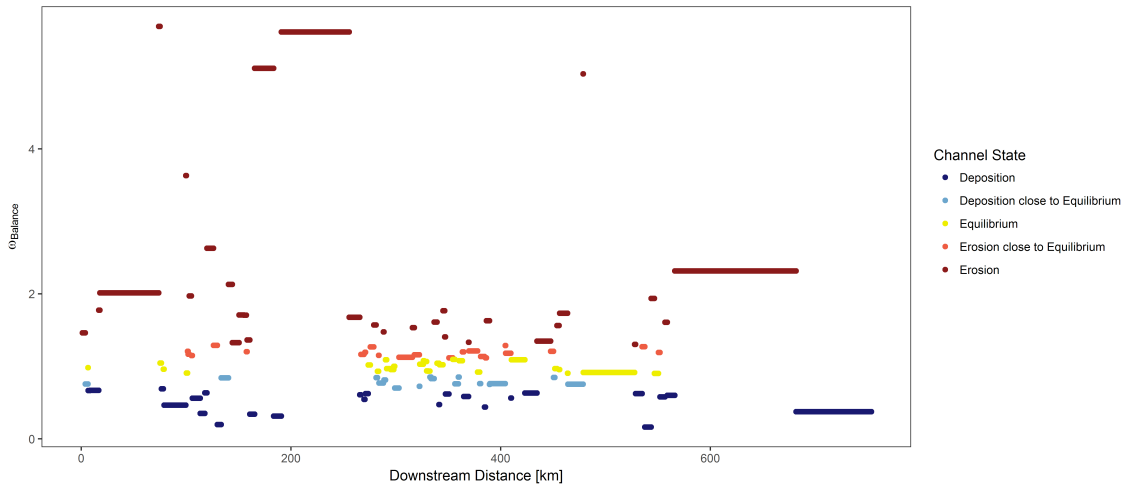


Figure 6.30: Longitudinal pattern of the balance values ($\omega_{\text{Balance}}$) of the reach averaged specific stream power

in balance. The states close to equilibrium contribute to 16.19% of the entire river, where the contribution of reaches with a tendency towards erosion or towards deposition is approximately the same. The relationship between stream power balance, channel state and river type is shown in figure 6.31. Clearly deposition dominated is the Toktogul reservoir with a median balance of

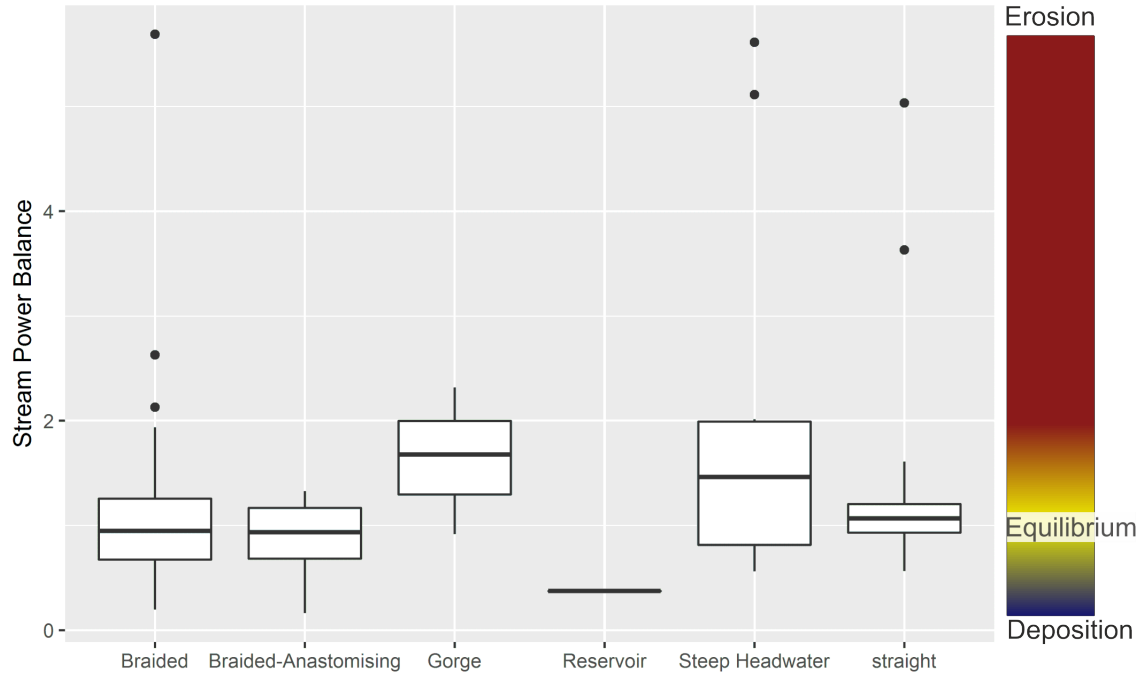


Figure 6.31: Stream power balance values grouped by river type

0.37. At the other end with high stream power balance values all greater than 1, i.e. all erosion

dominated, are the gorges with a median balance 1.68. In addition, the steep headwater reaches show high stream power balances (median=1.46). The majority of the straight reaches have values close to 1, i.e. close to equilibrium (median=1.07). However, the interpretation of the boxplot suggests that straight reaches are more likely to have a tendency towards erosion than to deposition. Contrary, braided and braided-anastomising reaches have a higher tendency towards deposition, even if their median stream power balance of 0.95 and 0.94 indicate a state close to equilibrium.

## 6.4 Spatial and statistical analysis of the river corridor

In this chapter, manifold river corridor parameters have been derived from diverse remote sensing sources. Now it is time to place them in context and analyze the spatial structure of the Naryn River. A straightforward approach is to link the different parameters with the mapped river types to give a descriptive overview before rising the question of the potential drivers. At first, we can have a look at the contribution of each river type to the riparian zone (Fig. 6.32). When having the river

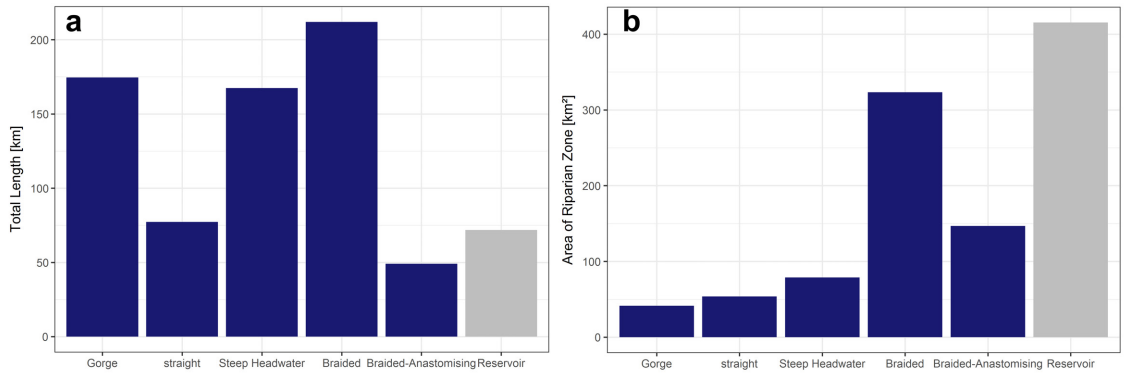


Figure 6.32: Contribution of the different river types to the total length of the Naryn River (a) and the riparian zone area (b)

length in focus, there is a similar occurrence of braided reaches, gorges and steep headwaters while straight and braided-anastomising reaches contribute are less relevant (Fig. 6.32a). The picture changes, when taking the contribution of the different river types to the riparian zone area into account. The entire riparian zone along the Naryn River covers an area of 1,059.75 km$^2$. 415.45 km$^2$ are covered by the Toktogul reservoir, a totally anthropogenic system. The other 644.30 km$^2$ (60.80%) can be considered to operate under widely natural conditions. Braided reaches contribute with an area of 323.35 km$^2$ to 50.19% of the entire natural river corridor. In addition, braided-anastomising reaches make up 146.86 km$^2$ (72.98%). Together, braided and braided-anastomising contribute to 72.98% of the natural riparian zone and can be considered as the dominating river types in the river corridor. Steep headwaters with a riparian zone area of 78.79 km$^2$ contribute to another 12.23% of the river corridor area. The gorges and straight reaches have a similar area of 41.48 km$^2$ (6.44%) and 53.82 km$^2$ (8.35%) respectively. Thus, analyzing the Naryn from a longitudinal perspective results in the conclusion that braided and braided-anastomising reaches make up only a minor part of the entire river with steep headwaters and gorges being significant parts of the river corridor as well (Fig. 6.32a). However, when having the area of the riparian zone in mind, the braided and braided-anastomising reaches in the central part of the catchment are by far the most relevant river type.

Second main interest is the distribution of riparian vegetation within the different river types. Figure 6.33 shows this distribution. Beside the visual comparison, a Kruskal-Wallis test along with a Dunn-Bonferroni posthoc test has been performed to check for the significance of the differences. To account for the different reach lengths, the area of riparian vegetation has been normalized prior to performing the statistical test. 64.75% of the riparian vegetation is concentrated in the

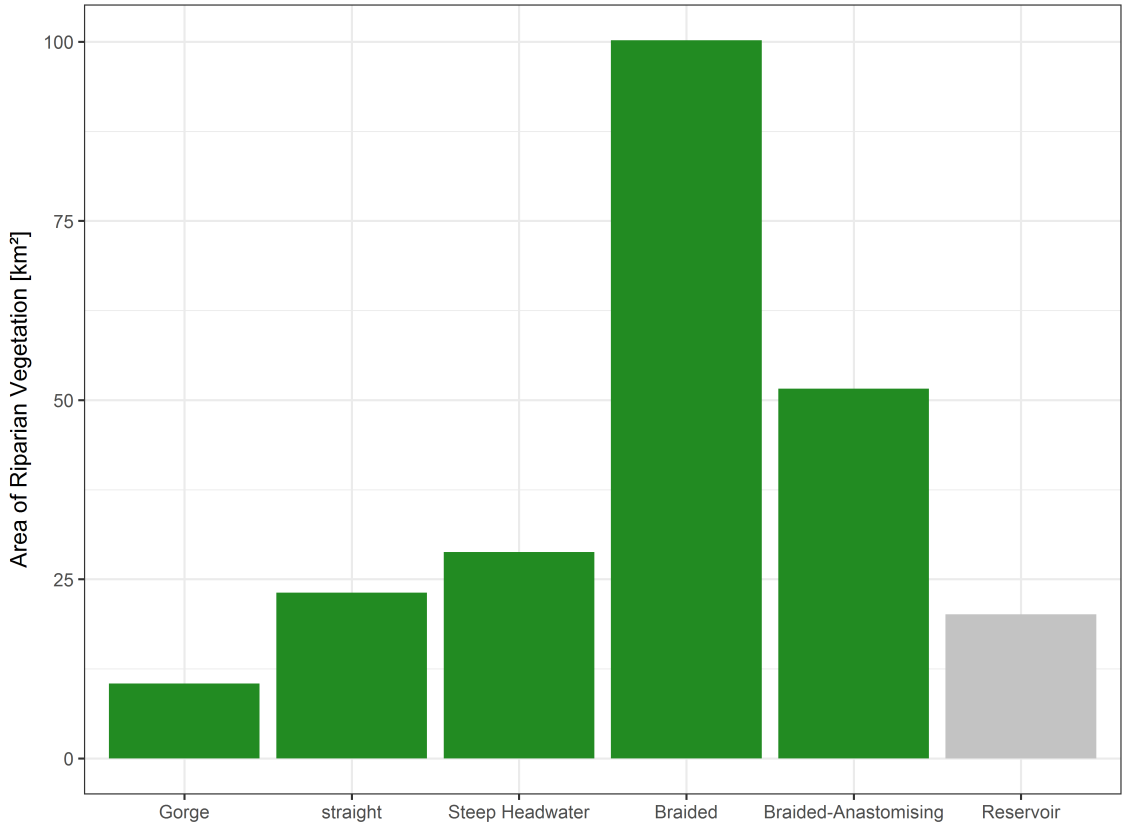


Figure 6.33: Area of riparian vegetation per river type

braided and braided-anastomising reaches with 100.21 km$^2$ and 51.59 km$^2$ respectively. The steep headwaters contribute to another 28.80 km$^2$, straight reaches to 23.13 km$^2$, the gorges to another 10.43 km$^2$. Also along the reservoir, a fringe of vegetation, in this area also partly agriculture, connected to the hydrological processes of the reservoir exists. Of course, we cannot consider this vegetation as natural riparian vegetation, nevertheless this area is is part of the river corridor. The visual impression of large differences of vegetation area is confirmed by the Kruskal-Wallis test on the vegetation area normalized by reach length. A chi-squared of 16.46 with a p-value of <0.001 clearly indicate that the observed differences are statistically significant. However, the picture becomes more heterogeneous when having a look at the results of the posthoc test in table 6.8. It becomes clear, that not all pairwise comparison results in significant differences. There is no statistically significant difference between the braided and braided-anastomising reaches as well as for the gorges and steep headwaters. This is a feasible result when thinking about the similar nature of these river types. More surprisingly is that also straight and braided as well as straight and braided-anastomising do not show a significant difference. On the contrary, significant differences

Table 6.8: Results of the Dunn-Bonferroni test comparing the normalized vegetation area of the different river types

| Comparison | Z-Score | P-Value | Significance | Effect Size |
|---|---|---|---|---|
| Braided - Braided-Anastomising | -0.43 | 0.67 | No | 0.04 |
| Braided - Gorge | 2.18 | 0.03 | 95%-level | 0.20 |
| Braided-Anastomising - Gorge | 2.18 | 0.03 | 95%-level | 0.20 |
| Braided - Steep Headwater | 2.57 | 0.01 | 99%-level | 0.24 |
| Braided-Anastomising - Steep Headwater | 2.28 | 0.02 | 95%-level | 0.21 |
| Gorge - Steep Headwater | -0.68 | 0.50 | No | 0.06 |
| Braided - straight | -1.38 | 0.17 | No | 0.13 |
| Braided-Anastomising - Straight | -0.41 | 0.69 | No | 0.04 |
| Gorge - Straight | -2.64 | 0.01 | 99%-level | 0.24 |
| Steep Headwater - Straight | -3.34 | <0.01 | 99%-level | 0.31 |

in the area of riparian vegetation exist between the braided/braided-anastomising reaches and the gorges as well as with the steep headwaters. In addition, gorges and steep headwaters differ also significantly in their amount of vegetation compared to the straight reaches.

*What controls the river types?*

After seeing the differences within the river types, one might rise the question what the drivers of the river type development are. As multiple drivers of planform development can be expected, a principal component analysis was carried out to allow an interpretation of the different variables in reduced dimensionality (Fig. 6.34). Prior to the principal component analysis, the data has been scaled and centered following the suggestion of Venables and Ripley (2002). When having a look at the different variables for the reaches in reduced data space, different associations between variables become obvious (Fig. 6.34 and table 6.4). The total stream power as measure of available energy in the river system is highly associated with the discharge and not the gradient. Thus, the energy is more controlled by the variable discharge then the gradient. This is also true for the specific stream power as indicator for the locally available energy though it is related to the confinement ratio (respectively its antipode, the active channel and river corridor width). High specific stream power values are likely to be associated with narrow river corridor sections with a high degree of confinement. Channel gradients are inversely related to the discharge. High gradients occur mostly in settings with low discharge, i.e. in the uppermost part of the river corridor as discharge is directly related to drainage area.
The different river types are located at specific positions within the reduced data space even if there is an obvious overlap between the normal data space indicated by the ellipses in figure 6.34. Especially braided and straight can occur under almost the same conditions, just braided reaches tend to have a higher active channel width and develop in settings with a lower confinement and higher river corridor width compared to straight reaches. More clearly distinct are braided-anastomising reaches which are associated with low confinement and high river corridor widths as well as with lower channel gradients and a low specific stream power. On the contrary, gorges are characterized by high confinement and high specific stream power values. The main discriminant of steep headwaters is their higher channel gradient compared to the other river types. In addition, they tend to have a certain degree of confinement indicated by the orientation on the confinement

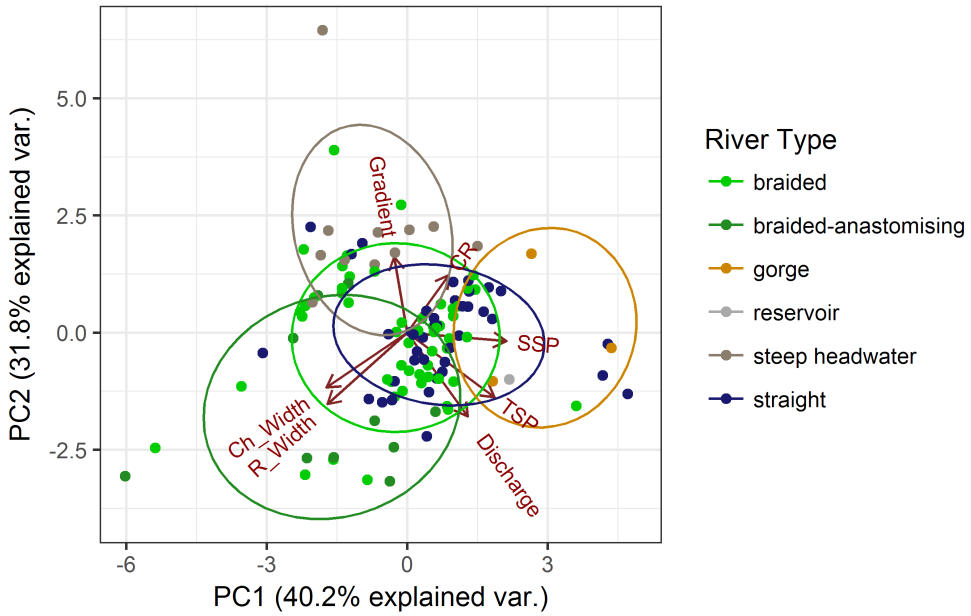


Figure 6.34: Graphical representation of the principal component analysis of the controlling variables (CR=confinement ratio, TSP=total stream power, SSP= specific stream power, Ch_Width=active channel width, R_Width=river corridor width)

ration axis. All in all, it becomes obvious that the main differences of the river types occur along the axis confinement ratio-active channel/river corridor width. This leads to the conclusion, that confinement is a major control of the process-form relationship of the Naryn River. This is in accordance of other work reporting confinement as major control of river planform development (Brierley and Fryirs, 2005; Fryirs et al., 2016). The confinement is also a major control of the specific stream power as widely recognized control of river processes (Nanson and Croke, 1992; Knighton, 1999; Ferguson, 2005; Barker et al., 2009; Fryirs and Brierley, 2013; Bizzi and Lerner, 2015). While the total stream power as a function of discharge and gradient is mainly controlled by the discharge as indicated by the similar value of the loadings of the first component (see table 6.4). The specific stream power, however, is influenced by the confinement as well as by the value of the total stream power (and thus discharge). The channel gradient seems to be only a minor control for the variations in stream power for the Naryn River.

Table 6.9: Loadings of the principal component analysis of the different controlling variables

| Variable | PC 1 | PC 2 | PC 3 | PC 4 | PC 5 | PC 6 | PC 7 |
|---|---|---|---|---|---|---|---|
| Total Stream Power | 0.46 | -0.38 | 0.15 | -0.23 | 0.02 | -0.67 | 0.34 |
| Specific Stream Power | 0.52 | -0.05 | 0.22 | -0.10 | 0.69 | 0.40 | -0.18 |
| Channel Gradient | -0.07 | 0.45 | 0.31 | -0.82 | -0.15 | 0.02 | -0.04 |
| Confinement Ratio | 0.22 | 0.34 | 0.70 | 0.47 | -0.27 | 0.05 | 0.21 |
| Discharge | 0.32 | -0.50 | 0.05 | -0.14 | -0.62 | 0.39 | -0.29 |
| Active Channel Width | -0.43 | -0.33 | 0.52 | 0.04 | 0.16 | -0.29 | -0.58 |
| River Corridor Width | -0.42 | -0.42 | 0.27 | -0.14 | 0.13 | 0.38 | 0.62 |

The confinement is mainly determined by geological control. Unfortunately no precise geological map is available to perform a statistical analysis of this controlling factor. However, when linking the remote sensing derived information about confinement with the information about geology available from literature, it turnes out that confinement is high upstream from Eki Naryn where the Naryn flows in the Hercynides of the Tian Shan, becomes lower when the Naryn flows into the tectonically formed Cenozoic Naryn Basin and becomes high again, when the river leaves the Cenozoic basin again downstream from Kazarman (see De Grave et al. 2011 and section 2.3 for an overview). The erosion/deposition model reveals in addition that the gorges and headwater reaches flowing outside the sedimentary fill of the Cenozoic basins are characterized by a high tendency towards erosion while the reaches within the basin are close to a dynamic equilibrium state. This leads to the assumption that within the unconsolidated sediments of the basin fills, the river could already develop towards an equilibrium state while this development was not possible in the bedrock confined sections of the Hercynides. Thus, the contemporary process-response system of the Naryn River is ultimately governed by the geological constraints. Only within the Cenozoic basins where partly confined and laterally unconfined reaches exist, the stream power can be considered as major driving force of river development.

*What controls the distribution of riparian vegetation?*

In the context of biogeomorphology but also for the assessment of ecosystem services and potential impacts of the planned hydropower dams, it is relevant to understand the control on the spatial distribution of riparian vegetation within the river corridor. While a first attempt was to link the riparian vegetation with the river types, in this section a more statistical test is applied to the disaggregated river corridor. Similar to Notebaert and Piégay (2013), a multiple linear model of the form $y = a + \beta_1 x_1 + \beta_2 x_2 + ... + \beta_i x_i$ relating the variable *y*, area of riparian vegetation per 100 m-segment, to the different controlling variables. Once the model is fitted, the resulting r-squared is deconstructed to check for the respective contribution of each variable for the explanatory power of the model using the partitioning method of Lindeman et al. (1980). Full details about the method of r-squared deconstruction can be found in Grömping (2015). The assumption is, that variables with a higher contribution to the r-squared of the linear model also have a higher relevance as controlling factor. I used the same variables as for the principal component analysis: *confinement ratio*, *specific stream power*, *total stream power*, *discharge*, *channel gradient*, *river corridor width* and *active channel width*. In addition, the parameters have been tested for their correlation with the downstream distance to test whether there is a significant scaling effect supporting the theory of the river continuum concept (Vannote et al., 1980).
For most variables, however, there is no significant downstream correlation. Beside an obvious relation between downstream distance and elevation and discharge, only the channel gradient shows a high correlation with a r of 0.689. A less strong relationship exists additionally between the total stream power (r=0.374) and the specific stream power (r=0.208) as well as with the area of riparian vegetation (r=-0.183). All other variables have a r<0.1. This leads to the conclusion that the downstream gradients have only a minor explanatory power for the Naryn River and further, super-ordinated controlling factors are abundant. The deconstructed r-squared values of the linear model gives more insights in the relevance of these controlling factors (Fig.6.35). The overall r-squared is 0.9182, i.e. the seven variables can explain 91.82% of the variability within the riparian vegetation area. Looking at the relative importance of the different variables, it turns out that the confinement related factors river corridor width, active channel width and confinement ratio have the highest contribution to the r-squared with 41.08%, 21.70% and 23.82% respectively (see also

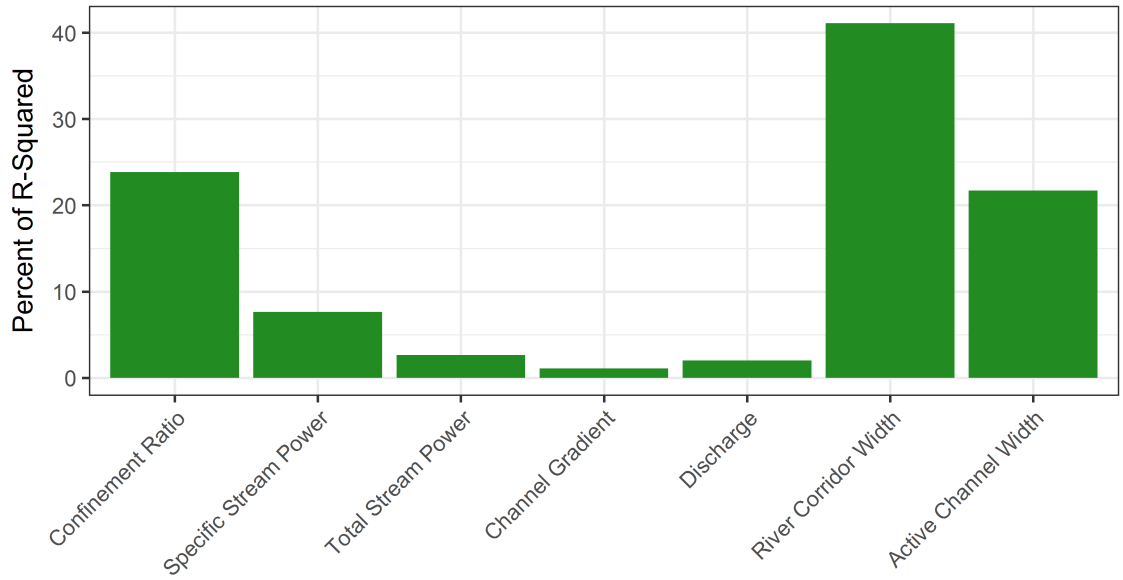


Figure 6.35: Relative contribution of the different controlling variables to the r-squared of the linear model explaining the area of riparian vegetation

Fig. 6.35). The specific stream power contributes to another 7.64% being a further relevant control. Total stream power, discharge and channel gradient, however, contribute only 2.65%, 2.02% and 1.08% to the r-squared of the linear model and can thus be considered as less important for the distribution of the riparian vegetation within the Naryn River corridor. Common for many environmental system variables, the controlling and response variables of the different components of the river corridor have not just simple process-response relationships but are partly intercorrelated as can be seen from the scatterplot matrix in figure 6.36.

Most relevant in the context of the linear modeling approach discussed above are the correlations between the river corridor width, the active channel width and the confinement ratio. The high correlation values indicate that these variables are similar expressions of the same issue - the space the river has for development as controlled by the geological constraints. An additional variable related to the confinement is the specific stream power (r=0.48). Stream power is in general closely related to the discharge as well as to the channel gradient. From having a look at the numeric correlation value alone, total stream power is closer related to discharge (r=0.14 for the gradient vs. r=0.37 for the discharge), while the specific stream power is closer related to the channel gradient (r=0.33 for the gradient vs. r=0.21 for the discharge). The scatterplots, however, shows that the different river corridor parameters are partly highly inter-correlated indicating a complex system of relationships.

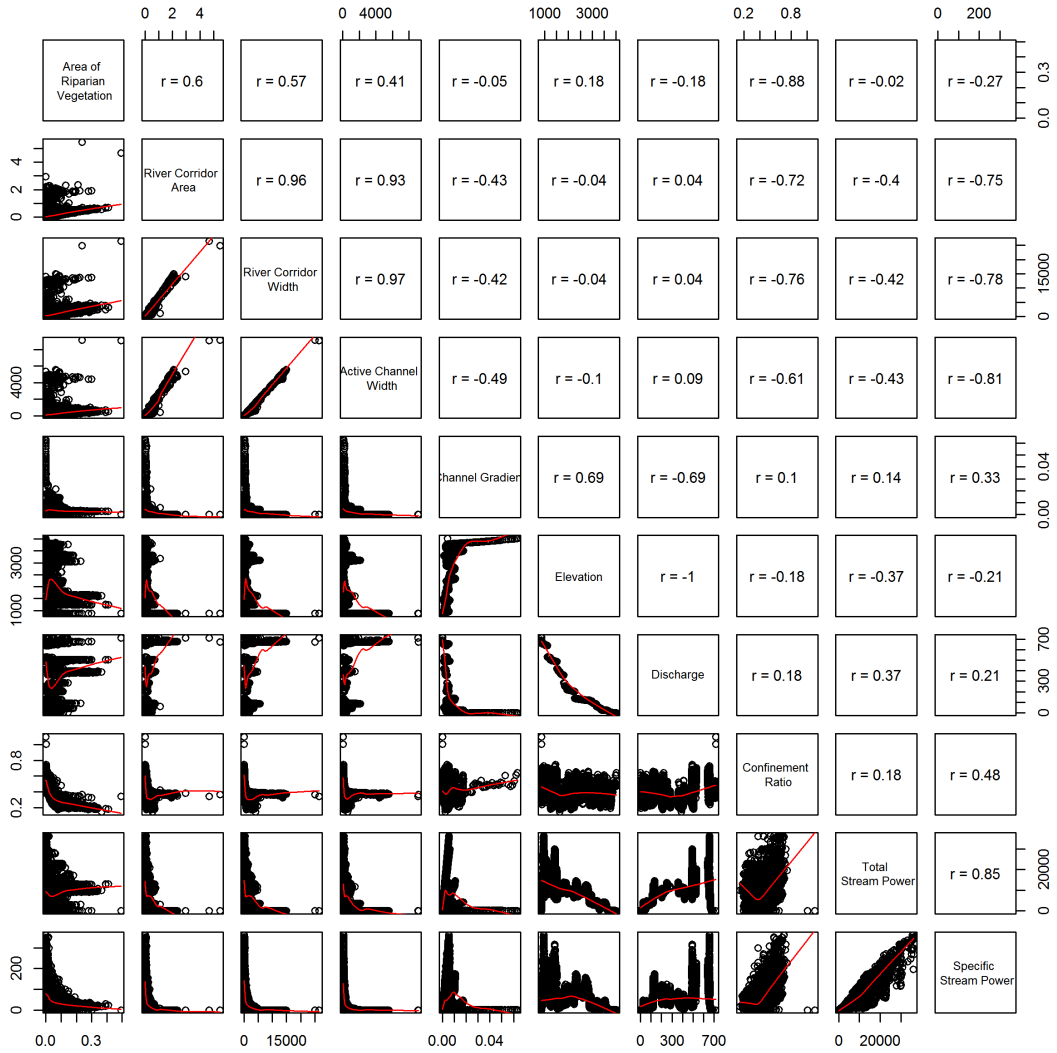


Figure 6.36: Scatterplot matrix showing the intercorrelation of different river corridor variables based on the disaggregated river corridor; The red lines in the scatterplots give a smoothed trend for orientation, the numeric correlation values are calculated as spearman's coefficient

# 7 Biogeomorphological Dynamics from Space

## 7.1 Biogeomorphology revisited

Biogeomorphology is the interaction of hydrological, geomorphological and ecological processes (see chapter 1 for a detailed review of the concept). Corenblit et al. (2007) suggested four different succession stages related to this interaction: A geomorphological stage, a pioneer stage, a biogeomorphological stage and an ecological stage. In addition to these four stages, I follow the suggestion of Gurnell et al. (2016a) and add permanently inundated zones as fifth stage. The

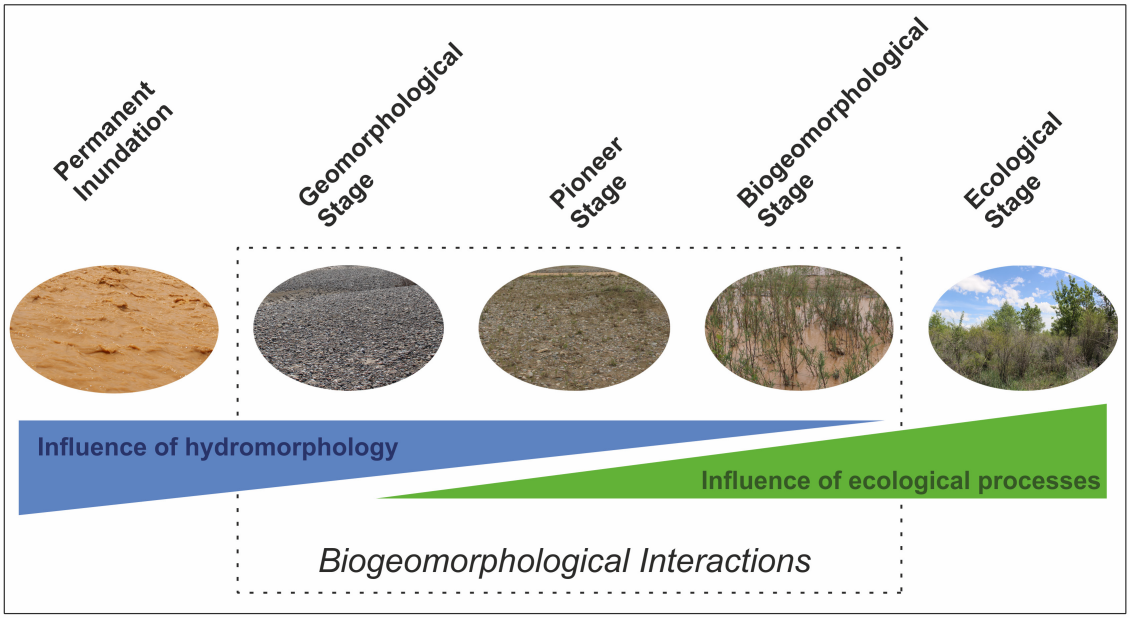


Figure 7.1: Schematic overview of the different biogeomorphological succession stages

different stages can represent a spatial distribution of different conditions at the same time but also a temporal development. From a process dynamics point of view, they can be thought as continuum along vegetation development and hydromorphological disturbance. Within the permanently inundated zones, hydrological processes are dominating, even the morphological development of bare sediment landforms is limited. In the geomorphological stage, deposition of - in the case of the Naryn - coarse sediment lead to the development of gravel bars. However, they are still likely to be flooded during the annual flood events. In the pioneer stage, juvenile vegetation can establish on the bare gravel surfaces, this is the point where vegetation occurs in the succession. Still hydromorphological disturbance governs the development. In the biogeomorphological stage, the vegetation has further developed beyond the juvenile state and becomes strong enough to resist

regular disturbance by flooding. As vegetation is still regular flooded, the interaction between hydromorphology and vegetation is strongest in this stage. In the ecological stage, the vegetation becomes disconnected from the regular disturbance and ecological processes such as the concurrence for light and nutrients control the community structure. This allows the establishment of species not adapted to regular flood disturbance.
On a more conceptual level, we can consider the different succession stages as operating under a certain process regime (see table 7.1). Thus, the different stages are defined by their specific process regime rather than by their structure or species composition. From a remote sensing per-

Table 7.1: Characteristics of the different biogeomorphological succession stages (based on Corenblit et al. 2007, Corenblit et al. 2009a and Gurnell et al. 2016a)

| Succession Stage | Natural Dynamics |
|---|---|
| Permanently inundated zone | Changes in water level, but absence of bare sediment and vegetation exposed to the air |
| Geomorphological Stage | Bare sediment surface, regularly flooded |
| Pioneer Stage | Beginning establishment of juvenile saplings on bare sediment surfaces, regularly flooded |
| Biogeomorphological Stage | Vegetation establishes and forms community structure dense enough to cause a stabilization of the underground as well as trapping of fine sediment; it is still flooded during regular flood events |
| Ecological Stage | Surfaces are located too high above the channel to be flooded during regular flood events; ecological processes like the concurrence for light and nutrients become more important than the disturbance by regular floods for ecosystem development and also species not adapted to the regular disturbance can establish |

spective, this dynamic character of biogeomorphological succession stages should be captured for a ecologically sound representation. This is especially true for analyzing the temporal behavior of biogeomorphological succession but remains relevant for the assessment of the spatial pattern at a certain point in time as well. As a consequence, time series of satellite imagery are considered to be more suitable for analyzing biogeomorphology from space than single date satellite scenes.

## 7.2 Satellite data available for time series modeling

In this thesis, I mainly focus on the use of Landsat imagery for the river corridor analysis. The major advantage of this imagery source is the long record going back until the 1970s. All in all four sensors cover that time span (Irons et al., 2012). In 1972, the MSS sensor has been launched. However, the resolution of 60 m is too coarse to assess the river corridor of the Naryn River. In 1984, Landsat 5 with the TM sensor was sent to the orbit. This sensor provided the spatial resolution of 30 m which is typical for the Landsat imagery till today. In 1999, Landsat 7 with the ETM+ sensor was launched to continue the Landsat mission. Contrary to Landsat 5, it is still in orbit and sends pictures while the TM sensor was decommissioned in 2011. However, due a failure of the scan line correction in 2003, ETM+ data contain a large amount of no-data cells. Since 2013, Landsat 8 sends imagery from the OLI sensor. Now, each pixel with the center coordinates $x_n, y_n$ can be considered as a single time series with time steps $t_1, t_2, ..., t_m$. For the area of interest within

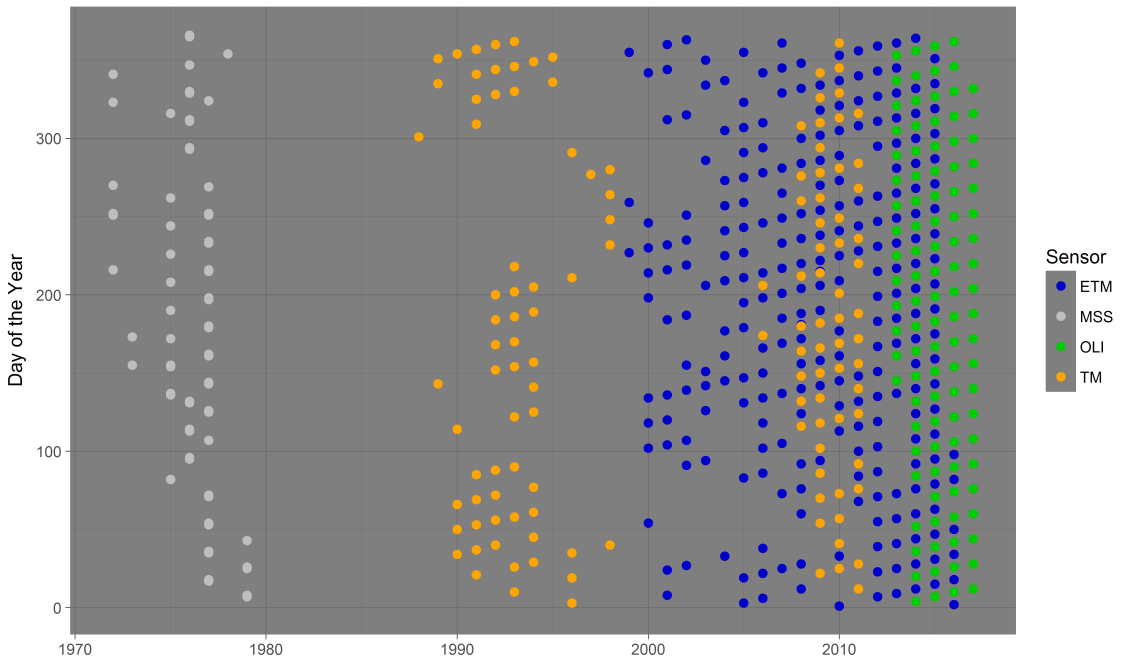


Figure 7.2: Landsat imagery available for analyzing biogeomorphological dynamics

the Naryn Basin in the central Naryn catchment, this results in 6,839,235 time series, each consisting of 475 observations (including no-data values due to clouds or sensor failures). However, the frequency of the observations is heterogeneous. Between 1988 and 1999, when Landsat 5 data only is available, there are large gaps in the imagery time series (Fig. 7.2). With the availability of ETM+ imagery, data gaps become smaller. Since at least from 2010, data at monthly coverage or even higher becomes available allowing detailed land surface phenology studies.

More recently, Sentinel-2 imagery has become available as an alternative data source (Drusch et al., 2012). For Kyrgyzstan, prior to 2017 only very few Sentinel-2 scenes are available. Since Sentinel-2 B completed Sentinel-2 A to the complete constellation, the time series density improved to a revisit time of 5 days what drastically improves the chance to get cloud-free scenes. Due to the limited time series length of Sentinel-2, I use Landsat for assessing time series of biogeomorphological succession while using Sentinel-2 to map the spatial pattern of biogeomorphological succession stages within the Naryn River corridor for the year 2017 only. The time series analysis approach suggested in this chapter is applicable to the Sentinel-2 imagery as well once the Sentinel archive has sufficient records.

In addition to the Landsat and Sentinel-2 imagery, 2 scenes of high resolution Planet Scope rgb images has been acquired for the braided-anastomising reach around Ak Tal for October 2015 and October 2016. These images serve as a reference for detecting changes caused by the 40 year return period flood in 2016 based on visual interpretation of these images. Automated analysis of these images is not possible due to spectral inconsistencies of Planet Scope imagery.

## 7.3 Exploring the multispectral and multitemporal representation of biogeomorphological dynamics

*Creating ground control points*

Mapping of ground control points of the different succession stages is a crucial step for the classification of the remote sensing imagery. The different succession stages are defined by the degree of interaction of hydro-morphological and ecological processes (Corenblit et al., 2007; Gurnell et al., 2016a). Thus, I base upon indicators representing the different process regimes. An overview of these indicators is given in table 7.2. Now, a stratified sampling design has been applied using

Table 7.2: Indicators for the different biogeomorphological succession stages for the field mapping of ground control points

| Succession Stage | Indicators |
|---|---|
| Permanently indundated zone | Covered by water during low flow season in early spring |
| Geomorphological Stage | Bare sediment surface; not flooded during the low flow season in early spring |
| Pioneer Stage | Juvenile individuals of woody species on bare sediment surface |
| Biogeomorphological Stage | Woody vegetation beyond the juvenile state; clear dominance of disturbance tolerant species; geomorphic evidence of disturbance like fresh fine sediment accumulation or flood marks; absence of herbal vegetation layer |
| Ecological Stage | Abundance of herbal vegetation layer and species intolerant to disturbance; consolidated sediment body with loamy texture |

the different succession stages as strata. Priority for the selection of the sampling points was the homogeneity within the area of one Landsat pixel rather than strict randomness. A total number of 111 ground control points have been collected in spring 2016, 20 in the pioneer stage, 23 in the geomorphological stage, 44 in the biogeomorphological stage and 24 in the ecological stage. For the permanent inundated areas, no direct field sampling is possible due to the lack of accessibility. Thus, 21 points for the class 'permanent inundation' have been added based on the visual interpretation of rgb-stacks of satellite images for the same time period as the field sampling. Additional points have been collected for the M.Sc. thesis of Alex Schechtel assessing the suitability of Sentinel-2 imagery for the supervised classification of biogeomorphological succession stages (see Schechtel, 2018). These points (218 in total) have been collected in spring 2017. Again, additional 36 points for the permanent inundation stage have been derived by the visual interpretation of rgb-image stacks from satellite imagery acquired in the low flow season in April 2017.

*Deriving spectral-temporal signatures of the biogeomorphological succession stages*

Optical remote sensing incorporates the use of spectral properties of the surfaces of the classes of interest, i.e. the amount of solar radiation absorbed or reflected in a certain spectrum of the sunlight. Figure 7.3 shows the spectral profiles of the biogeomorphological succession stages. These spectral profiles have been derived from Sentinel-2 imagery acquired on May 26 (discharge 406 $m^3s^{-1}$) and on November 2 (discharge 55 $m^3s^{-1}$). It becomes obvious, that spectral profiles

from the two dates show considerable differences especially in the near infrared spectrum (740 nm to 842 nm) and in the shortwave infrared (865 nm to 2190 nm). In the spring scene, there is

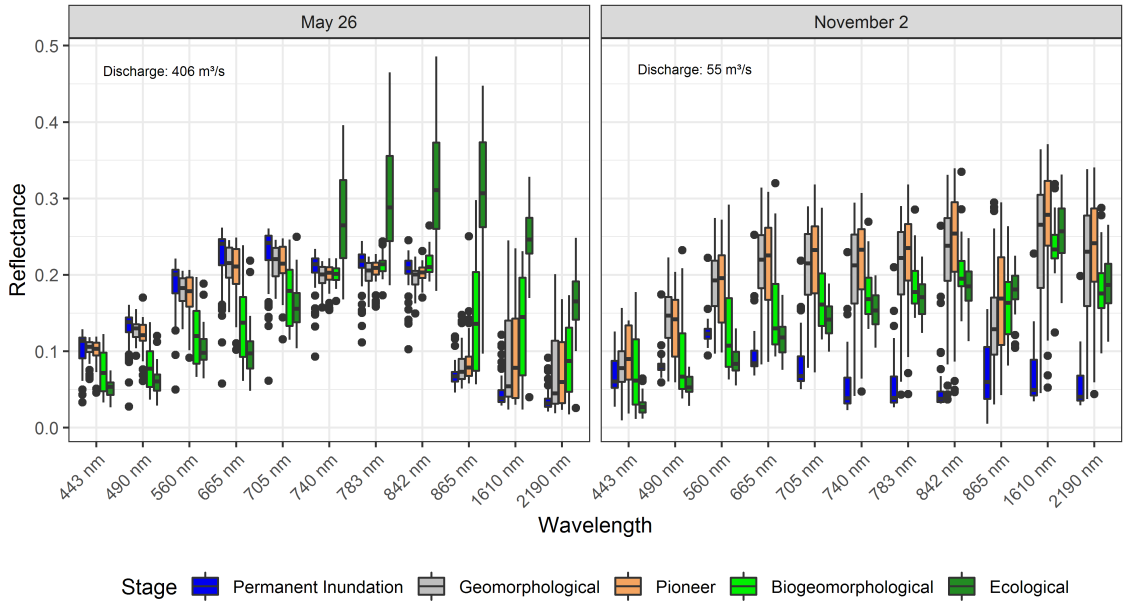


Figure 7.3: Spectral signatures of the five biogeomorphological succession stages for two different dates derived from Sentinel-2 imagery

a high reflectance in the infrared spectrum within the ecological stage indicating high photosynthetic activity. This assumption of photosynthetic activity is supported by the high absorbance in the red spectrum (665 nm) in spring which is reduced in the autumn scene. However, most relevant from the perspective of biogeomorphology assessment are the differences in the shortwave infrared spectrum. In May, in a high discharge situation, geomorphological, pioneer and biogeomorphological stage and the permanent inundation stage approach each other. On the contrary, in November when discharge is low, the permanent inundation stage and the other stages are clearly separable in the near and shortwave infrared spectra. This indicates that during the high discharge period end of May the field calibration plots of geomorphological, pioneer and biogeomorphological have been at least partly flooded causing a higher absorbance in the shortwave infrared as it is typical for inundated surfaces (Boschetti et al., 2014; Malinowski et al., 2017). The plots in the ecological stage have a significantly higher reflectance in the near infrared and the shortwave infrared in May what suggests that they have not been inundated at the time of satellite imagery acquisition (what is in agreement with field observation from May 2017). In November, the absorbance in the near infrared and shortwave infrared spectra are still high for the permanent inundation stage suggesting that these plots are still inundated during low flow. For the plots in the geomorphological, pioneer and biogeomorphological stage, the infrared absorbance is now lower than in May as they are not longer inundated at a discharge of 55 $m^3 s^{-1}$.
This observation suggests that there is a considerable dynamic of the surface reflectance due to the discharge regime. Thus, the spectral information at a single date does not tell the full story and the temporal trajectory of the surface reflectance should be considered as well. To avoid errors due to illumination differences, I use two spectral indices to describe temporal dynamics of surface reflectance. First, I use the Normalized Difference Vegetation Index (NDVI) to describe the

photosynthetic activity visible in the red and the near infrared spectra:

$$\text{NDVI} = \frac{\text{NIR} - \text{RED}}{\text{NIR} + \text{RED}} \tag{7.1}$$

where NIR is the reflectance in the near infrared spectrum and RED the reflectance in the red spectrum (Tucker, 1979). This index is used as an indicator for describing the vegetation behavior. To describe the absorbance in the shortwave infrared being an indicator of inundation, I use the Modified Normalized Difference Water Index (MNDWI) as a widely used index for detecting water (Malinowski et al., 2017)

$$\text{MNDWI} = \frac{\text{GREEN} - \text{SWIR}}{\text{GREEN} + \text{SWIR}} \tag{7.2}$$

In this equation, SWIR is the reflectance in the shortwave infrared spectrum and GREEN the reflectance in the green spectrum (Xu, 2006). Both indices have a theoretical value range from -1 to 1, where the maximum of 1 indicates the strongest signal regarding vegetation (for the NDVI) and water (for the MNDWI). On the contrary, values <0 are not related to vegetation or water respectively. To obtain a signal for vegetation and water only, negative index values are set to 0 assuming that the signal related to vegetation or water is minimal for these pixels. This time series with replaced negative values is called *positive* time series in the rest of the text.
Now, a time series of monthly average positive NDVI and MNDWI for 2015 have been generated as the landscape mapped in spring 2016 mainly reflects the result of the summer flood in 2015. The values for the locations of the ground control points have been grouped by succession stage to derive specific phenological curves of the NDVI and MNDWI. Figure 7.4 shows the result of the phenological curves. First, there is a lack of clear-sky observations between January and March. From April to December, there are sufficient observations to generate the curves. For the geomorphological state, NDVI values are generally low with a mean value of 0.03 and a maximum of 0.28. The values tend to be close to 0 during the flooding season in summer time and increase in autumn. On the contrary, the MNDWI values are high with a mean of 0.23 and a maximum of 0.84. The MNDWI shows a strong seasonal pattern with a sharp increase of the values in May, the highest values in July and a decrease in September. This pattern reflects the discharge regime of the Naryn River with a start of the flooding season in May, peak discharges in July and an end of the flooding season in September (see chapter 4).

## 7.4 Strategies for remote sensing assessment of biogeomorphological succession stages

I follow two complementary strategies for assessing biogeomorphology by satellite imagery. First, I use a machine learning based approach for supervised classification of the different biogeomorphological succession stages. This reveals the spatial dimension of the succession stages for the year 2017. Second, I use a time series modeling approach for assessing the temporal trajectory of locations over time. In this case, each pixel in a satellite imagery time series is considered as a single time series with a specific temporal behavior. For the single year assessment, I use Sentinel-2 imagery. For the time series modeling, I base upon Landsat as for Sentinel-2 time series are still considerable short. Especially the 2016 flood event with a return period of 40 years is not covered by Sentinel-2 imagery. Nevertheless, the single year comparison for 2017 is used to give a first estimation about the potential of Sentinel-2 imagery for large scale biogeomorphological research

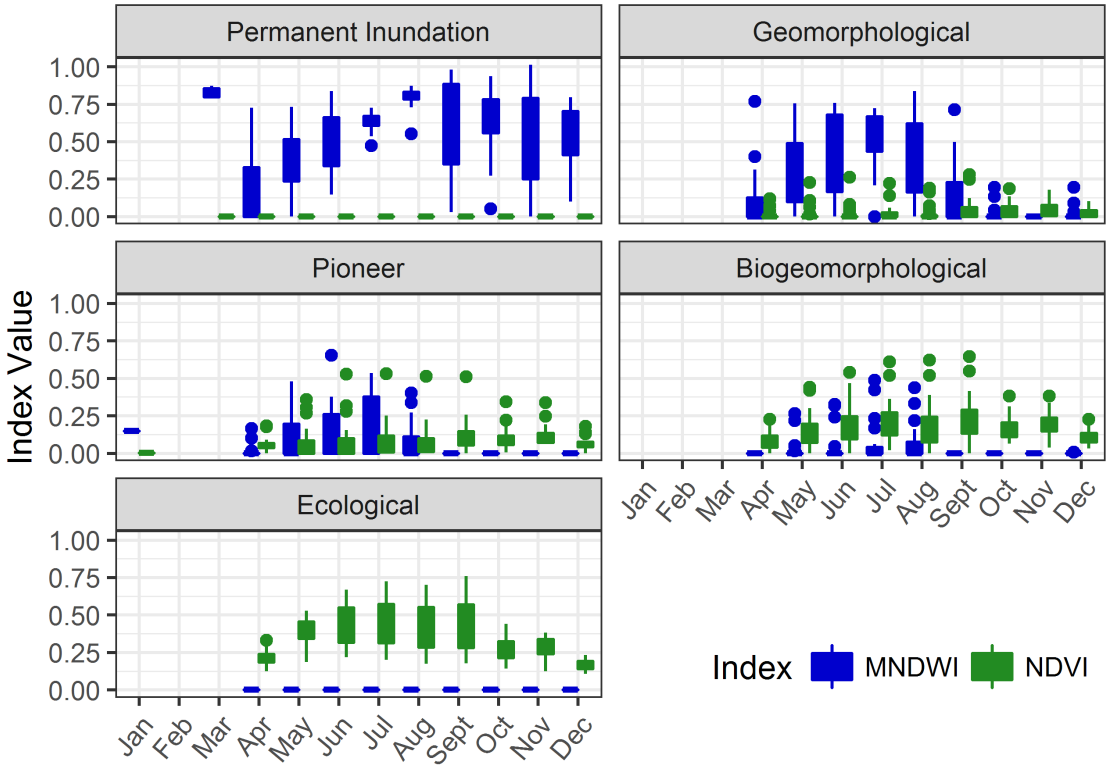


Figure 7.4: Seasonal cycle of Landsat derived NDVI and MNDWI for the different succession stages for the 111 ground control points

in river systems.

*Assessing the spatial pattern of biogeomorphological succession stages for a single year*

For the single year classification, I use a machine learning based supervised classification of digital elevation data and satellite imagery (Fig. 7.5). From the digital elevation data, the vertical distance to channel network, the horizontal distance to channel network as well as the multiresolution valley bottom flatness index and the modified topographic index have been derived. These indices are on the one hand used as predictors, on the other hand, they go into the fuzzy logic based delineation of the river corridor as presented in chapter 6. In addition, 8 Sentinel-2 scenes have been acquired and processed using the sen2r package (Ranghetti et al., 2020). This package has been used to download the imagery, apply an atmospheric correction and cloud masking as well as the computation of NDVI and MNDWI (see Ranghetti et al. 2020 for full details on the processing chain in sen2r). The indices of each single time step are now used to compute annually aggregated rasters of minimum, maximum and mean of NDVI and MNDWI. The values of all these raster datasets described above have been extracted at the location of the ground control points. The resulting dataset has been split randomly into a training dataset (75%) and a validation dataset (25%). Then, a random forest model has been trained, optimized and validated by means of the confusion matrix and the derived accuracy metrics. Model training and optimization have been carried out using the *caret* package in R (Kuhn, 2020). After the final model has been obtained, it has been used to predict the classes for the entire area of interest. This raster has been intersected

with the riparian zone delineation presented in chapter 6. In a final step, the river type mapping and the river corridor segmentation into 100 m segments (presented in chapter 6 as well) have been used for a spatial analysis of the results.

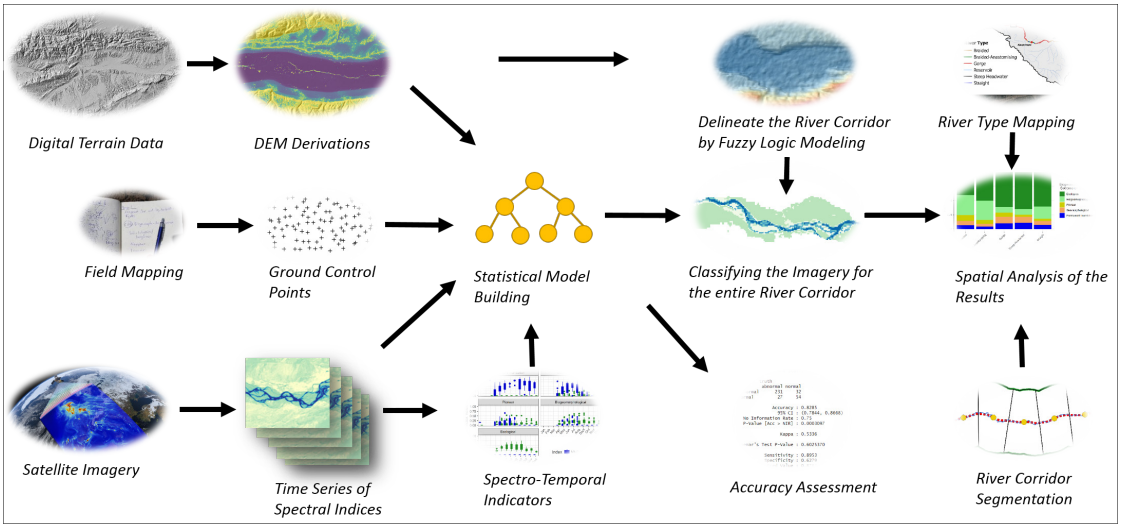


Figure 7.5: Workflow for supervised classification and spatial analysis of biogeomorphological succession stages

*Assessing temporal trajectories of biogeomorphological succession*

In addition to the spatial domain addressed in the section above, the temporal perspective is highly relevant for analyzing biogeomorphological succession. Here, Sentinel-2 data is not applicable as prior to 2017 (the year where the time range of interest of this thesis ends) Sentinel-2 imagery is not available as consistent time series. The Landsat data has been aggregated to monthly averages of NDVI and MNDWI. These layers have then been combined in a raster stack. In case, no imagery has been available for a specific month (an issue arising especially prior to the launch of Landsat 7 in 1999, see Fig. 7.2), a dummy layer consisting of NoData values only has been inserted to the stack in order to ensure consistent periodicity of the time series. For the river corridor in the central Naryn Basin, the area of interest for this analysis, this results in 6.8 million individual time series of NDVI and MNDWI (see Fig. 7.6). Prior to analysis, the time series have been gap filled by means of a spline interpolation and smoothed using a third order Savitzky-Golay filter (see Cai et al. 2017 for a discussion on satellite time series smoothing). These gap filled and smoothed time series are now the basis for further processing.
For analysis, I use an additive time series model describing each of the pixel time series by a trend, a seasonal and a remainder component (Verbesselt et al. 2010, 2012; Zhao et al. 2019, see equation 7.3).

$$y_i = S(t_i; \Theta_S) + T(t_i; \Theta_T) + \epsilon_i \tag{7.3}$$

In this equation, $y_i$ is the spectral index value at time i mathematically described by S and T being the seasonal and trend component of the time series at time $t_i$ with their respective parameters $\Theta_S$ and $\Theta_T$ at time $t_i$. $\epsilon_i$ is the remainder, i.e. the fraction of the decomposed time series which cannot be described by the seasonal component $S(t_i; \Theta_S)$ and the trend component $T(t_i; \Theta_T)$.
For estimating trend and changepoints in the time series of the NDVI and the MNDWI, it is

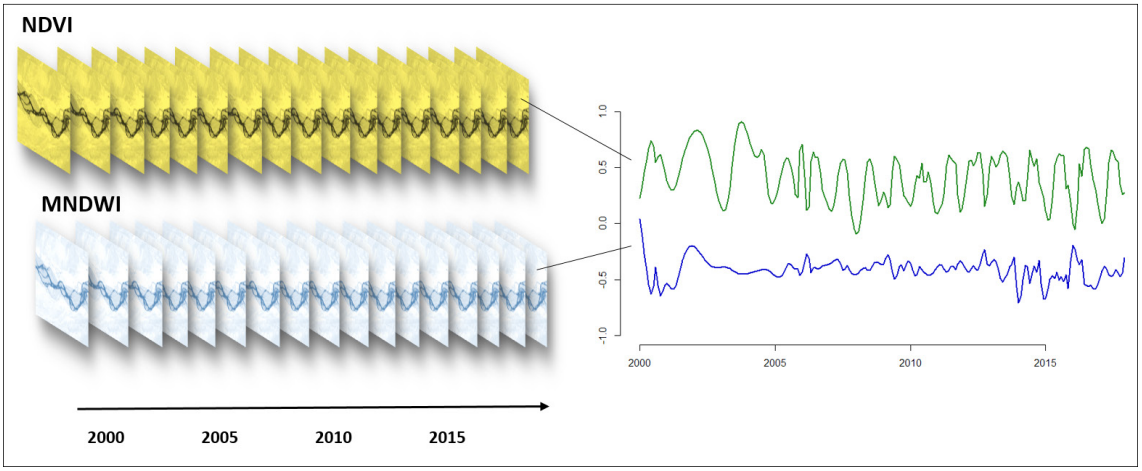


Figure 7.6: Datacube of NDVI and MNDWI for time series analysis

necessary to get estimates of the parameters $\Theta_S$ and $\Theta_T$. Following Verbesselt et al. (2012), equation 7.3 can be formulated as a combination of a linear and a harmonic regression model:

$$y_i = \alpha_1 + \alpha_2 i + \sum_{j=1}^{k} \gamma_j \sin(\frac{2\pi i}{f} + \delta_j) + \epsilon_i \tag{7.4}$$

In this equation, $\alpha_1$ is the intercept and $\alpha_2$ the slope of the linear regression. The parameters $\gamma_j$ and $\delta_j$ define the harmonic model. Parameter f is the known frequency of the time series, e.g. 12 observations per year for a monthly series as used in this thesis. $\epsilon_i$ is again the remainder. As this formulation can be treated as a ordinary least square regression problem, established methods like the moving sums approach can be used for estimating structural change in the time series and estimate changepoints and magnitude of change (Verbesselt et al., 2010, 2012). This approach has become increasingly popular for remote sensing based forest monitoring in recent years (Gómez et al., 2016).

In a recent development of time series modeling, Zhao et al. (2019) argued that a time series cannot be fully described by a single model as presented in equation 7.4 and suggested a Bayesian ensemble method instead. While the basic principle remains, i.e. a time series is formulated as a combination of a seasonal, trend and remainder component, no single 'best' estimate is generated for the parameters alpha, $\gamma$ and $\delta$ but a range of estimates along with their distribution function (Zhao et al., 2019). A full mathematical description of this approach is beyond the scope here, readers can refer to Zhao et al. (2019) instead. A major consequence of this Bayesian approach is the absence of absolute estimates about the location of changepoints. Instead, a probability for each location in the time series to be such a changepoint is predicted. This has also implications for the analysis of the Landsat time series in the context of biogeomorphological succession. For this analysis, I use two different spectral indices, MNDWI as indicator for hydromorphological disturbance and NDVI as indicator for vegetation. Using the Bayesian ensemble approach, it is possible to compute the probabilities of changepoints for the MNDWI as well as for the NDVI time series. A comprehensive estimate about biogeomorphological change can be estimated as the product of the MNDWI seasonal changepoint probailities $P_{MNDWI}$ and the NDVI seasonal

changepoint probabilities $P_{NDVI}$:

$$P_{Biogeo} = P_{NDVI} \times P_{MNDWI} \tag{7.5}$$

This reflects the idea that changepoints for instance in the NDVI time series might arise from anthropogenic disturbance like woodcutting. If, however, MNDWI time series show simultaneously a high changepoint probability, it is likely that the change in the NDVI time series arises from changes in the hydromorphological disturbance regime and can thus be interpreted as biogeomorphological change.

*Application of the temporal trajectory assessment*

The temporal assessment described in the previous section has been used for several analysis. First, I present results from several selected single time series along with their interpretation to demonstrate the principle of the analysis. Then, I classify the entire river corridor according to the predominant biogeomorphological dynamics distinguishing between three major classes: continuously in the ecological stage, continuously in the permanent inundation stage and biogeomorphologically dynamic. The first two classes refer to locations where no change has been detected in the time series between 2000 and 2017. The latter class refers to locations where at least one major change has been observed for the same time period. This analysis allows to detect 'hotspots' of biogeomorphological dynamics and is another descriptive parameter for the river corridor.
In a second step, I go into further detail and assess on the one hand the establishment and growth of vegetation between 2010 (the year of the last flood event prior to 2016) and the 40 year return period flood in 2016. Then, I analyze the consequences of the 2016 flood and detect changes from the biogeomorphological and ecological stage to the geomorphological or permanent inundation stage. In addition, I detect gravel bars formed during this flood event and marking the transition from the permanent inundation stage to the geomorphological stage.
A rigor validation of the time series analysis results is difficult due to the absence of high resolution reference data for multiple dates. For October 2015 and October 2016, rgb images with a resolution of 3 m from the Planet Scope satellites have been available for one braided-anastomising reach. These two images serve as a reference data set and allow to validate at least the detection of changes caused by the 2016 flood event.

## 7.5 Results

### 7.5.1 Single year classification

*Validation of the classification*

The overall accuracy of the random forest classification of the single year Sentinel-2 data is 81.5±11%. However, the accuracy is heterogeneous across the different classes. The accuracy metrics per class are given in table 7.3. It becomes obvious that the classes at the ends of the succession, permanent inundation and ecological stage, reveal the best accuracies. The lowest accuracy is achieved for the pioneer vegetation which tends to be confused with the geomorphic stage. This confusion is already manifested in the spectral signatures presented in figure 7.3. Carrying out a spectral separability analysis for these two classes by means of a Kruskal-Wallis test with a Dunn-Bonferroni posthoc test reveal values of 1 and 0.89 for May and November respectively. Thus, geomorphic stage and pioneer stage are not separable by means of their spectral profiles.

Table 7.3: Accuracy metrics of the classification of succession stages

| | Permanent Inundation | Geomorphic | Pioneer | Biogeomorphic | Ecologic |
|---|---|---|---|---|---|
| User's Accuracy | 0.9091 | 0.8889 | 0.3 | 0.875 | 0.9444 |
| Producer's Accuracy | 0.9815 | 0.8936 | 0.9818 | 0.9298 | 0.9787 |
| Balanced Accuracy | 0.9553 | 0.8913 | 0.6409 | 0.9024 | 0.9616 |

Using spectro-temporal metrics of the NDVI allows a certain recognition of pioneer vegetation, however this succession stage is still associated with uncertainties.

*Spatial pattern of succession stages in the river corridor*

Once having applied the model to the entire river corridor, the spatial pattern is analyzed. Figure 7.7 shows the pattern of the succession stages along the longitudinal profile as well as for selected river sections in order to show the heterogeneity of the spatial distribution of succession stages. First, it becomes obvious that there is no downstream trend in the pattern of the stages. This is supported by spearman correlation coefficients well below 0.1 for the correlation between the area of succession stage and the downstream distance. This is obvious when having a look at the example maps in figure 7.7. Between 300 km and 350 km downstream distance, straight reaches without extended instream bars or islands dominate. This leads to a dominance of the permanent inundation stage together with floodplains in the ecological stage. Further downstream, between 400 and 450 km downstream distance braided reaches are the characteristic planform type of the Naryn River. In this setting, the geomorphological and biogeomorphological stage are more dominant compared to the example reach further upstream. In the gorge further downstream, there is a clear dominance of the permanent inundation stage with only very few bars in the geomorphological stage and an absence of floodplains in the ecological stage.

Despite the insights in the river corridor arising from the longitudinal distribution of the succession stages presented in Fig. 7.7, these results tend to be hard to interpret in a concise manner. An analysis of the distribution of succession stages across the different river types and valley settings gives a clearer picture of their spatial pattern (Fig. 7.8). While I do not want to write out all the percentage values behind these figures, I want to draw some general ideas from this pattern. First, it becomes obvious that the ecological stage is dominating across all valley settings and river types. Nevertheless, there are differences as well. Regarding the valley setting, confined reaches have a higher percentage of 73.3% while partly confined reaches and laterally unconfined reaches show 63.75% respectively 68.89% of ecological stage[1]. This corresponds well with the river pattern of succession stages in the river types, where the gorges (78.03% ecological stage), steep headwaters (73.16% ecological stage) and straight reaches (77.15% ecological stage) with their tendency to a confined character have a high share of ecological stage as well. A similar picture can be observed for the permanent inundation stage. In the confined and partly confined reaches, this stage has a higher share of 8.84% and 6.93% compared to the laterally unconfined reaches with 4.88%. In the different river types, the gorges have the highest share of permanent inundation stage with 8.01% followed by the steep headwaters with 7.39% and straight reaches

[1]Please note that the percentages refer to the median of all reaches in a certain valley setting or river type. Thus, the sum does not necessarily result in 100%

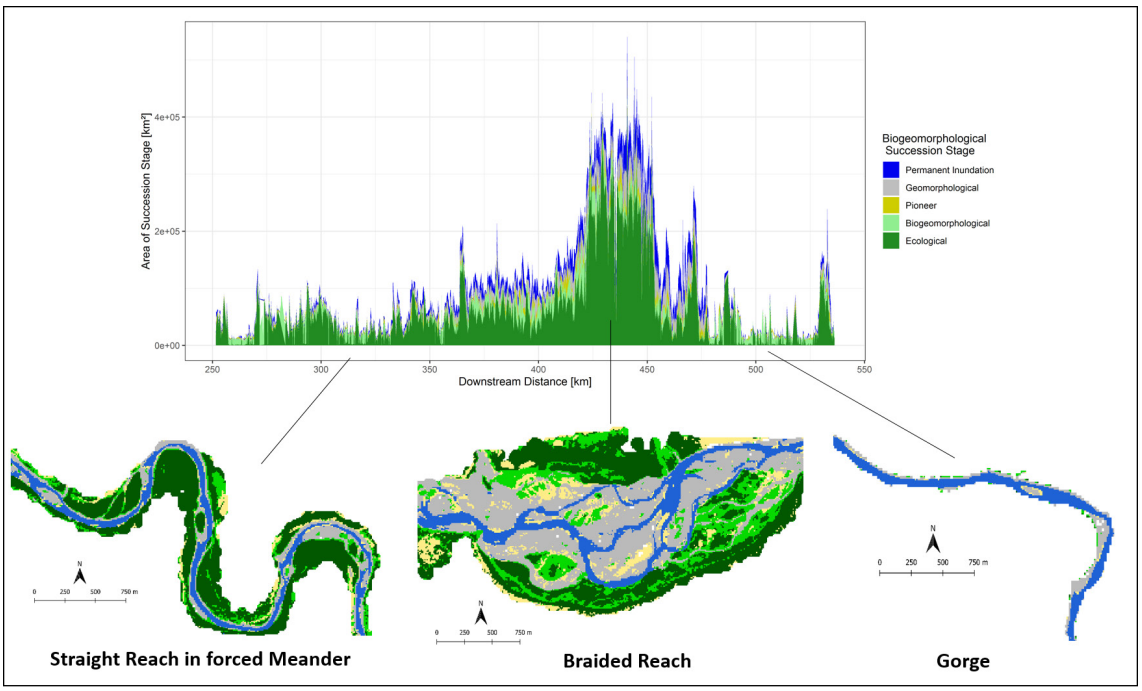


Figure 7.7: Results of the single year classification of the biogeomorphological succession stages

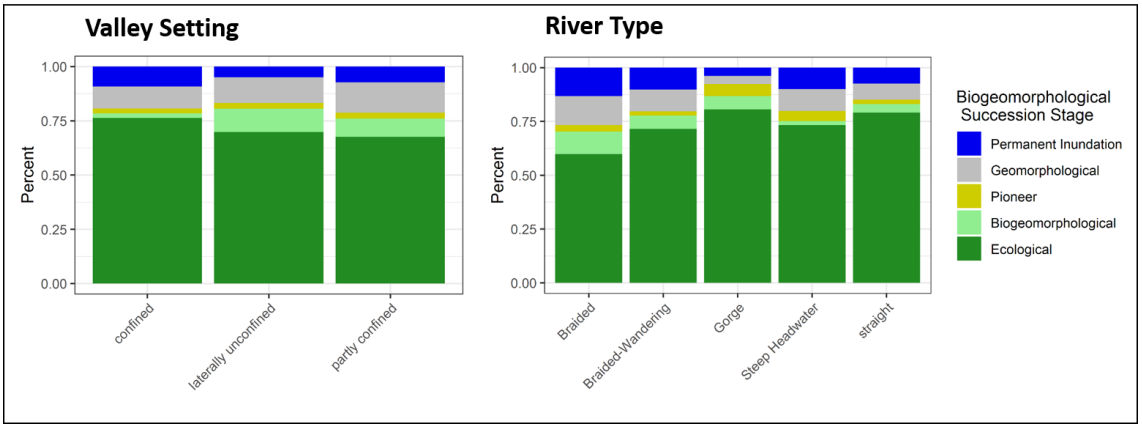


Figure 7.8: Distribution of succession stages across different valley settings and river types

with 6.57 %. Braided and braided-anastomising reaches tend to have a lower share of permanent inundation zone of 6.33% and 3.48% respectively. On the contrary, these river types tend to have a higher proportion of the geomorphological, pioneer and biogeomorphological succession stage. This is particularly true for the biogeomorphological stage, with 10.89% in braided reaches and 6.49 % in braided-anastomising reaches. For comparison, gorges have a share of biogeomorphological stage of 1.39%, steep headwaters have 1.60% and straight reaches have 2.97%.
In chapter 6, I demonstrated the relationship between the river types and different controlling factors. It has become obvious that the confinement plays a major role. In reaches with low confinement, the specific stream power becomes the relevant controlling factor. The relationship between valley setting as expression of confinement and the share of biogeomorphological suc-

cession stages is shown in figure 7.9. The trend lines in this figure indicate, that there is a general

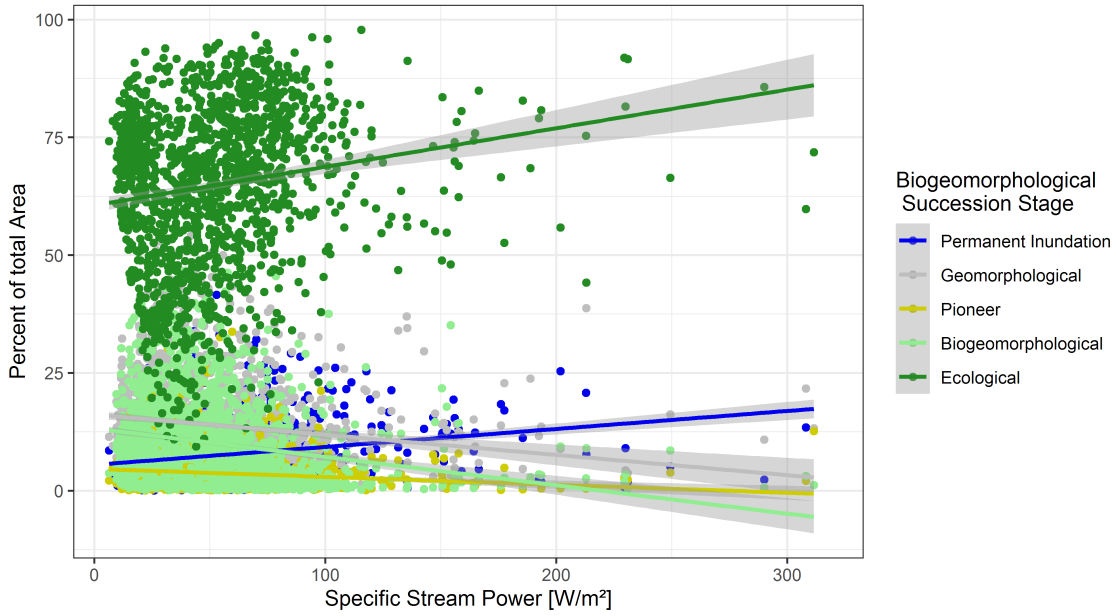


Figure 7.9: Relationship between specific stream power and share of succession stages

relationship between the specific stream power and the share of succession stages within each of the 100 m segments of the disaggregated river corridor. While the share of permanent inundation and ecological stage tend to increase with increasing stream power, the share of geomorphological and biogeomorphological stage clearly tend to decrease. The share of pioneer stage also tends to decrease, however, this decrease is less strong compared to geomorphological and biogeomorphological stage. Having a look at the linear models underlying the trend lines in figure 7.9, it is obvious that the relationship is only weak with r-squares between 0.02 and 0.06. However, the highly significant p-values ranging between $2.2 \times 10^{-16}$ for the biogeomorphological stage and $1.1 \times 10^{-8}$ for the geomorphological stage indicate that the slope of the regression lines is significantly different from 0. Thus, reach averaged specific stream power can be assumed to have a significant impact on the share of succession stages, even if other factors have to be considered as well as the explanatory power of the specific stream power is low.
In addition to the specific stream power alone, the simple erosion-deposition model basing upon the ratio of the stream power with the one from the upstream reach has been tested for a relationship with the pattern of biogeomorphological succession stages (Fig. 7.10). Due to the nature of stream power balance as indicator for erosion and deposition, a linear model is not feasible for showing the central tendency of the relationship. Thus, I use a locally estimated scatterplot smoothing (loess) model instead. There is a minor tendency of the share of ecological stage to be highest in reaches close to equilibrium. In addition, the geomorphological stage tends to become more dominant in reaches either clearly characterized by deposition or erosion. The biogeomorphological stage tends to be most dominant in reaches being in a slightly deposition oriented state. However, the relationship between stream power balance and share of succession stages is weak and remains unclear. Thus, a reach averaged and static characterization of the geomorphological process regime can be considered as insufficient for descriptor of biogeomorphological succession pattern even if the stream power balance is capable to describe general planform pattern in form

of the river types.

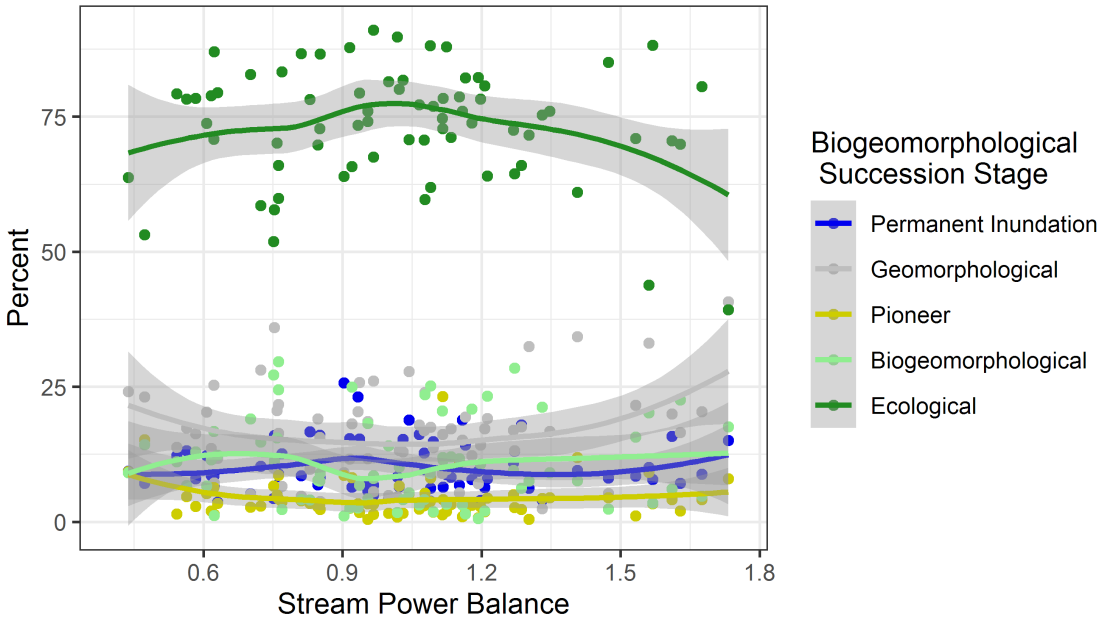


Figure 7.10: Relationship between stream power balance and share of succession stages; stream power balance can be interpreted as an indicator for the tendency towards erosion and deposition in a reach. Values close to 1 are expected to be in dynamic equilibrium, values smaller 1 tend towards deposition and values greater 1 towards erosion.

### 7.5.2 Temporal trajectories of biogeomorphological succession

*Time series examples of different biogeomorphological trajectories*

In this section, I explore several examples of biogeomorphological trajectories to illustrate the potential of dense, multispectral imagery time series to describe the temporal trajectory of biogeomorphological succession on a large scale. The examples have initially been selected to capture change (or no change) during the 40 year return period flood in 2016, but include also more interesting information from the past. All figures are organized in the same way. The solid green and blue lines gives the temporal trajectory of the NDVI respectively the MNDWI. The dotted lines give the trend component of the Bayesian time series decomposition as process indicator. The gray bars show the product of the seasonal changepoint probabilities of NDVI and MNDWI. They indicate the likelihood of change in the biogeomorphological succession stage. To support the interpretation, rgb images from before and after the 2016 flood event are included in the image. High resolution images prior to 2015 have not been available.
Figure 7.11 shows the first examples of 2 neighboring plots. In the lower figure (Fig. 7.11b), the location remained in the ecological stage for the entire period. This is clearly indicated by the consistently positive NDVI and negative MNDWI values. Throughout the entire time, there is no major trend. Also the seasonal signal of the NDVI values remains stable where the pronounced cycle refers to the phenology of the riparian vegetation. Consequently, there are also no relevant seasonal changepoints and the location is considered to be continuously in the ecological stage.

In contrast to location b, location a has a change in its biogeomorphological stage in 2016 (Fig.

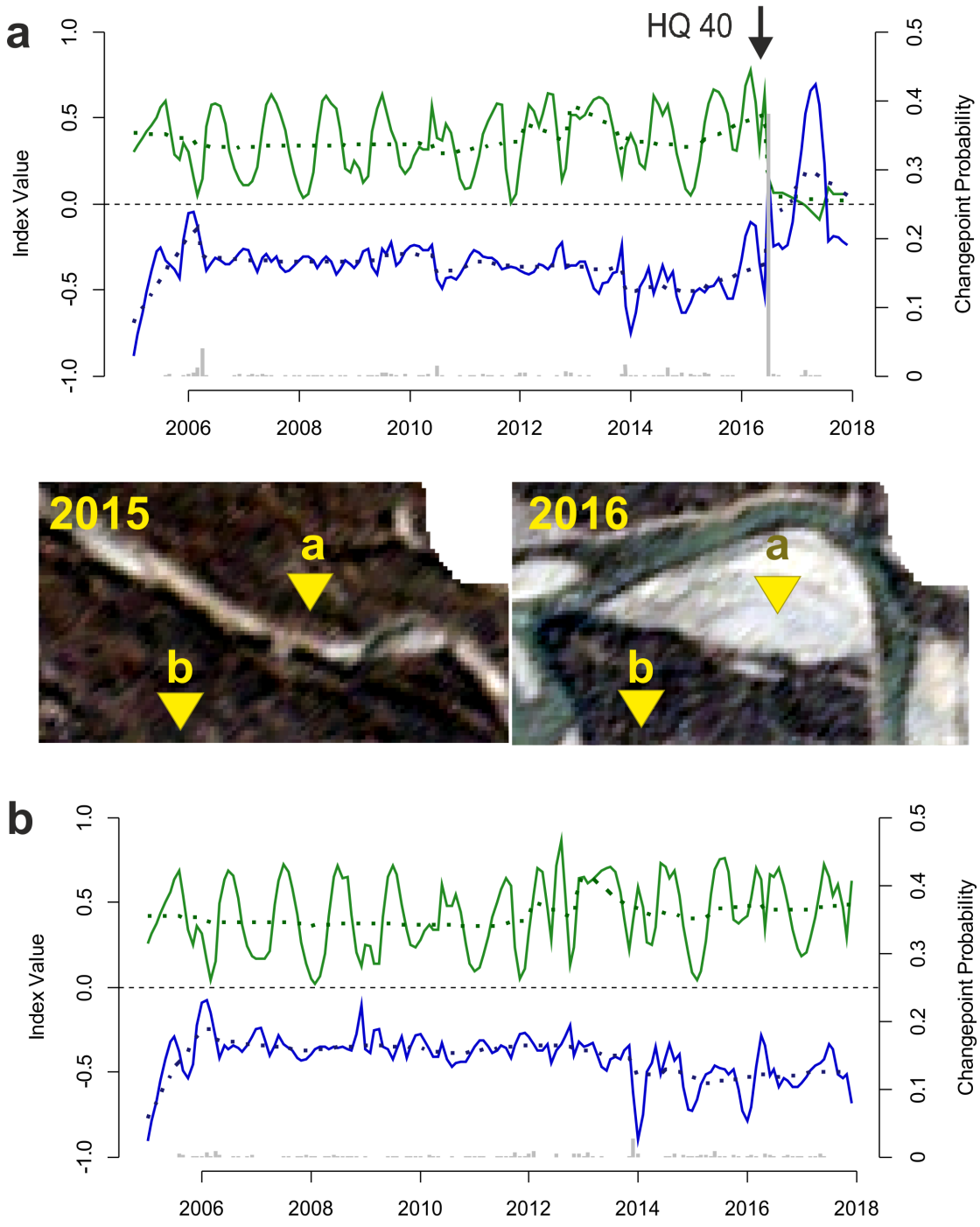


Figure 7.11: Time series indicating a change from the ecological to the geomorphological stage (a) and continuous ecological stage (b)

7.11). Prior to 2016, the behavior of this time series is similar to location a without changes in the trend or the seasonal signal. The positive NDVI with its accentuated seasonal cycle and negative

MNDWI values clearly indicate ecological stage. In 2016, a major change occurs as a consequence of the 40 year return period in this year (see chapter 4). There is a sharp decreasing NDVI trend along with an increasing MNDWI trend. This comes along with a rupture of the seasonal signal what is clearly indicated by a changepoint with a probability of 0.4. The satellite images show the reason of this time series behavior. Due to the flood event, an existing side channel was activated and reworked. As a consequence, the vegetation has been removed from the location and a new bar has formed. From a biogeomorphological perspective, the location has been set back from the ecological to the geomorphological stage.
A more complex example is shown in figure 7.12. This time series shows the development of a vegetation patch on a gravel bar (i.e. the development from the geomorphological/pioneer stage toward the biogeomorphological and ecological stage). This is indicated by the positive NDVI trend between 2005 and 2010. In this period, the MNDWI shows partly positive values indicating

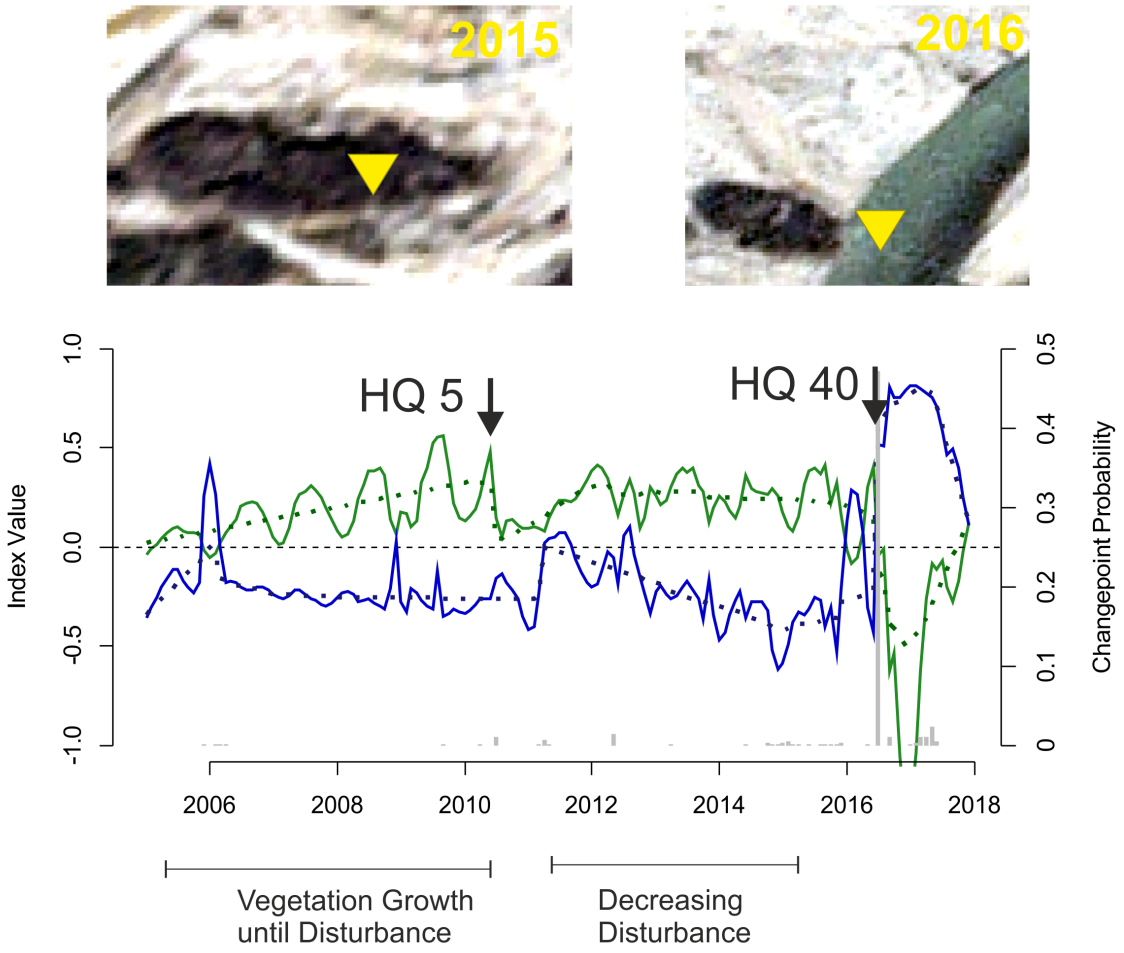


Figure 7.12: Time series indicating the development from vegetation colonization over the biogeomorphological stage towards ecological stage and reset during flood event

flooding of this location. A 5 year return period flood event in 2010 (see chapter 4) obviously caused a disturbance to the vegetation shown by the sharp decline of the NDVI. Between 2010 and 2016, there is no major trend in vegetation anymore. At the same time, the MNDWI shows

a decreasing trend, what is interpreted as a decreased hydromorphological disturbance of the location. The reason might for instance a shift of a channel on the braided plain disconnecting the location from regular flooding. In 2016, the flood caused the removal of the vegetation and a new side channel was initiated. This is reflected in a sharp decrease of the NDVI and increase of the MNDWI trend. In addition, there is a clear seasonal changepoint indicating a change from the just beginning ecological stage to the permanent inundation stage.
A third example is given in 7.13. This time series shows the formation of a gravel bar, the establishment and growth of vegetation and the set back to gravel bar in 2016. Between 2007 and 2010,

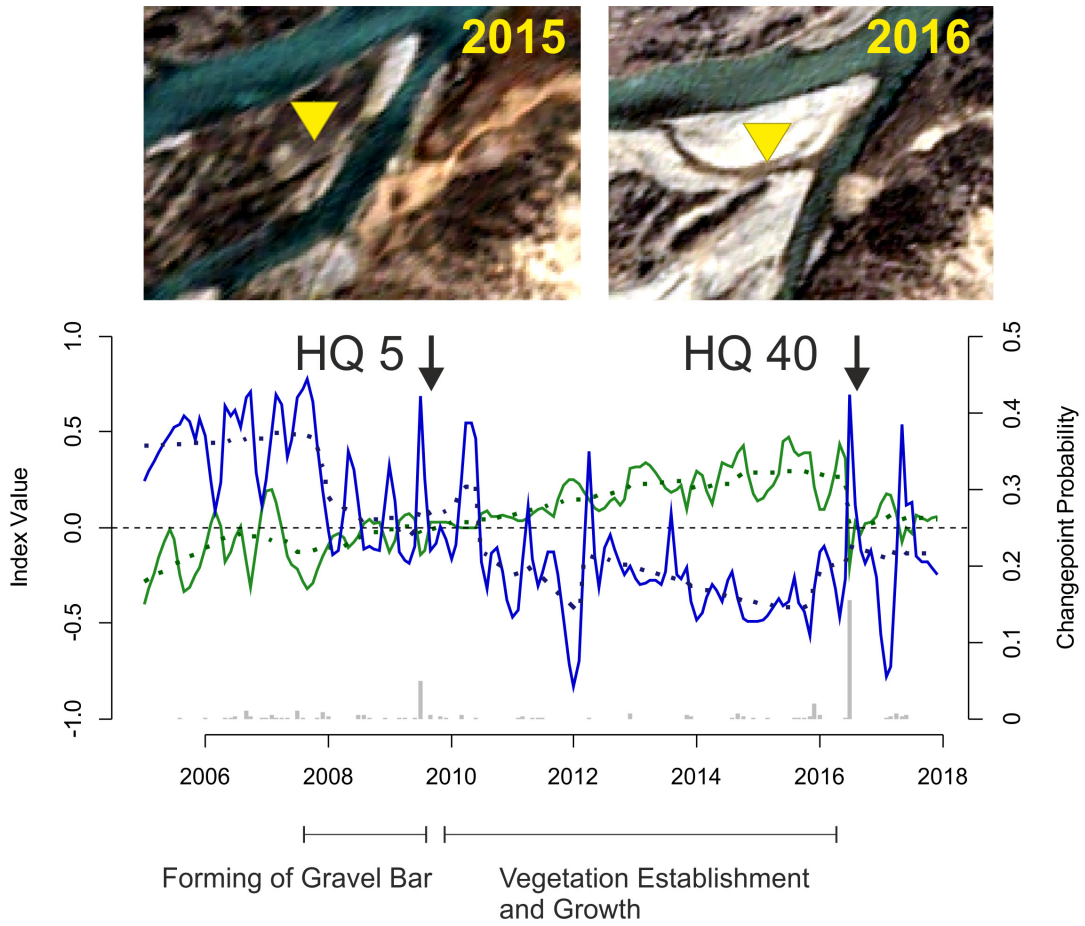


Figure 7.13: Time series indicating the formation of a gravel bar, establishment and growth of vegetation and set back during flood event

a gravel bar has formed at this location. This is shown by the sharp decrease of the MNDWI trend and the NDVI values starting to get positive. In 2010, a seasonal changepoint indicates a change in the biogeomorphological succession stage. As the NDVI trend is starting to increase from this year onwards, this is interpreted as the establishment and growth of vegetation, i.e. the transition from the geomorphological over the pioneer to the biogeomorphological stage. In 2016, the flood event caused a set back from the beginning ecological stage to the geomorphological stage as it is shown by the sharp decrease of NDVI and increase of MNDWI trend as well as the seasonal changepoint.

*Longterm classification of biogeomorphological status*

While the previous section focused on single time series taken as examples to illustrate the temporal trajectory of biogeomorphological succession, this section connects the spatial and the temporal perspective. First, the longterm biogeomorphological status has been assessed and the entire river corridor has been classified into the three major categories continuously ecological stage, continuously permanent inundation stage and biogeomorphologically dynamic (see Fig. 7.1). A location is considered as biogeomorphologically dynamic, if there has been at least one change in the succession stage between 2000 and 2017. This classification is a straightforward interpretation of the temporal trajectories and allows a simple, yet meaningful analysis of the spatio-temporal structure of the Naryn River corridor (see Fig. 7.14). Overall, there are 15.9 km$^2$ continuously

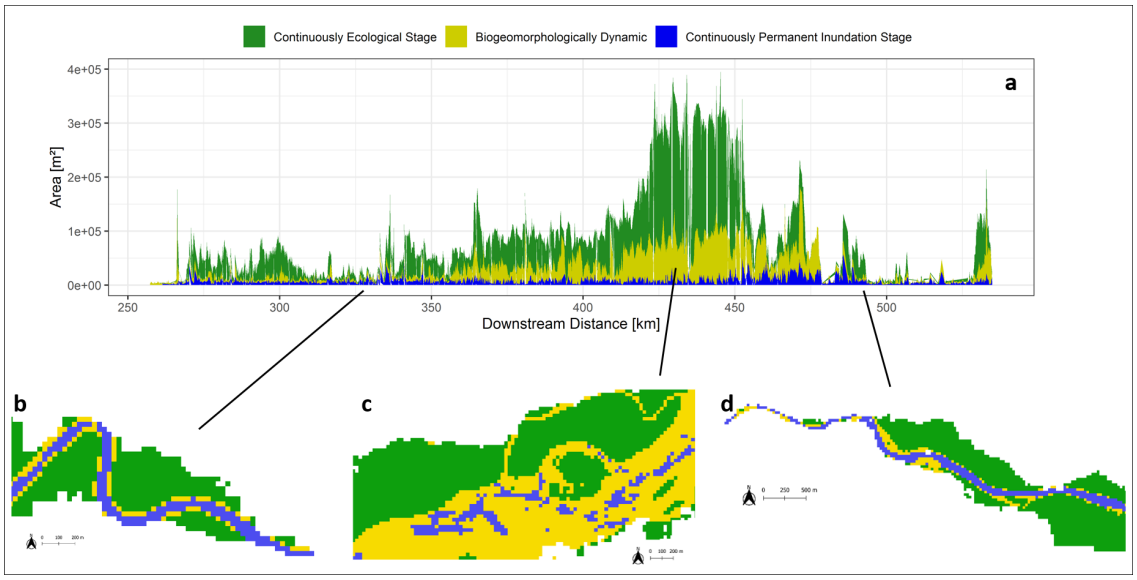


Figure 7.14: Longitudinal pattern of classified biogeomorphological status; please note, that contrary to Fig. 7.7, this figure contains the temporal perspective of biogeomorphological succession to find 'hotspots' of biogeomorphological dynamics in the Naryn River corridor; a is the longitudinal distribution, b an example of a straight reach in a forced meander, c is an example from a braided plain the central part of the catchment and d shows a straight reach and the beginning of the gorge

in the permanent inundation stage, 108.7 km$^2$ continuously in the ecological stage and 48.7 km$^2$ are biogeomorphologically dynamic. However, it is obvious that the areas are homogeneously distributed within the river corridor. Biogeomorphologically dynamic areas are predominantly found in the central part of the catchment between 350 and 500 km downstream distance where a laterally unconfined valley setting allows the formation of braided and braided-anastomising reaches (see chapter 6). Thus, a closer look at the distribution of the areas in a certain longterm biogeomorphological status across the different river types and valley settings is shown in figure 7.15. Across the valley settings, the share of biogeomorphologically dynamic areas is relatively homogeneous with values between 22% and 25%. However, the share of areas being continuously in the permanent inundation stage is higher in confined settings (25%) than in partly confined (13.5%) or laterally unconfined (7.5%) settings. Consequently, the share of areas continuously in the ecological stage varies as well and tends to be highest in laterally unconfined reaches. For the

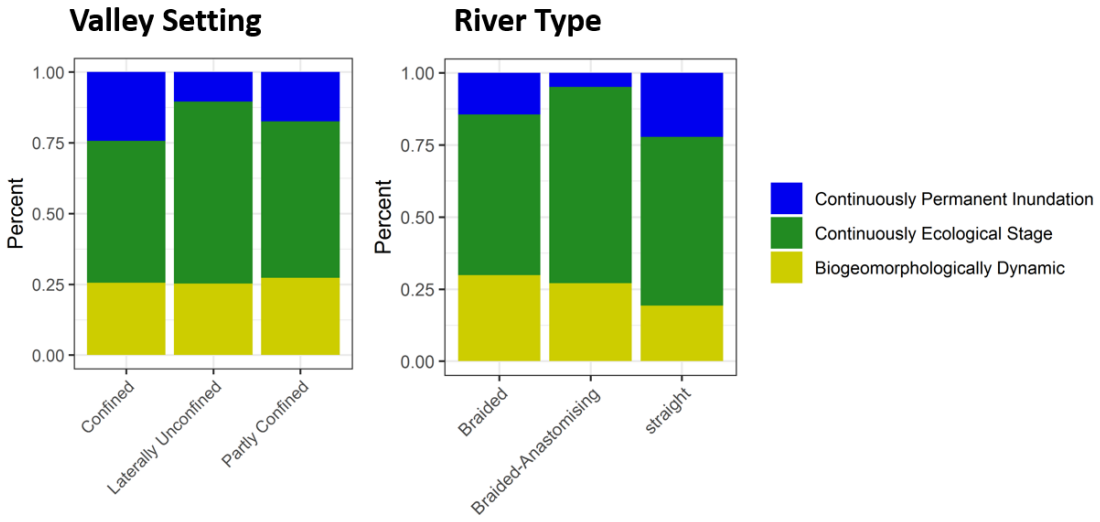


Figure 7.15: Distribution of the longterm (2000-20217) biogeomorphological status across the different valley settings and river types; the narrow river types *Gorge* and *Steep Headwater* are excluded from a detailed analysis due the issue of data gaps in this narrow river setting

different river types, there is a similar picture. Braided reaches have the highest share of biogeomorphologically active area (27.6%) while braided-anastomising and in particular straight reaches have a lower share of dynamic areas with 24.3% and 16.7% respectively. Braided-anastomising reaches have the highest share of areas continuously in the ecological stage (72.9%) followed by the straight and the braided reaches with 62.5% and 60.8% respectively. The share of area continuously in the permanent inundation stage is highest in the straight reaches (18.7%) while braided and braided-anastomising reaches show values of 9.8% and 3.1% respectively.
Having a look at this pattern, it seems that there is a relationship between the distribution of areas being in a particular class and the confinement. To support this assumption in a quantitative way, figure 7.16 shows the relationship between the confinement ratio (see chapter 6) and the classes in a particular class of longterm (2000-2017) biogeomorphological status. From this figure, the strong relationship between the confinement and share of continuously ecological and permanent inundation areas becomes clear. While the $R^2$ values of the linear models underlying the trend lines are relatively low with 0.5 (permanent inundation) and 0.4 (ecological stage), the p-values of the slopes are highly significant supporting the assumption that with increasing confinement, the share of areas in the ecological stage are significantly decreasing while the share of areas continuously in the permanent inundation stage is significantly increasing. This pattern reflects the strong control of confinement as an expression of geological constraints over the development of the river corridor which has already been addressed in chapter 6.

*Biogeomorphological change detection*

While the previous section addressed general and longterm pattern, this section will treat the detection of concrete biogeomorphological processes based on the time series of NDVI and MNDWI. First, the removal of vegetation and the formation of new gravel bars as a consequence of the 40 year return period flood in 2016 are assessed. This analysis has been restricted to biogeomorpho-

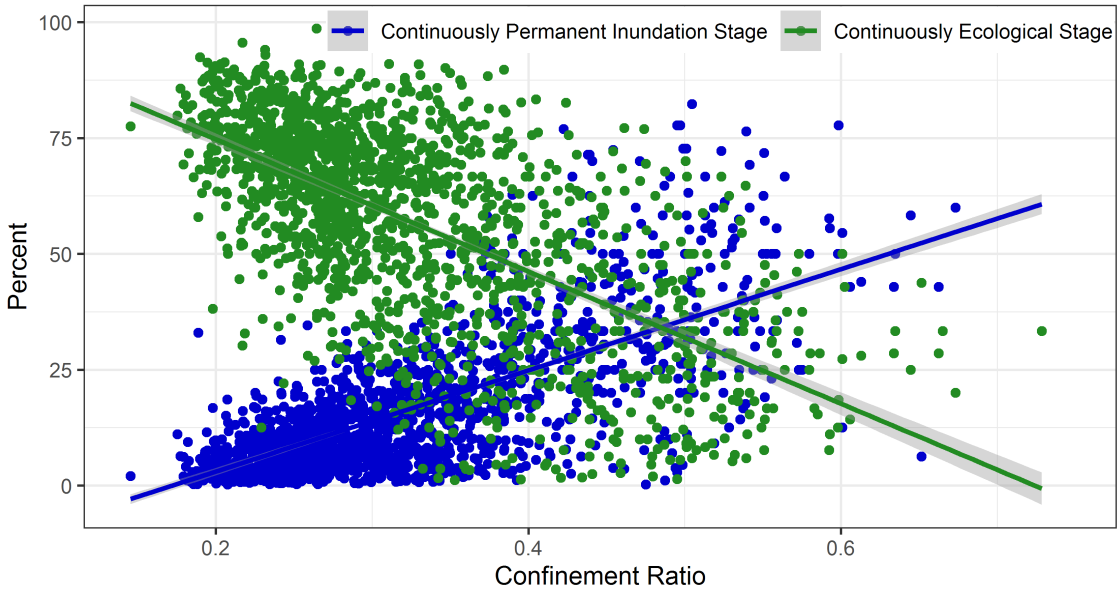


Figure 7.16: Relationship between distribution of classes of longterm (2000-2017) biogeomorphological status and confinement ratio; biogeomorphologically dynamic areas have been excluded for readability. For this class, there is no clear trend as it is indicated in figure 7.15

logically dynamic areas (see section above) to avoid a misinterpretation of vegetation stage e.g. due to wood cutting. Figure 7.17 shows the area of changes along the longitudinal profile. Check-

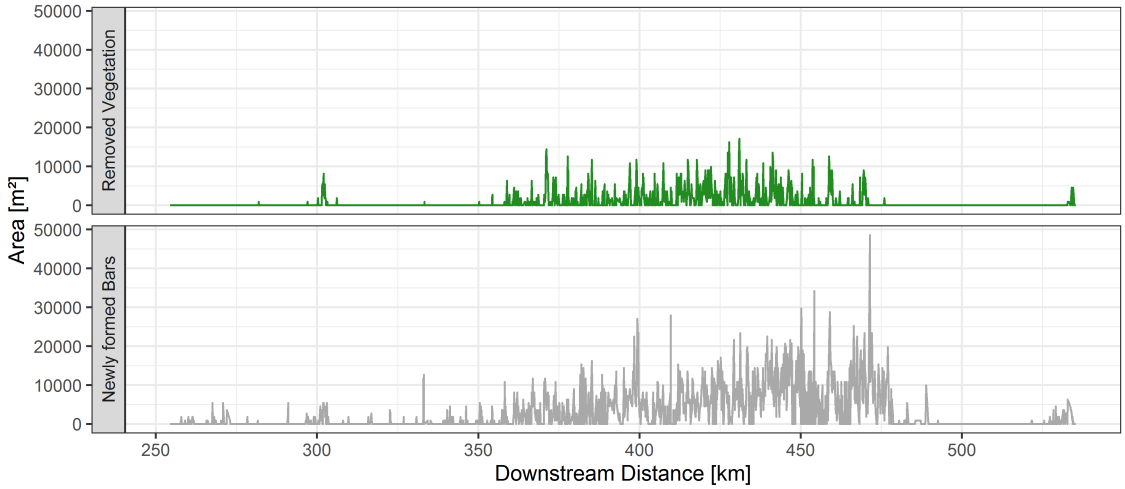


Figure 7.17: Biogeomorphological changes due to the 40 year return period flood in 2016

ing for the correctness of detected change at 50 points distributed across the reach in Ak Tal where the Planet Scope images are available reveals, that there is an agreement of 100% between the visually derived change and the automatically detected change. Thus, the Landsat based change detection is considered as reliable. All in all, 1.78 $km^2$ of vegetation have been reset from the

biogeomorphological or ecological stage to the permanent inundation or geomorphological stage. At the same time, a total area of 6.35 km$^2$ of new gravel bars have been formed bringing this area from the permanent inundation stage to the geomorphological stage. It is obvious, that the majority of change occurred between 350 km and 500 km downstream distance where the braided and braided-anastomising reaches are located. 75.1% of the vegetation removal occurred in braided reaches, another 19.9% in braided-anastomising reaches. The remaining 4.9% of change occurred in straight reaches while gorges and steep headwaters did not show any change. The bar formation gives a similar picture regarding the distribution across the river types. 76.1% of the total bar area has formed in braided reaches, another 17.9% in the braided-anastomising reaches. The majority of the remaining bar area has formed in the straight reaches (5.4%), while to a small extent bars have also formed in the steep headwater (0.03% of the total area) and the gorges (0.6%).
In addition to the changes caused by the flood event in 2016, the establishment and growth of vegetation between the last minor flood event in 2010 (5 year return period) and the flood event in 2016 has been analyzed. In this period, a total area of 13.43 km$^2$ has developed from the permanent inundation or geomorphological stage via the biogeomorphological towards the ecological stage (Fig. 7.18). In this period, 13.43 km$^2$ have developed towards biogeomorphological and eco-

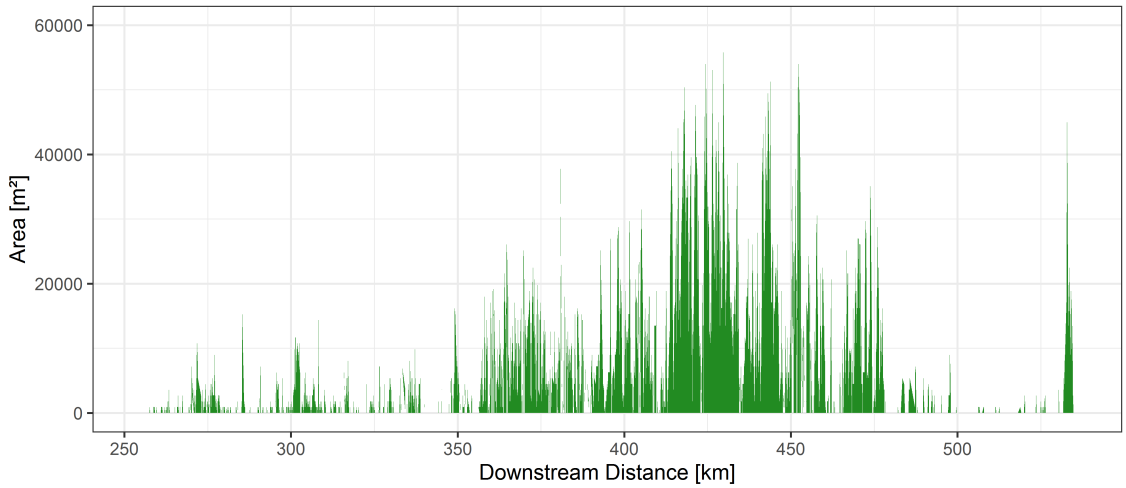


Figure 7.18: Establishment and growth of vegetation between 2010 and 2016

logical stage. Again, the majority of change happened in the braided and braided-anastomising reaches between 350 km and 500 km downstream distance. Within the braided reaches, 9.3 km$^2$ or 69.56% of the total area of vegetation established, in the braided-anastomising reaches 2.98 km$^2$ (22.18%). The remaining area is shared among the straight reaches (0.95 km$^2$), the gorges (0.15 km$^2$) and the steep headwater (0.0099 km$^2$).
For a deeper analysis of the driving forces behind these patterns, the erosion and deposition model presented in chapter 6 is used. This simplified model uses the balance between the specific stream power of a reach with the one of the upstream reach to give a statement about the predominant process regime of a reach, i.e. if it is erosion or deposition dominated or in respectively near a dynamic equilibrium state (see 6.2.14 for full details). Figure 7.19 brings together the results from this geomorphological model and the results from the biogeomorphological change detection. It shows the relationship between the predominant geomorphological channel process and the area of bars formed following the 2016 flood event respectively the vegetation establishment and growth

between 2010 and 2016. The boxplots give the distribution of areas across the different reaches. Reaches being in a state dominated by deposition or being deposition oriented but close to deposi-

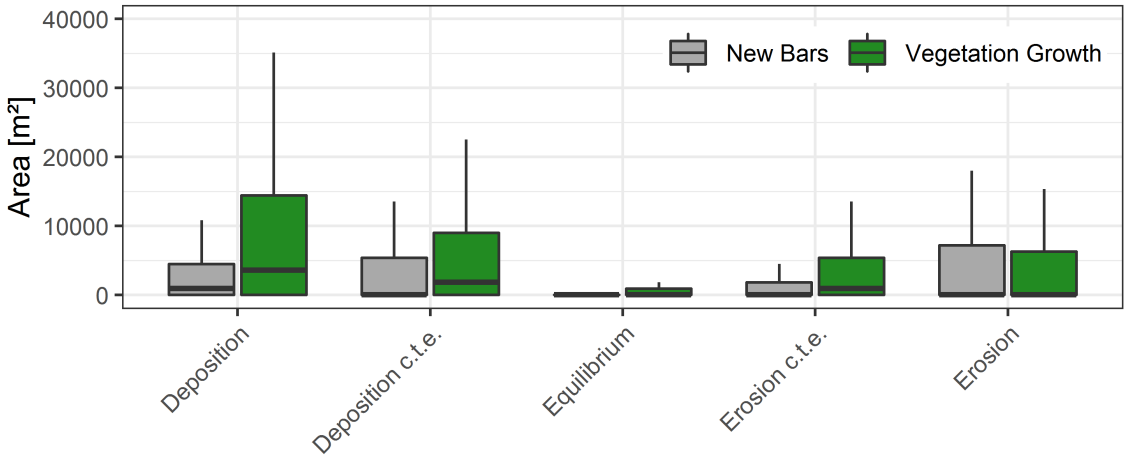


Figure 7.19: Relationship between vegetation establishment and growth, bar formation and predominant channel processes; c.t.e. refers to *'close to equilibrium'*

tion tend to have the largest areas of newly formed gravel bars with a median area of 900 $m^2$. The other classes have median bar areas of close to zero, but from the 75% quantile, it becomes clear that deposition oriented reaches close to equilibrium and reaches in an state dominated by erosion also show significant areas of new bars (5400 $m^2$ and 7200 $m^2$ respectively). Reaches in equilibrium and in an erosional, close to equilibrium state show less area of bars. While the formation of bars in deposition oriented reaches seems obvious, the bar formation in erosion oriented reaches might be explained by an excess of sediment availability in these reaches at the end of the 2016 flood event. The distribution of areas where vegetation has established and grown up is similar to the development of bars. The area is largest in reaches being dominated by deposition (median of 3600 $m^2$) followed by deposition oriented reaches close to equilibrium (1800 $m^2$). Reaches being characterized by erosion but being close to equilibrium experience also a certain vegetation growth with a median area of 900 $m^2$ while reaches in equilibrium and dominated by erosion have median vegetation growth areas of 0 $m^2$ and thus do not have significant vegetation growth.
When further analyzing the reasons of the distribution of vegetation establishment in the river corridor, one might look at the two major driving forces of the Naryn River corridor structure which have been identified in chapter 6: confinement and specific stream power (Fig. 7.20). Both parameters show a clear relationship with the area of vegetation establishment and growth. However, this relationship is nonlinear and seems to have a threshold character. Up to a confinement ratio of 0.4, the area of vegetation establishment and growth is highly variable even if there is a generally decreasing trend. From this value onwards, there is a sudden drop in the area except a few outliers. This value of 0.4 refers approximately to the change from a partly confined to a confined valley setting (see chapter 6). Obviously, there is a lack of opportunity for vegetation establishment in this setting except few locations as the outliers show. Above a confinement ratio of 0.6, a value occurring in the gorges and the steep headwater, no vegetation establishment occurs anymore. The pattern is similar for the specific stream power. Between 0 and 100 $Wm^{2-1}$, the area of vegetation establishment and growth shows a high variability around a sharply decreasing trend. Above a specific stream power value of approximately 100 $Wm^{2-1}$, there is no vegetation establishment

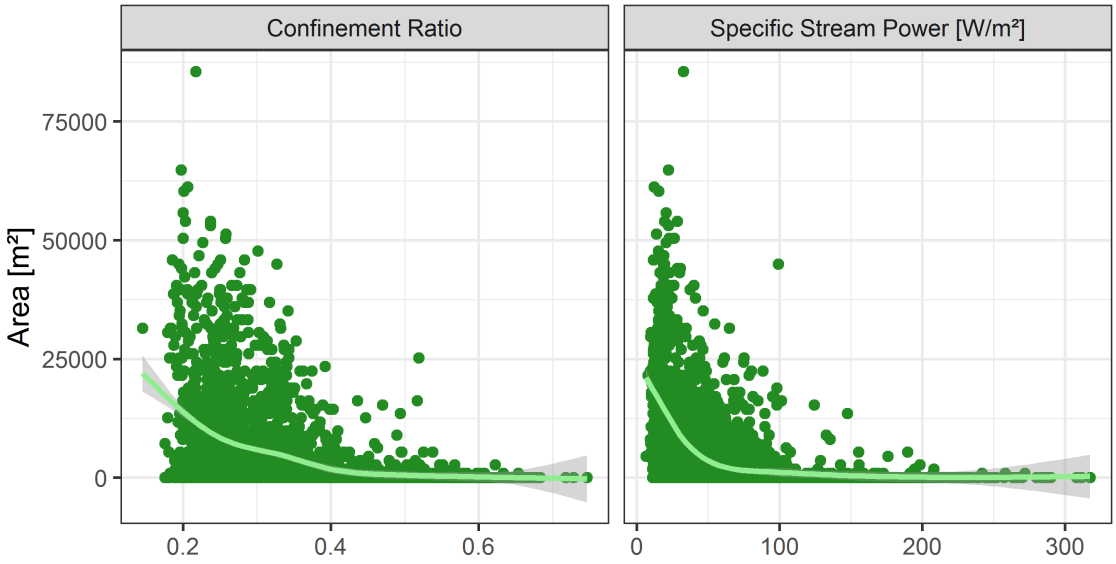


Figure 7.20: Relationship between confinement ratio, specific stream power and the area of establishment and growth of vegetation per 100 m segment

anymore except a few exceptions. Above a specific stream power value of 150 $Wm^{2-1}$, practically no vegetation establishment occurs anymore. Such high stream power occurs in the gorges and the straight reaches.

## 7.6 Interpreting the results in the light of biogeomorphological theory

This chapter is written against the background of biogeomorphological succession as suggested by Corenblit et al. (2007) and has been extended by Gurnell et al. (2016a) (see also chapter 1.3). The succession stages occurring in a river corridor at a certain time can be interpreted from a spatial as well as from a temporal perspective. First, different succession stages can exist at the same time and form a specific pattern of the river corridor. This is the perspective I take in the single year classification. This perspective is useful for characterizing the spatial pattern of a river corridor. Gurnell et al. (2016a) has suggested, that river corridors might have a zonation with a specific distribution of biogeomorphological succession stages. A single year classification approach as conducted in this chapter can help detecting this zonation in an objective and quantitative way, especially when combining it with further information on the river corridor like confinement or stream power. For the Naryn River for instance, there is a clear pattern with the majority of biogeomorphological interactions occurring in the central part of the corridor where the absence of confinement and a not too high specific stream power allow the formation of braided and braided-anastomising reaches. The formation of extensive bars or islands in these river types leads to extensive areas in the geomorphological stage which can then be colonized by vegetation and develop towards the biogeomorphological succession stage. This is reflected in the large areas being in the biogeomorphological stage. In the other river types, either the constraints by confinement or

by too high stream power lead to a higher share of the permanent inundation stage and ecological stage compared ot the braided and braided-anastomising reaches. Such an impact of confinement has already been postulated by Gurnell et al. (2016a) basing upon literature reviews and experience. Remote sensing in combination with a disaggregation/aggregation framework (Alber and Piégay, 2011), as applied in this thesis, allows a straightforward, data driven analysis of biogeomorphological pattern within a river corridor.
Second, the biogeomorphological succession can also be an expression of a temporal development over time where each location in the river corridor is considered to exist in a specific stage of the biogeomorphological stage and is continuously developing. This is potentially the more complex perspective, but acknowledges the dynamic character of rivers. In this thesis, time series of multispectral remote sensing imagery is used to assess the temporal trajectory of biogeomorphological succession. The use of remotely sensed data sources is not completely new to fluvial biogeomorphology and satellite imagery (Bertoldi et al., 2011; Henshaw et al., 2013) as well as aerial and UAV imagery (Vautier et al., 2016; Räpple et al., 2017) have been used for quantifying changes in vegetation and geomorphological landforms. However, these approaches use only relatively loose sampling points in time and analyze for instance the change between two single years. The analysis of dense time series as applied in this thesis allows a temporally continuous view. From a system perspective, this enables an observation of the behavior of a biogeomorphological system rather than just the change between two states. Recently, such system perspectives have become popular in biogeomorphology through the application of resilience theory. In this perspective, biogeomorphological succession is considered as set of adaptive cycles with each succession stage forming a specific cycle (Stallins and Corenblit, 2018, see chapter 1.3). While this is a promising theoretical concept for advancing biogeomorphology, there is still a lack of methods for a quantitative assessment (Stallins and Corenblit, 2018). The analysis of temporally dense satellite time series might be such a method. Figure 7.21 links the time series analysis conducted in this chapter and biogeomorphological resilience theory. Both, NDVI and MNDWI show a seasonal signal on the annual time scale. The seasonal signal of the (positive) MNDWI series can be interpreted as flood cycling, i.e. the annual cycle of high and low flow caused by the glacial discharge regime (see chapter 4). The seasonal cycle of the (positive) NDVI time series refers to the seasonal cycle of the vegetation caused by the phenological cycle of the vegetation with spring breakup in April and leaf fall in October. Negative signals of NDVI and MNDWI are caused by the spectral properties of water and vegetation and do not have a real-world meaning for flood cycle (MNDWI) or vegetation (NDVI). As long as the time series show a specific behavior of the seasonal signal (e.g. positive NDVI signal showing the seasonal cycling of the vegetation phenology), the location can be expected to remain within a specific biogeomorphological succession stage, i.e. the system remains in the same, yet dynamic state. Trends within the same seasonal signal can be interpreted as changes within a certain stage, e.g. vegetation is growing (what leads to an increasing NDVI), but nevertheless remaining in the biogeomorphological or ecological succession stage. If significant changes in the seasonal signal occur, this can be interpreted as the change of the system state or - in terms of biogeomorphology - the change from one succession stage to another one. The time series example in figure 7.21 illustrates these ideas. Prior to 2010, there is a clear dominance of the MNDWI signal indicating the dominance hydromorphological disturbance by the annual flood cycle. In 2010, there is a changepoint in the seasonal cycle of the spectral time series. The NDVI starts getting positive while the MNDWI shows positive values only during the peak of the seasonal cycle. This indicates that the disturbance by the annual flood cycle has been broken up (potentially by the formation of a gravel bar during the 5 year return period flood in 2010). Between 2010 and 2016, the NDVI shows a positive trend along with an increase of the seasonal

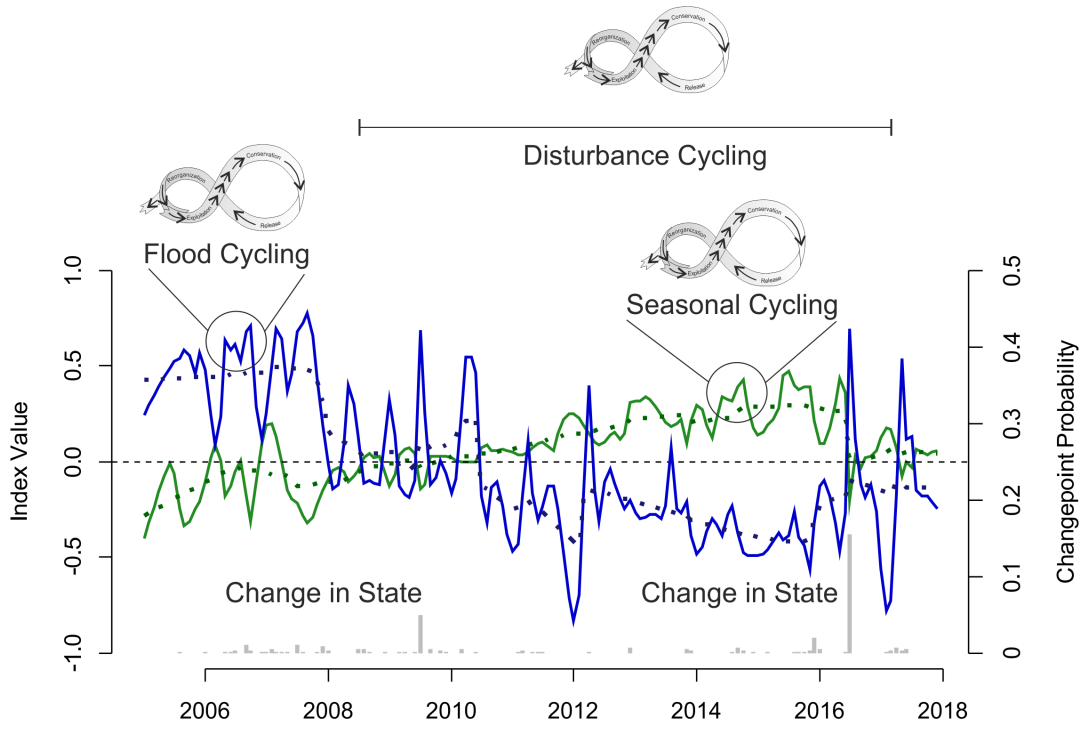


Figure 7.21: Linking multispectral index time series and resilience theory; the solid green and blue lines give the NDVI and MNDWI respectively; the dotted lines are the trend of the decomposed time series and the gray bars indicate the probability of changepoints in the seasonal signal

signal. This indicates the establishment and growth of vegetation having only a weak signal of seasonal cycling in the pioneer stage. This signal of seasonal cycle is quickly increasing with the growth of vegetation. In 2016, there is another significant changepoint in the seasonality. The rupture of the sesaonal signals of NDVI and MNDWI indicate the rupture of the seasonal cycle of vegetation and an re-initiation of the flood cycle. In terms of biogeomorphological succession, this indicates a set-back to the geomorphological stage. In addition to these annual cycles of flooding and vegetation phenology, there is another cycle on a different time scale. The entire development of the location between 2010 and 2016 from the geomorphological stage followed over the pioneer and the biogeomorphological and (early) ecological stage to the reset to geomorphological stage stands for a disturbance cycle.

# 8 Discussion

## 8.1 A comprehensive overview over the Naryn River corridor

One of the aims of this thesis is to give a comprehensive overview over the river corridor of the Naryn from the uppermost headwaters of the Big Naryn to the Toktogul reservoir. Still, these insights have a pioneering character as only very few studies on the Naryn River exist beyond the work of the author of this thesis and associated colleagues. The majority of these studies focuses on the issue of water resources against the background of climate change. Studies on fluvial geomorphology, riparian ecology or biogeomorphology as integrative field do not exist at all to my knowledge except the ones I (co-) authored. Thus, this discussion gives a comprehensive summary of the results and places them into general conceptual frameworks rather than discussing them against previous results. Ultimate goal is to contribute to a sustainable management of the river corridor by providing a comprehensive biophysical characterization. This characterization of the structure and functioning gives information about potential pressures on the river corridor and gives guidance for sustainable management and - in case of disturbed functions - suitable restoration measures (Gurnell et al. 2016b, see Fig. 8.1). The focus of this thesis is the first part

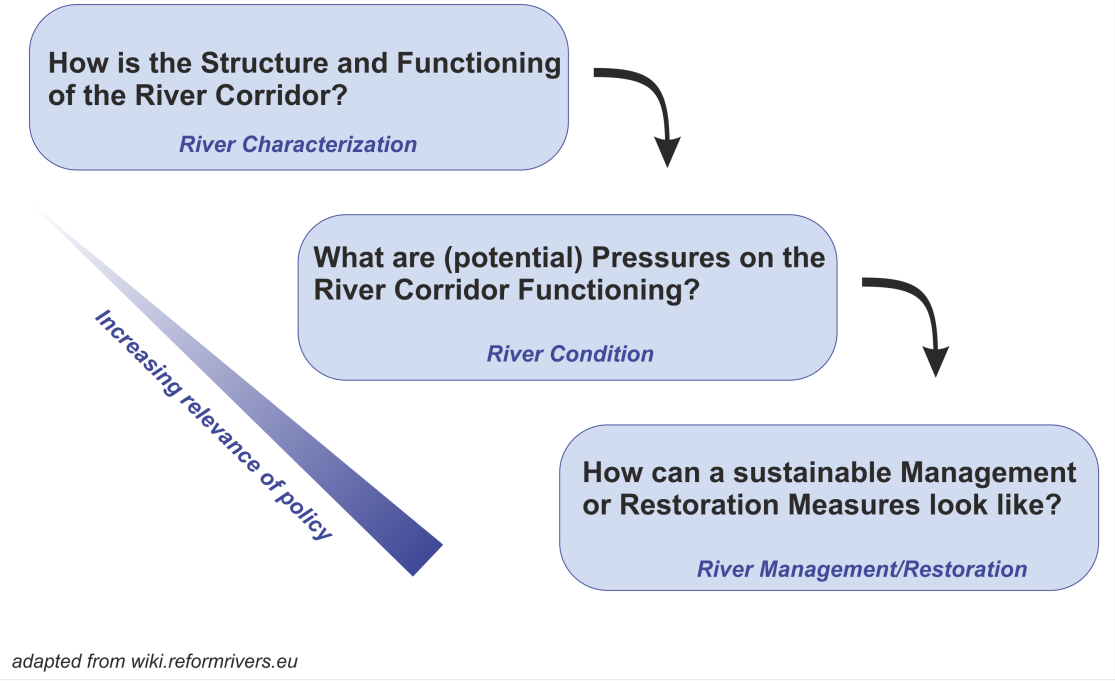


Figure 8.1: A modern approach to river management (modified from the REFORM project, wiki.reformrivers.eu, last access: 2020-12-28)

of this cascade. Thus, the major focus of this section of the discussion is on the large scale pattern

and functioning of the Naryn River corridor. Nevertheless, a brief summary of actual and potential pressures as well as perspectives for sustainable management are included here in order to give a complete picture.

### 8.1.1 River characterization: How is the large scale structure and functioning of the Naryn River corridor?

Prior to the work carried out within this thesis, no comprehensive study on the structure and functioning of the Naryn River has been available. In this section of the discussion, I develop a comprehensive overview of the Naryn River corridor based on the results presented in previous chapters of this thesis. This overview is focused on the scales between the river segment between Eki Naryn and Kazarman and the entire corridor of the Naryn River upstream from the Toktogul reservoir. The remote sensing based analysis of the river corridor (chapter 6) and the biogeomorphological succession (chapter 7) along with the hydrological analysis (chapter 4) and the field based analysis in four selected reaches (chapter 5) are used to disentangle the complex interactions governing the structure and functioning of the Naryn River corridor. A large scale, remote sensing based assessment as carried out in this thesis has the opportunity to deliver concise information for the scale under consideration. However, as many of the analysis presented here are derived from values aggregated to reach averages, not all local phenomena are fully captured. The potentials and limitations of such large scale characterization are discussed in section 8.2.

*Interpreting the structure of the river corridor*

Figure 8.2 shows the major structural zones of the Naryn River. In the uppermost part, the Naryn is still flowing for the majority of its course in a bedrock confined situation associated with very steep channel gradients. Downstream from Eki Naryn, the river is entering the Naryn basin and an interplay of straight and braided reaches dominate the riverscape. The gradient tends to become lower while the discharge is continuously increasing. In this part of the river corridor, terraces are a dominant feature of the riverscape forming the confining margin. Further downstream, the river corridor gradually becomes wider and the gradient becomes lower. In addition, the terraces disappear what leads to a laterally unconfined valley setting where braided and braided-anastomising planforms have developed (only interrupted by a gorge). Downstream from this braided/braided-anastomising section, the Naryn River is leaving the tectonically formed Naryn basin and enters a gorge directly leading to the Toktogul reservoir where the study area of this thesis is ending.
Discussing the parameters leading this specific pattern of planforms along with the specific spatial distribution of riparian vegetation is a challenging issue. The different parameters of the Naryn River show complex inter-correlations, thus there is no simple, straightforward explanation of the river corridor structure and functioning (see chapter 6). Nevertheless, I summarize the most relevant factors in a generalized way (Fig. 8.3). Tectonics respectively geology and climate form the boundary conditions under which the river system is operating. Tectonics and geology control the channel gradient and the confinement respectively river corridor width. Within the headwater and the gorges, the Naryn River is flowing in a bedrock confined situation with steep gradients in a narrow river corridor. On the contrary, within the Cenozoic basins, channel gradients tend to be lower and the river corridor tends to be wider. In addition, tectonics also have a minor impact on climate via the local topography. Climate has several impacts on the system. First, it is relevant for glaciation and being highly relevant for the discharge regime of the Naryn River. Runoff generation by snow melt and precipitation are controlled by climate as well. Climate change is obvious

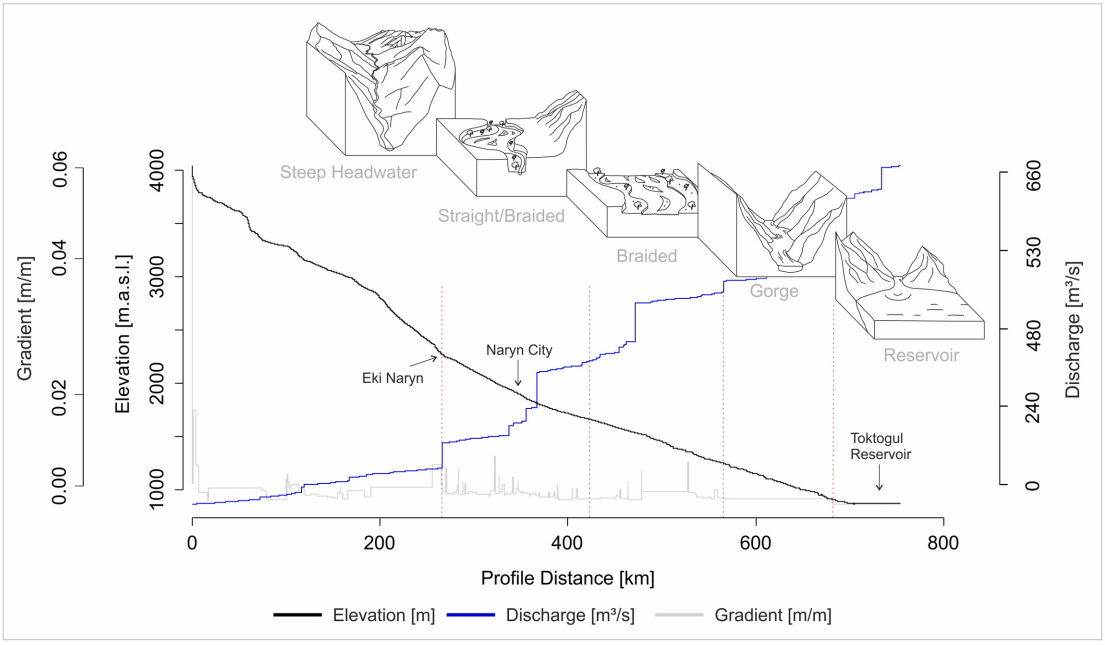


Figure 8.2: Large scale structure of the Naryn River (*river type sketches prepared by Magdalena Lauermann*)

in Central Asia (Unger-Shayesteh et al., 2013). Rising temperatures lead to enhanced glacier melt with increasing summer discharge until a tipping point is reached where the glacier cannot sustain the runoff anymore and summer discharges decrease. This tipping point has already been crossed for one sub-catchment of the Naryn River (see chapter 4). As also precipitation is decreasing, the natural flow regime might change in future. However, despite the trends visible in the discharge time series, the flow regime did not show a significant change regarding seasonality and magnitude of flow. Another, minor link exists between climate and riparian vegetation via the length of the vegetation period. However, this link has not been explored in detail in this thesis.

The width of the river corridor is then a major control on the development of specific river types and riparian vegetation along with its biogeomorphological feedbacks. In the confined reaches characterized as steep headwaters, straight reaches or gorges, the combination of limited space for development and high specific stream power does not allow the formation of extensive floodplains or instream features like bars or islands. In this setting, confinement as an expression of the specific geological history is considered as the major control of river development. Only, when the river has enough space to develop, braided and braided-anastomising rivers develop along with extended patches of riparian vegetation. These reaches are the 'hotspots' of biogeomorphological interaction in the corridor of the Naryn River. From the spatial perspective, the majority of the area in the pioneer or biogeomorphological stage occurs here. From the temporal perspective, the majority of changes could be observed there as well. This observation is true for the formation of new gravel bars and the removal of vegetation during a 40 year flood event as well as the establishment and growth of vegetation between a 5 year flood event in 2010 and the flood event in 2016.

Summarizing these findings, confinement caused by the tectonic and geological boundary conditions is the major control of the Naryn River. Only in unconfined reaches, the stream power along with biogeomorphological interactions controls the planform development. This combination of

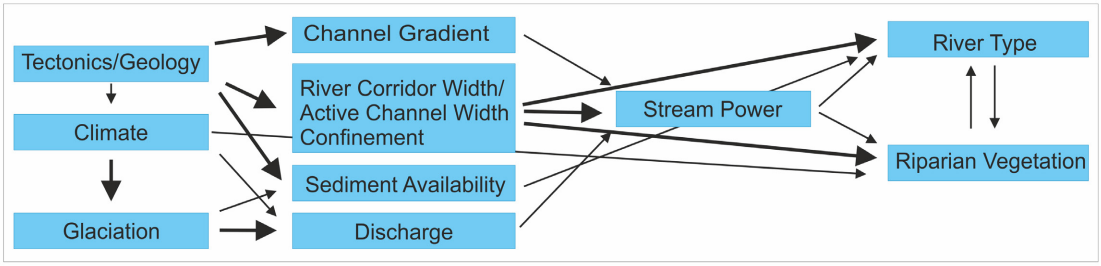


Figure 8.3: Conceptual understanding how selected river corridor parameters influence the occurrence of different river types and riparian vegetation (inspired from Notebaert and Piégay 2013)

geological boundary conditions and recent processes shaping contemporary riverine landscapes is a widely recognized phenomenon (Phillips, 2007; Fryirs, 2017). This impact of geological boundary conditions lead to a longitudinally heterogeneous pattern of the Naryn River what supports the view on rivers being organized in a patchy, discontinuous way rather than in a downstream continuum (Poole, 2002; Thorp et al., 2006). Due to their dynamics, the braided and braided-anastomising reaches between Eki Naryn and Kazarman are of particular interest for further, biogeomorphology oriented research. As they are highly sensitive to change, they should also be a focus area for decision making and future, ecology oriented monitoring incentives.

### 8.1.2 River condition: What are actual and potential pressures?

Despite the fact, that the contemporary Naryn River upstream from the Toktogul is still in a widely natural condition compared to most other rivers in the world, there are several (potential) pressures threatening this river corridor. The major issues I like to consider here are:

- Climate Change leading to hydrological changes and potential future water scarcity
- Dam Construction causing a disturbance of the natural flow regime and sediment connectivity
- Degradation of floodplain vegetation due to wood cutting and livestock grazing

*Climate change*

Climate change is expected to cause far-reaching changes in the hydrological systems of Central Asia (Immerzeel et al., 2010; Bernauer and Siegfried, 2012; Sorg et al., 2014; Xenarios et al., 2018). In chapter 4, I have carried out an in-depth analysis of climate and discharge trends in the Naryn River catchment. The results of these analysis suggest, that there are already significant changes of the hydrology. However, these changes are not homogeneous across the catchment. In sub-catchments with high glaciation, enhanced glacier melt is causing increased runoff and leads to increased discharge during the summer months. This increase will continue until the water equivalent stored in the glaciers becomes to small to sustain the runoff. After this tipping point, the runoff will decrease. Once the tipping point has been crossed, the (summer) discharge will start to decrease (Sorg et al., 2014). In the sub-catchment of the Small Naryn, this tipping point already seems to be crossed as summer discharges show a significantly decreasing trend. The Naryn itself

has not reached this tipping point yet, as summer discharge still shows an increasing trend (see chapter 4). Sub-catchments with a lower glaciation where runoff generation is dominated by snow melt and precipitation experience only minor changes in discharge so far. This has been proved for the Naryn catchment for the gauges Chichkan and Ustasai. However, a decreasing precipitation and and potentially changes in the snow cover may lead to a higher discharge variability in future (Deng et al., 2019). To date, these hydrological changes did not lead to statistically significant changes in the natural flow regime of the Naryn River even if a tendency towards a longer flood season has been observed. This development will continue until the glacier runoff starts to decrease. Once the glaciers become less relevant for the discharge in the Naryn River, the flow regime is expected to become more variable with less predictable timing of the peak flows towards the end of this century (Gan et al., 2015).
In an overall evaluation, the effects of climate change do not yet have a strong effect on the riparian ecosystems along with their biogeomorphological feedbacks. But in future, the hydrological changes might have a more significant impact on flow regime (Gan et al., 2015). In addition, there might be further consequences of climate change beyond hydrology as well. For instance, the vegetation period might change causing a modification of the phenology of riparian vegetation (Jiang et al., 2017). Furthermore, glacier melt will expose vast amounts of sediment and makes it available for transport in the fluvial system. (Heckmann et al., 2015; Heckmann and Morche, 2019). These issues are considered as remaining research gaps which should be filled in future research projects.

*Dam construction*

In the short term, dams are expected to have a greater impact than climate change. Currently, two dams exist upstream from the Toktogul reservoir. Directly upstream from the Toktogul reservoir, there is the first dam of the Kambar Ata cascade and further upstream there is the At Bashe dam. In addition, there are concrete plans for further hydropower dams in the Naryn catchment (see chapter 2.6). A quantitative measure of the fragmentation of a river network is the dendritic connectivity index suggested by Cote et al. (2009). This index takes a value of 100% in case there are no dams in a catchment and decreases with increasing fragmentation. If we take into account the existing dams - Kambar Ata and At Bashe - the index takes a value of 66.65%. If the Naryn cascade and the Emgek Talaa hydropower plant (HPP) were built, the connectivity index would decrease to 33.76%. An overview about the potential fragmentation is given in figure 8.4. However, the connectivity index values alone do not tell the full story. The Kambar Ata dam is directly at the inflow of the Toktogul reservoir. Thus, the impacts on the downstream section of the Naryn is minimal as there are already no natural conditions anymore. The At Bashe dam is disconnecting a relevant tributary of the Naryn River. The At Bashe River contributes to approximately 18% of the annual average discharge. The impact on the natural flow regime of the Naryn River is nevertheless minimal (see chapter 4). This can be explained by the glacial dominance of the flow regime and the distribution of the glaciers in the catchment. The At Bashe sub-catchment contains only 8% of the glacier area in the Naryn catchment while 70% of the glaciers are in the headwaters of the Big and Small Naryn. The Emgek Talaa HPP and in particular the Naryn cascade with several dams up to 75 m height would disconnect these highly glaciated sub-catchments. In addition, they are upstream from the braided and braided-anastomising reaches in the central part of the Naryn catchment. As the purpose of these dams is mainly energy production and the highest energy demand is in winter time, water release is expected mainly in winter time (Xenarios et al., 2020, see also chapter 2.6). Thus, the annual flood pulses in summer time caused by glacier

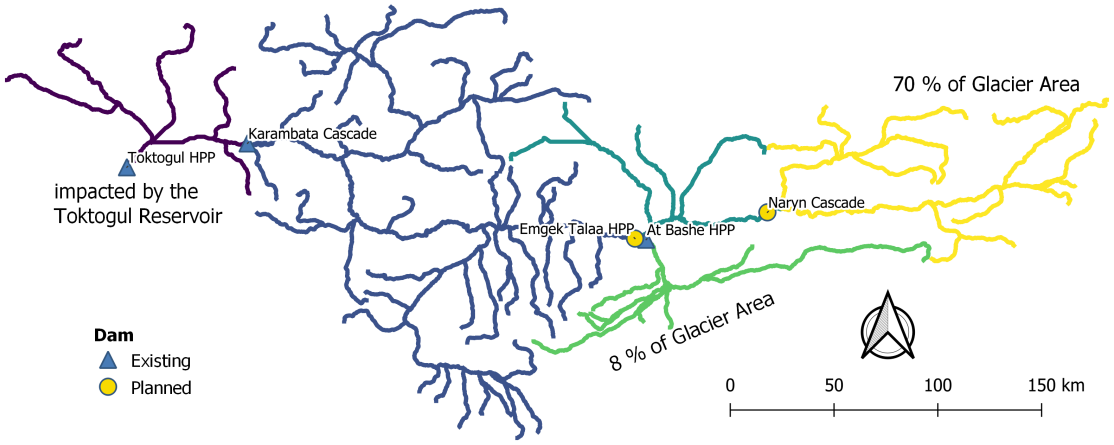


Figure 8.4: Potential fragmentation of the river network of the Naryn catchment

melt are expected to be significantly reduced. This flow regime modification has already been observed for the gauge Uchkurgan directly downstream from the Toktogul dam (Fig. 8.5). After

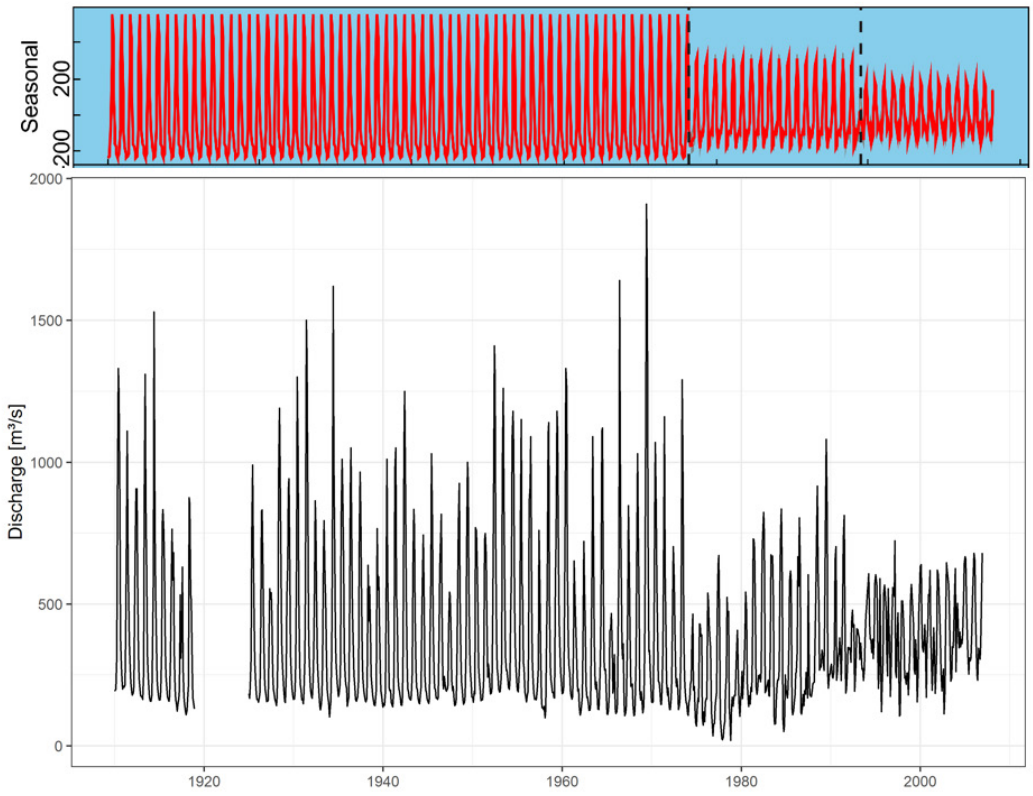


Figure 8.5: Monthly discharge of the gauge Uchkurgan right downstream from the Toktogul reservoir; the red line gives the seasonal signal of the decomposed time series, the dashed line show significant changes in the seasonality

the closure of the dam in the 1970s, the peak flows in summer time have significantly changed due to the reservoir management. This became even more obvious after the independence of Kyrgyzstan 1991, when the Kyrgyz authorities started to focus on energy production in winter time instead of irrigation in summer time. Thus, looking at the gauge Uchkurgan might help to get an understanding how a modified flow regime of the Naryn River might look like downstream from a hydropower dam dedicated to energy production in winter time. For the Central Asian rivers, there has been no intensive discussion about the ecological and geomorphological consequences of dam construction so far, neither in academia nor in practice. However, there are many studies on the impact of dams on river systems from other parts of the world (Poff and Zimmerman, 2010; Hayes et al., 2018). Hayes et al. (2018) gives a comprehensive summary of expected impacts of flow regime modification on hydromorphology, flora and fauna. A key message of this review is, that flow regime modifications as anticipated for the Naryn River in case of the construction of one or several dams will result in a decrease of dynamics and thus a decrease of habitat diversity and a terrestrialization of the floodplain vegetation.
In this thesis, I identified 'hotspots' of riparian ecosystem dynamics in the braided and braided-anastomising reaches in the central part of the catchment between Eki Naryn and Kazarman. With an impact on these reaches, 65% of the area of riparian ecosystems along the entire Naryn River are likely to undergo a negative development regarding dynamics and habitat diversity. The time series analysis approach introduced in chapter 7 offers an efficient tool for monitoring habitat dynamics at a large scale. The monthly time series of spectral indices have proved to deliver reliable indicators for biogeomorphological dynamics. Especially the recently available Sentinel-2 imagery has the potential to serve as a basis for large scale monitoring of riparian habitat dynamics.

*Degradation of floodplain vegetation due to wood cutting and overgrazing*

The provision of firewood and pastoral land are important ecosystem services of the Naryn floodplain forests (see chapter 3). The exploitation of the forest resources, however, can lead to a degradation of the floodplain vegetation. The Landsat time series used for the assessment of biogeomorphological dynamics can also be used for getting an idea of the floodplain forest development. An in-depth analysis of this issue would be a study for its own, but nevertheless, I give an impression in figure 8.6. Negative NDVI trends indicate decrease in vegetation cover, positive values an increase. The negative trends on the floodplain are an indicator for deforestation and grazing. The park like landscape with low tree density is interpreted as the result of timber extraction. The island is not easily accessible, neither for humans nor for livestock. This is reflected in positive NDVI values or values close to 0 except for the flow facing side in the east where potentially lateral erosion removed trees or shrubs close to the edge of the river bank. The statistical distribution of the NDVI values for the entire floodplain areas along the Naryn River show a slight tendency towards negative values with a mean of $3 \times 10^{-5}$. Thus, in general there is the long term tendency of decrease of vegetation cover on the floodplains. Interviews during the work on ecosystem services revealed, that there has been particular intensive wood cutting between the breakdown of the Soviet Union and the mid 1990s (see also Schmidt, 2013 for a discussion on forest resource use in the post-soviet era). Today, the demand for forest resources is still high and existing control mechanisms for limiting their exploitation are weak (see chapter 3).
The field based overview of the floodplain forests showed, that there is a lack of rejuvenation in the ecological stage (see chapter 5). In these areas, vegetation development is controlled by anthropogenic impact in form of pollarding and livestock grazing. In areas shaped by the high dynamics of the annual flood pulses, the natural, biogeomorphological succession governs vegetation

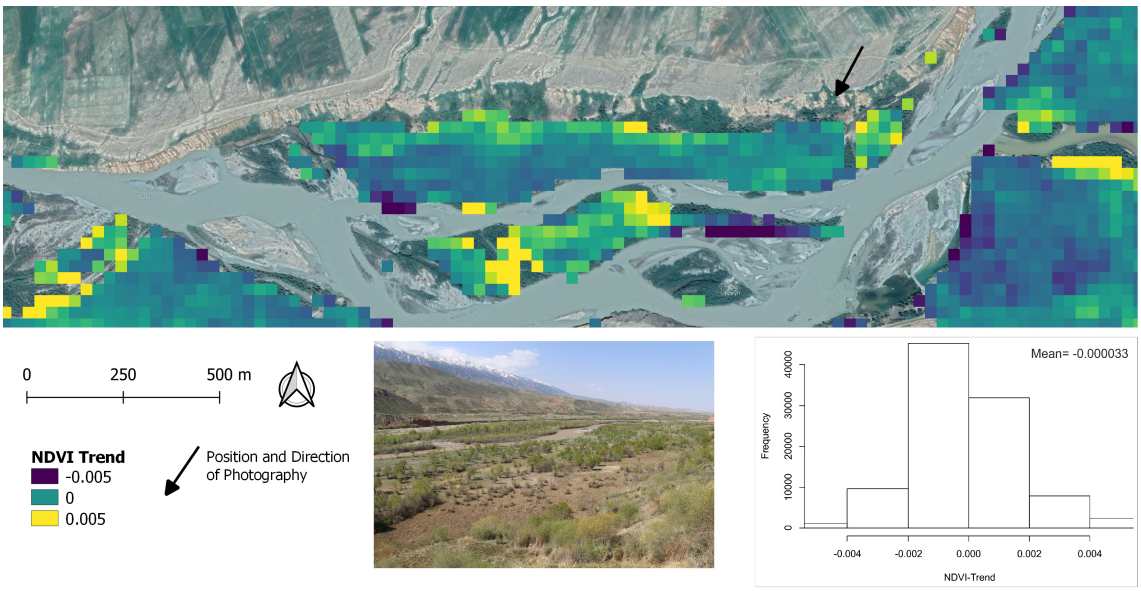


Figure 8.6: NDVI trend from 1990 to 2017 for the Emgek Talaa field site (background image: Google Earth); the photography gives an impression of the landscape on the map, the histogram gives the statistical distribution of the NDVI for all floodplain areas along the Naryn River (morphologically active areas have been excluded from analysis)

development.

### 8.1.3 River management: A vision for sustainable development of the Naryn River corridor

Figure 8.7 shows the linkage between science as it is the focus of this thesis and environmental policy (see also Cyffka, 2001). The guiding principle clarifies the focus of environmental decision makers. These principles are then put in more concrete terms in the environmental quality objectives defining for instance which ecological functions to protect or which resources to elaborate. Environmental quality standards are then the reference scale and define environmental indicators measuring the degree of achievement of the quality objectives. These indicators are (ideally) established based on scientific research, are able to fully capture the environmental condition of interest and allow efficient monitoring.

When thinking about the guiding principle of river management in Kyrgyzstan and in Central Asia in general, the focus is on a water resource perspective seeing rivers mainly as a certain amount of water flowing from upstream to downstream (Sorg et al., 2014; Xenarios et al., 2020). Consequently, the environmental objectives, standards and indicators focus on the amount of water delivered countries at the time when water resources are needed. The reason for this is certainly the ongoing international water conflict with the downstream countries Uzbekistan and Kazakhstan (see chapter 2.6). At the same time, the riparian ecosystems of the upstream countries are highly valuable from a nature conservation and biodiversity perspective as riverine ecosystems with undisturbed natural dynamics have become extremely rare worldwide (Zarfl et al., 2014; Grill et al., 2019). Thus, for a comprehensive management of the Naryn River, an adjustment of the guiding principle from a water resource focus to an integrated management would be nec-

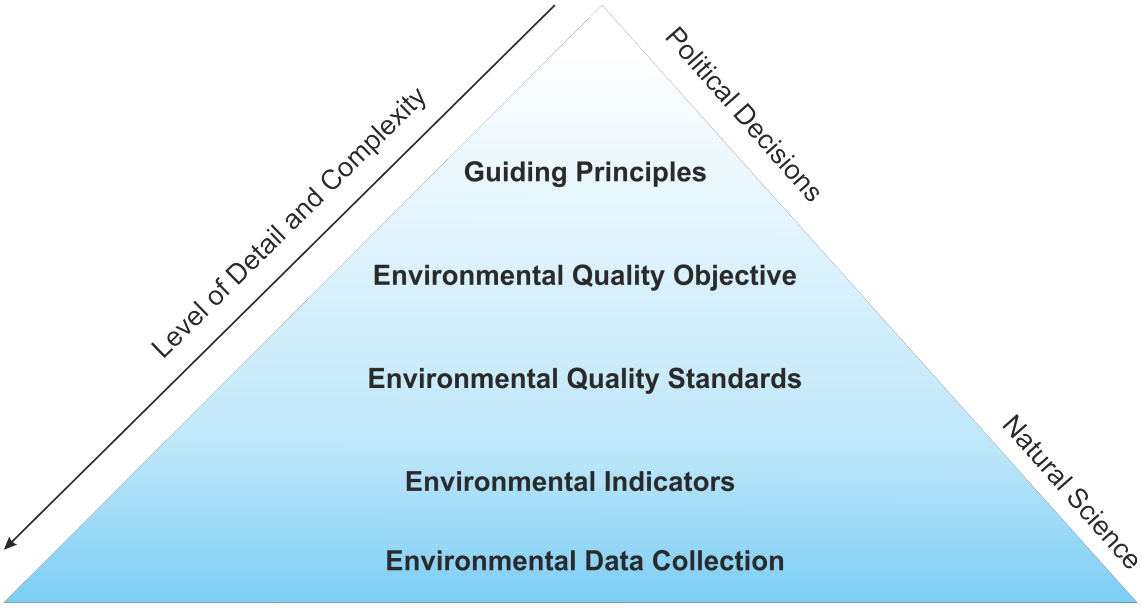


Figure 8.7: From guiding principle to environmental data collection: Linkage between natural science and policy (modified from Cyffka, 2001)

essary taking into account hydrology, hydromorphology, ecology and human resource demand. Consequently, the environmental quality objectives should include also the conservation of riparian ecosystems depending on the habitat dynamics caused by a natural flow regime (see chapters 4 and 7). Against this background, the potential impacts of hydropower exploitation on the natural dynamics and the ecosystems should be critically evaluated. One possible environmental objective could be the avoidance of hydropower by using photovoltaic as an alternative (Lauermann et al., 2020). If the plans for hydropower persist, an environmental flow management is highly recommended taking into account the functions of timing, magnitude and frequency of discharge (Hayes et al., 2018). For instance, periodic high flow events are needed to initiate habitat turnover and maintain habitat diversity. The concept of fluvial biogeomorphology as used in this thesis is a potential template for an assessment of these dynamics. To optimize environmental flow management, model based predictions about the effects of flows on the biogeomorphological dynamics are suggested as a tool (see e.g. Egger et al., 2013). To achieve the objective of maintaining a dynamic riverine landscape, standards in particular about the environmental flow management have to be defined. Then, comprehensive indicators are needed to monitor the achievements. The remote sensing approach for analyzing biogeomorphological dynamics suggested in chapter 7 has the potential for efficient monitoring of river dynamics delivering temporally and spatially continuous observations (see also the discussion on remote sensing in chapter 8.2).

While the construction of dams is certainly the most serious potential threat for the ecosystems along the Naryn River, the use of the floodplain forests for timber collection and livestock grazing cause a certain pressure as well. Contrary to the management of hydrology, there are existing management schemes for balancing resource exploitation and nature conservation (Schmidt, 2013, see also chapter 3). Guiding principle here is to protect the floodplain forest, the concrete environmental objectives are formulated in the forest code of Kyrgyzstan (Zholdosheva, 2010). Despite this clear objective, there is a gap between legislation and actual management practice in the villages. Officially, there are clear restrictions of forest resource exploitation which should be controlled

by the local forest authorities by means of a ticket system. In practice, this access limitation is not working due to a lack of control (see chapter 3). This lack of control is partly caused by the absence of a monitoring scheme. Reporting on forest condition is the responsibility of local foresters. Interviews with local foresters and forest authorities on the Rayon and Oblast level reveal significant differences in the reported amount of timber extracted from the forests (personal communication with Siegmund Missall). Thus, on the one hand objective indicators for monitoring the forest condition are required for improving the current management scheme. Beside improving field based forest inventories, remote sensing has proved to be a valuable alternative for forest assessment of the Naryn floodplain forests (Chymyrov et al., 2019). On the other hand, alternatives to the exploitation of the forest resources by local people need to be provided to maintain the livelihood in the villages along the Naryn River. For instance, short rotation coppices might offer a sustainable alternative for timber from the natural forests or improved isolation of buildings might reduce energy demand for heating (Lauermann et al., 2020).
Basing upon several years of research in a transdisciplinary context in Kyrgyzstan showed that the Kyrgyz authorities have a great openness regarding solutions for sustainable environmental management and nature conservation. However, in the context of river and floodplain management, the highly sectoral organization of Kyrgyz authorities limits their ability to offer comprehensive solutions (Lauermann et al., 2020). Currently, an international, transdisciplinary project is working on comprehensive management recommendations for the Naryn floodplain ecosystems including the elaboration of alternatives for satisfying peoples' resource demand and the assessment of hydrological impacts of hydropower exploitation (Lauermann et al., 2020, see also `www.bmbf-client.de/en/projects/OekoFlussPlan`). This thesis directly contributes to the aims of this project by providing comprehensive information about the local situation and an in-depth analysis of the large scale structure and functioning of the Naryn River corridor.

## 8.2 Remote sensing for the characterization of river corridors

### 8.2.1 Potentials and limitations of open source approaches for riverscape analysis [1]

Remote sensing and terrain analysis are the core methods used in this thesis for large scale characterization of the Naryn River corridor. Such technical approaches have become increasingly popular in river science over the past decade (Piégay et al., 2019; Tomsett and Leyland, 2019). Remote sensing has demonstrated to deliver spatially continuous data over large scales overcoming the issue of spatially loose sampling points unable to cope with the heterogeneity of riverscapes (Carbonneau et al., 2012; Notebaert and Piégay, 2013). Today, the high potential of automated remote sensing and GIS procedures for riverscape analysis has become commonly accepted and science has started to incorporate these methods and existing conceptual models and frameworks (Fryirs et al., 2019). Except very few examples (e.g. Schmitt et al., 2014 or Betz et al., 2020), studies tend to focus on regions where data like LiDAR derived DEMs or aerial imagery is available. This leads to the consequence that rivers in remote regions of the world tend to be underrepresented in the scientific literature while at the same time many of the few remaining free flowing (and thus ecologically valuable) rivers are located in such data-scarce environments (Grill et al., 2019). The Naryn River studied in this thesis is a typical example of this issue. Kyrgyzstan as a developing country does not routinely collect aerial imagery or LiDAR elevation data which

[1] Several aspects of this section of the discussion have been published in Betz et al. 2020.

could be purchased from a mapping agency. At the same time, high resolution spaceborne data is extremely costly. For instance, a state-of-the-art high resolution DEM derived from satellite imagery has costs of 100 € per square kilometer. This results in total costs of 5.2 million € for the entire catchment. Such costs are simply not feasible for common research projects or management applications. Thus, I focus on the use of open access data like the SRTM-1 DEM or Landsat imagery for river corridor characterization as an alternative to LiDAR DEMs and aerial imagery. Open access data allows large scale river characterization for low costs. The riverscape mapping approach demonstrated in chapter 6 fully relies on open access data and a minimum of field calibration data only. Nevertheless, it is capable to deliver a realistic representation of the river corridor for both, the longitudinal as well as the lateral dimension. Despite this low data demand, the results derived for the Naryn River in chapter 6 show sufficiently high accuracies even for complex parameters like the active channel width. Thus, it potentially enables studies on other large rivers in data-scarce regions which might remain unexplored otherwise.
Despite its potentials, the use of open access data has limitations as well. First, the spatial resolution of the data needs to fit to the size of the river under investigation. The ratio of pixel size and river width gives an estimate of the suitability of open access data (Legleiter and Fonstad, 2012). For smaller rivers, the 30 m resolution used in this thesis is certainly not sufficient (Henshaw et al., 2013). While the recently available Sentinel-2 imagery with its higher spatial resolution might overcome this challenge for the multispectral data, the bottleneck remains the availability of open access digital elevation data with sufficiently high resolution and accuracy. Even for large rivers, the suggested approach delivers information averaged for the disaggregated 100 m segments only. Elements of the river corridor like single geomorphological units like single bars or islands are not considered individually contrary to high resolution remote sensing studies. As a consequence, the results of the open access riverscape characterization approach developed in this thesis is suitable to deliver information on the scale of entire river corridors. Such information is relevant for a quantitative overview needed for the objective selection of study reaches or sampling sites (Fausch et al., 2002).

### 8.2.2 Extending the idea of riverscapes to the temporal domain

The merit of the original idea of riverscapes is to move beyond spatially loose sampling points or simple scaling laws like the river continuum concept (Vannote et al., 1980) or the downstream hydraulic geometry Leopold and Maddock (1953). Rather, rivers are treated as spatially continuous, yet complex objects in the landscape (Fausch et al., 2002; Thorp et al., 2006). While there has been a considerable progress in the spatial realization of riverscape studies (e.g. Carbonneau et al., 2012), the temporal dynamics emphasized in conceptual frameworks (Junk et al., 1989; Ward et al., 2002) remains unstudied on a large spatial scale. Of course, river scientists have studied the changes of river structures for a long time mainly based on the use of archival aerial images (Carbonneau and Piégay, 2012; Piégay et al., 2019). The limitation of this data source is the limited temporal frequency. For Bavaria (Germany) for instance, there is one aerial image every second year. Results of the analysis from such imagery is highly dependent on the river conditions at the acquisition date. What is the discharge? What is the phenological stage of the vegetation? Thus, from a temporal perspective, these aerial images or similar infrequent observations are similar to the spatially loose sampling points in the spatial domain. Most recently, UAV surveys allow to theoretically collect more frequent aerial imagery (Piégay et al., 2019). However, UAV surveys are limited in their spatial coverage and are not suitable beyond the scale of a single reach. In addition, they have a high pre-processing demand regarding georeferencing, orthorecti-

fication and spectral calibration making the creation of image time series a labor intensive task. Over the past decade, the use of temporally dense satellite time series has become increasingly popular due to the availability of open access satellite archives and the increasing computational power (Gómez et al., 2016; Wulder et al., 2018). The time series algorithms developed for the analysis of satellite imagery time series have mainly focused on the detection of forest disturbance (Kennedy et al., 2010; Verbesselt et al., 2012; DeVries et al., 2015; Reiche et al., 2018). Within the context of river science, satellite time series have the potential to extend the idea of spatially continuous riverscapes to include the temporal dimension. From a conceptual perspective, each location in space is characterized by the spectral characteristics of a single pixel while the temporal aspect is covered by the observation of the trajectory of the spectral values of this pixel (see Fig. 8.8). The analysis of Landsat time series in chapter 7 showed, that monthly time series of NDVI

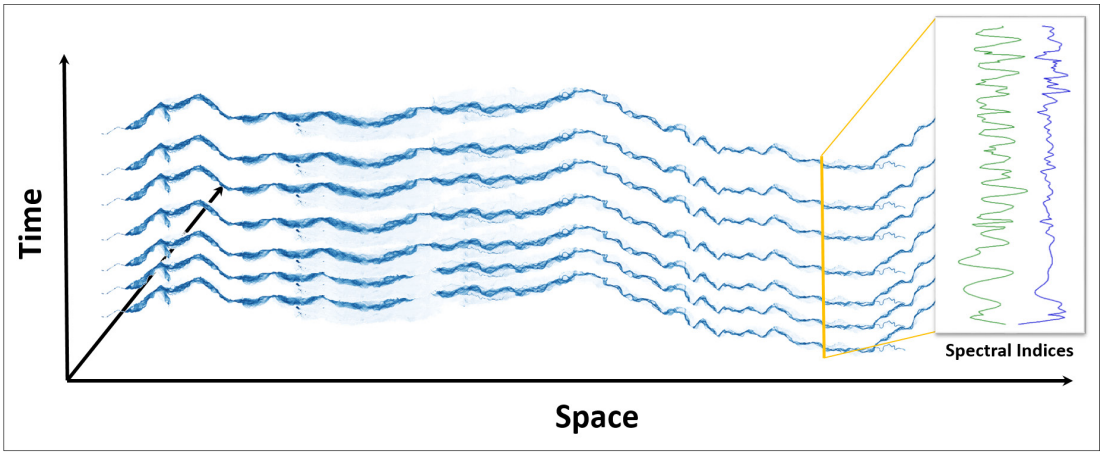


Figure 8.8: Extending the idea of continuous observation of rivers from the spatial to the temporal domain; each location in space is represented by the spectral characteristics of one single pixel while the temporal aspect is represented by the trajectory of the values of spectral indices

as indicator for vegetation and MNDWI as indicator for hydromorphological disturbance are able to capture the temporal trajectory of biogeomorphological dynamics of a river. The continuous temporal observation allows a process oriented analysis against the background of biogeomorphological theory (see chapter 7.6). Despite this successful demonstration, the Landsat sensors have limitations due to their spatial resolution of 30 m only (Henshaw et al., 2013). At the same time, an approach depending on a vast amount of satellite imagery for time series analysis is likely to depend on open access data (Wulder et al., 2012). The recently available imagery from the Sentinel earth observation mission by the European Space Agency have the potential to fulfill both requirements - open access data and sufficient spatial and temporal resolution (Malenovský et al., 2012). The multispectral satellite constellation Sentinel-2 offers data in a spatial resolution of 10 m and a revisit time of 5 days giving it a high potential for monitoring of dynamic earth surface processes Drusch et al. (2012). The derivation of the spatial pattern of biogeomorphological succession stages based on Sentinel-2 imagery as it has been demonstrated in chapter 7 shows very promising results. While the data record of Sentinel-2 has been not sufficient for carrying out the time series analysis presented in this thesis, the conceptual approach presented based on Landsat data is fully applicable to Sentinel-2 time series as well. An application of the dense time series analysis as presented in this thesis based on Sentinel-2 imagery is expected to deliver continuous

measurements of fluvial biogeomorphology in river corridors in space and time on the scale of geomorphological units. This will give new opportunities for river science to observe (biogeomorphological) processes for entire river corridors and analyze their emergent pattern.

### 8.2.3 Towards multi-scale biogeomorphology

In the previous section of the discussion, I elaborated the idea of spatially and temporally continuous large scale observation of biogeomorphological processes for entire river corridors. Despite this great potential, satellite observations alone are not sufficient for a comprehensive study of the dynamic interactions of hydrology, geomorphology and ecology. From a technical perspective, remote sensing is dependent on field data for calibration and validation. But also from a conceptual perspective, satellite analysis needs to be accomplished by further research. This is due to the fact, that satellite observations deliver indicators rather than the biophysical foundation of biogeomorphological processes. At the same time, field measurements deliver information for a single point in space and time only. For a complete picture, methods across scales need to combined (Räpple et al., 2017; Gurnell et al., 2020, see Fig. 8.9). On the scale of river elements like single pieces of

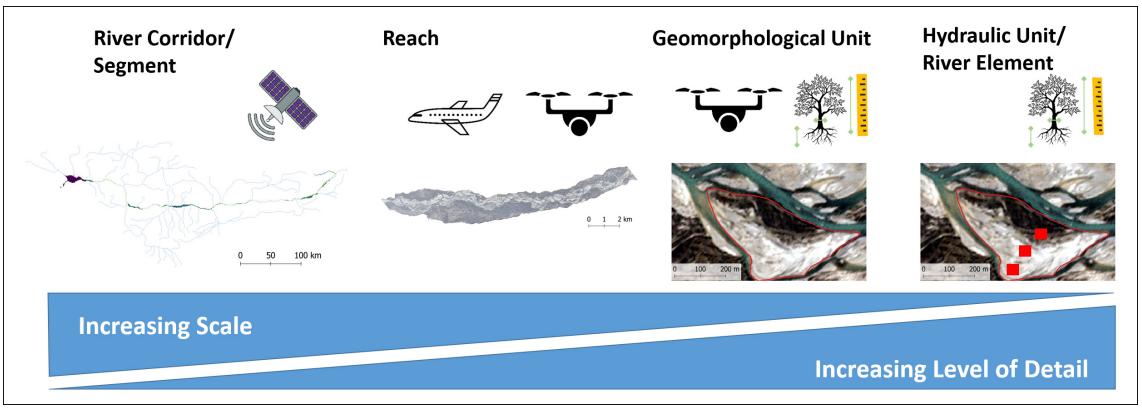


Figure 8.9: Scheme of multi-scale biogeomorphological research; a definition of scales is given in chapter 1.2 (icons from www.colourbox.de)

deadwood as well as on the scale of hydraulic units, field measurements in plots deliver detailed information on woody debris metrics, sediment and soil characteristics or plant traits. On the scale of geomorphological units, still a high level of detail is required and field measurements might be combined with UAV based surveys for detecting changes. For instance, mapping of the vegetation composition might be combined with topographical change detection based on terrestrial or UAV based photogrammetry (Räpple et al., 2017). For entire reaches, field based methods are not longer suitable. Here, UAV or aerial surveys deliver combined information on both - vegetation and topographical change (Vautier et al., 2016). When recalling the state-of-the-art review in the introduction (1.3), most of the studies are working on the spatial scales between hydraulic units and single study reaches. This thesis extends the spatial scale of biogeomorphological analysis to the entire river corridor. On such large scales, satellite remote sensing becomes the method of choice (Piégay et al., 2019). On this spatial scale, the use of indicators for biogeomorphological processes allows to study large scale spatial patterns along with their relevant driving forces.
Each study approach on each scale gives specific insights in the structure and functioning of entire river corridors. While detailed field methods on the scale of hydraulic or geomorphological units

give insights in the detailed mechanisms behind biogeomorphological feedbacks, they do not allow an observation of spatial structures emerging from the local scale processes. Often, the reach has been used to bridge the gap between the scales. For instance, Francis et al. (2009) studied the emergence of vegetated islands in a braided river as consequence of local scale feedbacks between vegetation, hydraulic forces and sediment deposition and fixation (to mention just one example, see also chapter 1.3). However, there are differences between the reaches within a river corridor or network as well emerging from the specific conditions of available energy, sediment availability and geological constraints in terms of confinement (Gurnell et al., 2016b, 2020). Combining the information from the different scales from the single river element to the entire corridor or network allows to disentangle the complex, nested relationships in river systems. This thesis introduces innovative remote sensing techniques to extend biogeomorphological analysis beyond the reach scale. This analysis is conducted having such a multi-scale biogeomorphological research in mind which will potentially give further insights in the functioning of the Naryn River or other dynamic river systems.

# 9 Conclusion

In this thesis, I presented the first comprehensive scientific study on the corridor of the Naryn River in Kyrgyzstan combining an up-to-date riverscape approach with a biogeomorphological perspective and remote sensing methods. Due to the lack of previous scientific work, I follow a holistic river science approach and address topics from hydrology, geomorphology, ecology as well as from socio-economy. The Naryn River is today still in a widely natural condition. High natural dynamics caused by a glacial discharge regime shape the active channel where the permanent inundation, geomorphological, pioneer and biogeomorphological stage of biogeomorphological succession can be found. In this part of the river corridor, there is practically no anthropogenic impact today and the structure and processes can be explored from a purely natural science perspective. On the contrary, the floodplains in the ecological stage of biogeomorphological succession are used by the local people for cutting firewood, grazing livestock or for recreational purposes. Wile these are important ecosystem services for local people, the resource exploitation causes also a certain pressure on the ecosystems and management adaptation is required for a longterm conservation of these areas. However, the major focus of this thesis is on the natural processes shaping the structure of the Naryn River. Due to the large size with a catchment area of 52,130 $km^2$ and a river length of more than 700 km, the analysis is challenging. Thus, this thesis focuses on the use of remote sensing methods for a spatially continuous characterization. As Kyrgyzstan is a data-scarce region where no aerial imagery, high resolution elevation or LiDAR data is available, an open source approach is developed for a characterization. In a first part of the analysis I derive a static template of the river corridor including a derivation of the riparian zone, active channel width and a range of parameters for a quantitative description of the river corridor including a simple, stream power based erosion/deposition model. Validating the results shows, that such an open source approach delivers reliable results for a large scale analysis of river corridors in data-scarce regions. Basing upon this template, I take an explicitly biogeomorphological perspective and analyze the large scale pattern of biogeomorphological succession in the Naryn River corridor based on multispectral satellite imagery time series. This analysis is done in a twofold way. Using recently available Sentinel-2 imagery, the spatial distribution of biogeomorphological succession stages is derived for one single year. Then, Landsat time series with a monthly resolution are used to analyze the temporal perspective on biogeomorphological succession. This analysis shows, that multispectral satellite imagery time series have a high potential for a temporally and spatially continuous analysis of processes of biogeomorphological succession such as the formation of new gravel bars, vegetation establishment and growth and reset from the biogeomorphological or ecological stage to the geomorphological or permanent inundation stage. This satellite time series approach has a great potential for tracking biogeomorphological processes over large areas in a temporal continuous way. This allows to extend the idea of riverscapes as spatially continuous measurements along river corridors to spatially *and* temporally continuous observations of river corridors.

The results of the static river corridor characterization as well as the remote sensing analysis of biogeomorphology reveal, that the large scale structure of the Naryn River corridor is controlled mainly by its confinement caused by either by hillslopes in the headwaters, terraces or bedrock in

two gorges. Only in the central part of the catchment, the Naryn is flowing in a tectonically formed basin where laterally unconfined reaches exist. In this setting, the specific stream power is considered to be the major driving force of planform development and braided and braided-anastomising river types develop. These reaches are also the 'hotspots' of biogeomorphological interactions as on the extensive bars of the braided plains there is vast space for the establishment and growth of vegetation leading in turn to biogeomorphological feedbacks via the stabilization and trapping of sediment. In other river types with a higher degree of confinement, almost no biogeomorphological feedbacks happen due to the lack of space for the formation of bars and too high hydraulic forces. This spatial heterogeneity becomes also obvious when analyzing biogeomorphological changes caused by a 40 year return period flood in 2016. The majority of changes occurred in the braided and braided-anastomising reaches in the central part of the catchment.
The natural processes are unlikely to change in near future. An analysis of hydrological and climatic changes in the Naryn catchment reveals, that there are significant changes in the discharge, but they do not have a significant effect on the natural flow regime yet. In the longer term perspective, glacier melt as a consequence of climate change will lead to reduced glacier runoff and thus potentially to a higher discharge variability in summer and a slightly changed seasonality. However, a higher threat for the natural flow regime are the plans for the construction of several hydropower dams in the Naryn River. Two of these hydropower projects, the upper Naryn cascade and the Emgek Talaa hydropower plant would directly affect the braided reaches with their highly dynamic interaction of hydromorphology and vegetation. To date, it is unclear if or when these projects will be realized. Nevertheless, it is unlikely that these plans will be off the table on the short run as this would require a major change of the guiding principles of contemporary Kyrgyz environmental policy. This thesis delivers data, information and methods which can form the basis for further research on the Naryn River, but can also contribute to informed decision making in river management and longterm monitoring of the river system.

# Bibliography


Abbink, K., Moller, L.C., O'Hara, S., 2010. Sources of mistrust: An experimental case study of a central asian water conflict. Environmental and Resource Economics 45, 283–318. doi:10.1007/s10640-009-9316-2.

Abdrakhmatov, K.Y., Aldazhanov, S., Hager, B., Hamburger, M., Herring, T., Kalabaev, K., Makarov, V., Molnar, P., Panasyuk, S., Prilepin, M., et al., 1996. Relatively recent construction of the Tien Shan inferred from GPS measurements of present-day crustal deformation rates. Nature 384, 450. doi:10.1038/384450a0.

AG Boden, 2005. Bodenkundliche Kartieranleitung. 5 ed., Stuttgart. In German.

Agarwal, A., Maheswaran, R., Kurths, J., Khosa, R., 2016. Wavelet spectrum and self-organizing maps-based approach for hydrologic regionalization -a case study in the western united states. Water Resources Management 30, 4399–4413. doi:10.1007/s11269-016-1428-1.

Aiken, S.J., Brierley, G.J., 2013. Analysis of longitudinal profiles along the eastern margin of the Qinghai-Tibetan Plateau. Journal of Mountain Science 10, 643–657. doi:10.1007/s11629-013-2814-2.

Aizen, V.B., Aizen, E.M., Kuzmichonok, V.a., 2007. Glaciers and hydrological changes in the Tien Shan: simulation and prediction. Environmental Research Letters 2, 045019. doi:10.1088/1748-9326/2/4/045019.

Aizen, V.B., Aizen, E.M., Melack, J.M., 1995. Climate, snow cover, glaciers, and runoff in the Tien Shan, Central Asia. Journal of the American Water Resources Association 31, 1113–1129. doi:10.1111/j.1752-1688.1995.tb03426.x.

Alber, A., Piégay, H., 2011. Spatial disaggregation and aggregation procedures for characterizing fluvial features at the network-scale: Application to the Rhône basin (France). Geomorphology 125, 343–360. doi:10.1016/j.geomorph.2010.09.009.

Alber, A., Piégay, H., 2017. Characterizing and modelling river channel migration rates at a regional scale: Case study of south-east france. Journal of Environmental Management 202, 479 – 493. doi:10.1016/j.jenvman.2016.10.055.

Allen, C., Holling, C., 2010. Novelty, adaptive capacity, and resilience. Ecology and society 15, 24–38.

Allen, C.R., Angeler, D.G., Garmestani, A.S., Gunderson, L.H., Holling, C.S., 2014. Panarchy: Theory and application. Ecosystems 17, 578–589. doi:10.1007/s10021-013-9744-2.

Amoros, C., Bornette, G., 2002. Connectivity and biocomplexity in waterbodies of riverine floodplains. Freshwater Biology 47, 761–776. doi:10.1046/j.1365-2427.2002.00905.x.

Anderson, J., 1999. Kyrgyzstan. Central Asia's island of democracy? Harwood Academic Publishers, Amsterdam.

Antipova, E., Zyryanov, A., McKinney, D., Savitsky, A., 2002. Optimization of syr darya water and energy uses. Water International 27, 504–516. doi:10.1080/02508060208687038.

Arthington, A.H., Bunn, S.E., Poff, N.L., Naiman, R.J., 2006. The challenge of providing environmental flow rules to sustain river ecosystems. Ecological Applications 16, 1311–1318. doi:10.1890/1051-0761(2006)016[1311:TCOPEF]2.0.CO;2.

Avouac, J.P., Tapponnier, P., Bai, M., You, H., Wang, G., 1993. Active thrusting and folding along the northern Tien Shan and Late Cenozoic rotation of the Tarim relative to Dzungaria and Kazakhstan. Journal of Geophysical Research: Solid Earth 98, 6755–6804. doi:10.1029/92JB01963.

Baig, M.H.A., Zhang, L., Shuai, T., Tong, Q., 2014. Derivation of a tasseled cap transformation based on Landsat 8 at-satellite reflectance. Remote Sensing Letters 5, 423–431. doi:10.1080/2150704X.2014.915434.

Bailly, J.S., Kinzel, P., Allouis, T., Feurer, D., Le Coarer, Y., 2012. Airborne lidar methods applied to riverine environments, in: Carbonneau, P., Piégay, H. (Eds.), Fluvial Remote Sensing for Science and Management. Wiley-Blackwell. chapter 7, pp. 141–161. doi:10.1002/9781119940791.ch7.

Bakker, M., Lane, S., 2017. Archival photogrammetric analysis of river–floodplain systems using structure from motion (sfm) methods. Earth Surface Processes and Landforms 42, 1274–1286. doi:10.1002/esp.4085.

Balke, T., Herman, P.M.J., Bouma, T.J., 2014. Critical transitions in disturbance-driven ecosystems: identifying windows of opportunity for recovery. Journal of Ecology 102, 700–708. doi:10.1111/1365-2745.12241.

Barker, D.M., Lawler, D.M., Knight, D.W., Morris, D.G., Davies, H.N., Stewart, E.J., 2009. Longitudinal distribution of river flood power: the combined automated flood, elevation and stream power (CAFES) methodology. Earth Surface Processes and Landforms 34, 280–290. doi:10.1002/esp.

Benda, L., Poff, N.L., Miller, D., Dunne, T., Reeves, G., Pess, G., Pollock, M., 2004. The network dynamics hypothesis: How channel networks structure riverine habitats. BioScience 54, 413–427. doi:10.1641/0006-3568(2004)054[0413:TNDHHC]2.0.CO;2.

Bendix, J., Hupp, C.R., 2000. Hydrological and geomorphological impacts on riparian plant communities. Hydrological Processes 14, 2977–2990.

Bernauer, T., Siegfried, T., 2012. Climate change and international water conflict in Central Asia. Journal of Peace Research 49, 227–239. doi:10.1177/0022343311425843.

Bertoldi, W., Drake, N.A., Gurnell, A.M., 2011. Interactions between river flows and colonizing vegetation on a braided river: Exploring spatial and temporal dynamics in riparian vegetation cover using satellite data. Earth Surface Processes and Landforms 36, 1474–1486. doi:10.1002/esp.2166.

Bertrand, M., Piégay, H., Pont, D., Liébault, F., Sauquet, E., 2013. Sensitivity analysis of environmental changes associated with riverscape evolutions following sediment reintroduction: geomatic approach on the drôme river network, france. International Journal of River Basin Management 11, 19–32. doi:10.1080/15715124.2012.754444.

Betz, F., Halik, Ü., Cyffka, B., Kurban, A., Chymyrov, A., Baibagyshov, E., Ding, J., 2015a. Using GIS for environmental management along the Central Asian rivers Tarim and Naryn, in: Proceedings of the GIS in Central Asia Conference – GISCA 2015, pp. 13–18.

Betz, F., Keyimu, M., Halik, U., Cyffka, B., 2015b. Ökosystemdienstleistungen von Flussauen in Zentralasien: Der Tarim und der Naryn als Fallbeispiele, in: U. Feit, H. (Ed.), Treffpunkt Biologische Vielfalt XIV. BfN, pp. 59–63. URL: https://www.bfn.de/fileadmin/BfN/service/Dokumente/skripten/skript397.pdf. In German.

Betz, F., Lauermann, M., Cyffka, B., 2018. Delineation of the riparian zone in data-scarce regions using fuzzy membership functions: An evaluation based on the case of the Naryn River in Kyrgyzstan. Geomorphology 306, 170–181. doi:10.1016/j.geomorph.2018.01.024.

Betz, F., Lauermann, M., Cyffka, B., 2020. Open source riverscapes: analyzing the corridor of the Naryn River in Kyrgyzstan based on open access data. Remote Sensing 12, 2533. doi:10.3390/rs12162533.

Betz, F., Rauschenberger, J., Lauermann, M., Cyffka, B., 2016. Using GIS and Remote Sensing for Assessing Raparian Ecosystems along the Naryn River, Kyrgyzstan. International Journal of Geoinformatics 12, 25–30.

Bishop, M.P., Shroder, J.F., Bonk, R., Olsenholler, J., 2002. Geomorphic change in high mountains: a western himalayan perspective. Global and Planetary Change 32, 311 – 329. doi:10.1016/S0921-8181(02)00073-5.

Bizzi, S., Demarchi, L., Grabowski, R.C., Weissteiner, C.J., Van de Bund, W., 2016. The use of remote sensing to characterise hydromorphological properties of European rivers. Aquatic Sciences 78, 57–70. doi:10.1007/s00027-015-0430-7.

Bizzi, S., Lerner, D.N., 2012. Characterizing physical habitats in rivers using map-derived drivers of fluvial geomorphic processes. Geomorphology 169-170, 64–73. doi:10.1016/j.geomorph.2012.04.009.

Bizzi, S., Lerner, D.N., 2015. The use of stream power as an indicator of channel sensitivity to erosion and deposition processes. River research and applications 31, 16–27. doi:10.1002/rra.2717.

Bizzi, S., Piégay, H., Demarchi, L., Van de Bund, W., Weissteiner, C., Gob, F., 2019. LiDAR-based fluvial remote sensing to assess 50–100-year human-driven channel changes at a regional level: The case of the Piedmont Region, Italy. Earth Surface Processes and Landforms 44, 471–489. doi:10.1002/esp.4509.

Black, M., Carbonneau, P., Church, M., Warburton, J., 2014. Mapping sub-pixel fluvial grain sizes with hyperspatial imagery. Sedimentology 61, 691–711. doi:10.1111/sed.12072.

Bornette, G., Tabacchi, E., Hupp, C., Puijalon, S., Rostan, J.C., 2008. A model of plant strategies in fluvial hydrosystems. Freshwater Biology 53, 1692–1705. doi:10.1111/j.1365-2427.2008.01994.x.

Boschetti, L., Flasse, S.P., Brivio, P.A., 2004. Analysis of the conflict between omission and commission in low spatial resolution dichotomic thematic products: The pareto boundary. Remote Sensing of Environment 91, 280 – 292. doi:10.1016/j.rse.2004.02.015.

Boschetti, M., Nutini, F., Manfron, G., Brivio, P.A., Nelson, A., 2014. Comparative analysis of normalised difference spectral indices derived from MODIS for detecting surface water in flooded rice cropping systems. PLOS ONE 9, e88741. doi:10.1371/journal.pone.0088741.

Braat, L.C., de Groot, R., 2012. The ecosystem services agenda: bridging the worlds of natural science and economics, conservation and development, and public and private policy. Ecosystem Services 1, 4–15. doi:10.1016/j.ecoser.2012.07.011.

Brenden, T., Wang, L., Seelbach, P., Clark, R., Wiley, M., Sparks-Jackson, B., 2008. A spatially constrained clustering program for river valley segment delineation from gis digital river networks. Environmental Modelling & Software 23, 638 – 649. doi:10.1016/j.envsoft.2007.09.004.

Brierley, G.J., 2015. Linking science to practice: tools to assess river status and guide rehabilitation to optimize river basin management, in: Angelous, N., Buijse, A.D., et al. (Eds.), Proceedings of the International Conference on River and Stream Restoration "Novel Approaches to Assess and Rehabilitate Modified Rivers". FP7 REFORM deliverable 7.5., pp. 20–26.

Brierley, G.J., Fryirs, K.A., 2005. Geomorphology and River Management. Applications of the River Styles Framework. Blackwell, Oxford.

Burgette, R.J., Weldon, R.J., Abdrakhmatov, K.Y., Ormukov, C., Owen, L.A., Thompson, S.C., 2017. Timing and process of river and lake terrace formation in the Kyrgyz Tien Shan. Quaternary Science Reviews 159, 15–34. doi:10.1016/j.quascirev.2017.01.003.

Burtman, V.S., 2012. Geodymanics of Tibet, Tarim, and the Tien Shan in the Late Cenozoic. Geotectonics 46, 185–211. doi:10.1134/S0016852112030028.

Cai, Z., Jönsson, P., Jin, H., Eklundh, L., 2017. Performance of smoothing methods for reconstructing ndvi time-series and estimating vegetation phenology from modis data. Remote Sensing 9, 1271. doi:10.3390/rs9121271.

Carbonneau, P., Fonstad, M.A., Marcus, W.A., Dugdale, S.J., 2012. Making riverscapes real. Geomorphology 137, 74–86. doi:10.1016/j.geomorph.2010.09.030.

Carbonneau, P., Piégay, H., 2012. Fluvial Remote Sensing for Science and Management. Wiley-Blackwell, Oxford.

Carbonneau, P.E., Lane, S.N., Bergeron, N.E., 2004. Catchment-scale mapping of surface grain size in gravel bed rivers using airborne digital imagery. Water Resources Research 40, W07202. doi:10.1029/2003WR002759.

Cheterian, V., 2010. Dritter Versuch in Kirgistan. Le Monde Diplomatique 05/2010.

Church, M., 2002. Geomorphic thresholds in riverine landscapes. Freshwater Biology 47, 541–557. doi:10.1046/j.1365-2427.2002.00919.x.

Chymyrov, A., Betz, F., Baibagyshov, E., Kurban, A., Cyffka, B., Halik, U., 2019. Floodplain forest mapping with Sentinel-2 imagery: Case study of Naryn River, Kyrgyzstan, in: Egamberdieva, D., Ozturk, M. (Eds.), Vegetation of Central Asia and Environs. Springer, Cham, pp. 335–347. doi:10.1007/978-3-319-99728-5_14.

CIESIN, 2005. Gridded Population of the World, Version 3 (GPWv3). Technical Report. Columbia University. Palisades, NY.

Clerici, N., Weissteiner, C., Paracchini, M.L., Strobl, P., 2011. Riparian zones: where green and blue networks meet. Pan-European zonation modelling based on remote sensing and GIS.and GIS. JRC63959. JRC Scientific Reports. Publications Office of the European Union. doi:10.2788/80271.

Clerici, N., Weissteiner, C.J., Paracchini, M.L., Boschetti, L., Baraldi, A., Strobl, P., 2013. Pan-European distribution modelling of stream riparian zones based on multi-source Earth Observation data. Ecological Indicators 24, 211–223. doi:10.1016/j.ecolind.2012.06.002.

Cohen, S., Willgoose, G., Hancock, G., 2008. A methodology for calculating the spatial distribution of the area-slope equation and the hypsometric integral within a catchment. Journal of Geophysical Research: Earth Surface 113, n/a–n/a. doi:10.1029/2007JF000820. f03027.

Coles, S., 2001. An introduction to statistical modeling of extreme values. Springer, London.

Collins, B.D., Montgomery, D.R., Fetherston, K.L., Abbe, T.B., 2012. The floodplain large-wood cycle hypothesis: A mechanism for the physical and biotic structuring of temperate forested alluvial valleys in the North Pacific coastal ecoregion. Geomorphology 139-140, 460–470. doi:10.1016/j.geomorph.2011.11.011.

Comber, A., Wulder, M., 2019. Considering spatiotemporal processes in big data analysis: Insights from remote sensing of land cover and land use. Transactions in GIS 23, 879–891. doi:10.1111/tgis.12559.

Conrad, O., Bechtel, B., Bock, M., Dietrich, H., Fischer, E., Gerlitz, L., Wehberg, J., Wichmann, V., Boehner, J., 2015. System for Automated Geoscientific Analyses (SAGA) v. 2.1.4. Geoscientific Model Development 8, 1991–2007. doi:10.5194/gmd-8-1991-2015.

Corenblit, D., Baas, A., Balke, T., Bouma, T., Fromard, F., Garafano-Gomez, V., Gonzalez, E., Gurnell, A.M., Hortobagyi, B., Julien, F., Kim, D., Lambs, L., Stallins, J.A., Steiger, J., Tabacchi, E., Walcker, R., 2015a. Engineer pioneer plants respond to and affect geomorphic constraints similarly along water-terrestrial interfaces world-wide. Global Ecology and Biogeography 24, 1363–1376. doi:10.1111/geb.12373.

Corenblit, D., Davies, N.S., Steiger, J., Gibling, M.R., Bornette, G., 2015b. Considering river structure and stability in the light of evolution: Feedbacks between riparian vegetation and hydrogeomorphology. Earth Surface Processes and Landforms 40, 189–207. doi:10.1002/esp.3643.

Corenblit, D., Steiger, J., Gurnell, A.M., Naiman, R.J., 2009a. Plants intertwine fluvial landform dynamics with ecological succession and natural selection: A niche construction perspective for riparian systems. Global Ecology and Biogeography 18, 507–520. doi:10.1111/j.1466-8238.2009.00461.x.

Corenblit, D., Steiger, J., Gurnell, A.M., Tabacchi, E., Roques, L., 2009b. Control of sediment dynamics by vegetation as a key function driving biogeomorphic succession within fluvial corridors. Earth Surface Processes and Landforms 34, 1790–1810. doi:10.1002/esp.1876.

Corenblit, D., Tabacchi, E., Steiger, J., Gurnell, A.M., 2007. Reciprocal interactions and adjustments between fluvial landforms and vegetation dynamics in river corridors: A review of complementary approaches. Earth-Science Reviews 84, 56–86. doi:10.1016/j.earscirev.2007.05.004.

Costanza, R., de Groot, R., Braat, L., Kubiszewski, I., Fioramonti, L., Sutton, P., Farber, S., Grasso, M., 2017. Twenty years of ecosystem services: How far have we come and how far do we still need to go? Ecosystem Services 28, 1 – 16. doi:10.1016/j.ecoser.2017.09.008.

Cote, D., Kehler, D., Bourne, C., Wiersma, Y., 2009. A new measure of longitudinal connectivity for stream networks. Landscape Ecology 24, 101–113. doi:10.1007/s10980-008-9283-y.

Crist, E.P., Cicone, R.C., 1984. A physically-based transformation of Thematic Mapper data—The TM Tasseled Cap. IEEE Transactions on Geoscience and Remote sensing , 256–263.

Crutzen, P.J., 2002. Geology of mankind. Nature 415, 23. doi:10.1038/415023a.

Cyffka, B., 2001. Möglichkeiten der dauerhaft-umweltgerechten Entwicklung einer stark belasteten Landschaft in Russisch-Lappland durch gezielten strukturellen Landnutzungswandel, in: Pörtge, Karl-Heinz (Ed.), Göttinger Geographische Abhandlungen 108. In German.

Davies, W., 1899. The geographical cycle. The Geographical Journal 14, 481–504.

De Grave, J., Glorie, S., Buslov, M.M., Izmer, A., Fournier-Carrie, A., Batalev, V.Y., Vanhaecke, F., Elburg, M., Van den haute, P., 2011. The thermo-tectonic history of the Song-Kul plateau, Kyrgyz Tien Shan: Constraints by apatite and titanite thermochronometry and zircon U/Pb dating. Gondwana Research 20, 745–763. doi:10.1016/j.gr.2011.03.011.

Demarchi, L., Bizzi, S., Piégay, H., 2016. Hierarchical object-based mapping of riverscape units and in-stream mesohabitats using lidar and vhr imagery. Remote Sensing 8, 97. doi:10.3390/rs8020097.

Deng, H., Chen, Y., Li, Q., Lin, G., 2019. Loss of terrestrial water storage in the Tian Shan mountains from 2003 to 2015. International Journal of Remote Sensing 40, 8342–8358. doi:10.1080/01431161.2019.1608392.

Deutsches Auswaertiges Amt, 2016. Länderinformationen Kirgisistan. URL: https://www.auswaertiges-amt.de/de/aussenpolitik/laender/kirgisistan-node.

DeVries, B., Verbesselt, J., Kooistra, L., Herold, M., 2015. Robust monitoring of small-scale forest disturbances in a tropical montane forest using Landsat time series. Remote Sensing of Environment 161, 107 – 121. doi:10.1016/j.rse.2015.02.012.

Dierschke, H., 1994. Pflanzensoziologie. Ulmer, Stuttgart. In German.

Döll, P., Zhang, J., 2010. Impact of climate change on freshwater ecosystems: a global-scale analysis of ecologically relevant river flow alterations. Hydrology and Earth System Sciences 14, 783–799. doi:10.5194/hess-14-783-2010.

Dollar, E., James, C., Rogers, K., Thoms, M., 2007. A framework for interdisciplinary understanding of rivers as ecosystems. Geomorphology 89, 147 – 162. doi:10.1016/j.geomorph.2006.07.022.

Drusch, M., Bello, U.D., Carlier, S., Colin, O., Fernandez, V., Gascon, F., Hoersch, B., Isola, C., Laberinti, P., Martimort, P., Meygret, A., Spoto, F., Sy, O., Marchese, F., Bargellini, P., 2012. Sentinel-2: ESA's Optical High-Resolution Mission for GMES Operational Services. Remote Sensing of Environment 120, 25 – 36. doi:10.1016/j.rse.2011.11.026.

Dubashov, B., Kruse, A., Ismailakhunova, S., 2017. Kyrgyz Republic: A robust recovery with underlying weaknesses: Economic update with a special focus on labor migration. Technical Report. World Bank. Washington. URL: http://documents.worldbank.org/curated/en/727401517229479407/pdf/122978-NWP-PUBLIC-Kyrgz-no-6-add-series.pdf.

Easmus, D., Huete, A., Yu, Q., 2016. Vegetation Dynamics. A Synthesis of Plant Ecophyisiology, Remote Sensing and Modelling. Cambridge University Press, New York.

Edwards, P., Kollmann, J., Gurnell, A., Petts, G., Tockner, K., Ward, J., 1999. A conceptual model of vegetation dynamics on gravel bars of a large alpine river. Wetlands Ecology and Management 7, 141–153. doi:10.1023/A:1008411311774.

Egger, G., Politti, E., Garófano-Gómez, V., Blamauer, B., Ferreira, T., Rivaes, R., Benjankar, R., Habersack, H., 2013. Embodying Interactions Between Riparian Vegetation and Fluvial Hydraulic Processes Within a Dynamic Floodplain Model: Concepts and Applications. John Wiley & Sons, Ltd. chapter 24. pp. 407–427. doi:10.1002/9781118526576.ch24.

Egozi, R., Ashmore, P., 2008. Defining and measuring braiding intensity. Earth Surface Processes and Landforms 33, 2121–2138. doi:10.1002/esp.1658.

Eichel, J., Corenblit, D., Dikau, R., 2016. Conditions for feedbacks between geomorphic and vegetation dynamics on lateral moraine slopes: a biogeomorphic feedback window. Earth Surface Processes and Landforms 41, 406–419. doi:10.1002/esp.3859.

Farr, T.G., Rosen, P.A., Caro, E., Crippen, R., Duren, R., Hensley, S., Kobrick, M., Paller, M., Rodriguez, E., Roth, L., Seal, D., Shaffer, S., Shimada, J., Umland, J., Werner, M., Oskin, M., Burbank, D., Alsdorf, D., 2007. The shuttle radar topography mission. Reviews of Geophysics 45, RG2004. doi:10.1029/2005RG000183.

Farrington, J.D., 2005. De-development in eastern Kyrgyzstan and persistence of semi-nomadic livestock herding. Nomadic Peoples 9, 171–197. doi:10.3167/082279405781826191.

Fausch, K.D., Torgersen, C.E., Baxter, C.V., Ll, H.W., 2002. Landscapes to Riverscapes: Bridging the Gap between Research and Conservation of Stream Fishes. BioScience 52, 483–498. doi:10.1641/0006-3568(2002)052[0483:LTRBTG]2.0.CO;2.

Ferguson, R., 1986. Hydraulics and hydraulic geometry. Progress in Physical Geography 10, 1–31. doi:10.1177/030913338601000101.

Ferguson, R., 2005. Estimating critical stream power for bedload transport calculations in gravel-bed rivers. Geomorphology 70, 33 – 41. doi:10.1016/j.geomorph.2005.03.009.

Fisher, R., Schmidt, K., Steenhof, B., Akenshaev, N., 2004. Poverty and forestry. A case study of Kyrgyzstan with reference to other countries in West and Central Asia. LSP Working Paper 13. URL: http://www.fao.org/docrep/007/j2603e/j2603e00.htm#Contents.

Fonstad, M.A., Andrew Marcus, W., 2010. High resolution, basin extent observations and implications for understanding river form and process. Earth Surface Processes and Landforms 35, 680–698. doi:10.1002/esp.1969.

Forkel, M., Carvalhais, N., Verbesselt, J., Mahecha, M.D., Neigh, C.S., Reichstein, M., 2013. Trend change detection in ndvi time series: Effects of inter-annual variability and methodology. Remote Sensing 5, 2113–2144. doi:10.3390/rs5052113.

Forkel, M., Migliavacca, M., Thonicke, K., Reichstein, M., Schaphoff, S., Weber, U., Carvalhais, N., 2015. Codominant water control on global interannual variability and trends in land surface phenology and greenness. Global Change Biology 21, 3414–3435. doi:10.1111/gcb.12950.

Francis, R.A., Corenblit, D., Edwards, P.J., 2009. Perspectives on biogeomorphology, ecosystem engineering and self-organisation in island-braided fluvial ecosystems. Aquatic Sciences 71, 290. doi:10.1007/s00027-009-9182-6.

Frissell, C.A., Liss, W.J., Warren, C.E., Hurley, M.D., 1986. A hierarchical framework for stream habitat classification: Viewing streams in a watershed context. Environmental Management 10, 199–214. doi:10.1007/BF01867358.

Fryirs, K.A., 2017. River sensitivity: a lost foundation concept in fluvial geomorphology. Earth Surface Processes and Landforms 42, 55–70. doi:10.1002/esp.3940.

Fryirs, K.A., Brierley, G.J., 2013. Geomorphic analysis of river systems: an approach to reading the landscape. Wiley-Blackwell, Oxford.

Fryirs, K.A., Wheaton, J.M., Bizzi, S., Williams, R., Brierley, G.J., 2019. To plug–in or not to plug–in? Geomorphic analysis of rivers using the River Styles Framework in an era of big data acquisition and automation. Wiley Interdisciplinary Reviews: Water 321, 146. doi:10.1002/wat2.1372.

Fryirs, K.A., Wheaton, J.M., Brierley, G.J., 2016. An approach for measuring confinement and assessing the influence of valley setting on river forms and processes. Earth Surface Processes and Landforms 41, 701–710. doi:10.1002/esp.3893.

Gallant, J.C., Dowling, T.I., 2003. A multiresolution index of valley bottom flatness for mapping depositional areas. Water Resources Research 39. doi:10.1029/2002WR001426.

Gan, R., Luo, Y., Zuo, Q., Sun, L., 2015. Effects of projected climate change on the glacier and runoff generation in the Naryn River Basin, Central Asia. Journal of Hydrology 523, 240–251. doi:10.1016/j.jhydrol.2015.01.057.

Ghose, S., Hamburger, M.W., Ammon, C.J., 1998. Source parameters of moderate-sized earthquakes in the Tien Shan, central Asia from regional moment tensor inversion. Geophysical Research Letters 25, 3181–3184. doi:10.1029/98GL02362.

Giese, E., Bahro, G., Betke, D., 1998. Umweltzerstörungen in Trockengebieten Zentralasiens (West- und Ost-Turkestan): Ursachen, Auswirkungen, Maßnahmen. Steiner, Stuttgart. In German.

Giese, E., Mossig, I., Rybski, D., Bunde, A., 2007. Long-Term Analysis of Air Temperature Trends in Central Asia. Erdkunde 61, 186–202.

Gilbert, G., 1914. The tranportation of debris by running water. Technical Report. Washington.

Gilvear, D.J., Bryant, R.G., 2016. Analysis of remotely sensed data for fluvial geomorphology and river science, in: Kondolf, M., Piégay, H. (Eds.), Tools in Fluvial Geomorphology. Wiley, Chichester, pp. 103–132.

Gilvear, D.J., Greenwood, M.D., Thoms, M.C., Wood, P.J., 2016a. River Science: Research and Management for the 21st Century. Wiley-Blackwell, Chichester.

Gilvear, D.J., Hunter, P., Stewardson, M., 2016b. Remote sensing: Mapping natural and managed river corridors from the micro to the network scale, in: Gilvear, D.J., Greenwood, M.D., Thoms, M.C., Wood, P.J. (Eds.), River science. Research and management for the 21st century. Wiley-Blackwell, Chichester, p. 171.196.

Gleason, C.J., 2015. Hydraulic geometry of natural rivers: A review and future directions. Progress in Physical Geography: Earth and Environment 39, 337–360. doi:10.1177/0309133314567584.

Gómez, C., White, J.C., Wulder, M.A., 2016. Optical remotely sensed time series data for land cover classification: A review. ISPRS Journal of Photogrammetry and Remote Sensing 116, 55 – 72. doi:10.1016/j.isprsjprs.2016.03.008.

Grill, G., Lehner, B., Lumsdon, A.E., MacDonald, G.K., Zarfl, C., Liermann, C.R., 2015. An index-based framework for assessing patterns and trends in river fragmentation and flow regulation by global dams at multiple scales. Environmental Research Letters 10, 015001. doi:10.1088/1748-9326/10/1/015001.

Grill, G., Lehner, B., Thieme, M., Geenen, B., Tickner, D., Antonelli, F., Babu, S., Borrelli, P., Cheng, L., Crochetiere, H., Macedo, H.E., Filgueiras, R., Goichot, M., Higgins, J., Hogan, Z., Lip, B., McClain, M.E., Meng, J., Mulligan, M., Nilsson, C., Olden, J.D., Opperman, J.J., Petry, P., Liermann, C.R., Sáenz, L., Salinas-Rodríguez, S., Schelle, P., Schmitt, R.J.P., Snider, J., Tan, F., Tockner, K., Valdujo, P.H., van Soesbergen, A., Zarfl, C., 2019. Mapping the world's free-flowing rivers. Nature 569, 215–221. doi:10.1038/s41586-019-1111-9.

Groisman, P.Y., Bartalev, S.A., 2007. Northern Eurasia earth science partnership initiative (NEESPI), science plan overview. Global and Planetary Change 56, 215–234. doi:10.1016/j.gloplacha.2006.07.027.

Grömping, U., 2015. Variable importance in regression models. Wiley Interdisciplinary Reviews: Computational Statistics 7, 137–152. doi:10.1002/wics.1346.

Grubov, V.I., 2010. Schlussbetrachtung zum Florenwerk Rastenija Centralnoj Azii [Die Pflanzen Zentralasiens] und die Begründung der Eigenständigkeit der mongolischen Flora. Feddes Repertorium 121, 7–13. doi:10.1002/fedr.201011123. In German.

Gunderson, L., Holling, C., 2002. Panarchy: Understanding transformations in human and natural systems. Island Press, Washington.

Gunderson, L.H., Allen, C.R., Holling, C.S., 2012. Foundations of ecological resilience. Island Press.

Gurnell, A., 2014. Plants as river system engineers. Earth Surface Processes and Landforms 39, 4–25. doi:10.1002/esp.3671.

Gurnell, A., Petts, G., 2006. Trees as riparian engineers: the Tagliamento river, Italy. Earth Surface Processes and Landforms 31, 1558–1574. doi:10.1002/esp.1342.

Gurnell, A., Tockner, K., Edwards, P., Petts, G., 2005. Effects of deposited wood on biocomplexity of river corridors. Frontiers in Ecology and the Environment 3, 377–382. doi:10.1890/1540-9295(2005)003[0377:EODWOB]2.0.CO;2.

Gurnell, A.M., Corenblit, D., Garcia de Jalon, D., Gonzalez del Tanago, M., Grabowski, R.C., O'Hare, M.T., Szewczyk, M., 2016a. A conceptual model of vegetation-hydrogeomrophology interactions within river corridors. River research and applications 32, 142–163. doi:10.1002/rra.2928.

Gurnell, A.M., Petts, G.E., Hannah, D.M., Smith, B.P.G., Edwards, P.J., Kollmann, J., Ward, J.V., Tockner, K., 2001. Riparian vegetation and island formation along the gravel-bed Fiume Tagliamento, Italy. Earth Surface Processes and Landforms 26, 31–62.

Gurnell, A.M., Rinaldi, M., Belletti, B., Bizzi, S., Blamauer, B., Braca, G., Buijse, A.D., Bussettini, M., Camenen, B., Comiti, F., Demarchi, L., García de Jalón, D., González del Tánago, M., Grabowski, R.C., Gunn, I.D.M., Habersack, H., Hendriks, D., Henshaw, A.J., Klösch, M., Lastoria, B., Latapie, A., Marcinkowski, P., Martínez-Fernández, V., Mosselman, E., Mountford, J.O., Nardi, L., Okruszko, T., O'Hare, M.T., Palma, M., Percopo, C., Surian, N., van de Bund, W., Weissteiner, C., Ziliani, L., 2016b. A multi-scale hierarchical framework for developing understanding of river behaviour to support river management. Aquatic Sciences 78, 1–16. doi:10.1007/s00027-015-0424-5.

Gurnell, A.M., Scott, S.J., England, J., Gurnell, D., Jeffries, R., Shuker, L., Wharton, G., 2020. Assessing river condition: A multiscale approach designed for operational application in the context of biodiversity net gain. River Research and Applications doi:10.1002/rra.3673.

Habersack, H.M., 2000. The river-scaling concept (rsc): a basis for ecological assessments, in: Jungwirth, M., Muhar, S., Schmutz, S. (Eds.), Assessing the Ecological Integrity of Running Waters. Springer Netherlands, Dordrecht, pp. 49–60.

Hack, J., 1960. Interpretation of erosional topography in humid temperate regions. Amer. Jour. Sci. 258, 80–97.

Hagg, W., Braun, L., Kuhn, M., Nesgaard, T., 2007. Modelling of hydrological response to climate change in glacierized Central Asian catchments. Journal of Hydrology 332, 40 – 53. doi:10.1016/j.jhydrol.2006.06.021.

Hagg, W., Mayer, C., Lambrecht, A., Kriegel, D., Azizov, E., 2013. Glacier changes in the Big Naryn basin, Central Tian Shan. Global and Planetary Change 110, 40–50. doi:10.1016/j.gloplacha.2012.07.010.

Hayakawa, Y.S., Oguchi, T., 2006. Dem-based identification of fluvial knickzones and its application to japanese mountain rivers. Geomorphology 78, 90 – 106. doi:10.1016/j.geomorph.2006.01.018.

Hayes, D.S., Brändle, J.M., Seliger, C., Zeiringer, B., Ferreira, T., Schmutz, S., 2018. Advancing towards functional environmental flows for temperate floodplain rivers. Science of the Total Environment 633, 1089–1104. doi:10.1016/j.scitotenv.2018.03.221.

Heckmann, T., McColl, S., Morche, D., 2015. Retreating ice: research in pro-glacial areas matters. Earth Surface Processes and Landforms 41, 271–276. doi:10.1002/esp.3858.

Heckmann, T., Morche, D. (Eds.), 2019. Geomorphology of proglacial systems: Landform and sediment dynamics in recently deglaciated alpine landscapes. Geography of the Physical Environment, Springer International Publishing, Cham. doi:10.1007/978-3-319-94184-4.

Hengl, T., Grohmann, C., Bivand, R., Conrad, O., Lobo, A., 2009. SAGA vs GRASS: A Comparative Analysis of the Two Open Source Desktop GIS for the Automated Analysis of Elevation Data. Proceedings of Geomorphometry 2009 , 22–27.

Henshaw, A.J., Gurnell, A.M., Bertoldi, W., Drake, N.A., 2013. An assessment of the degree to which Landsat TM data can support the assessment of fluvial dynamics, as revealed by changes in vegetation extent and channel position, along a large river. Geomorphology 202, 74–85. doi:10.1016/j.geomorph.2013.01.011.

Hilbig, W., Jäger, E., 2010. Valerij Ivanovic Grubov (1917–2009) und die pflanzengeographische Gliederung Zentralasiens. Feddes Repertorium 121, 1–6. doi:110.1002/fedr.201011122. In German.

Hoppe, F., Zhusui Kyzy, T., Usupbaev, A., Schickhoff, U., 2016. Rangeland degradation assessment in Kyrgyzstan: vegetation and soils as indicators of grazing pressure in Naryn Oblast. Journal of Mountain Science 13, 1567–1583. doi:10.1007/s11629-016-3915-5.

Hortobagyi, B., Corenblit, D., Vautier, F., Steiger, J., Roussel, E., Burkart, A., Peiry, J.L., 2016. A multi-scale approach of fluvial biogeomorphic dynamics using photogrammetry. Journal of Environmental Management , 1–15doi:10.1016/j.jenvman.2016.08.069.

Hortobágyi, B., Corenblit, D., Steiger, J., Peiry, J.L., 2017. Niche construction within riparian corridors. Part I: Exploring biogeomorphic feedback windows of three pioneer riparian species (Allier River, France). Geomorphology doi:10.1016/j.geomorph.2017.08.048.

Hugue, F., Lapointe, M., Eaton, B., Lepoutre, A., 2016. Satellite-based remote sensing of running water habitats at large riverscape scales: Tools to analyze habitat heterogeneity for river ecosystem management. Geomorphology 253, 353 – 369. doi:10.1016/j.geomorph.2015.10.025.

Hupp, C.R., Osterkamp, W.R., 1996. Riparian vegetation and fluvial geomorphic processes. Geomorphology 14, 277–295. doi:10.1016/0169-555X(95)00042-4.

Hupp, C.R., Osterkamp, W.R., 2013. Vegetation Ecogeomorphology, Dynamic Equilibrium, and Disturbance. volume 12. Elsevier Ltd. doi:10.1016/B978-0-12-374739-6.00324-9.

Imanberdieva, N., 2015. Flora and Plant Formations Distributed in At-Bashy Valleys–Internal Tien Shan in Kyrgyzstan and Interactions with Climate, in: Öztürk, M., Hakeem, K.R., Faridah-Hanum, I., Efe, R. (Eds.), Climate Change Impacts on High-Altitude Ecosystems. Springer International Publishing, Cham, pp. 569–590. doi:10.1007/978-3-319-12859-7_22.

Immerzeel, W.W., van Beek, L.P.H., Bierkens, M.F.P., 2010. Climate change will affect the Asian water towers. Science (New York, N.Y.) 328, 1382–5. doi:10.1126/science.1183188.

Irons, J.R., Dwyer, J.L., Barsi, J.A., 2012. The next landsat satellite: The landsat data continuity mission. Remote Sensing of Environment 122, 11 – 21. doi:10.1016/j.rse.2011.08.026.

Ivits, E., Cherlet, M., Mehl, W., Sommer, S., 2009. Estimating the ecological status and change of riparian zones in Andalusia assessed by multi-temporal AVHHR datasets. Ecological Indicators 9, 422–431. doi:10.1016/j.ecolind.2008.05.013.

Jain, V., Preston, N., Fryirs, K., Brierley, G., 2006. Comparative assessment of three approaches for deriving stream power plots along long profiles in the upper hunter river catchment, new south wales, australia. Geomorphology 74, 297 – 317. doi:10.1016/j.geomorph.2005.08.012.

Jasiewicz, J., Metz, M., 2011. A new GRASS GIS toolkit for Hortonian analysis of drainage networks. Computers and Geosciences 37, 1162–1173. doi:10.1016/j.cageo.2011.03.003.

Jiang, L., Guli·Jiapaer, Bao, A., Guo, H., Ndayisaba, F., 2017. Vegetation dynamics and responses to climate change and human activities in Central Asia. Science of the Total Environment 599-600, 967 – 980. doi:10.1016/j.scitotenv.2017.05.012.

Jones, C.G., Lawton, J.H., Shachak, M., 1994. Organisms as ecosystem engineers. Oikos 69, 373–386. doi:10.2307/3545850.

Junk, W.J., Baylay, P., Sparks, R.E., 1989. The flood-pulse concept in river-floodplain systems. Canadian Special Publication of Fisheries and Aquatic Sciences 106, 110–127.

Karrenberg, S., Blaser, S., Kollmann, J., Speck, T., Edwards, P.J., 2003. Root anchorage of saplings and cuttings of woody pioneer species in a riparian environment. Functional Ecology 17, 170–177. doi:10.1046/j.1365-2435.2003.00709.x.

Karrenberg, S., Edwards, P.J., Kollmann, J., 2002. The life history of salicaceae living in the active zone of floodplains. Freshwater Biology 47, 733–748. doi:10.1046/j.1365-2427.2002.00894.x.

Karthe, D., Chalov, S., Borchardt, D., 2015. Water resources and their management in central Asia in the early twenty first century: status, challenges and future prospects. Environmental Earth Sciences 73, 487–499. doi:10.1007/s12665-014-3789-1.

Kauth, R., Thomas, G., 1976. The Tasseled Cap—A Graphic Description of the Spectral-temporal Development of Agricultural Crops as Seen by Landsat. LARS Symp .

Kennedy, R.E., Yang, Z., Cohen, W.B., 2010. Detecting trends in forest disturbance and recovery using yearly Landsat time series: 1. LandTrendr — Temporal segmentation algorithms. Remote Sensing of Environment 114, 2897–2910. doi:10.1016/j.rse.2010.07.008.

King, C., 1966. Techniques in Geomorphology. Arnold, London.

Knighton, A., 1999. Downstream variation in stream power. Geomorphology 29, 293 – 306. doi:10.1016/S0169-555X(99)00015-X.

Kollmann, J., Vieli, M., Edwards, P., Tockner, K., Ward, J., 1999. Interactions between vegetation development and island formation in the Alpine river Tagliamento. Applied Vegetation Science 2, 25–36. doi:10.2307/1478878.

Kondolf, M., Piégay, H., Schmitt, L., Montgomery, D.R., 2016. Geomorphic classification of rivers and streams, in: Kondolf, M., Piégay, H. (Eds.), Tools in Fluvial Geomorphology. Wiley-Blackwell, Chichester, pp. 133–158.

Korup, O., Strom, A.L., Weidinger, J.T., 2006. Fluvial response to large rock-slope failures: Examples from the Himalayas, the Tien Shan, and the Southern Alps in New Zealand. Geomorphology 78, 3 – 21. doi:10.1016/j.geomorph.2006.01.020.

Kriegel, D., Mayer, C., Hagg, W., Vorogushyn, S., Duethmann, D., Gafurov, A., Farinotti, D., 2013. Changes in glacierisation, climate and runoff in the second half of the 20th century in the Naryn basin, Central Asia. Global and Planetary Change 110, 51–61. doi:10.1016/j.gloplacha.2013.05.014.

Kuhn, M., 2020. caret: Classification and Regression Training. URL: https://CRAN.R-project.org/package=caret. r package version 6.0-86.

Kundzewicz, Z.W., Robson, A.J., 2004. Change detection in hydrological records - a review of the methodology. Hydrological Sciences Journal-journal Des Sciences Hydrologiques 49, 7–19. doi:10.1623/hysj.49.1.7.53993.

Kwiatkowski, D., Phillips, P.C., Schmidt, P., Shin, Y., 1992. Testing the null hypothesis of stationarity against the alternative of a unit root: How sure are we that economic time series have a unit root? Journal of Econometrics 54, 159 – 178. doi:10.1016/0304-4076(92)90104-Y.

Lane, E., 1955. The importance of fluvial morphology in hydraulic engineering. Proceedings of the American Society of Civil Engineering 81, 1–17.

Lane, S., Widdison, P.E., Thomas, R.E., Ashworth, P.J., Best, J.L., Lunt, I.A., Sambrook-Smith, G.H., Simpson, C.J., 2010. Quantification of braided river channel change using archival digital image analysis. Earth Surface Processes and Landforms 35, 971–985. doi:10.1002/esp.2015.

Lane, S.N., 2007. Assessment of rainfall-runoff models based upon wavelet analysis. Hydrological Processes 21, 586–607. doi:10.1002/hyp.6249.

Lane, S.N., Richards, K.S., 1997. Linking river channel form and process: Time, space and causality revisited. Earth Surface Processes and Landforms 22, 249–260.

Lauermann, M., 2016. Fluviale Dynamik am Mittellauf des Naryn. Eine GIS-basierte Modellierung. Unpublished M.Sc. Thesis at the Catcholic University Eichstaett-Ingolstadt. In German.

Lauermann, M., Betz, F., Cyffka, B., 2016. Channel Network Derivation from Digital Elevation Models – An Evaluation of Open Source Approaches. Bulletin of KSUCTA 3, 154–161. URL: https://goo.gl/5PKMwf.

Lauermann, M., Betz, F., Mehta, K., Thevs, N., Ehrenwirth, M., Zörner, W., Cyffka, B., 2020. Preservation of selected ecosystem services in the floodplains of the Naryn River (Kyrgyzstan): Introducing the ÖkoFlussPlan Project. Geographica Augustana 31, 47–53.

Legendre, P., Legendre, L., 2012. Numerical ecology. volume 24. 3rd english ed. ed., Elsevier, Amsterdam and Boston.

Legleiter, C.J., Fonstad, M.A., 2012. An introduction to the physical basis for deriving river information by optical remote sensing, in: Carbonneau, P., Piégay, H. (Eds.), Fluvial Remote Sensing for Science and Management. Wiley-Blackwell, Chichester, pp. 43–69.

Legleiter, C.J., Goodchild, M.F., 2005. Alternative representations of in-stream habitat: classification using remote sensing, hydraulic modeling, and fuzzy logic. International Journal of Geographical Information Science 19, 29–50. doi:10.1080/13658810412331280220.

Legleiter, C.J., Roberts, D.A., 2009. A forward image model for passive optical remote sensing of river bathymetry. Remote Sensing of Environment 113, 1025 – 1045. doi:10.1016/j.rse.2009.01.018.

Legleiter, C.J., Roberts, D.A., Lawrence, R.L., 2009. Spectrally based remote sensing of river bathymetry. Earth Surface Processes and Landforms 34, 1039–1059. doi:10.1002/esp.1787.

Legleiter, C.J., Roberts, D.A., Marcus, W.A., Fonstad, M.A., 2004. Passive optical remote sensing of river channel morphology and in-stream habitat: Physical basis and feasibility. Remote Sensing of Environment 93, 493 – 510. doi:10.1016/j.rse.2004.07.019.

Legleiter, C.J., Stegman, T.K., Overstreet, B.T., 2016. Spectrally based mapping of riverbed composition. Geomorphology 264, 61 – 79. doi:10.1016/j.geomorph.2016.04.006.

Leopold, L., Maddock, T., 1953. The hydraulic geometry of stream channels and some physiographic implications. US Geol. Survey Prof. Paper 252.

Leopold, L., Marchand, M.O., 1968. On the quantitative inventory of the riverscape. Water Resources Research 4, 709–717. doi:10.1029/WR004i004p00709.

Leopold, L.B., Wolman, M.G., Miller, J.P., 1964. Fluvial processes in geomorphology. Freeman.

Leutner, B., Horning, N., 2016. RStoolbox: Tools for Remote Sensing Data Analysis. URL: https://CRAN.R-project.org/package=RStoolbox. r package version 0.1.6.

Leviandier, T., Alber, A., Ber, F.L., Piégay, H., 2012. Comparison of statistical algorithms for detecting homogeneous river reaches along a longitudinal continuum. Geomorphology 138, 130 – 144. doi:10.1016/j.geomorph.2011.08.031.

Lindeman, R., Merenda, P., Gold, R., 1980. Introduction to Bivariate and Multivariate Analysis. Foresman, Gleview.

Lovelace, R., Nowosad, J., Muenchow, J., 2018. Geocomputation with R. Chapman & Hall, London. URL: https://geocompr.robinlovelace.net/.

MA, 2005. Millennium ecosystem assessment report. Ecosystems and human wellbeing: a framework for assessment Washington, DC: Island Press .

Malenovský, Z., Rott, H., Cihlar, J., Schaepman, M.E., García-Santos, G., Fernandes, R., Berger, M., 2012. Sentinels for science: Potential of Sentinel-1, -2, and -3 missions for scientific observations of ocean, cryosphere, and land. Remote Sensing of Environment 120, 91–101. doi:10.1016/j.rse.2011.09.026.

Malinowski, R., Groom, G.B., Heckrath, G., Schwanghart, W., 2017. Do Remote Sensing Mapping Practices Adequately Address Localized Flooding ? A Critical Overview. Springer Science Reviews doi:10.1007/s40362-017-0043-8.

Manfreda, S., Sole, A., Fiorentino, M., 2008. Can the basin morphology alone provide an insight into floodplain delineation. WIT Transactions on Ecology and the Environment 118, 47–56. doi:10.2495/FRIAR080051.

Maniak, U., 2016. Hydrologie und Wasserwirtschaft: eine Einführung für Ingenieure. Springer Vieweg, Berlin. In German.

Mann, H.B., 1945. Nonparametric tests against trend. Econometrica: Journal of the Econometric Society , 245–259.

Marchetti, Z., Minotti, P., Ramonell, C., Schivo, F., Kandus, P., 2016. NDVI patterns as indicator of morphodynamic activity in the middle Paraná River floodplain. Geomorphology 253, 146 – 158. doi:10.1016/j.geomorph.2015.10.003.

Marchetti, Z., Ramonell, C., Brumnich, F., Alberdi, R., Kandus, P., 2020. Vegetation and hydrogeomorphic features of a large lowland river: NDVI patterns summarizing fluvial dynamics and supporting interpretations of ecological patterns. Earth Surface Processes and Landforms 45, 694–706. doi:10.1002/esp.4766.

Marcus, W., Legleiter, C.J., Aspinall, R.J., Boardman, J.W., Crabtree, R.L., 2003. High spatial resolution hyperspectral mapping of in-stream habitats, depths, and woody debris in mountain streams. Geomorphology 55, 363 – 380. doi:10.1016/S0169-555X(03)00150-8.

Marcus, W.A., Fonstad, M.A., 2008. Optical remote mapping of rivers at sub-meter resolution and watershed extents. Earth Surface Processes and Landforms 33, 4–24. doi:10.1002/esp.1637.

Markham, B., Barsi, J., Kvaran, G., Ong, L., Kaita, E., Biggar, S., Czapla-Myers, J., Mishra, N., Helder, D., 2014. Landsat-8 operational land imager radiometric calibration and stability. Remote Sensing 6, 12275–12308. doi:10.3390/rs61212275.

Martínez-Fernández, V., Solana-Gutiérrez, J., del Tánago, M.G., de Jalón, D.G., 2016. Automatic procedures for river reach delineation: Univariate and multivariate approaches in a fluvial context. Geomorphology 253, 38 – 47. doi:10.1016/j.geomorph.2015.09.029.

Martínez-Fernández, V., del Tánago, M.G., de Jalón, D.G., 2019. Selecting geomorphic variables for automatic river segmentation: Trade-offs between information gained and effort required. Geomorphology 329, 248 – 258. doi:10.1016/j.geomorph.2019.01.005.

von Maydell, H.J., 1983. Forst- und Holzwirtschaft der Sowjetunion. Teil 4: Kasachstan und die mittelasiatischen Sowjetrepubliken Usbekistan, Kirgisien, Tadshikistan, Turkmenistan. Mitteilungen der Bundesforschungsanstalt für Forst und Holzwirtschaft. Kommissionsverlag Buchhandlung Max Wiedebusch.

McCabe, M.F., Aragon, B., Houborg, R., Mascaro, J., 2017. Cubesats in hydrology: Ultrahigh-resolution insights into vegetation dynamics and terrestrial evaporation. Water Resources Research 53, 10017–10024. doi:10.1002/2017WR022240.

Mestre, I., 2017. When Shepherds Mine Mountains: The Impact of Artisanal Mining on Agropastoral Systems in Kyrgyzstan. Case Study of Naryn Province. Journal of Alpine Research – Revue de Géographie Alpine 105. URL: http://rga.revues.org/3611.

Metz, M., Mitasova, H., Harmon, R.S., 2011. Efficient extraction of drainage networks from massive, radar-based elevation models with least cost path search. Hydrology and Earth System Sciences 15, 667–678. doi:10.5194/hess-15-667-2011.

Michez, A., Piégay, H., Lejeune, P., Claessens, H., 2017. Multi-temporal monitoring of a regional riparian buffer network (>12,000 km) with LiDAR and photogrammetric point clouds. Journal of Environmental Management , 1–13doi:10.1016/j.jenvman.2017.02.034.

Micklin, P., 1988. Desiccation of the aral sea: A water management disaster in the soviet union. Science 241, 1170–1176. doi:10.1126/science.241.4870.1170.

Micklin, P., 2016. The future aral sea: hope and despair. Environmental Earth Sciences 75, 844. doi:10.1007/s12665-016-5614-5.

Milner, A.M., Khamis, K., Battin, T.J., Brittain, J.E., Barrand, N.E., Füreder, L., Cauvy-Fraunié, S., Gíslason, G.M., Jacobsen, D., Hannah, D.M., Hodson, A.J., Hood, E., Lencioni, V., Ólafsson, J.S., Robinson, C.T., Tranter, M., Brown, L.E., 2017. Glacier shrinkage driving global changes in downstream systems. Proceedings of the National Academy of Sciences 114, 9770–9778. doi:10.1073/pnas.1619807114.

Mohadjer, S., Ehlers, T.A., Bendick, R., Stübner, K., Strube, T., 2016. A Quaternary fault database for central Asia. Natural Hazards and Earth System Sciences 16, 529–542. doi:10.5194/nhess-16-529-2016.

Montgomery, D.R., 1999. Process domains and the river continuum. JAWRA Journal of the American Water Resources Association 35, 397–410. doi:10.1111/j.1752-1688.1999.tb03598.x.

Montgomery, D.R., Buffington, J.M., 1997. Channel-reach morphology in mountain drainage basins. Geological Society of America Bulletin 109, 596–611.

Montgomery, D.R., Buffington, J.M., 1998. Channel processes, classification, and response. River Ecology and Management: Lessons from the Pacific Coastal Ecoregion, RJ Naiman and RE Bilby (Editors). Springer-Verlag, New York, New York , 13–42.

Naiman, R.J., Décamps, H., 1997. The ecology of interfaces: Riparian zones. Annual Review of Ecology and Systematics 28, 621–658. doi:10.1146/annurev.ecolsys.28.1.621.

Naiman, R.J., Décamps, H., McClain, M.E., 2005. Riparia. Ecology, conservation and management of streamside communities. Elsevier Academics, Amsterdam.

Nanson, G.C., Croke, J.C., 1992. A genetic classification of floodplains. Geomorphology 4, 459–486. doi:10.1016/0169-555X(92)90039-Q.

Nicoll, T.J., Hickin, E.J., 2010. Planform geometry and channel migration of confined meandering rivers on the Canadian prairies. Geomorphology 116, 37 – 47. doi:10.1016/j.geomorph.2009.10.005.

Nilsson, C., Reidy, C., Dynesius, M., Revenga, C., 2005. Fragmentation and Flow Regulation of the World's Large River Systems. Science 308, 405–408. doi:10.1126/science.1107887.

Notebaert, B., Piégay, H., 2013. Multi-scale factors controlling the pattern of floodplain width at a network scale: The case of the Rhône basin, France. Geomorphology 200, 155 – 171. doi:10.1016/j.geomorph.2013.03.014.

Odling-Smee, F.J., Laland, K.N., Feldman, M.W., 2003. Niche construction: the neglected process in evolution. 37, Princeton University Press.

Olofsson, P., Foody, G.M., Herold, M., Stehman, S.V., Woodcock, C.E., Wulder, M.A., 2014. Good practices for estimating area and assessing accuracy of land change. Remote Sensing of Environment 148, 42 – 57. doi:10.1016/j.rse.2014.02.015.

Parker, C., Clifford, N.J., Thorne, C.R., 2012. Automatic delineation of functional river reach boundaries for river research and applications. River Research and Applications 28, 1708–1725. doi:10.1002/rra.1568.

Parker, C., Thorne, C.R., Clifford, N.J., 2015. Development of ST:REAM: a reach-based stream power balance approach for predicting alluvial river channel adjustment. Earth Surface Processes and Landforms 40, 403–413. doi:10.1002/esp.3641.

Petts, G., Amoros, C., 1996. Fluvial hydrosystems. Chapman & Hall, London.

Petts, G.E., Gurnell, A.M., 2005. Dams and geomorphology: Research progress and future directions. Geomorphology 71, 27 – 47. doi:10.1016/j.geomorph.2004.02.015.

Pfaff, B., McNeil, A., 2012. evir: Extreme Values in R. URL: https://CRAN.R-project.org/package=evir. r package version 1.7-3.

Phillips, J.D., 2007. The perfect landscape. Geomorphology 84, 159 – 169. doi:10.1016/j.geomorph.2006.01.039.

Phillips, J.D., 2011. Emergence and pseudo-equilibrium in geomorphology. Geomorphology 132, 319 – 326. doi:10.1016/j.geomorph.2011.05.017.

Piégay, H., 2016. System approaches in fluvial geomorphology, in: Tools in Fluvial Geomorphology. Wiley-Blackwell, Chichester, pp. 79–102.

Piégay, H., Arnaud, F., Belletti, B., Bertrand, M., Bizzi, S., Carbonneau, P., Dufour, S., Liebault, F., Ruiz-Villanueva, V., Slater, L., 2019. Remotely sensed rivers in the anthropocene: State of the art and prospects. Earth Surface Processes and Landforms doi:10.1002/esp.4787.

Piégay, H., Gurnell, A., 1997. Large woody debris and river geomorphological pattern: examples from S.E. France and S. England. Geomorphology 19, 99 – 116. doi:10.1016/S0169-555X(96)00045-1.

Planchon, O., Darboux, F., 2002. A fast, simple and versatile algorithm to fill the depressions of digital elevation models. Catena 46, 159–176. doi:10.1016/S0341-8162(01)00164-3.

Poff, N.L., Allan, J.D., Bain, M.B., Karr, J.R., Prestegaard, K.L., Richter, B.D., Sparks, R.E., Stromberg, J.C., 1997. The natural flow regime. BioScience 47, 769–784. doi:10.2307/1313099.

Poff, N.L., Zimmerman, J.K.H., 2010. Ecological responses to altered flow regimes: a literature review to inform the science and management of environmental flows. Freshwater Biology 55, 194–205. doi:10.1111/j.1365-2427.2009.02272.x.

Politti, E., Bertoldi, W., Gurnell, A., Henshaw, A., 2018. Feedbacks between the riparian salicaceae and hydrogeomorphic processes: A quantitative review. Earth-Science Reviews 176, 147 – 165. doi:10.1016/j.earscirev.2017.07.018.

Pollen-Bankhead, N., Simon, A., 2010. Hydrologic and hydraulic effects of riparian root networks on streambank stability: Is mechanical root-reinforcement the whole story? Geomorphology 116, 353 – 362. doi:10.1016/j.geomorph.2009.11.013.

Poole, G.C., 2002. Fluvial landscape ecology: addressing uniqueness within the river discontinuum. Freshwater Biology 47, 641–660. doi:10.1046/j.1365-2427.2002.00922.x.

Potschin, M.B., Haines-Young, R.H., 2011. Ecosystem services: Exploring a geographical perspective. Progress in Physical Geography 35, 575–594. doi:10.1177/0309133311423172.

Potschin-Young, M., Haines-Young, R., Görg, C., Heink, U., Jax, K., Schleyer, C., 2017. Understanding the role of conceptual frameworks: Reading the ecosystem service cascade. Ecosystem Services 29, 428 – 440. doi:10.1016/j.ecoser.2017.05.015.

Powell, S.L., Cohen, W.B., Healey, S.P., Kennedy, R.E., Moisen, G.G., Pierce, K.B., Ohmann, J.L., 2010. Quantification of live aboveground forest biomass dynamics with Landsat time-series and field inventory data: A comparison of empirical modeling approaches. Remote Sensing of Environment 114, 1053 – 1068. doi:10.1016/j.rse.2009.12.018.

Pulvirenti, L., Chini, M., Pierdicca, N., Guerriero, L., Ferrazzoli, P., 2011. Flood monitoring using multi-temporal cosmo-skymed data: Image segmentation and signature interpretation. Remote Sensing of Environment 115, 990 – 1002. doi:10.1016/j.rse.2010.12.002.

QGIS Development Team, 2009. QGIS Geographic Information System. Open Source Geospatial Foundation. URL: http://qgis.osgeo.org.

Ranghetti, L., Boschetti, M., Nutini, F., Busetto, L., 2020. "sen2r": An R toolbox for automatically downloading and preprocessing Sentinel-2 satellite data. Computers & Geosciences 139, 104473. doi:10.1016/j.cageo.2020.104473.

Räpple, B., Piégay, H., Stella, J.C., Mercier, D., 2017. What drives riparian vegetation encroachment in braided river channels at patch to reach scales? Insights from annual airborne surveys (Drôme River, SE France, 2005–2011). Ecohydrology 10, e1886–n/a. doi:10.1002/eco.1886.

Rauschenberger, J., 2016. Standortanalyse juveniler Phanerophyten in der Narynaue, Kirgistan. Unpublished M.Sc. Thesis at the Catcholic University Eichstaett-Ingolstadt. In German.

Reiche, J., Hamunyela, E., Verbesselt, J., Hoekman, D., Herold, M., 2018. Improving near-real time deforestation monitoring in tropical dry forests by combining dense Sentinel-1 time series with Landsat and ALOS-2 PALSAR-2. Remote Sensing of Environment 204, 147–161. doi:10.1016/j.rse.2017.10.034.

Reinfelds, I., Cohen, T., Batten, P., Brierley, G., 2004. Assessment of downstream trends in channel gradient, total and specific stream power: a GIS approach. Geomorphology 60, 403 – 416. doi:10.1016/j.geomorph.2003.10.003.

Richter, B.D., Baumgartner, J.V., Powell, J., Braun, D.P., 1996. A method for assessing hydrologic alteration within ecosystems. Conservation Biology 10, 1163–1174. doi:10.1046/j.1523-1739.1996.10041163.x.

Rinaldi, M., Gurnell, A.M., del Tánago, M.G., Bussettini, M., Hendriks, D., 2016. Classification of river morphology and hydrology to support management and restoration. Aquatic Sciences 78, 17–33. doi:10.1007/s00027-015-0438-z.

Rinaldi, M., Surian, N., Comiti, F., Bussettini, M., 2013. A method for the assessment and analysis of the hydromorphological condition of Italian streams: The Morphological Quality Index (MQI). Geomorphology 180-181, 96 – 108. doi:10.1016/j.geomorph.2012.09.009.

Rinaldi, M., Surian, N., Comiti, F., Bussettini, M., 2015. A methodological framework for hydromorphological assessment, analysis and monitoring (IDRAIM) aimed at promoting integrated river management. Geomorphology 251, 122 – 136. doi:10.1016/j.geomorph.2015.05.010.

Ritz, C., Streibig, J., 2008. Nonlinear Regression with R. Springer, Heidelberg.

Robertson, K.M., Augspurger, C.K., 1999. Geomorphic processes and spatial patterns of primary forest succession on the Bogue Chitto River, USA. Journal of Ecology 87, 1052–1063. doi:10.1046/j.1365-2745.1999.00416.x.

Rost, K.T., Ratfelder, G., Topbaev, O., 2015. Problems of rural drinking water supply management in Central Kyrgyzstan: a case study from Kara-Suu village, Naryn Oblast. Environmental Earth Sciences 73, 863–872. doi:10.1007/s12665-014-3299-1.

Rougé, C., Ge, Y., Cai, X., 2013. Detecting gradual and abrupt changes in hydrological records. Advances in Water Resources 53, 33–44. doi:10.1016/j.advwatres.2012.09.008.

Roux, C., Alber, A., Bertrand, M., Vaudor, L., Piégay, H., 2015. "FluvialCorridor": A new ArcGIS toolbox package for multiscale riverscape exploration. Geomorphology 242, 29–37. doi:10.1016/j.geomorph.2014.04.018.

Schechtel, A., 2018. Die Erfassung von Sukzessionsstadien der Auenvegetation am Naryn (Kirgistan) mit Hilfe von Fernerkundung. Unpublished M.Sc. Thesis at the Catcholic University Eichstaett-Ingolstadt. In German.

Scheuber, M., Müller, U., Köhl, M., 2000. Wald- und Forstwirtschaft Kirgistans. Schweizerische Zeitschrift für Forstwesen 151, 69–74. In German.

Schlaffer, S., Matgen, P., Hollaus, M., Wagner, W., 2015. Flood detection from multi-temporal SAR data using harmonic analysis and change detection. International Journal of Applied Earth Observation and Geoinformation 38, 15 – 24. doi:10.1016/j.jag.2014.12.001.

Schmidt, M., 2007. Die Erfindung Kirgistans und der unvollendete Prozess der Nationenbildung. Europa Regional 15, 209–223. URL: https://goo.gl/ktdqDB. In German.

Schmidt, M., 2013. Mensch und Umwelt in Kirgistan. Politische Ökologie im postkolonialen und postsozialistischen Kontext. Steiner, Stuttgart. In German.

Schmidt, M., 2014. Die Walnuss-Wildobst-Wälder Kirgistans im Fokus divergierender Interessen und Akteure, in: Schmidt, M. (Ed.), Aktuelle Forschungen zu den Mensch-Umwelt-Verhältnissen in Kirgistan. Hannoversche Geographische Arbeiten ed.. Berlin, pp. 21–36. In German.

Schmidt, M., 2017. Human Geography of Post-Socialist Mountain Regions. An Introduction. Journal of Alpine Research – Revue de Géographie Alpine 115, 1–7. URL: http://journals.openedition.org/rga/3573.

Schmidt, M., Sagynbekova, L., 2008. Migration past and present: changing patterns in Kyrgyzstan. Central Asian Survey 27, 111–127. doi:10.1080/02634930802355030.

Schmidt, P., 2001. The scientific world and the farmer's reality: Agricultural research and extension in Kyrgyzstan. Mountain Research and Development 21, 109–112. doi:10.1659/0276-4741(2001)021[0109:TSWATF]2.0.CO;2.

Schmitt, R., Bizzi, S., Castelletti, A., 2014. Characterizing fluvial systems at basin scale by fuzzy signatures of hydromorphological drivers in data scarce environments. Geomorphology 214, 69–83. doi:10.1016/j.geomorph.2014.02.024.

Schoch, N., Steimann, B., Thieme, S., 2010. Migration and animal husbandry: Competing or complementary livelihood strategies. Evidence from Kyrgyzstan. Natural Resources Forum 34, 211–221. doi:10.1111/j.1477-8947.2010.01306.x.

Schultz, J., 2005. The ecozones of the world : the ecological divisions of the geosphere. Springer.

Schumm, S., 1977. The fluvial system. Wiley, New York.

Schumm, S., Lichty, R., 1965. Time, Space and Causality in Geomorphology. American Journal of Science 263, 110–119.

Schuyler, E., 1876. Turkestan. Notes of a journey in Russian Turkestan, Kokand, Bukhara and Kuldja. Ed. by G. Wheeler, New York 1966.

Schwanghart, W., Heckmann, T., 2012. Fuzzy delineation of drainage basins through probabilistic interpretation of diverging flow algorithms. Environmental Modelling and Software 33, 106 – 113. doi:10.1016/j.envsoft.2012.01.016.

Schwanghart, W., Scherler, D., 2017. Bumps in river profiles: uncertainty assessment and smoothing using quantile regression techniques. Earth Surface Dynamics 5, 821–839. doi:10.5194/esurf-5-821-2017.

Sear, D., Newson, M.D., Thorne, C.R., 2010. Guidebook of Applied Fluvial Geomorphology. Thomas Telford, London.

Shahgedanova, M., 2002. The physical geography of northern Eurasia. Oxford University Press, Oxford.

Shamsiev, B., 2007. Kyrgyz Republic livestock sector review: embracing the new challenges. Technical Report. World Bank. Bishkek.

Shigaeva, J., Wolgram, B., Chad, D., 2013. Sustainable Land Management in Kyrgyzstan and Tajikistan: A Research Review. MSRI Background Paper. URL: http://msri.ucentralasia.org/events.asp?Nid=589.

Simon, A., Collison, A.J.C., 2002. Quantifying the mechanical and hydrologic effects of riparian vegetation on streambank stability. Earth Surface Processes and Landforms 27, 527–546. doi:10.1002/esp.325.

Soar, P.J., Wallerstein, N.P., Thorne, C.R., 2017. Quantifying river channel stability at the basin scale. Water 9, 133. doi:10.3390/w9020133.

Sorg, A., Bolch, T., Stoffel, M., Solomina, O., Beniston, M., 2012. Climate change impacts on glaciers and runoff in Tien Shan (Central Asia). Nature Climate Change 2, 725–731. doi:10.1038/nclimate1592.

Sorg, A., Mosello, B., Shalpykova, G., Allan, A., Hill Clarvis, M., Stoffel, M., 2014. Coping with changing water resources: The case of the Syr Darya river basin in Central Asia. Environmental Science and Policy 43, 68–77. doi:10.1016/j.envsci.2013.11.003.

Spangenberg, J.H., Görg, C., Settele, J., 2015. Stakeholder involvement in ESS research and governance: Between conceptual ambition and practical experiences - risks, challenges and tested tools. Ecosystem Services 16, 201–211. doi:10.1016/j.ecoser.2015.10.006.

Spangenberg, J.H., von Haaren, C., Settele, J., 2014. The ecosystem service cascade: Further developing the metaphor. Integrating societal processes to accommodate social processes and planning, and the case of bioenergy. Ecological Economics 104, 22 – 32. doi:10.1016/j.ecolecon.2014.04.025.

Spangenberg, J.H., Settele, J., 2010. Precisely incorrect? Monetising the value of ecosystem services. Ecological Complexity 7, 327–337. doi:10.1016/j.ecocom.2010.04.007.

Spiess, A.N., Neumeyer, N., 2010. An evaluation of R squared as an inadequate measure for nonlinear models in pharmacological and biochemical research: a Monte Carlo approach. BMC Pharmacology 10, 1–11. doi:10.1186/1471-2210-10-6.

Stallins, J.A., Corenblit, D., 2018. Interdependence of geomorphic and ecologic resilience properties in a geographic context. Geomorphology 305, 76 – 93. doi:10.1016/j.geomorph.2017.09.012.

Steimann, B., 2011. Making a living in uncertainty. Agro-pastoral livelihoods and institutional transformations in post-socialist rural Kyrgyzstan. Al Salam Print House, Bishkek and Zurich.

Strahler, A., 1952. Hypsometric (area–altitude) analysis of erosional topography. Geol. Soc. Am. Bull. 63, 1117–1142.

Strom, A.L., Korup, O., 2006. Extremely large rockslides and rock avalanches in the Tien Shan Mountains, Kyrgyzstan. Landslides 3, 125–136. doi:10.1007/s10346-005-0027-7.

Tabacchi, E., Correll, D.L., Hauer, R., Pinay, G., Planty-Tabacchi, A.M., Wissmar, R.C., 1998. Development, maintenance and role of riparian vegetation in the river landscape. Freshwater Biology 40, 497–516. doi:10.1046/j.1365-2427.1998.00381.x.

Thapa, R., Thoms, M.C., Parsons, M., Reid, M., 2016. Adaptive cycles of floodplain vegetation response to flooding and drying. Earth Surface Dynamics 4, 175–191. doi:10.5194/esurf-4-175-2016.

Thompson, S.C., Weldon, R.J., Rubin, C.M., Abdrakhmatov, K., Molnar, Peter, B., Glenn, W., 2002. Late Quaternary slip rates across the central Tien Shan, Kyrgyzstan, Central Asia. Journal of Geophysical Research 107. doi:10.1029/2001JB000596.

Thoms, M.C., Parsons, M., 2002. Eco-geomorphology: an interdisciplinary approach to river science. International Association of Hydrological Sciences, Publication 276, 113–119p.

Thoms, M.C., Piégay, H., Parsons, M., 2018. What do you mean, 'resilient geomorphic systems'? Geomorphology 305, 8 – 19. doi:10.1016/j.geomorph.2017.09.003.

Thorp, J.H., Thoms, M.C., Delong, M.D., 2006. The riverine ecosystem synthesis: Biocomplexity in river networks across space and time. River Research and Applications 22, 123–147. doi:10.1002/rra.901.

Thorp, J.H., Thoms, M.C., Delong, M.D., 2008. The riverine ecosystem synthesis: Towards conceptual cohesiveness of river science. Elsevier Academics, Amsterdam.

Tibaldi, A., Corazzato, C., Rust, D., Bonali, F.L., Pasquare Mariotto, F.A., Korzhenkov, A.M., Oppizzi, P., Bonzanigo, L., 2015. Tectonic and gravity-induced deformation along the active Talas-Fergana Fault, Tien Shan, Kyrgyzstan. Tectonophysics 657, 38–62. doi:10.1016/j.tecto.2015.06.020.

Tockner, K., Lorang, M.S., Stanford, J.A., 2010. River flood plains are model ecosystems to test hydrogeomorphic and ecological concepts. River research and applications 26, 76–86. doi:10.1002/rra.1328.

Tockner, K., Stanford, J.a., 2002. Riverine flood plains: present state and future trends. Environmental Conservation 29, 308–330. doi:10.1017/S037689290200022X.

Tomsett, C., Leyland, J., 2019. Remote sensing of river corridors: A review of current trends and future directions. River Research and Applications 35, 779–803. doi:10.1002/rra.3479.

Tremp, H., 2005. Aufnahme und Analyse vegetationsökologischer Daten. volume 8299. Ulmer and UTB, Stuttgart. In German.

Trouchine, A., Giese, E., 2006. Aktuelle Probleme der Energiewirtschaft und Energiepolitik in Zentralasien. Discussion papers/Zentrum für internationale Entwicklungs- und Umweltforschung, No. 28. In German.

Tucker, C.J., 1979. Red and photographic infrared linear combinations for monitoring vegetation. Remote Sensing of Environment 8, 127 – 150. doi:10.1016/0034-4257(79)90013-0.

Unger-Shayesteh, K., Gerlitz, L., Vorogushyn, S., 2016. Technical Note : Why Methods Matter . A Guidance for Data-based Climate and Hydrological Change Assessments. IRWM 1, 1–12.

Unger-Shayesteh, K., Vorogushyn, S., Farinotti, D., Gafurov, A., Duethmann, D., Mandychev, A., Merz, B., 2013. What do we know about past changes in the water cycle of Central Asian headwaters? A review. Global and Planetary Change 110, 4–25. doi:10.1016/j.gloplacha.2013.02.004.

Urmambetova, T., Chymyrov, A., 2017. Geoenvironmental Impact Studies for Hydro-Energy Projects: Naryn River in Kyrgyzstan. Studia Universitatis Babeș-Bolyai Geographia 62, 59–66. doi:10.24193/subbgeogr.2017.1.04.

Vannote, R.L., Minshall, G.W., Cummins, K.W., Sedell, J.R., Cushing, C.E., 1980. The river continuum concept. Canadian Journal of Fisheries and Aquatic Sciences 37, 130–137. doi:10.1139/f80-017.

Vautier, F., Corenblit, D., Hortobagyi, B., Fafournoux, L., Steiger, J., 2016. Monitoring and reconstructing past biogeomorphic succession within fluvial corridors using stereophotogrammetry. Earth Surface Processes and Landforms 41, 1448–1463. doi:10.1002/esp.3962.

Venables, W.N., Ripley, B.D., 2002. Modern Applied Statistics with S. Fourth ed., Springer, New York. URL: http://www.stats.ox.ac.uk/pub/MASS4.

Verbesselt, J., Hyndman, R., Newnham, G., Culvenor, D., 2010. Detecting trend and seasonal changes in satellite image time series. Remote Sensing of Environment 114, 106 – 115. doi:10.1016/j.rse.2009.08.014.

Verbesselt, J., Umlauf, N., Hirota, M., Holmgren, M., Van Nes, E.H., Herold, M., Zeileis, A., Scheffer, M., 2016. Remotely sensed resilience of tropical forests. Nature Climate Change 6, 1028.

Verbesselt, J., Zeileis, A., Herold, M., 2012. Near real-time disturbance detection using satellite image time series. Remote Sensing of Environment 123, 98 – 108. URL: http://www.sciencedirect.com/science/article/pii/S0034425712001150, doi:https://doi.org/10.1016/j.rse.2012.02.022.

Vermote, E., Justice, C., Claverie, M., Franch, B., 2016. Preliminary analysis of the performance of the Landsat 8/OLI land surface reflectance product. Remote Sensing of Environment 185, 46 – 56. doi:10.1016/j.rse.2016.04.008.

Vogel, R.M., Fennessey, N.M., 1994. Flow Duration Curves I: New interpretation and Confidence Intervals. Journal of Water Resources Planning and Management 120, 485–504. doi:10.1061/(ASCE)0733-9496(1994)120:4(485).

Vogel, R.M., Fennessey, N.M., 1995. Flow Duration Curves II: A review of applications in water resource planning. JAWRA Journal of the American Water Resources Association 31, 1029–1039. doi:10.1111/j.1752-1688.1995.tb03419.x.

Wang, L., Liu, H., 2006. An efficient method for identifying and filling surface depressions in digital elevation models for hydrologic analysis and modelling. International Journal of Geographical Information Science 20, 193–213. doi:10.1080/13658810500433453.

Ward, J.V., 1989. The four-dimensional nature of lotic ecosystems. Journal of the North American Benthological Society 8, 2–8. doi:10.2307/1467397.

Ward, J.V., Tockner, K., Arscott, D.B., Claret, C., 2002. Riverine landscape diversity. Freshwater Biology 47, 517–539. doi:10.1046/j.1365-2427.2002.00893.x.

Weissteiner, C., Ickerott, M., Ott, H., Probeck, M., Ramminger, G., Clerici, N., Dufourmont, H., de Sousa, A., 2016. Europe's Green Arteries—A Continental Dataset of Riparian Zones. Remote Sensing 8, 925. doi:10.3390/rs8110925.

Wharton, G., 1995. The channel-geometry method: Guidelines and applications. Earth Surface Processes and Landforms 20, 649–660. doi:10.1002/esp.3290200707.

Wheaton, J.M., Fryirs, K.A., Brierley, G., Bangen, S.G., Bouwes, N., O'Brien, G., 2015. Geomorphic mapping and taxonomy of fluvial landforms. Geomorphology 248, 273–295. doi:10.1016/j.geomorph.2015.07.010.

Wheaton, J.M., Gibbins, C., Wainwright, J., Larsen, L., McElroy, B., 2011. Preface: Multiscale Feedbacks in Ecogeomorphology. Geomorphology 126, 265–268. doi:10.1016/j.geomorph.2011.01.002.

White, M.A., Schmidt, J.C., Topping, D.J., 2005. Application of wavelet analysis for monitoring the hydrologic effects of dam operation: Glen Canyon Dam and the Colorado River at Lees Ferry, Arizona. River Research and Applications 21, 551–565. doi:10.1002/rra.827.

Wiens, J.A., 2002. Riverine landscapes: taking landscape ecology into the water. Freshwater Biology 47, 501–515.

Wildi, O., 2017. Data analysis in vegetation ecology. CABI, Oxfordshire.

Willgoose, G., Hancock, G., 1998. Revisiting the hypsometric curve as an indicator of form and process in transport-limited catchment. Earth Surface Processes and Landforms 23, 611–623.

Williams, W.A., Jensen, M.E., Winne, J.C., Redmond, R.L., 2000. An automated technique for delineating and characterizing valley-bottom settings. Environmental Monitoring and Assessment 64, 105–114. doi:10.1023/A:1006471427421.

Wintenberger, C.L., Rodrigues, S., Bréhéret, J.G., Villar, M., 2015. Fluvial islands: First stage of development from nonmigrating (forced) bars and woody-vegetation interactions. Geomorphology 246, 305 – 320. doi:10.1016/j.geomorph.2015.06.026.

Wohl, E., 2013. Floodplains and wood. Earth-Science Reviews 123, 194 – 212. doi:10.1016/j.earscirev.2013.04.009.

Wohl, E., 2014. Time and the rivers flowing: Fluvial geomorphology since 1960. Geomorphology 216, 263 – 282. doi:10.1016/j.geomorph.2014.04.012.

Wohl, E., 2017. Bridging the gaps: An overview of wood across time and space in diverse rivers. Geomorphology 279, 3 – 26. doi:10.1016/j.geomorph.2016.04.014.

Wohl, E., Scott, D.N., 2017. Wood and sediment storage and dynamics in river corridors. Earth Surface Processes and Landforms 42, 5–23. doi:10.1002/esp.3909.

World Bank, 2016. State and Trends of Carbon Pricing. World Bank, Washington.

Wulder, M., Coops, N., 2014. Satellites: Make earth observations open access. Nature 513, 30–31. doi:10.1038/513030a.

Wulder, M.A., Coops, N.C., Roy, D.P., White, J.C., Hermosilla, T., 2018. Land cover 2.0. International Journal of Remote Sensing 39, 4254–4284. doi:10.1080/01431161.2018.1452075.

Wulder, M.A., Masek, J.G., Cohen, W.B., Loveland, T.R., Woodcock, C.E., 2012. Opening the archive: How free data has enabled the science and monitoring promise of Landsat. Remote Sensing of Environment 122, 2 – 10. doi:10.1016/j.rse.2012.01.010.

Xenarios, S., Assubayeva, A., Xie, L., Sehring, J., Amirkhanov, D., Sultanov, A., Fazli, S., 2020. A bibliometric review of water security concept in central asia. Environmental Research Letters doi:10.1088/1748-9326/abc717.

Xenarios, S., Gafurov, A., Schmidt-Vogt, D., Sehring, J., Manandhar, S., Hergarten, C., Shigaeva, J., Foggin, M., 2018. Climate change and adaptation of mountain societies in Central Asia: uncertainties, knowledge gaps, and data constraints. Regional Environmental Change doi:10.1007/s10113-018-1384-9.

Xu, H., 2006. Modification of normalised difference water index (NDWI) to enhance open water features in remotely sensed imagery. International Journal of Remote Sensing 27, 3025–3033. doi:10.1080/01431160600589179.

Young, N.E., Anderson, R.S., Chignell, S.M., Vorster, A.G., Lawrence, R., Evangelista, P.H., 2017. A survival guide to Landsat preprocessing. Ecology 98, 920–932. doi:10.1002/ecy.1730.

Zarfl, C., Lumsdon, A.E., Berlekamp, J., Tydecks, L., Tockner, K., 2014. A global boom in hydropower dam construction. Aquatic Sciences 77, 161–170. doi:10.1007/s00027-014-0377-0.

Zhao, K., Wulder, M.A., Hu, T., Bright, R., Wu, Q., Qin, H., Li, Y., Toman, E., Mallick, B., Zhang, X., Brown, M., 2019. Detecting change-point, trend, and seasonality in satellite time series data to track abrupt changes and nonlinear dynamics: A bayesian ensemble algorithm. Remote Sensing of Environment 232, 111181. doi:10.1016/j.rse.2019.04.034.

Zholdosheva, E., 2010. Review of the existing information, policies and proposed or implemented climate change measures in Kyrgyzstan. Technical Report. FAO. URL: http://www.fao.org/docrep/014/k9589e/k9589e10.pdf.

Zhu, Z., Wang, S., Woodcock, C.E., 2015. Improvement and expansion of the Fmask algorithm: cloud, cloud shadow, and snow detection for Landsats 4–7, 8, and Sentinel 2 images. Remote Sensing of Environment 159, 269 – 277. doi:10.1016/j.rse.2014.12.014.

Zhu, Z., Woodcock, C.E., 2012. Object-based cloud and cloud shadow detection in Landsat imagery. Remote Sensing of Environment 118, 83 – 94. doi:10.1016/j.rse.2011.10.028.